Associative Polymers as Antimisting Agents and Other Functional Materials via Thiol-Ene Coupling

Thesis by

Ralph Leonard Ameri David

In Partial Fulfillment of the Requirements for the Degree of Doctor of Philosophy

California Institute of Technology

Pasadena, California

2008

(Defended March 7, 2008)

Dedicated to:

my mother, for devotion in educating my child's mind,

my father, for unwavering support,

and my wife, for enduring friendship.

Acknowledgements

I feel profoundly grateful for my associations with members and friends of the Caltech community. My interactions with so many individuals who are at once fine people and outstanding scientists have combined to afford an immensely rewarding experience both on a personal and a professional level. I wish to express appreciation for the support and contributions I received from the following individuals: my advisor, Julie Kornfield, for allowing creativity and initiative to flourish, and for her kindness; the members of the Kornfield lab, for technical assistance and friendship; fellow students Jeremy Wei, David Liu, and Alessa Gambardella who participated directly in my research experiments; our many collaborators, including the Robert Grubbs and John Bercaw groups at the California Institute of Technology, Brett Bathel and Prof. Al Ratner at the University of Iowa, and Dr. Jan Plog of Thermo Fisher Scientific; and the members of my research committee, Prof. Robert Grubbs, Prof. Zhen-Gang Wang, and Dr. Virendra Sarohia, for guidance and countless fruitful discussions. I express loving appreciation to my wife Kristi, our daughters Charley and Madeleine, and our families and friends, for generating life outside of the laboratory. Finally, I acknowledge the financial support of the Milliken Grant, the Grubstake Grant, and the John and Ursula Kanel Charitable Fellowship.

Abstract

Associating polymers of varying molecular design were studied as potential additives to aviation fuel, aimed to suppress misting and thereby reduce the fuel's fire hazard in crash scenarios. Molecular architectures investigated varied from random placement along polymer chains of associating groups (referred to throughout this work as "stickers") to selective clustering of the stickers at chain ends. Linear chains possessing associating functional groups grafted at random positions along the entire chain were investigated first. Model polymers with matched backbone length were synthesized to examine the effects of degree of functionalization and type of interaction (self-associating or donor-acceptor) on shear and extensional rheology of both dilute and semi-dilute solutions in non-polar hydrocarbon solvents. We found that intramolecular associations dominate the behavior of self-associating chains even in semi-dilute concentrations, leading to chain collapse and reduced shear and extensional viscosities. Mixtures of donor-acceptor chains show much more favorable intermolecular pairing in dilute solutions (as evidenced by the formation of large aggregates), but nevertheless display reduced solution elasticity and extensional viscosity relative to unmodified homologues: sticker pairing interfered with the stretching of the chains in elongational flow. Molecular designs that overcome chain collapse by clustering stickers at the ends of polymer chains were studied next. We showed by theoretical modeling that symmetric linear chains displaying strongly associating endgroups suffer instead from loop formation, which traps the bulk of the polymer into small cyclic aggregates with low mist-control properties. Therefore, we suggest molecular architectures that preclude formation of cyclic supramolecules by employing several different donor-acceptor pairs that do not affect one another ("orthogonal" pairs). This presents a synthetic challenge, i.e., the development of simple and rapid protocols for the preparation of functional polymer materials of controlled architecture and functionality. We developed such convenient protocols (fast, non-wasteful, and scalable procedures) for the functionalization of polybutadiene by thiol-ene addition to yield functional polymers of narrow polydispersity. These powerful, versatile synthetic tools can potentially be applied to add any side-group onto any polymer, copolymer, or block copolymer displaying pendant vinyl groups, with exciting potential applications in fields ranging from organic electronics to drug delivery.

Table of Contents

List of Illustrations and Tables

Foreword

The subject of the present doctoral contribution is at the intersection of two exciting segments of macromolecular science in which the Kornfield lab has been involved for over a decade: the study of polymer self-assembly and the study of functional polymers. Our contribution is twofold. First, we increase the understanding of the behavior of associative functional polymers of various architectures (random, blocky) and type of interactions (self-associating versus specific, directional bonding) in dilute and semi-dilute solutions. In particular, we address the nature of the competition between inter- and intra-chain associations, and the effect of polymer molecular design and molecular parameters on aggregate structure and ultimately on rheological solution properties. Second, we expand the polymer scientist's toolkit for the preparation of well-defined materials with tailored properties by functionalization of polymers bearing pendant vinyl groups via thiol-ene coupling. That is, we present facile, high-yield, and scalable synthetic methods that optimize the combined tasks of (i) synthesizing new functional thiols and (ii) grafting them to polymer chains, in an efficient, rapid, and controlled manner.

Chapter I Introduction to Associating Polymers for Improved Fuel Fire Safety

1.1 Technological Need

The research presented here has been motivated by the technological need to improve the fire safety of jet fuel, motivated by both aviation safety and antiterrorism. Our efforts have sought to develop a polymer additive capable of suppressing the misting of aviation fuel, thereby delaying and abating the intensity of fires following the crash of a jet aircraft.[1-3]

Over the last 4 decades, on average 2 air carrier accidents have occurred monthly within the US and 15 worldwide. This level persists despite ongoing efforts to eliminate human error and improve security. Of these, an estimated 70% occur on takeoff or landing and are impact survivable. It is further estimated that 40% of the fatalities in such crashes are due to fire caused by combustion of aviation fuel. Thus, some 500–1000 lives per year can be saved by the development of an effective antimisting fuel system.

Perhaps more important is the issue of homeland security: the destructive power of a fully fueled aircraft inspires terrorists to subvert any security measures put in place. This destructive power comes from the fuel—not kinetic energy (in the September 11 attack on the World Trade Center, for instance, both towers absorbed the aircrafts' momentum and survived the initial impact). Threats to high-rise buildings, sports arenas, nuclear power facilities, and other important targets result from the explosion and intense post-crash fire. Thus, the successful incorporation of an antimisting fuel additive would greatly reduce the loss of life and property caused by plane accidents, and render passenger aircraft fuel ineffective as a weapon.

Presently there are no implemented technologies to reduce the fire hazard of fuel in crash scenarios. Our objective has been to develop an antimisting polymer additive to be used at concentrations below 0.1 wt % and at a cost of 1–2 cents per gallon of fuel. At a consumption rate of 19.5 billion gallons of jet fuel for the US airline industry (worldwide consumption is roughly twice that number), the estimated annual global market for such a polymer additive would be on the order of $0.5–1 billion/year. The requirements of a viable polymer additive for mist control of aviation fuel are given in Table 1.1.

1.2 Historical Developments of Polymer Research for Improved Fuel Fire Safety

Attempts in the past to mitigate aircraft crash fires has led to the incorporation of firewalls, flame arresters, fuel-line isolation, fire extinguishing systems, fire-resistant materials, etc., with limited success. As stated in a 1997 NRC report,[4] "the reduction of the fire hazard of [the] fuel [itself] is critical in improving survivability in past crashes." Candidate technologies aimed to provide a post-impact fire-safe fuel were evaluated in the January 2000 report of the Southwest Research Institute, prepared by Bernard Wright under contract to NASA.[5] Based on an extensive review of fuel vulnerability studies and discussions with industry-knowledgeable sources, Mist-Controlled Kerosene (MCK) technology was rated as the most promising and highest priority to date. MCK is conventional Jet-A to which a small concentration (say < 0.3 wt %) of high molecular weight (MW) polymer has been added. When fuel is released from ruptured tanks into the airflow around a crashing aircraft, the polymer interferes mechanically with the formation of mist.

1.2.1 Ultra-High Molecular Weight Linear Chains

It has been known since the 1960s that low concentrations of very high molar mass polymers (on the order of 10^7 g/mol) have potent effects on both hydrodynamic drag in turbulent flows and on the breakup of liquid jets and drops. Drag reduction refers to the spectacular decrease in the frictional losses under turbulent flow that can result from the addition of part-per-million levels (as low as 0.02 ppm)[6] of long-chain polymer to a fluid. The addition of small quantities of polymer is known to affect the behavior of liquids in jet breakup, spray atomization, and splashing, and has long been used to control drop size in technologies ranging from inkjet printing to agricultural spraying.

1.2.1.1 Basis of Effectiveness

What is the molecular basis for mist suppression and drag reduction by ultra-long polymer chains, and are the phenomena related? Control of drop size using polymer additives is determined by the polymer behavior in elongational flow, which is the dominant mode of deformation in the necking and breakup of fluid elements. Presumably, the stretching of the polymer chains results in large tensile stresses (as observed by large values of extensional viscosity)[7-11] which resist extensional deformation. In capillary breakup

experiments, this behavior serves to greatly extend the lifetime of filaments of Boger fluids, as seen in Figure 1.1. In jet breakup experiments of viscoelastic fluids, polymer molecules damp disturbances, promoting the formation of connecting filaments to produce a beads-on-string morphology[9, 12-14] (Figure 1.2). Mun et al.[10] and Christanti and Walker[15] showed that in jet breakup of dilute and semi-dilute polymer solutions due to natural disturbances, fluids with higher apparent extensional viscosity have larger breakup lengths, larger droplets, and fewer (if any) satellite droplets than Newtonian fluids of equal shear viscosity, density, and surface tension. The most important parameters in characterizing satellite drop suppression of viscoelastic fluids in elongational flow are the fluid's relaxation time and extensional viscosity.[7-9, 11]

Mist suppression and drag reduction seem to share the same origin in viscous and elastic effects arising from the distortion and relaxation of long polymer chains.[16, 17] Experimental and computational studies have confirmed that polymer chains in turbulent flow become highly extended compared to their equilibrium conformations, especially near the wall, and that the ability of the polymers to stretch is essential to drag reduction. Lumley[18, 19] and others[20, 21] proposed that drag reduction originates from the large increase in elongational viscosity associated with chain stretching, resulting in the damping of small eddies and thickening of the viscous sublayer. de Gennes[22] and others[23] suggested that drag reduction is caused instead by the elastic properties of the polymers, i.e., that the polymer molecules prevent production of turbulent velocity fluctuations on small scales by absorbing the small-scale turbulence energy as elastic energy. This energy can then be dissipated by polymer relaxation.[17, 24-26]

1.2.1.2 The Longer the Better

Ultra-high molecular weight linear chains have been shown to be extremely effective mist-control agents.[8, 27] Chao et al. reported that linear polyisobutylene (PIB) chains of molecular weight $5–10 \times 10^6$ g/mol were effective at reducing flammability of sprays of Jet-A fuel at concentrations as low as 50 ppm, and that mist-control ability increased with both increasing molecular weight and concentration.[8] With increasing concentration of 6×10^6 g/mol PIB, the effect progressed from suppression of smaller droplets to formation of continuous large filaments with no liquid breakup (Figure 1.3). Chao and coworkers reported that the single most important parameter in determining antimisting effectiveness was the

elongational viscosity of the solution (determined by tubeless siphon height measurements). This result was confirmed by Smolinski et al. for dilute PIB/mineral oil solutions by a combination of experiments and computations using an FENE-P dumbbell model.[11]

1.2.1.3 Shear Degradation

As a rough criterion, Chao and coworkers[8] proposed that polymer additives for antimisting in jet fuels must be of MW ~ 10^7 g/mol to be truly effective. Unfortunately, linear chains of such size undergo scission in high strain regions of turbulent flow, rendering their use impractical (the additive must be reintroduced after each pumping station or added at the point of delivery). One manifestation of this flow-induced degradation is the decrease in drag reduction activity with distance along a pipe segment.[24]

1.2.2 Associating Polymers

It has been suggested that shear degradation of polymer drag-reduction/mist-control additives may be overcome by turning to associative polymers, i.e., polymer chains capable of interacting through non-covalent bonds (e.g., hydrogen bonds). The objective then is to design shear-stable chains of molecular weight on the order of 1×10^6 g/mol that can aggregate at polymer concentration on the order of 1000 ppm into large clusters that themselves are effective mist-control/drag-reducing agents.

Two important examples of associating materials that have been investigated as potential mist-control/drag-reduction additives are ABA triblock copolymers designed so that the solvent is selectively good for one block and poor for the other (such as Kratons), and linear chains possessing hydrogen-bonding functional groups grafted at random positions along the entire chains (Figures 1.4 and 1.5). Kratons are polystyrene-*b*-polybutadiene-*b*-polystyrene (SBS) rubbers that can form flower-like micelle structures by association of the poorly soluble polystyrene endblocks in solvents such as heptane and kerosene, resulting in significantly enhanced shear viscosity. Experiments showed that although Kratons are able to increase droplet size in atomization due to higher values of shear viscosity, they do not lead to any enhancement in elongational viscosity relative to shear viscosity (i.e., $\mathrm{Tr} \equiv \eta_E / \eta_s \cong 3$, as expected for Newtonian fluids), and are therefore poor mist-control additives.[28]

Linear polymer chains possessing hydrogen-bonding functional groups grafted at random positions along the entire chains received the most attention. An important class of such polymers involves functional side-groups capable of pair-wise self-associations, such as ICI's FM-9 polymer (Figure 1.4a), and Exxon's alpha-olefin derivatives (Figure 1.4b). These were shown to be effective mist-control agents in the semi-dilute regime, but suffered from unacceptably high shear viscosity enhancements at these concentrations, as well as from poor solubility in non-polar hydrocarbon solvents such as jet fuel. More sophisticated attempts involved the development of systems with "directional bonding"[29-31] from a hydrogen-bond donor to a hydrogen-bond acceptor (Figure 1.5), expected to achieve control of extensional rheological properties at lower concentrations than self-associating systems. Malik and Mashelkar[30] (Figure 1.5b) demonstrated that mixing two polymers bearing complementary proton-accepting and proton-donating groups leads to the formation of interpolymer complexes even at concentrations below the overlap concentration of the individual polymers. These interpolymer complexes (IPC) were reported to enhance drag-reduction activity, both in terms of greater initial drag-reduction activity (by up to a factor of 6 when comparing IPCs with their non-associating precursors),[30] and in terms of increased resistance to shear degradation.[29-31] That is, molecules involved in IPCs were found to have increased shear-stability compared to non-associating polymer of the same molecular weight—a more stringent criterion than merely improving on the stability of ultra-long polymers.

1.2.3 Termination of Research

To date, the most extensive and most successful attempt to develop a polymer-modified fuel that improves fire-safety was the FAA-funded Anti-Misting Kerosene (AMK) program centered on ICI's proprietary FM-9 polymer. AMK was an engineering-focused program with emphasis on practical testing. By trial and error a fuel formulation was produced that reduced the post-crash fire; however, the program eventually failed because it lacked the scientific effort necessary to obtain fundamental understanding of how to make necessary adjustments.

The termination of research on polymer additives for mist control of jet fuels was precipitated by negative publicity arising from a controlled impact demonstration (CID) conducted by the FAA and NASA on December 1, 1984. The intent of the CID was to test

the effectiveness of Mist-Controlled Kerosene under realistic conditions of a survivable crash, using a 3000 ppm FM-9 formulation. Unfortunately, the test was not performed as planned and the remotely piloted Boeing 720 commercial aircraft was landed at a high yaw angle of 13^{o}, resulting in a huge fireball. Despite appearances, careful review of the CID photographic evidence revealed that the large initial plume of burning fuel self-quenched, did not penetrate the interior of the aircraft, and left the fuselage with only minor fire damage,[3] so that a large number of passengers could have safely escaped during the ~ 1 ½ minute time interval over which the fire subsided. Similar controlled crashes with untreated Jet-A produced such an intense fireball that the fuselage melted and its contents were engulfed in flames. Thus, MCK *did* perform as intended. Nevertheless, by 1986 the Department of Transportation had cancelled the entire program. Without the prospect of a market, industry followed suit.

1.3 Overview of the Present Work

As mentioned earlier, prior efforts failed because they did not aim to obtain a molecular understanding of material properties. Our interest has been to develop such a fundamental understanding, i.e., to provide the scientific foundation for utilizing non-covalent interactions in the preparation of functional polymers which are both resistant to shear degradation and effective mist-control/drag-reducing agents. The specific materials and selection of properties to investigate reflect the specific engineering objective that motivated our research: improving the fire-safety of fuels, especially aviation fuel. Technologically, the results can be expected to have broad relevance to suppression of splashing and misting in applications as diverse as agricultural spraying and ink-jet printing.

1.3.1 Objectives

We address the knowledge gap in the existing literature. In particular, the few reports of promising effects of randomly functionalized associating polymers have not examined the role of molecular variables, such as chain length or sticker density. Our first objective was therefore to establish the relationship between molecular properties and solution behavior, i.e., the connections between molecular design, aggregate structure, rheological properties, and performance in drag reduction and mist suppression (Figure 1.6) for randomly functionalized associative polymers. Our next objective was to use that understanding to molecularly design, synthesize, and test new generations of associative polymers. Our

technological objective was to eventually develop a polymer formulation that enables control of the extensional rheological properties of dilute solutions, while satisfying the requirements set out in Table 1.1.

1.3.2 Materials Studied

We investigated four generations of polymer additives (Figure 1.7), starting where the literature stopped, i.e., with the study of randomly functionalized chains with self-associating side-groups, and the study of randomly functionalized chains with complementary side-groups. A critical aspect of our work is that we prepared model molecules that allowed us to isolate the effect of associations from that of other parameters, such as chain size. More precisely, the synthetic methods we used allowed us to prepare homologous series of polymer chains identical in every respect (in length, architecture, chemical makeup, etc.) except for the nature and number of the functional groups. Our solution to that synthetic challenge enabled us to achieve the molecular control necessary to generate the fundamental understanding which was lacking in prior studies.

1.3.3 Organization

Chapter 2 deals with the solution properties of linear chains possessing self-associating functional groups grafted at random positions along the entire chains (Figure 1.7.1). Their shear and extensional rheological properties are presented in conjunction with new theoretical insight into structural changes arising from interactions. Chapter 3 tests the literature assertion that randomly functionalized linear chains featuring complementary groups (Figure 1.7.2) can provide satisfactory mist control at dilute or semi-dilute concentrations. New understanding generated in the above studies led to molecular designs that cluster interacting groups at chain ends. Computational modeling of the association behavior of linear chains displaying strongly associating endgroups (Figure 1.7.3) is reported in Chapter 4. We conclude our discussion of associating polymers for improved fuel fire safety with promising directions indicated by model predictions.

In Chapter 5, we carefully investigate the general usefulness of our chosen synthetic method for the preparation of homologous series of well-defined, functional polymers. We present fast, efficient, and scalable protocols for the synthesis and addition by thiol-ene coupling of various functional side-groups to polymers bearing pendant vinyl groups. The

procedure preserves the structure of the prepolymer material and allows powerful tuning of molecular properties by control of the nature and extent of functionalization.

1.4 Figures and Tables

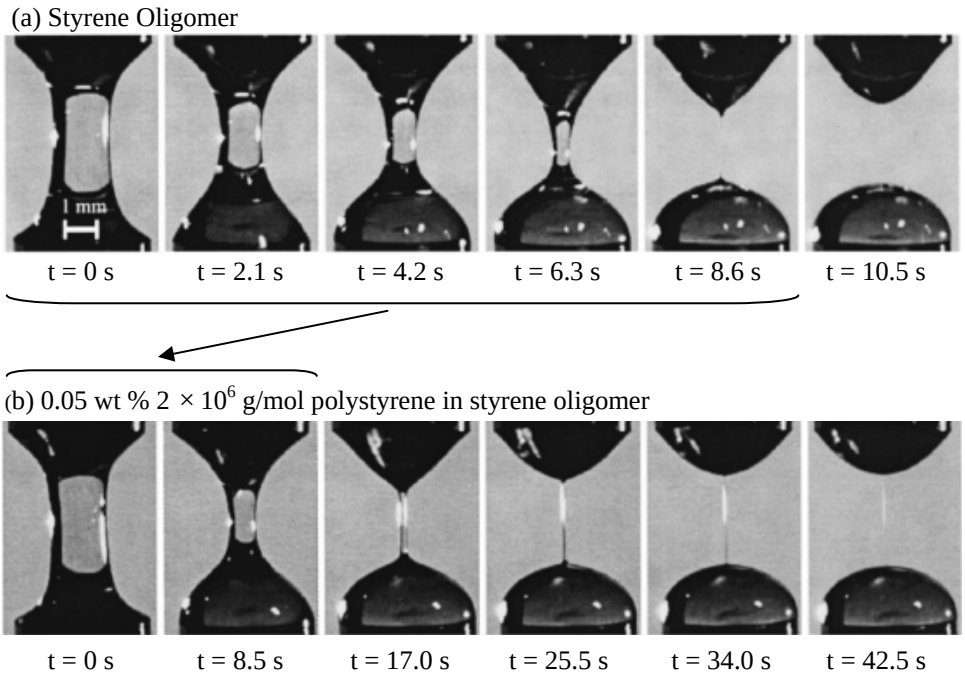

Figure 1.1 Sequence of video images showing capillary thinning and breakup for Newtonian and viscoelastic filaments. The plate diameter in both sequences is 3 mm. Note that the Newtonian filament (top row) is axially non-uniform due to gravitational sagging, while the Boger fluid (bottom row) forms a nearly cylindrical filament that persists much longer than a Newtonian filament of the same viscosity.[7] (Reproduced with permission.)

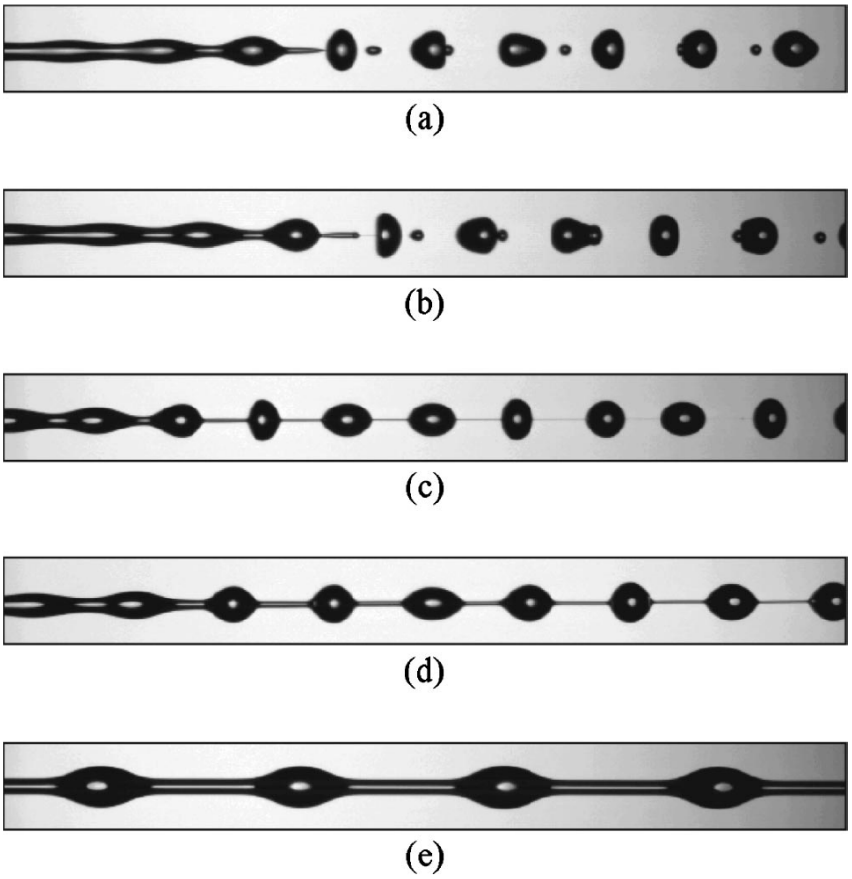

Figure 1.2 Effect of viscoelasticity on jet breakup due to a forced disturbance for PEO/glycerol/water solutions of nearly constant shear viscosity, surface tension, and density.[9] (a) 50% glycerol/water, (b) 0.3% 1×10^5 g/mol PEO, (c) 0.1% 3×10^5 g/mol PEO, (d) 0.05% 1×10^6 g/mol PEO, and (e) 0.043% 5×10^6 g/mol PEO. Flow direction is from left to right; image size is 20,000 μm × 2,000 μm. Note the nonlinear decrease in concentration required to achieve a given breakup morphology as polymer MW increases; e.g., $1/20^{th}$ the concentration of 1×10^6 g/mol PEO is sufficient to produce the effect of 3×10^5 g/mol PEO. (Reproduced with permission.)

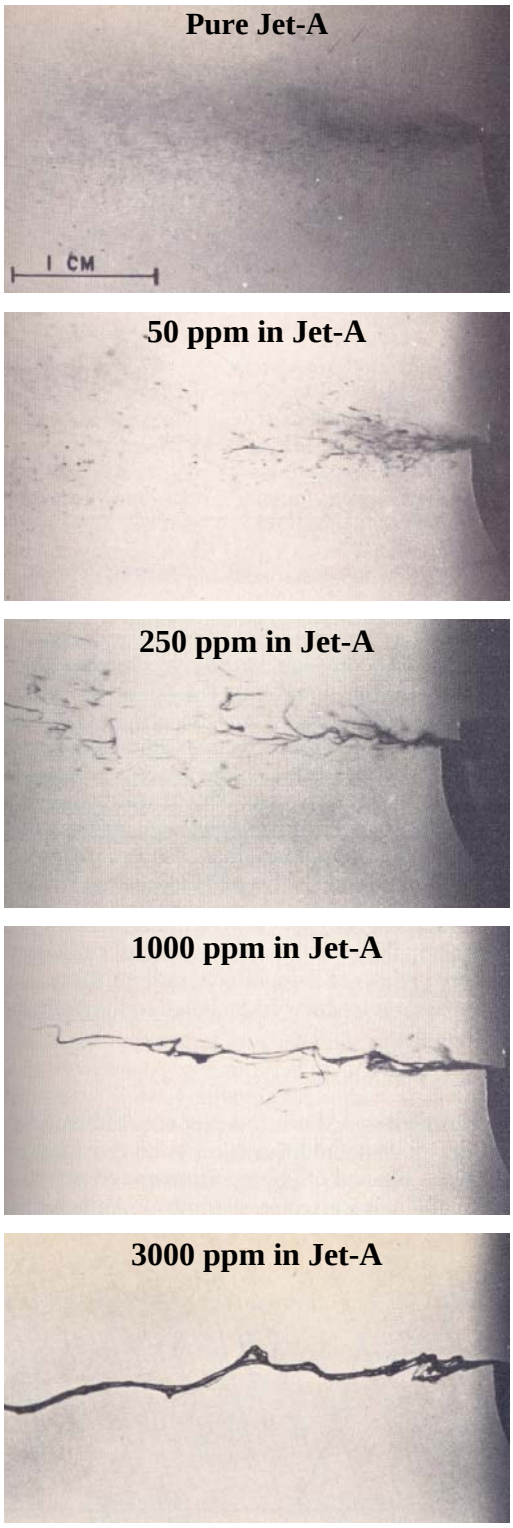

Figure 1.3 Effect of mist control additive concentration on spray morphology, as seen for polyisobutylene of $M_w = 6 \times 10^6$ g/mol and $M_w/M_n = 4.3$ in Jet-A at air velocity of 67 m/s and fuel flow of 0.33 cm^3/s.[8] (Reproduced with permission.)

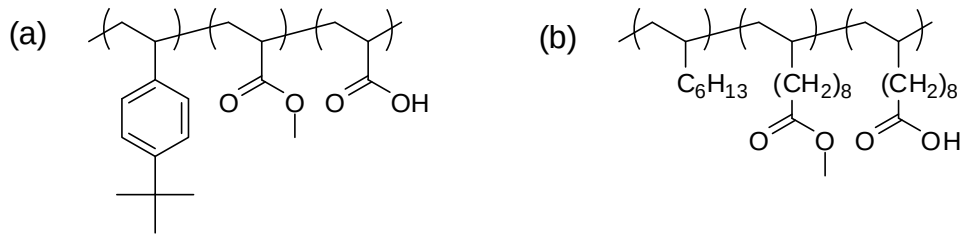

Figure 1.4 Examples of self-associating polymers. Interactions are pair-wise via dimerization of carboxylic acid side groups. (a) FM-9 random copolymer developed by ICI having undisclosed composition and molar mass,[32] (b) copolymer of 1-octene (99 mol %), methyl undecenoate (< 1 mol %), and undecenoic acid (0.02–0.5 mol %) of molecular weight $2–5\times 10^6$ g/mol developed by Schulz and coworkers at Exxon.[29, 31]

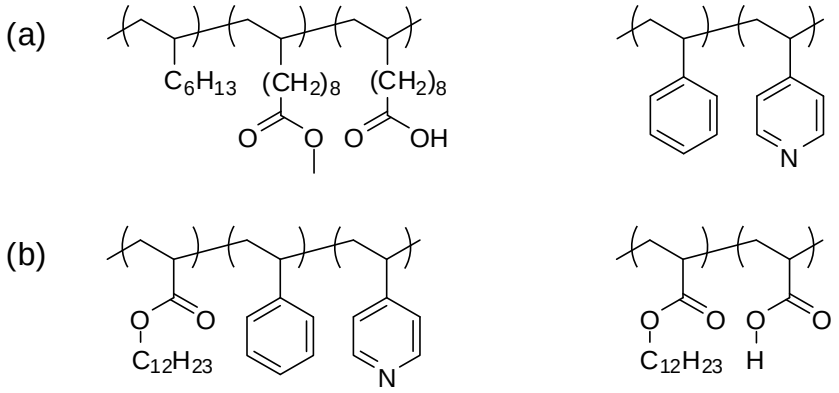

Figure 1.5 Examples of hydrogen-bond donor/acceptor random copolymer pairs. (a) Carboxylic acid groups as proton donors (polymer structure was given in Figure 1.4b) and pyridine moieties as proton acceptors (~ 8 mol %) on chains of $M_w \sim 2\times 10^6$ g/mol, developed at Exxon.[29, 31] (b) Carboxylic acid groups as proton donors (~ 3 wt % methacrylic acid) on chains of $M_w \sim 4.7\times 10^5$ g/mol, and pyridine groups as proton acceptors (~ 4 wt %) on chains of $M_w \sim 2.1\times 10^6$ g/mol, developed by Malik and Mashelkar.[30]

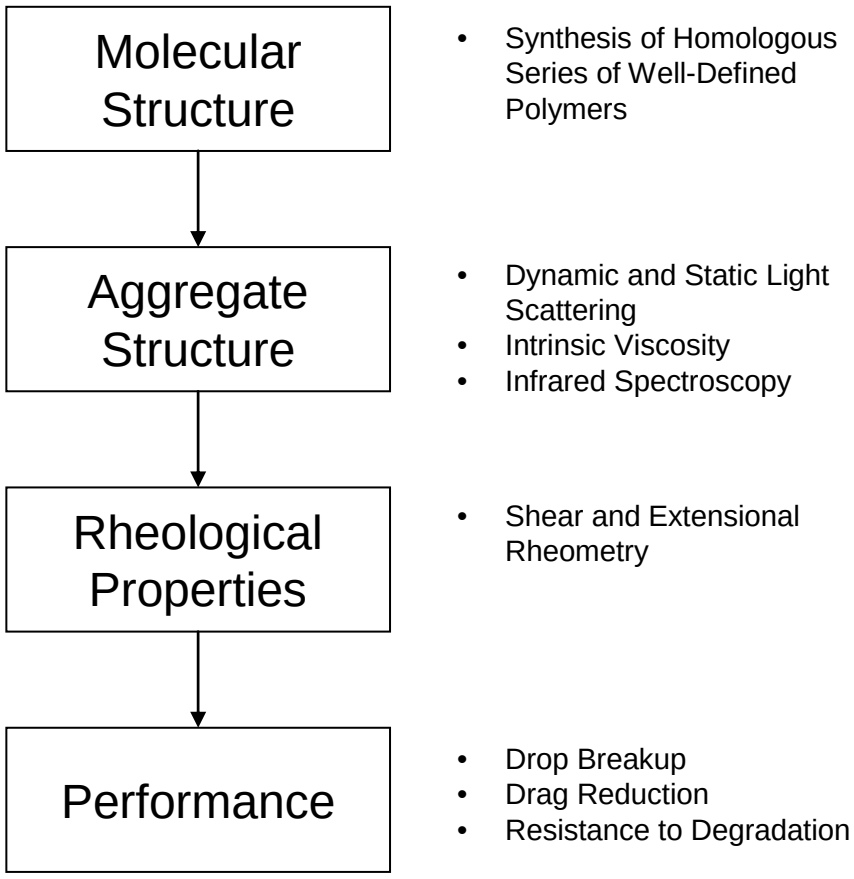

Figure 1.6 Our objectives are to establish the connections between polymer molecular structure, polymer self-assembly, solution rheological properties, and polymer performance in drag reduction and mist suppression.

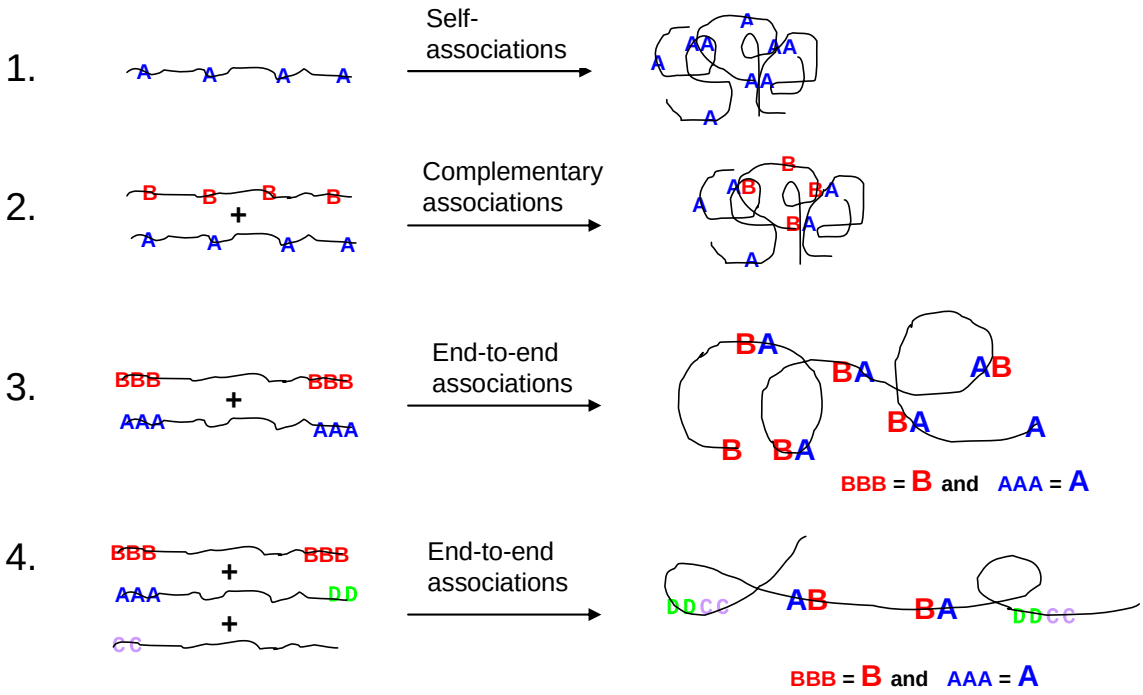

Figure 1.7 Alternative strategies using self-assembly of associating polymers in dilute solutions to control drop breakup in elongational flow.

Table 1.1 Fundamental Requirements of an Ideal Polymer Additive for Mist Control of Aviation Fuel

Criteria	Fluid Physical and Chemical Requirements
Improved fire safety	Fuel must not produce fine drops when accidentally released during a crash
Compatibility with aircraft fuel system	Addition of antimisting agent must not cause significant changes to other fuel physical and chemical properties, such as shear viscosity, acidity, etc.
	Fuel must remain single-phase over a wide range of use conditions
Ease of transport, storage, and use	Polymer design must confer sufficient stability that additives introduced at the point of production survive to the point of delivery
Low cost	Selection of polymer backbone and functional groups must take into account feasibility and cost of large scale production
Environmentally friendly	Polymer must burn cleanly
Marginal water uptake	Polymer must have low affinity for water

1.5 References

1. In *Fuel safety research*, Workshop Proceeding, FAA, Alexandria, Virginia, 29 October–1 November, 1985.

2. Sarohia, V., Research on anti-misting fuel for suppression of post-crash fires. In *AIAA paper 86-0573*.

3. Yaffee, M., Anti-misting fuel research and development for commercial aircraft—final report. In *DOT/FAA/CT-86/7*, April 1986.

4. In *Aviation fuels with improved fire safety*, NRC Proceeding, NMAB-490; Washington D.C., 1997; p. 41.

5. Wright, B. *Assessment of concepts and research for commercial aviation fire-safe fuel*; Southwest Research Institute, funded by NASA Glenn: January 2000.

6. Oliver, D. R.; Bakhtiyarov, S. I., Drag reduction in exceptionally dilute polymer-solutions. *Journal of Non-Newtonian Fluid Mechanics* **1983,** 12, (1), 113–118.

7. Anna, S. L.; McKinley, G. H., Elasto-capillary thinning and breakup of model elastic liquids. *Journal of Rheology* **2001,** 45, (1), 115–138.

8. Chao, K. K.; Child, C. A.; Grens, E. A.; Williams, M. C., Antimisting action of polymeric additives in jet fuels. *AICHE Journal* **1984,** 30, (1), 111–120.

9. Christanti, Y.; Walker, L. M., Effect of fluid relaxation time of dilute polymer solutions on jet breakup due to a forced disturbance. *Journal of Rheology* **2002,** 46, (3), 733–748.

10. Mun, R. P.; Byars, J. A.; Boger, D. V., The effects of polymer concentration and molecular weight on the breakup of laminar capillary jets. *Journal of Non-Newtonian Fluid Mechanics* **1998,** 74, 285–297.

11. Smolinski, J. M.; Gulari, E.; Manke, C. W., Atomization of dilute polyisobutylene mineral oil solutions. *AICHE Journal* **1996,** 42, (5), 1201–1212.

12. Entov, V. M.; Yarin, A. L., Influence of elastic stresses on the capillary breakup of jets of dilute polymer solutions. *Fluid Dynamics* **1984,** 19, (1), 21–29.

13. Goldin, M.; Yerushal, J.; Pfeffer, R.; Shinnar, R., Breakup of a laminar capillary jet of a viscoelastic fluid. *Journal of Fluid Mechanics* **1969,** 38, 689.

14. Gordon, M.; Yerushal, J.; Shinnar, R., Instability of jets of non-Newtonian fluids. *Transactions of the Society of Rheology* **1973,** 17, (2), 303–324.

15. Christanti, Y.; Walker, L. M., Surface tension driven jet break up of strain-hardening polymer solutions. *Journal of Non-Newtonian Fluid Mechanics* **2001,** 100, 9–26.

16. Matthys, E. F., Heat-transfer, drag reduction, and fluid characterization for turbulent-flow of polymer-solutions—recent results and research needs. *Journal of Non-Newtonian Fluid Mechanics* **1991,** 38, 313–342.

17. Ptasinski, P. K.; Boersma, B. J.; Nieuwstadt, F. T. M.; Hulsen, M. A.; Van den Brule, B. H. A. A.; Hunt, J. C. R., Turbulent channel flow near maximum drag reduction: simulations, experiments and mechanisms. *Journal of Fluid Mechanics* **2003,** 490, 251–291.

18. Lumley, J. L., Drag reduction by additives. *Annual Review of Fluid Mechanics* **1969,** 1, 367.

19. Lumley, J. L., Drag reduction in turbulent flow by polymer additives. *Journal of Polymer Science: Macromolecular Reviews* **1973,** 7, (1), 263–290.

20. Bewersdorff, H. W.; Berman, N. S., The influence of flow-induced non-Newtonian fluid properties on turbulent drag reduction. *Rheologica Acta* **1988,** 27, (2), 130–136.

21. Gadd, G. E., Turbulence damping and drag reduction produced by certain additives in water. *Nature* **1965,** 206, (4983), 463.

22. de Gennes, P. G., *Introduction to Polymer Dynamics*. Cambridge University Press: 1990.

23. Sreenivasan, K. R.; White, C. M., The onset of drag reduction by dilute polymer additives, and the maximum drag reduction asymptote. *Journal of Fluid Mechanics* **2000,** 409, 149–164.

24. Brostow, W., Drag reduction and mechanical degradation in polymer-solutions in flow. *Polymer* **1983,** 24, (5), 631–638.

25. Brostow, W.; Majumdar, S.; Singh, R. P., Drag reduction and solvation in polymer solutions. *Macromolecular Rapid Communications* **1999,** 20, (3), 144–147.

26. Min, T.; Jung, Y. Y.; Choi, H.; Joseph, D. D., Drag reduction by polymer additives in a turbulent channel flow. *Journal of Fluid Mechanics* **2003,** 486, 213–238.

27. Motier, J. F. *Hydrocarbon fuels containing antimisting agents*. European Patent 0177649, 1986.

28. Ergungor, Z.; Manke, C. W.; Gulari, E., Atomization and elongational viscosity of associating triblock copolymer solutions. *Journal of Non-Newtonian Fluid Mechanics* **2001,** 97, 159–167.

29. Kowalik, R. M.; Duvdevani, I.; Peiffer, D. G.; Lundberg, R. D.; Kitano, K.; Schulz, D. N., Enhanced drag reduction via interpolymer associations. *Journal of Non-Newtonian Fluid Mechanics* **1987,** 24, (1), 1–10.

30. Malik, S.; Mashelkar, R. A., Hydrogen-bonding mediated shear stable clusters as drag reducers. *Chemical Engineering Science* **1995,** 50, (1), 105–116.

31. Schulz, D. N.; Kitano, K.; Duvdevani, I.; Kowalik, R. M.; Eckert, J. A., Hydrocarbon-soluble associating polymers as antimisting and drag-reducing agents. *ACS Symposium Series* **1991,** 462, 176–189.

32. Knight, J. *Antimisting additives for aviation fuels*. United States patent 4,396,398, 1983.

Chapter II Randomly Functionalized Linear Chains with Self-Associating Groups

2.1 Introduction

Suppressing misting of fluids has long been achieved in water (e.g., controlling the coherence of a water jet) and in lubricating oils (e.g., cutting fluids in large-scale machining operations) by simply introducing an extremely long linear polymer at the point of application of the fluid (e.g., in the water tanks of fire-fighting equipment or the dispensing robot in a machine shop). The unmet challenge is developing an additive that will behave like the ultralong linear chains even after the fluid has been transported, stored, and filtered. The most promising strategies emerging from the era of intensive effort on antimisting kerosene (AMK) were polymer molecules that associate with one another via functional groups statistically distributed along the chains. Unfortunately, a survey of the literature reveals that the physical phenomena whereby associations drive mist suppression are poorly understood. In the case of FM-9 polymer (Figure 1.4a), the patent literature[1] reveals an engineering approach with emphasis on practical testing, aimed at developing a working anti-misting formulation for aviation fuel by trial and error. At each step of the way additional complexity was introduced, but without commensurate generation of new understanding. The result was a formulation whose behavior and mist-control effectiveness under high rates of deformation remains a mystery.[1-3]

We begin our study of associating polymers as mist-suppressing agents with the simplest molecular design, i.e., randomly functionalized linear chains with self-associating groups similar to FM-9. To generate understanding of physical phenomena, we designed and synthesized model polymers: chains of matched length and narrow length distribution (anionically synthesized linear polybutadienes of 510 and 1250 kg/mol) were functionalized with systematically varied extent of pair-wise “stickers” (carboxylic acid side groups incorporated by grafting 3-mercaptopropionic acid to the pendant double bonds of 1,2-units in the polybutadiene chains).

The model polymers were subjected to complementary measurements to evaluate the size of the supramolecular aggregates that they form, and the consequences those aggregates have on rheological properties and mist suppression. Attention was focused on low concentration

solutions relevant to antimisting of aviation fuel. Viscosity measurements of entangled solutions are included to test existing theory of the gelation of self-association polymers. The specific viscosity results indicate a significant degree of chain collapse, which is absent from prior theoretical models; therefore, we present a theoretical treatment of chain size at infinite dilution to gain insight into the role of chain collapse.

The body of results presented here calls into question many of the widely accepted conclusions presented in the prior literature. We find that inadequate attention was given to issues of phase separation and to the compact conformations that chains adopt when they are decorated with self-associating stickers. Therefore, alternative strategies to achieve antimisting polymers that resist shear degradation are suggested.

2.2 Experimental

2.2.1 Materials

Prepolymer polybutadiene (PB) chains of weight-average molecular weight M_w = 510 kg/mol (containing ~ 98% 1,2 units and with M_w/M_n = 1.15), hereafter referred to as 510kPB, were kindly provided by Dr. Steven Smith of Procter and Gamble Company. Prepolymer PB chains of M_w = 1250 kg/mol, hereafter referred to as 1250kPB, were purchased from Polymer Source, Inc. (product ID P1914-Bd, containing ~ 8% 1,2 adducts, with M_w/M_n = 1.09). Polyisobutylene of M_w = 4200 kg/mol, hereafter referred to as 4200kPIB, was purchased from Aldrich (product number 181498, with M_w/M_n = 1.35). 2,6-Di-*tert*-butyl-4-methylphenol (BHT), 3-mercaptopropionic acid (MPA), and 2,2′-azobis(2-methylpropionitrile) (AIBN) were obtained at 99% purity from Sigma-Aldrich. AIBN was recrystallized biweekly in methanol (10 mL solvent per g AIBN) and stored at 4 ºC; all other reagents (as well as solvents) were stored at room temperature and used as received without further purification.

2.2.2 Representative Procedure for PB Functionalization with MPA

To 510kPB (3.6 g, 67 mmol of repeat units) dissolved in 175 mL tetrahydrofuran (THF) in a 500-mL Schlenk round bottom flask was added a 25 mL THF solution of MPA (0.45 g, 4.2 mmol) and AIBN (113 mg, 0.69 mmol). The contents of the Schlenk flask were degassed in 3 freeze-pump-thaw cycles, warmed to 55 ºC, and then allowed to react at 55 ºC for 105 min. Following the reaction, the polymer solution was transferred to a 500-mL jar containing

a small amount of BHT, cooled in liquid nitrogen, and precipitated by addition of 200 mL of cold methanol. The polymer was purified by reprecipitation from a THF solution (containing ca. 1 wt % BHT) with cold methanol, followed by drying to constant weight under vacuum at room temperature. Reaction conditions and results are summarized in Table 2.1 (entry 510kPB1.8A).

2.2.3 Polymer Characterization

The extent of incorporation of MPA units into PB polymer was determined by analysis of ^{1}H NMR spectra, obtained using a Varian Mercury 300 spectrometer (300 MHz). All spectra were recorded in $CDCl_3$ and referenced to tetramethylsilane. Measurements of polymer molecular weight distributions by gel permeation chromatography (GPC) were carried out in THF at 25 ºC eluting at 0.9 mL/min through four PLgel 10-μm analytical columns (Polymer Labs, 10^6 to 10^3 Å in pore size) connected to a Waters 410 differential refractometer detector (λ = 930 nm). All GPC measurements were analyzed based on calibration using polystyrene standards. Polystyrene-equivalent molecular weights determined in this manner were substantially larger for PB than values provided by the suppliers of the polymers. The latter values, which were obtained by light scattering in conjunction with GPC, are reported above.

2.2.4 Viscosity and Size Measurements

Polymer solutions for viscosity measurements were prepared by combining polymer and solvent in clean 20 mL scintillation vials which were placed on a Wrist-Action Shaker (Burrell Scientific) for up to 72 hrs to allow the polymer to dissolve fully and homogenously. For solutions of viscosities $\geq$ 10 Pa.s, homogeneity was achieved by first preparing diluted solutions using dichloromethane (DCM) as co-solvent, followed by selective and complete evaporation of the DCM under reduced pressure (this method was enabled by the > 100 ºC difference in normal boiling points between DCM and the solvents we used). Shear viscosity measurements were performed under steady-state flow using an AR1000 rheometer from TA Instruments. The following complementary geometries enabled measurements of viscosities ranging from 10^{-3} to 10^5 Pa.s: (i) an aluminum cone of 60 mm diameter, 1^o angle, and 29 μm truncation, (ii) a steel cone of 40 mm diameter, 2^o angle, and 55 μm truncation, and (iii) a steel plate of 25 mm diameter.

Polymer samples used for measurements of hydrodynamic diameter by dynamic light scattering were prepared by filtration of dilute polymer solutions through a 0.4-μm pore PTFE membrane with Acrodisc CR 25-mm syringe filters. A ZetaPALS (Brookhaven Instruments Corporation) instrument was used to perform the size measurements. Experiments were carried out using a laser source with wavelength of 532 nm, and the scattered light was collected at an angle of 90º. The built-in Particle Size Software was used to analyze the acquired raw data. Reported apparent hydrodynamic radii represent averages of 9 runs of 1 minute each.

2.2.5 Characterization of Fluid Breakup and Atomization

The elasticity and relaxation time of polymer solutions under elongational deformation was studied using capillary breakup extentional rheometry using a Thermo Haake CaBER1 instrument (measurements courtesy of Dr. Jan P. Plog of Thermo Fisher Scientific). The effect of polymer on fluid breakup was characterized using two methods. The first investigates the splashing, spreading, and breakup processes of individual drops impacting a smooth, solid surface. The second experiment involves the spraying of fuel with a simple paint gun (HUSKY Gravity Feed Spray Gun, model HDS 780) and visualizing the resulting spray pattern.

The three methods above are chosen for their complimentary advantages and limitations. For the present solutions, CaBER is restricted to $c > c_{min} > c^*$, where $c^* \approx 2500$ ppm by wt for 1250kPB in Jet-A, and droplet impact only led to breakup if $c < c_{max} < c^*$. The only method that is applicable across a wide range of concentrations spanning c^* is the spray experiment. CaBER provides the most quantitative measurements of effective extensional properties of dilute polymer solutions, but for practical purposes it is limited to the testing of solutions of sufficiently high extensional viscosity[4] (for Newtonian fluids the shear viscosity must exceed ~ 100 mPa.s; fluids of lower viscosity can only be examined if they have high elasticity, e.g., solutions of linear polymers having $M_w > 10^7$ g/mol). High-speed imaging of drop spreading and breakup generates high deformation rates ($> 10^3$ s^{-1}) and is remarkably reproducible, but analysis is difficult, and for the present polymers, concentrations below 1000 ppm were required to permit breakup. Spray experiments are strictly qualitative, in part because spray patterns on 2-dimensional surfaces vary greatly based on experimental settings such as the position of the gun relative to the surface and the air pressure. The appeal of the

method, however, is that it can be used to evaluate in a rapid, although coarse manner, the extent of mist suppression imparted by a polymer additive of *any* molecular weight at *any* concentration in solution.

Capillary breakup rheometry and its application to the measurement of elongational properties of low-viscosity elastic fluids have been established by McKinley and coworkers.[4, 5] The CaBER1 system measures the effective extensional properties of a fluid confined to a small column between parallel discs of diameter D_0 = 4–8 mm, by first imposing a rapid axial step strain of prescribed magnitude to induce a statically unstable "neck" shape, and then by measuring with a laser the thinning and breakup of the resultant filament under the action of capillary forces. Filament thinning, driven by the capillary pressure, is resisted by the extensional stress in the fluid. The principal experimental results obtained are the evolution of the midpoint diameter $D_{mid}(t)$ and the critical time to breakup. The Hencky strain ε_H and the apparent extensional viscosity η_{ext} are determined as follows:

$$\varepsilon_H(t) = 2\ln\left(\frac{D_0}{D_{mid}(t)}\right) \tag{2.1}$$

$$\eta_{ext}(t) = \frac{\sigma}{-\mathrm{d}D_{mid}/\mathrm{d}t} \tag{2.2}$$

where σ is the surface tension. As the fluid filament thins, a window of time in which D_{mid} decays exponentially is typically observed for sufficiently elastic fluids; this regime is used to extract a characteristic relaxation time λ of the fluid ($D_{mid} \sim \exp[-t/3\lambda]$).

Drop impact experiments were done in collaboration with Prof. Albert Ratner at the University of Iowa, according to methods developed in his lab.[6] Droplets of diameter 3 mm were carefully forced out of a needle (one at a time) and allowed to impact a smooth quartz surface at velocities of 3 m/s, while a high-speed, high-resolution camera captured the deformation and breakup behavior at frame rates of 4 kHz and spatial resolution of 15 μm/pixel (Figure 2.1). Criteria for characterizing breakup include investigation of the amount of splashing, the amount of fluid ejected, and the survival time of fluid filaments. The latter is most readily quantified and serves as our primary criterion for comparing differently functionalized polymers.

All spray measurements were performed according to the following conditions: Solution aliquots of volume ½ mL were sprayed in a fume hood at horizontal angle from a vertical height of 30 cm using 10 psi air pressure, and images of the sedimenting droplet pattern on the bench surface were recorded 80 cm downstream from the spraying source (Figure 2.2, top). Spray patterns for solutions of 4200kPIB polymer in Jet-A (Figure 2.2, compare with Figure 1.3) demonstrate that this simple experiment is able to expose the mist-suppressing action of known mist-suppressing materials.

2.3 Results

2.3.1 Synthesis of Acid-Functionalized Polybutadiene

Reaction of PB prepolymer according to Scheme 2.1 using reaction conditions summarized in Table 2.1 allows controlled incorporation of carboxylic acid side-groups by radical addition of MPA to the pendant double bonds of 1,2-PB units (Table 2.1, Figure 2.3). Consistent with general results for PB modification by thiol-ene coupling under similar conditions, we found that the functionalization reaction occurs with minimal degradation of the precursor material (refer to Chapter 5). Because our studies spanned several months, the stability of functionalized polymer over time was investigated. We found that cross-linking occurs slowly (Table 2.1, Figure 2.4), but that this process could be minimized by stabilizing the polymer with a small amount of BHT and storing it in the dark below 0 ºC. Under these conditions, polymer crosslinking caused M_w/M_n to increase by < 0.1 over time periods of up to 18 months. As an example, the polydispersity of 510kPB0.2A increased from $M_w/M_n \sim 1.16$ after reaction to $M_w/M_n \sim 1.24$ after 18 months, compared with $M_w/M_n \sim 1.15$ for 510kPB prepolymer.

As documented in Chapter 5, possible cyclization of neighboring 1,2-PB adducts (when present) results in the formation of 5-member ring structures, so that in fact the predominant polymer structure arising from functionalization of 1,2-PB chains at low thiol concentration is that shown in Scheme 2.1a. In other words, the 510kPB chains documented in Table 2.1 contain roughly the same number of cyclic structures as MPA groups. However, because all of the molecules which were further studied contained < 2% side-groups, it seems reasonable to expect that structural changes to the polymer backbone are of little consequence compared to the effects arising from the incorporation of the self-associating carboxylic acid functionalities. The extent of MPA incorporation was determined upon analysis of ^{1}H NMR

spectra by integration of backbone and side-group peaks, as explained in the footnotes.[7] It proved difficult to achieve target levels of functionalization by kinetic control of the reaction, due to poor reproducibility of the reaction rates (refer to last column of Table 2.1). For example, nearly identical reaction conditions were used during synthesis of 1250PB0.6A and 1250PB0.4A. Investigation of the kinetics of the radical functionalization reaction is beyond the scope of this study.

2.3.2 Phase Behavior

Incorporation of carboxylic acid functional groups onto PB chains decreases polymer solubility due to unfavorable solvent-sticker interactions. Intra- and inter-molecular polymer associations further drive phase separation of the polymer into a dense phase, which is observed to occur above a maximum MPA content (Table 2.2) even at low polymer concentrations (500-2500 ppm).

As shown in Table 2.2, the maximum MPA content that is compatible with polymer solubility increases with solvents of increasing polarity, consistent with the known decrease in the strength of associations with increasing solvent polarity.[8] Solvent effects on the maximum MPA content compatible with single-phase solutions were also consistent with solvent quality for the polymer backbone. In the least polar solvent (dodecane), the tendency to phase separate as MPA units are added is more severe for 1,4-PB than for 1,2-PB, in accord with the more favorable polymer-solvent interactions for 1,2-PB in *n*-alkanes: C_5–C_8 *n*-alkanes at 60 ºC are approximately θ-solvents for 1,4-PB (the Flory-Huggins interaction parameter is $\chi \sim 0.5$-0.6 for chains of size $\sim 10^4$ g/mol), while they are fair solvents for 1,2-PB ($\chi \sim 0.3$–0.4 for chains of comparable size).[9] In addition, the tendency for polymer phase separation was found to be lower in chlorinated or aromatic hydrocarbons (the latter are present at 10–40 % in aviation fuels such as Jet-A) than in less polar solvents, consistent with the higher affinity of the polybutadiene backbones for halogenated and aromatic solvents: at 60 ºC for both 1,2-PB and 1,4-PB chains of size $\sim 10^4$ g/mol, χ values are smaller by about 0.1 for 1-chloropentane compared to *n*-pentane, $\chi \sim 0.1$ for chloroform, and $\chi \sim 0.1$–0.2 in toluene.[9] Thus, the observed trends in phase behavior indicate that increasing solvent polarity expands the single-phase region due to the combined effects of increased solubility of the chain backbone and decreased strength of hydrogen bonding.

2.3.3 Effects of Stickers on Shear Viscosity for Homogeneous Solutions

Our first observation is that stickers cause a decrease in η_{sp} in dilute solutions and an increase in η_{sp} in semi-dilute solutions, for both 510 kg/mol 1,2-PB chains in 1-chlorododecane (CDD) (Figure 2.5, with $\phi^* \cong 0.003$ for the unfunctionalized prepolymer) and 1250 kg/mol 1,4-PB chains in Jet-A (Table 2.3, with $c^* \sim 0.25$ wt % for the unfunctionalized prepolymer). This result is evidence of the competing effects between intra- and inter-molecular interactions. On the one hand, intramolecular associations collapse chains and thereby decrease shear viscosity; this effect is dominant at dilute concentrations. On the other hand, intermolecular associations result in viscosity enhancements, and the magnitude of this effect increases with increasing polymer concentration above the overlap. The crossover of the η_{sp} vs. c curves for associating and non-associating polymer solutions depends on the competition between these two opposing effects, but occurs for all polymer investigated here at a polymer volume fraction that is greater than ϕ^* of the unfunctionalized polymer (Figure 2.5, Table 2.3).

Our attempts to isolate the effects of intramolecular associations on the conformation of individual chains by measuring the viscosity of dilute solutions were not successful. Based on the Einstein relationship,[10] the specific viscosity η_{sp} in dilute solution is proportional to the hydrodynamic volume occupied by individual chains. Therefore, in principle the collapse of individual chains can be measured by the ratio of the specific viscosity of an associative polymer solution to that of the corresponding unfunctionalized polymer solution at infinite dilution: $\lim_{c\to 0}\left[r_{\eta,sp} = (\eta - \eta_{solvent})/(\eta_{ref} - \eta_{solvent}) \right]$. In our case, however, $r_{\eta,sp}$ could be determined with good accuracy only when $\eta_{sp} > 0.5$ (which required concentrations > ½ ϕ^*) using the 60-mm cone-and-plate geometry (a Couette geometry was available, but in that case measurement accuracy suffered from poorer temperature control).

A second observation is that the magnitude of the effects of stickers on solution shear viscosity was small over the entire range from dilute to entangled concentrations. Even at polymer volume fraction above the overlap of the strands between stickers ϕ_s (such that interchain associations are more probable than intrachain associations), stickers generated enhancements in η_{sp} no larger than 10-fold for all 510 kg/mol 1,2-PB polymer solutions investigated (Figure 2.5). We were surprised to find such small increases in viscosity,

particularly at the highest degrees of functionalization and polymer concentration investigated. Indeed, for 510kPB1.8A polymer at 30 vol % in CDD, polymer concentration is twice ϕ_s, and the strand length between stickers is ~ 3000 g/mol, leading us to anticipate a dramatic viscosity increase due to the formation of an entangled thermoreversible network. The anticipated[11-13] steep increase in shear viscosity with increasing polymer concentration in the vicinity of ϕ_s, due to transitioning of intra- to inter-molecular pairing, was not observed.

Effects of solvent and temperature were evaluated in the concentration regime in which stickers increase η_0, using ϕ = 0.10. With increasing temperature the specific viscosity decreases, as expected, with stickers generally giving a stronger temperature dependence than the unfunctionalized parent polymer (Figure 2.6). Solvent effects accord with qualitative expectations: shifting from a non-polar solvent (dodecane, DD) to a slightly polar solvent (CDD) has little effect on the viscosity of solutions of the unfunctionalized polymer and strongly reduces the viscosity of the polymer with 0.4% stickers. The magnitude of solvent effects, however, was somewhat unexpected. For example, the change from DD to CDD results in larger changes in viscosity than the change from CDD to tetrachloroethane (TCE). To further place the magnitude of these effects in perspective, note that for 510kPB0.3A polymer the reduction of solution viscosity resulting from changing from DD to CDD is comparable to the reduction of viscosity produced by a 6-fold decrease of sticker content holding solvent fixed (from 510kPB1.8A to 510kPB0.3A in CDD solvent at both 8 ºC and 20 ºC). Evidently, small changes in polarity for non-polar solvents can be more important than major changes in molecular structure.

Based on existing reports of shear thickening in associative polymers,[14, 15] we examined the shear rate dependence of the viscosity. Monotonic shear thinning was observed in all but a very few cases, two of which are shown in Figure 2.7. Thickening was the exception, not the rule, and when it was found, its magnitude was not significant (rising only 20% above the zero-shear viscosity before the onset of shear-thinning). The effect was very weak compared to that described in the prior literature (see Section 2.4.1).

2.3.4 Effects of Stickers on Hydrodynamic Size

The observed viscosities indicate that coils adopt more compact configurations as stickers are added (e.g., $r_{\eta,sp}$ = 0.74 for 1250kPB0.6A polymer near the overlap concentration of the prepolymer in Jet-A; refer to Table 2.3). We wished to determine whether dynamic

light scattering measurements could be performed under sufficiently dilute solutions to accurately measure the hydrodynamic radius R_h of single, isolated chains. We found that measurement sensitivity unfortunately limited the concentration range to ≥ 0.05 wt % (~ $c^*/5$ based on unmodified 1250kPB in Jet-A). This was not sufficiently dilute to reach the single-chain limit: as shown in Table 2.4, a significant concentration dependence remains, indicating that inter-chain hydrogen-bonding contributes (making the apparent hydrodynamic size greater than that of a single chain).

2.3.5 Modeling of Chain Collapse at Infinite Dilution in θ-Solvent

Confronted by experimental limitations that precluded direct observation of the effects of intramolecular associations on individual chain dimensions, we developed a model of single-chain statistics at infinite dilution in θ-solvent. Consider a polymer chain containing N monomers and f stickers separated by $l = N/(f-1)$ monomers (meaning there are stickers at each chain end), with pairwise association of the stickers of energy εkT. Time-average properties of such a chain were calculated by tracking the evolution of the chain through a large number of bond-forming and bond-breaking events. This stochastic process corresponds to a semi-Markov chain,[16] such that a state of the process (corresponding to a state of the polymer chain) is fully specified by identifying which pairs of stickers form bonds, and the chain transitions from one state to the next by either breaking a bond or forming a new bond. Let the stickers be indexed from 1 to f (refer to Figure A.1 of Appendix A); let $\vec{R}_n - \vec{R}_m$ be the position of sticker m relative to sticker n; and let $L_{n,m}$ refer to the number of monomers in the shortest connected path between stickers n and m. Because the strand corresponding to the shortest path between stickers is unrestricted by associations and has Gaussian statistics in θ-solvent, the dimensionless root-mean-square end-to-end (1-to-f) distance for any given state is:

$$\sqrt{\left\langle R^2/b^2 \right\rangle} = L_{1,f}{}^{1/2} \tag{2.3}$$

where b is the monomer Kuhn length. The dimensionless radius of gyration of the chain in any specific state is:

$$\sqrt{\left\langle \frac{R_g^2}{b^2} \right\rangle} = \frac{1}{f \cdot b}\left(\sum_{n=1}^{f}\sum_{m=n}^{f} \left\langle \left(\vec{R}_n - \vec{R}_m \right)^2 \right\rangle \right)^{1/2} = \frac{1}{f}\left(\sum_{n=1}^{f}\sum_{m=n}^{f} L_{n,m} \right)^{1/2}. \tag{2.4}$$

Averaging over a large number of successive states and accounting for the time spent in each state yields the time-average properties, such as the average size of the chain. A full description of the model is given in Appendix A.

Computer simulations according to the above model allowed us to quantify the effects of bond strength (Figure 2.8), degree of functionalization (Figure 2.9), and chain length (Figure 2.10) on chain configuration. In addition to overall measures of coil size (chain end-to-end distance and radius of gyration), we examined the fraction of stickers that are paired (*fps*) and the average number of backbone units between paired stickers (*adps*), i.e., the distance between them along the chain in its stretched, unassociated state (Figure A.1). Model predictions show that intrachain associations reduce both the end-to-end distance and the radius of gyration (Figure 2.8-2.10), with the end-to-end distance decreasing more strongly. The reduction in coil dimensions with increasing strength of association arises from two effects: an increase in the fraction of stickers that are paired, and an increase in the fraction of "bonds" that occur between stickers that are widely separated along the backbone (Figure 2.8). Interestingly, the decrease of chain size with increasing extent of functionalization corresponds to remarkably straight lines on a log-normal plot (Figure 2.9). Finally, the increase in chain size upon increasing N at fixed l and ε does not follow a power-law (Figure 2.10), meaning that the chains do not behave as fractals.

2.3.6 Elasticity and Mist Suppression

2.3.6.1 Drop Impact Experiments

The effect of self-associating stickers on solution elasticity and drop breakup in very dilute solutions is manifested in drop impact experiments (Figure 2.11). Results for a reference solution of 4200 kg/mol PIB polymer show the famous effect of polymer elasticity in extensional deformation: at 180 ppm in Jet-A, these chains promote the formation of fluid filaments which completely suppress the ejection of satellite droplets (Figure 2.11a), in sharp contrast with the rapid fragmentation of ejected fluid in the absence of polymer (Figure 2.1b). Results for 1250kPB prepolymer at the same concentration (Figure 2.11b) reveal the pronounced effect of chain length on polymer elasticity: in contrast to the 4200 kg/mol PIB solution, there is more splashing of fluid initially upon impact, followed by rapid breakup of the ejected fluid. Nevertheless, the 1250kPB chains display sufficient elasticity to visibly hinder the necking and pinching processes involved in the breakup of individual droplets:

filaments that form between beads of fluid survive for ~ 2 ms (Figure 2.11b). The ability of 1250kPB to hinder drop breakup is reduced by incorporation of carboxylic side-groups at random positions along the chains, evidenced by a decrease in the lifetimes of fluid filaments for 1250kPB0.3A and 1250kPB0.6A solutions to 1.5 and 1 ms, respectively.

Suppression of breakup was enhanced significantly by increasing the polymer concentration (Figure 2.12): at 450 ppm, the lifetimes of fluid filaments were 2.5, 2.5, and 2 ms for solutions of 1250kPB, 1250kPB0.3A, and 1250kPB0.6A, respectively. This corresponds to a steeper increase with concentration of breakup suppression for the acid-functionalized chains than for the prepolymer. That observation begs for comparison of solution elasticity and extensional viscosity at higher concentrations. Because complete suppression of fluid breakup occurred for all 1250kPB solutions at polymer concentrations $\geq c^* = 2500$ ppm, characterization of fluid breakup at the overlap concentration and in the semi-dilute regime was conducted via spray experiments and capillary breakup experiments.

2.3.6.2 Spray and CaBER Experiments

Spray experiments for 1250kPB polymer at the overlap concentration of 2500 ppm by wt in Jet-A reveal that 0.2–0.6 mol % of carboxylic acid stickers do not shift droplet size to higher values during atomization of the fuel (Figure 2.13). This simple qualitative experiment successfully detects mist suppression by 4200 kg/mol PIB (Figure 2.2), showing a pronounced increase in drop size as concentration is increased even from 50 ppm to 200 ppm. By comparison, the drop size is remarkably insensitive to the addition of stickers to 1250kPB. In terms of mist suppression, what slight effects stickers have are unfavorable: the size of droplets appears to decrease as functionalization increases from 0 to 0.3 mol %, and only recovers to be similar to that for the unmodified polymer as functionalization is increased further to the 0.6 mol % solubility limit.

To place the above qualitative effects on a more rigorous foundation, quantitative measurements of extensional viscosity and relaxation time were attempted using capillary breakup rheology. Unfortunately, solution elasticity was too low to be measured for 1250 kg/mol 1,4-PB chains at concentrations below 1.5 wt % in Jet-A solvent (corresponding to $c = 6c^*$). CaBER results for solutions of 1250kPB0.3A and 1250kPB0.6A polymers show that, at 1.5 wt % polymer in Jet-A, associations caused 60–200% increases in the breakup

time of filaments, the solution's relaxation time, and the solution's apparent extensional viscosity (Figures 2.14 and 2.15). This amounts to considerably smaller effects of stickers on extensional viscosity than reported behavior for similar systems (Section 2.4.1, Figure 2.16c): relative to shear viscosity, the increases in relaxation time compared to the prepolymer solution were only 50% for 1250kPB0.3A and 60% for 1250kPB0.6A.

2.4 Discussion

The object of the present study is to obtain a fundamental understanding of the behavior of self-associating polymers through the study of homologous series of narrow-dispersed chains of controlled molecular properties. The effects of carboxylic-acid side-groups (pairwise "stickers") on rheological behavior were investigated as a function of number density of side-groups, polymer concentration, chain length, and solvent polarity.

2.4.1 Low-Concentration Solutions (Dilute and Unentangled Semidilute)

In contrast to the extensive literature on polymers that associate in solution through many-body interactions (such as ionic interactions in low polarity solvents or hydrophobic interactions in aqueous media), the literature on pairwise associating stickers is sparse, particularly in relation to the low concentration regime pertinent to fuel additives. Indeed, there are only two bodies of work that we have found focusing on dilute and semidilute solutions of polymer bearing pairwise, self-associating stickers: studies of ICI's FM-9 polymer[2, 3] and studies of Exxon's polyoctene copolymers[14, 15, 17] (Figure 1.4). Our experiments confirmed the reduction in shear viscosity (Figure 2.5) reported for dilute solutions ($c < c^*$ in Figure 2.16a). We found that the reduction of shear viscosity was accompanied by a reduction in the apparent extentional viscosity, as seen in drop breakup experiments (Figures 2.11 and 2.12). These behaviors are a consequence of the previously recognized phenomenon[14, 17] of chain collapse driven by intramolecular associations in dilute solutions. Computations confirm that for chains of ~ 10^4 Kuhn monomers, containing ~1 mol % side-groups that associate pairwise with energy ~ 10 kT (closely matching our 1250kPB0.6A polymer in DD), chain collapse is severe (Figure 2.10).

A number of salient rheological characteristics attributed to pairwise stickers in the prior literature are conspicuously absent in the present systems. Expected features include an extremely nonlinear increase in viscosity in the semidilute unentangled regime, pronounced

shear thickening, and strongly enhanced extensional viscosity (Figure 2.16). Plausible explanations for the discrepancies include the substantially higher MW or acid content of the molecules tested in earlier studies: the polyoctene copolymers prepared by Schulz[15, 17] had $M_n \sim 2\text{-}5 \times 10^6$ g/mol, so M_w up to $10\text{–}20 \times 10^6$ g/mol;[18] on the other hand the carboxylic acid content of FM-9 was 5–7 wt % methacrylic acid, according to the preferred composition divulged in the patent literature.[1] Different solvent-polymer and solvent-sticker interactions in the respective systems investigated are likely to contribute substantially to discrepancies among studies. Our data show that small changes in solvent polarity dramatically alter the phase behavior of non-polar polymers bearing polar stickers. Given the importance of solvent effects and the prevalence of phase separation that we observed, it is striking that the previous studies[2, 3, 14, 15, 17] do not provide solubility data. In view of the present results, we deduce that the high degree of functionalization in FM-9 would drive phase separation of the solutions; indeed, the patent literature describes the solutions as "hazy" and "opalescent."[1] As a result of the limited amount of experimental detail in the prior literature, it is impossible to determine which rheological features pertain to microscopically homogenous solutions, and which correspond to phase-separated mixtures.

Our results for solutions of concentration $\geq c^*$ uncover physical phenomena overlooked in the prior literature. We observed that at c^*, adding stickers produces measurable *reductions* in shear viscosity (Table 2.3, Figure 2.5) and in polymer-induced mist suppression in spray tests (indicative of a reduction in extensional viscosity; Figure 2.13). For $c >> c^*$ we observed that the effects of stickers on both shear and apparent extensional viscosity (Figure 2.5, Figure 2.15) were remarkably weak in comparison to those shown in Figure 2.16. These results reveal that the effects of chain collapse due to intrachain pairing are important beyond the dilute regime. This physical insight was lacking in the prior literature, according to which intermolecular interactions are believed to dominate solution behavior above c^*. The implications for mist control of aviation fuel are that self-associating polymers of acceptable solubility in the fuel are not superior to non-associating polymers even at concentrations several times above overlap.

2.4.2 Entangled Solutions

The viscosity versus concentration results we obtained for entangled solutions of 510 kg/mol PB chains (Figure 2.5) were in good agreement with the only experimental body of

work reporting on the dynamics of solutions of pairwise associating polymer:[19] Stadler and de Lucca Freitas modified anionically synthesized PB with hydrogen-bonding 1,2,4-triazolidine-3,5-dione side-groups, and reported a $\eta \sim \phi^6$ concentration dependence of zero-shear viscosity for squalene solutions of 1% modified chains of 2×10^5 g/mol, over nearly one decade in concentration corresponding to $0.1 < \phi < 1$. Note that this concentration dependence is identical to that which we observed for 510kPB1.8A polymer at volume fractions $\phi > 0.08$ in CDD (Figure 2.5). Given the $\eta \sim \phi^{5.3}$ relationship measured for unfunctionalized 510kPB prepolymer, this observed increase in the exponent of the concentration dependence of viscosity due to stickers seems very moderate.

The measured effect of self-associating, pair-wise polymer interactions on solution viscosity is much weaker than anticipated based on theoretical literature models of such systems. For example, Rubinstein and Semenov[11-13] predicted scaling exponents up to 8.5 in a concentration regime corresponding to a transition from predominantly intramolecular to predominantly intermolecular interactions (Figure 2.17, refer to footnotes[20] for a brief description of the model). For 510 kg/mol PB chains with carboxylic acid content up to 1.8 mol %, the observed shape of the viscosity vs. concentration curves was strikingly similar to that of the unmodified polymer, by comparison with model predictions (compare Figures 2.5 and 2.17).

Why the differences? First, it is difficult to meet Rubinstein and Semenov's model assumptions for homogenous solutions, particularly in term of the strength of associations for pairwise stickers. Second, the theory seems to give inadequate consideration to the effect of intramolecular interactions on the chain statistics. We discuss these two aspects in turn.

Satisfying Model Assumptions. We have already mentioned the apparent void in the literature dealing with solutions of linear polymers associating via binary interactions. In fact, for lack of a better choice, Rubinstein and Semenov[12] compared predictions of their model with experimental results of polymer systems interacting through many-body (rather than pairwise) association of hydrophobic groups in aqueous solutions. Given the binary nature of carboxylic acid associations, and equipped with the molecular control to vary bond strength, extent of functionalization, or chain length while holding other parameters constant, we felt that our materials were particularly well-suited for the testing of Rubinstein and Semenov's model predictions.

However, in spite of our best efforts in selecting the nature of the associations, the structure of the backbone, and the set of solvents, we unfortunately cannot be certain that our system is truly an experimental realization of their model. Regarding model assumptions concerning solvent quality and strengths of interactions, two key assumptions[12] underpin the concentration dependence of the viscosity of entangled reversible networks shown in Figure 2.17: the solvent is good (monomer excluded volume parameter v on the order of b^3), and associations are strong (such that $e^{\varepsilon} > l^{2.225}$). Our best estimate of the association energy for dimerization of carboxylic acids in CDD[21] corresponds to $\varepsilon \approx 8$–10. Assuming a Kuhn monomer of molar mass ~ 100 g/mol, the distances between stickers are $l \sim 180$, 55, and 30 Kuhn monomers for 0.3%, 1%, and 1.8% functionalized chains, so that the assumption of strong association is expected to hold for 510kPB1.0A and 510kPB1.8A, but is questionable for 510kPB0.3A. Further, our best estimate of the solvent quality for 510kPB chains in CDD[22] corresponds to $v/b^3 \sim 0.2$ or $\chi \sim 0.4$ (this number compares favorably with measured χ values for PB in shorter chloroalkanes reported by Alessi et al.).[9] Because Rubinstein and Semenov's theoretical treatment is limited to a description of scaling behavior without knowledge of the prefactors, it is difficult to assert from the above estimates of v/b^3 and ε that our system fully satisfies the model requirements of "good solvent" and "strong interactions."

In practice, the "good solvent" and "strong associations" assumptions defined above tend to be largely incompatible. Hydrogen-bonding systems model binary associations; however, their strengths of interaction are greatest in very non-polar solvents such as *n*-alkanes, which are marginal solvents for all common polymers. On the other hand, efforts to satisfy the assumption of good solvent by using, for instance, chlorinated hydrocarbons or aromatic solvents, compromise the strengths of hydrogen bond interactions. The relationship between the "good solvent" and "strong associations" criteria is further complicated by solvent-sticker interactions: Quantitative pairing of the stickers in a system requires low values of l and high values of ε, meaning high levels of functionalization with stickers exhibiting very favorable sticker-sticker interactions and, unfortunately, unfavorable sticker-solvent interactions. In this case, phase separation of the functional chains driven by adverse solvent-side group interactions is likely to occur regardless of solvent quality for the polymer backbone itself. These solvent-side group interactions which significantly impact the solubility and phase

behavior of functionalized chains were not accounted for in Rubinstein and Semenov's model.

Role of Intrachain Associations. The effect of chain collapse even above c^*, unnoticed in previous experimental work (Section 2.4.1), was also overlooked in theoretical descriptions of self-associating polymer systems. Specifically, Rubinstein and Semenov's theory fails to account for the effects of intramolecular bonds on the chains statistics. Intrachain associations are physical cross-links that cause polymer molecules to collapse onto themselves, even at concentrations >> c^*, so that expressions for segment sizes and relaxation times that are applicable to linear chains without stickers no longer hold for self-associating polymer molecules. As a result, corrections must be made to expressions of chain size R, correlation length ξ, number of monomers per correlation blob g, Zimm time of correlation blobs, tube length $a(\phi)$, etc.; Rubinstein and Semenov did not make such corrections. Calculations of chains collapse (Figures 2.8–2.10) confirm the intuitive expectation that the changes in polymer configuration due to same-chain associations are substantial, especially for long chains and strong associations.

2.5 Conclusion

The results of this study challenge the pre-existing understanding of the rheology of self-associating polymers (Figures 2.16 and 2.17), and suggest that previously accepted assertions regarding the effects of pairwise stickers on the rheology of polymer solutions deserve re-evaluation. Properly controlled studies (using functionalized and unmodified polymer homologues of matched, well-defined length) that include light scattering and rheological characterization can provide definitive tests of prior beliefs.

For 510 kg/mol and 1250 kg/mol PB chains of low polydispersity, we find that incorporation of carboxylic acid side-groups results in a strong tendency for phase separation, and observe that for homogeneous solutions, enhancements in shear and extentional viscosity due to stickers are relatively small even at polymer concentrations >> c^*, in contrast with prior expectations. Our results reveal that the effects of chain collapse due to intrachain pairing are important beyond the dilute regime—behavior unaccounted for in earlier experimental and theoretical studies. The implications for mist control of aviation fuel are that self-associating polymers of acceptable solubility in the fuel are not superior to non-associating polymers even at concentrations several times above overlap. Therefore,

alternative strategies to improve antimisting based on polymer associations in dilute solutions are needed. In the next chapter, we consider randomly functionalized linear chains bearing complementary stickers (Figure 1.7.2).

2.6 Figures, Schemes, and Tables

(a)

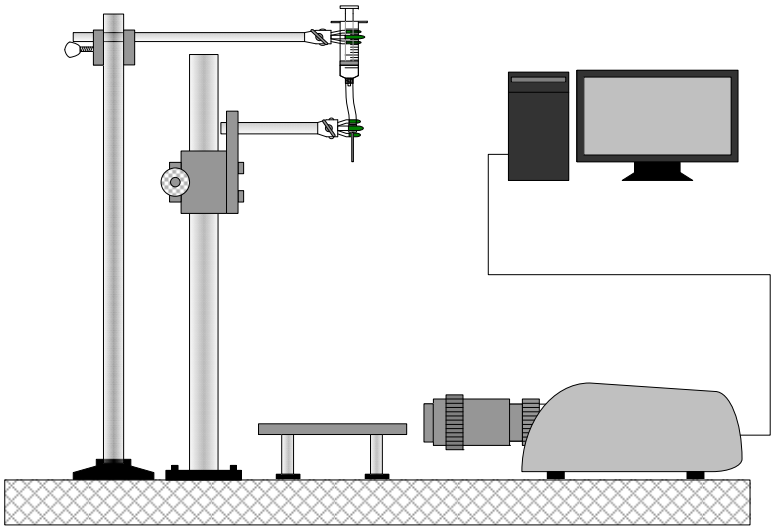

(b) Jet A solvent, 0.25 ms intervals, 15 μm/pixel resolution

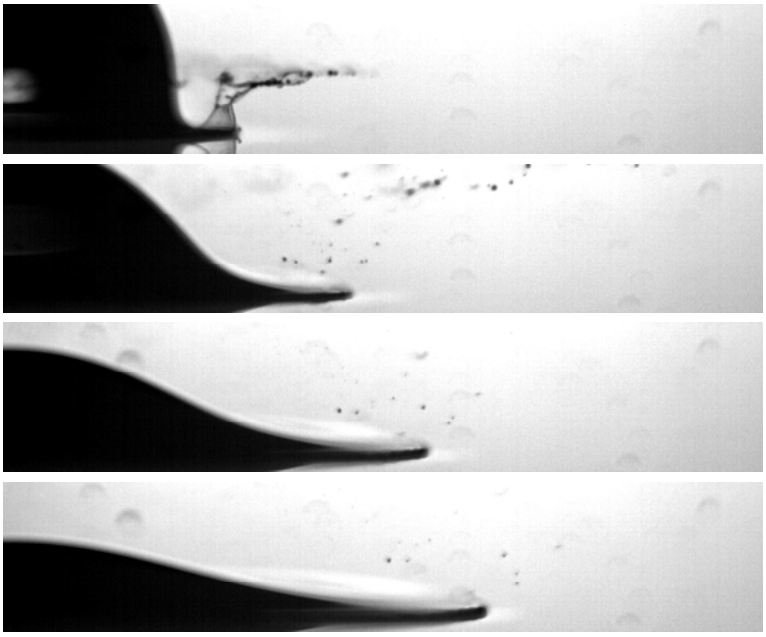

Figure 2.1 Experimental apparatus for the characterization of drop splashing, spreading, and breakup (a), and results for Jet-A solvent (b). Notice that the ejected fluid breaks up so quickly that only a small number of individual droplets can be resolved after 0.5 ms.

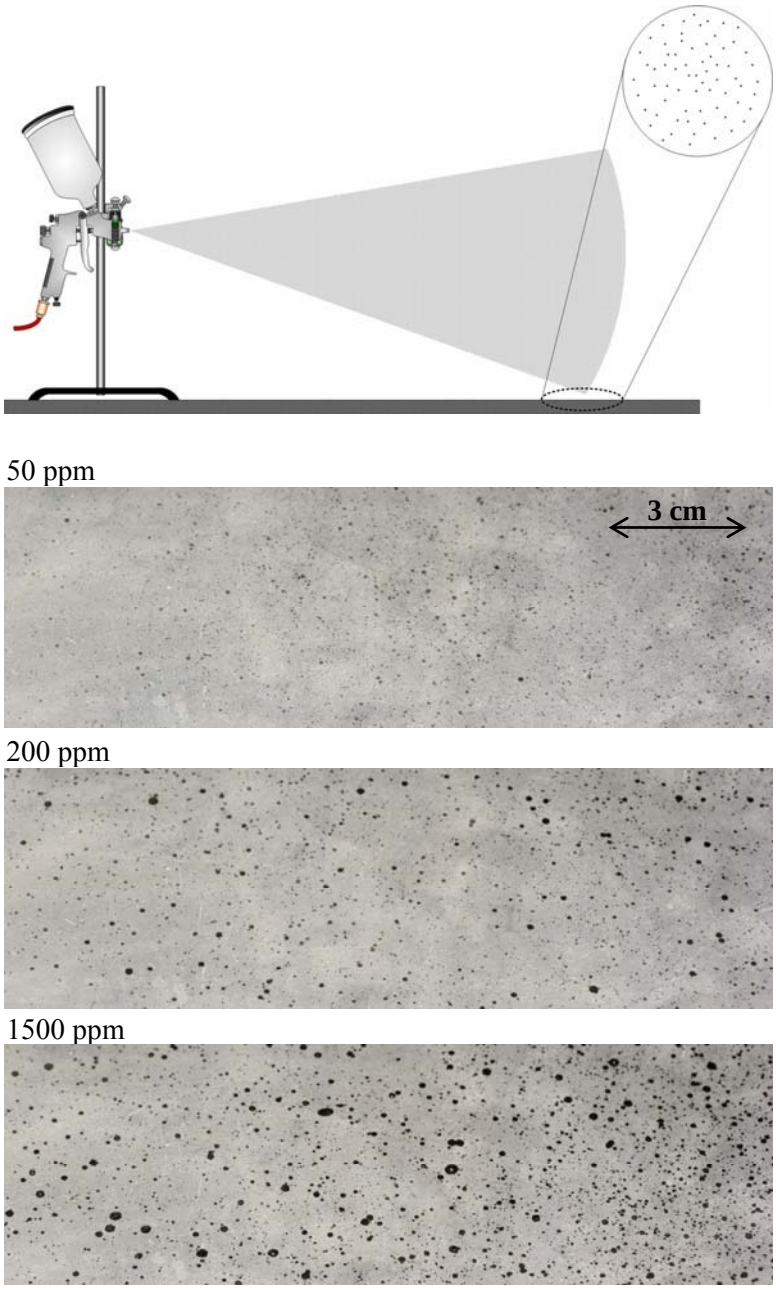

Figure 2.2 Experimental apparatus for the characterization of fuel atomization during spraying (top), and spray patterns for reference solutions of 4200 kg/mol polyisobutylene polymer at increasing weight fraction in Jet-A (bottom three photographs). Pure Jet-A is atomized so finely that there is no observable spray pattern: the fine mist is entrained by the upward air flow of the fume hood and does not settle onto the surface.

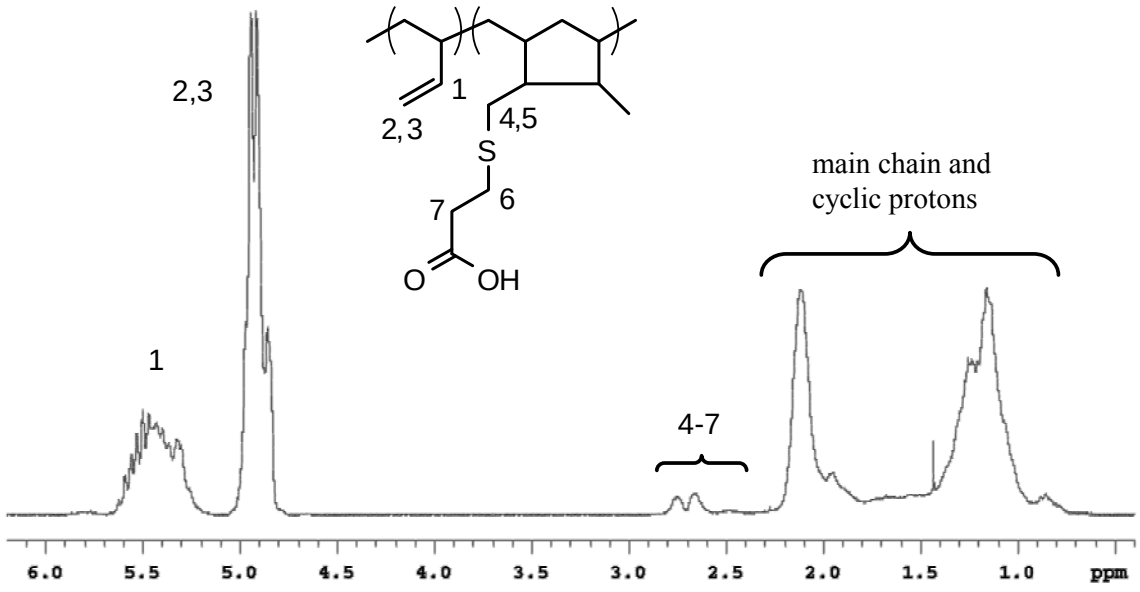

Figure 2.3 Representative ^{1}H NMR spectrum of acid-functionalized polybutadiene polymer (510kPB1.8A, refer to Table 2.1). Note that protons 4 and 5 are not equivalent.

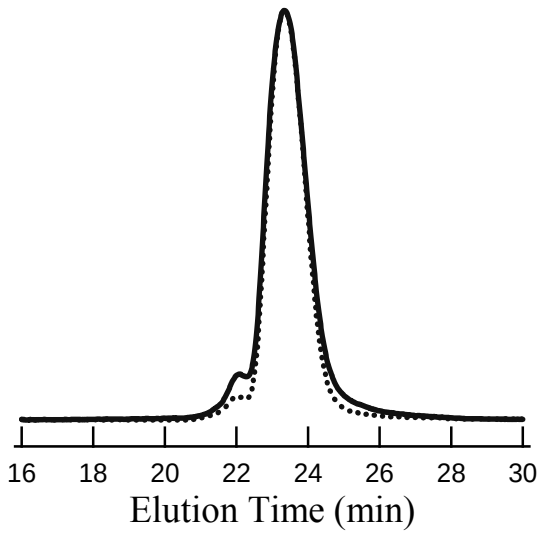

Figure 2.4 Representative gel permeation chromatography trace of acid-functionalized polybutadiene polymer. The solid line corresponds to 1250kPB0.2A (after 10 months of storage; refer to Table 2.1); the dashed line is 1250kPB prepolymer.

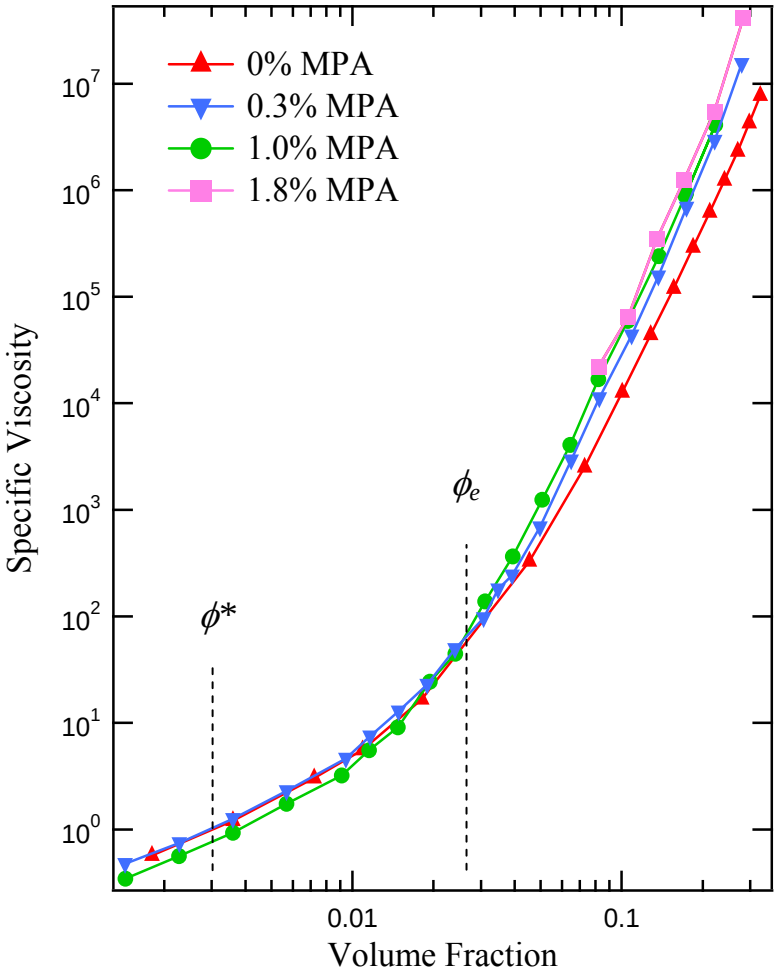

Figure 2.5 Zero-shear specific viscosity ($\eta_{sp} \equiv \eta_{solution}/\eta_{solvent} - 1$, where $\eta_{solvent}$ = 2.72 mPa.s) of 510 kg/mol 1,2-polybutadiene chains in chlorododecane at 20 ºC, as a function of 3-mercaptopropionic acid (MPA) content. For 510kPB prepolymer, the overlap concentration corresponds to $\phi^* \cong 0.003$ according to the criterion $[\eta]\phi^* \cong 1$, and the entanglement concentration is $\phi_e \cong 0.026$ (determined as the intersection of the semi-dilute and entangled regimes, corresponding to $\eta_{sp} \sim \phi^{1.3}$ and $\eta_{sp} \sim \phi^{5.3}$ regimes, respectively). The overlap concentrations of the strands between stickers were determined using the expression[23] $\phi_s = \phi^*(MW_{chain}/MW_{strand})^{-0.76}$ to be ϕ_s = 0.04, 0.10, and 0.15 for polymer chains containing 0.3%, 1.0%, and 1.8% MPA side-groups, respectively.

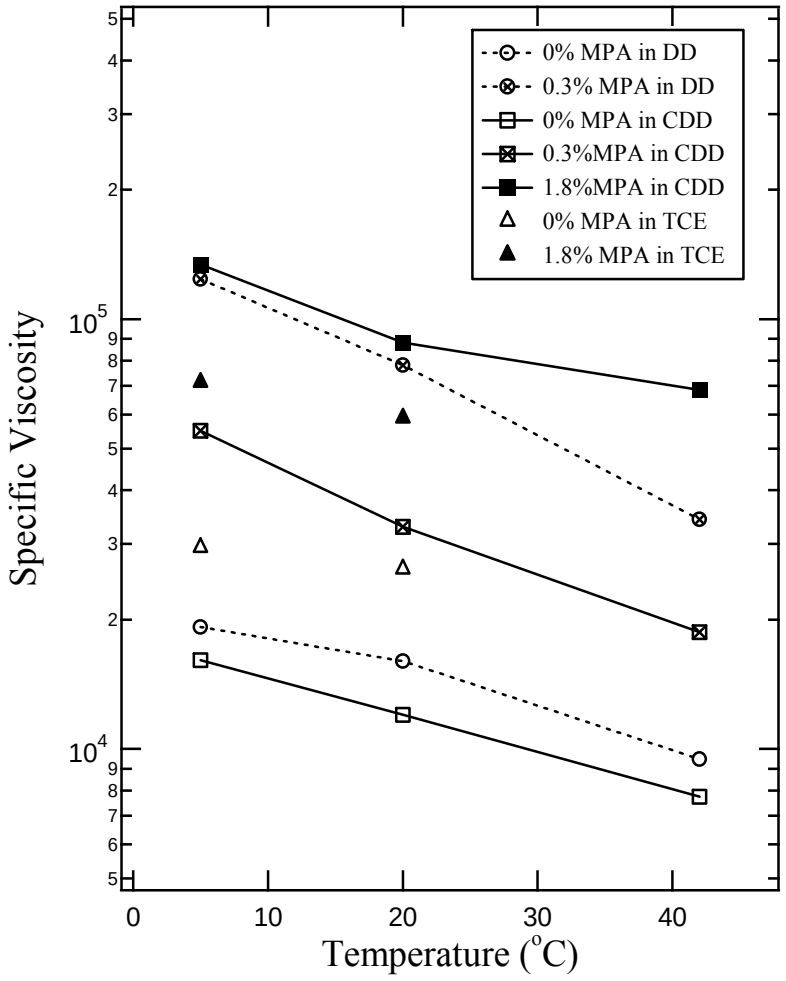

Figure 2.6 Temperature and solvent effects on specific viscosity ($\eta_{sp} \equiv \eta_{solution}/\eta_{solvent} - 1$) of 10 vol % solutions of 510 kg/mol 1,2-polybutadiene chains as a function of mercaptopropionic acid (MPA) content. Note that experiments in TCE were limited to temperatures ≤ 20 ºC due to solvent volatility, and that experiments with 1.8% stickers were not possible in DD due to phase separation.

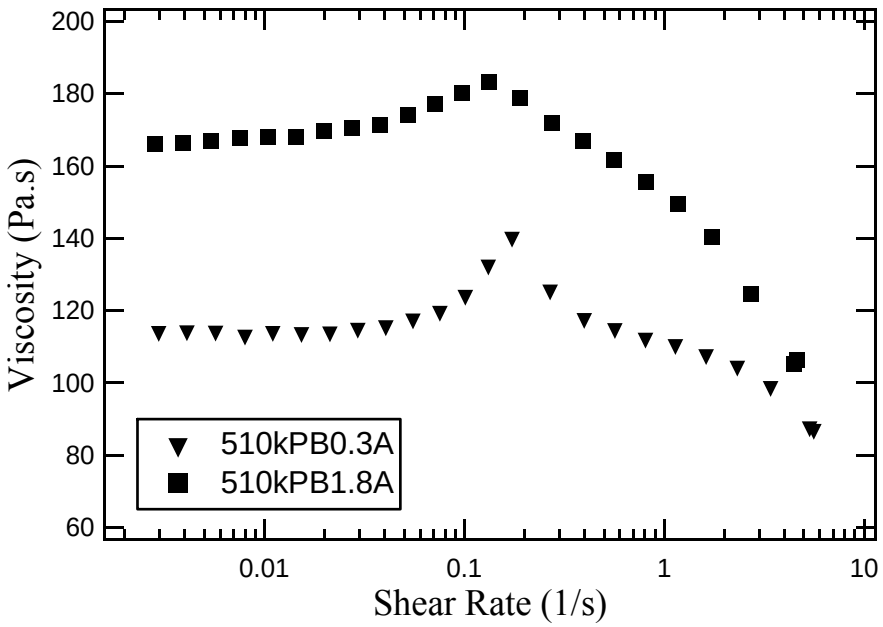

Figure 2.7 Shear viscosity as a function of shear rate for 10 vol % 510 kg/mol 1,2-polybutadiene solutions in tetrachloroethane at 20 ºC.

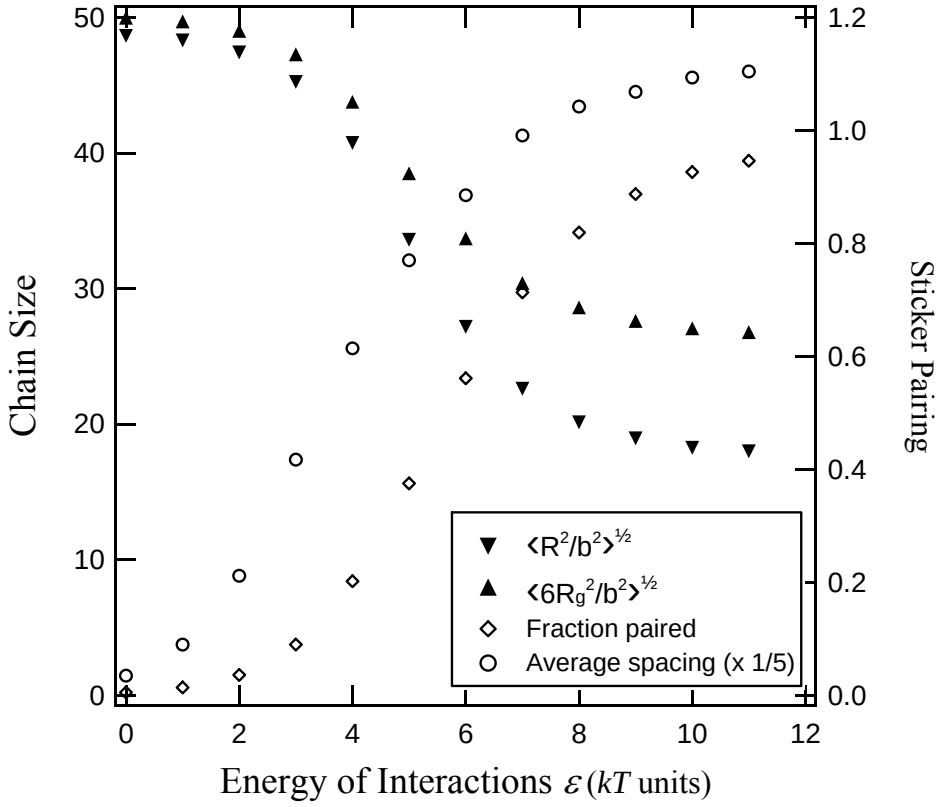

Figure 2.8 Simulation results of the end-to-end distance, radius of gyration, fraction of stickers paired (*fps*), and average spacing between paired stickers (*adps* = $\langle p\text{-}p' \rangle$, where p and p' are the indexes of stickers involved in pairs; refer to Figure A.1 of Appendix A), as a function of energy of interaction εkT for a chain with $f = 25$ stickers and $l = 100$ monomers between stickers. The bond volume was taken to be $V_b = b^3$, and the time-evolution of the chain was tracked over 2×10^5 bond-breaking or bond-forming events.

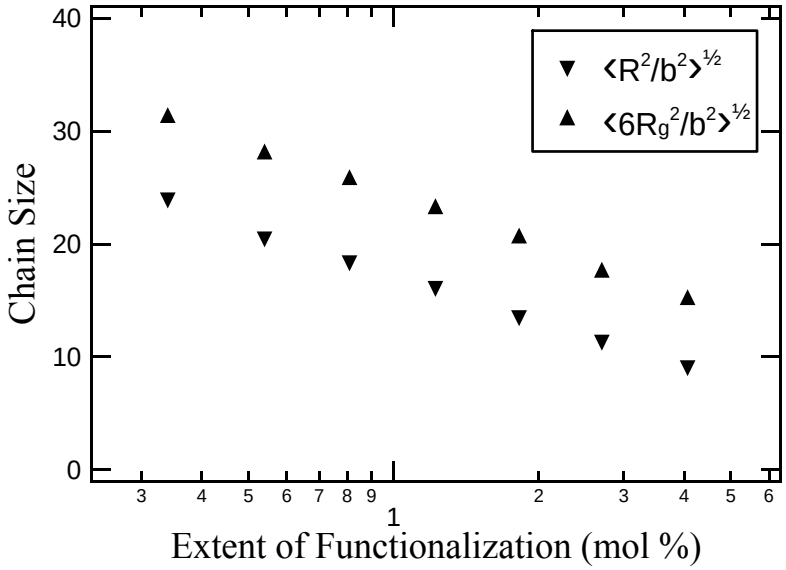

Figure 2.9 Simulation results of the end-to-end distance and radius of gyration as a function of the fraction of monomers bearing stickers (in mol %) for a chain with $N = 1500$ monomers at fixed energy of interaction $10kT$. The bond volume was taken to be $V_b = b^3$, and the time-evolution of the chain was tracked over 4×10^4 bond-breaking or bond-forming events.

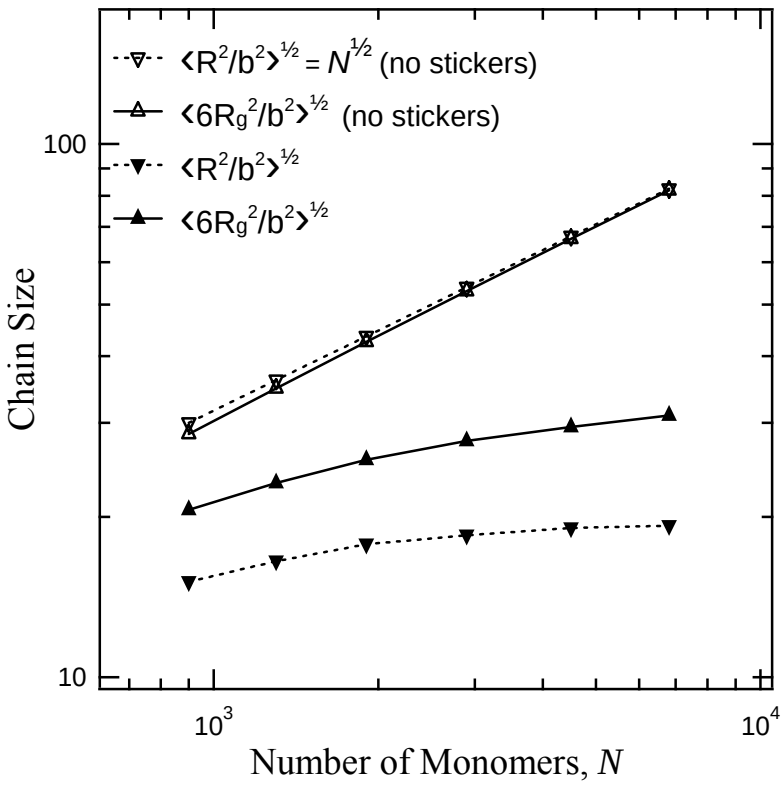

Figure 2.10 Simulation results of the end-to-end distance and radius of gyration as a function of chain length for a chain at fixed l = 100 and fixed energy of interaction 10kT (under these conditions the stickers spend the majority of their time in pairs). Open symbols correspond to chain size, calculated using Equations 2.3 and 2.4, for chains of matched length without stickers. The bond volume was taken to be $V_b = b^3$, and the time-evolution of the chain was tracked over 10^5 bond-breaking or bond-forming events.

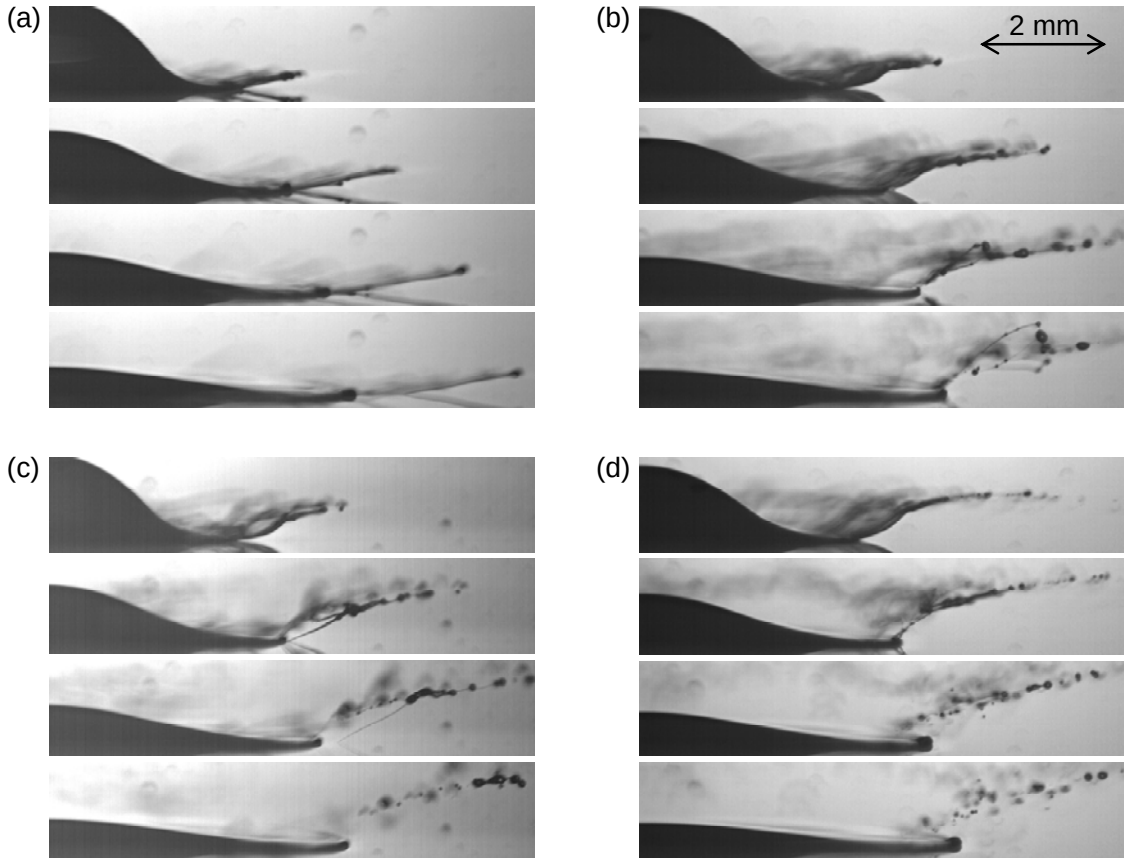

Figure 2.11 High-speed imaging of drop breakup of polymer solutions at 180 ppm by wt in Jet-A: (a) 4200 kg/mol linear, non-associating polyisobutylene chains; (b) 1250 kg/mol linear, unfunctionalized 1,4-polybutadiene chains; (c) 1250kPB0.3A chains; and (d) 1250kPB0.6A chains (refer to Table 2.1). For 4200kPIB, satellite droplets were never fully ejected; on the other hand all visible fluid filaments connecting "beads" of fluid together had broken 2 ms, 1.5 ms, and 1 ms after impact for solutions b, c, and d, respectively. The interval between frames is 0.25 ms in all cases.

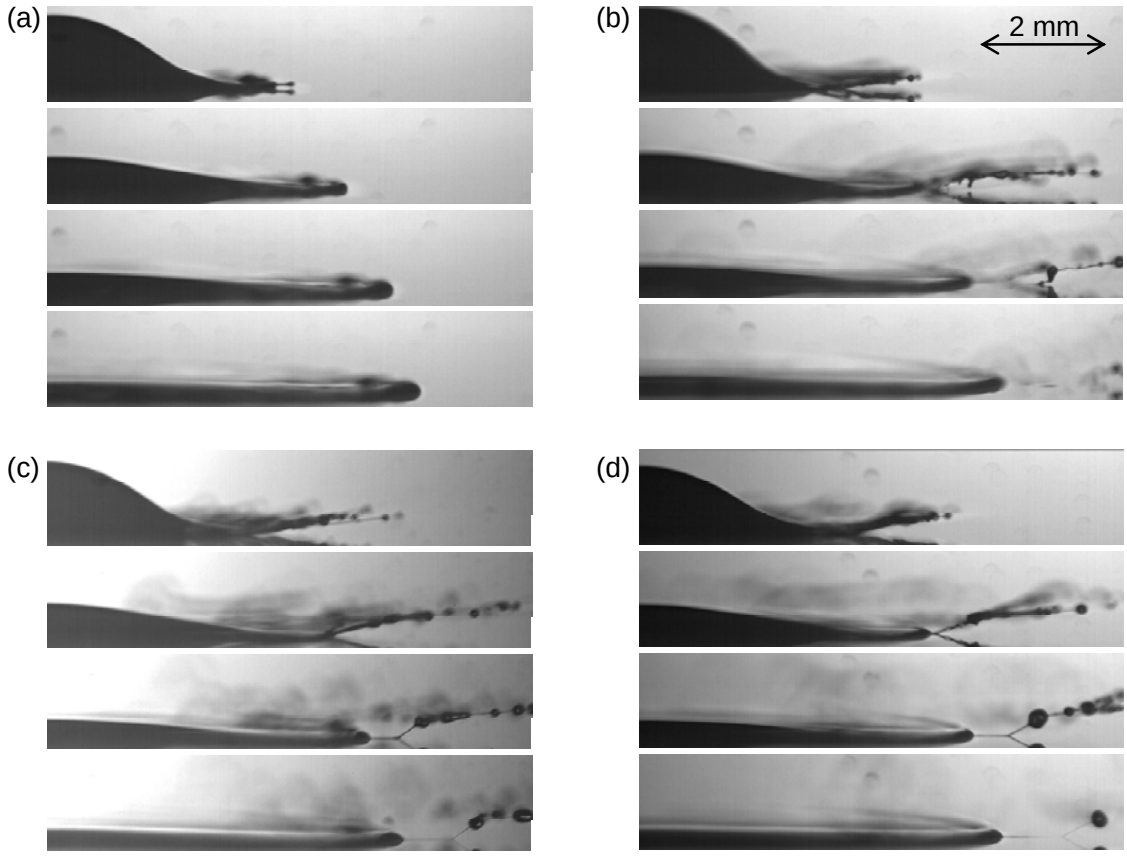

Figure 2.12 High-speed imaging of drop breakup of polymer solutions at 450 ppm by wt in Jet-A: (a) 4200 kg/mol linear, non-associating polyisobutylene chains; (b) 1250 kg/mol linear, unfunctionalized 1,4-polybutadiene chains; (c) 1250kPB0.3A chains; and (d) 1250kPB0.6A chains (refer to Table 2.1). For 4200kPIB, there is nearly complete suppression of breakup, without formation of satellite droplets; on the other hand all visible fluid filaments connecting "beads" of fluid together had broken 2.5 ms, 1.25 ms, and 0.75 ms after impact for solutions b, c, and d, respectively. The interval between frames is 0.5 ms in all cases.

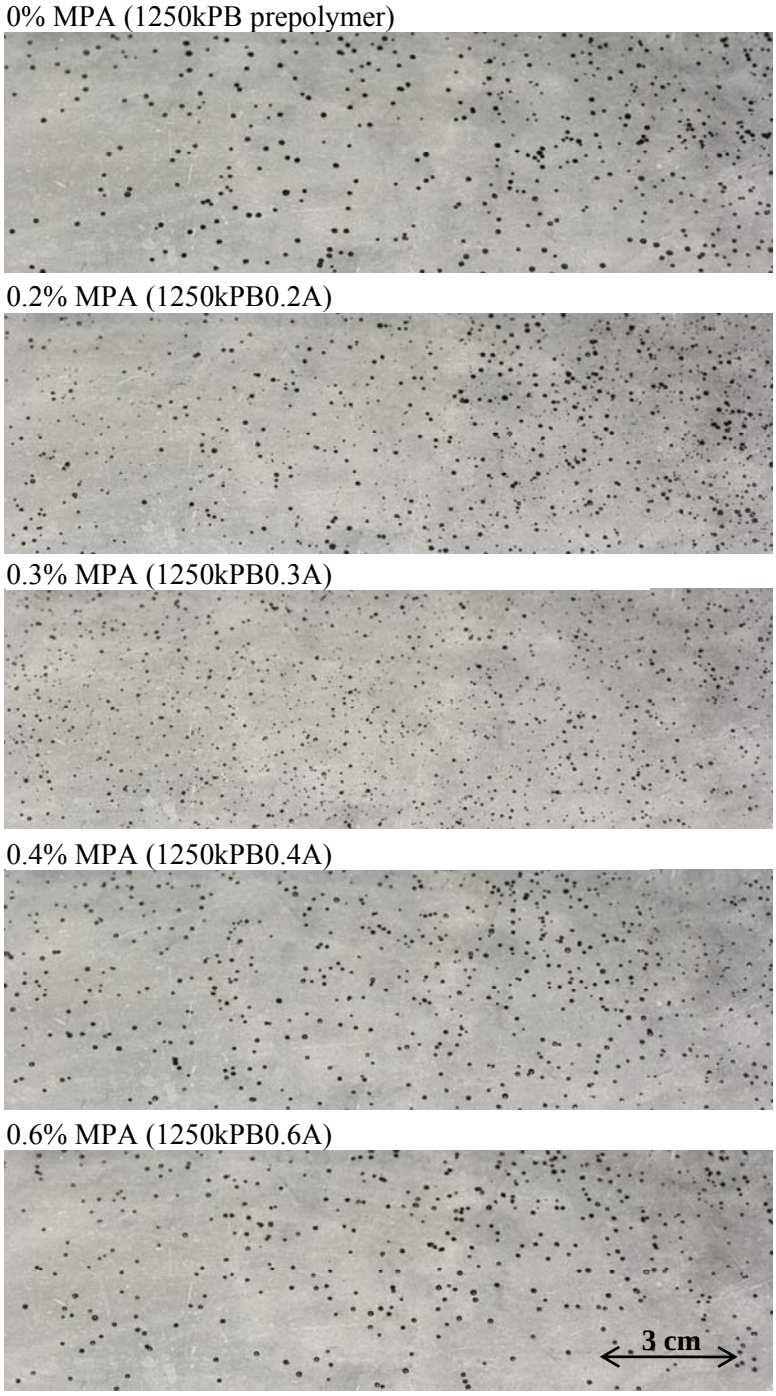

Figure 2.13 Spray patterns of solutions of 1250 kg/mol 1,4-polybutadiene chains (refer to Table 2.1) at 2500 ppm by wt in Jet-A as a function of increasing mercaptopropionic acid content.

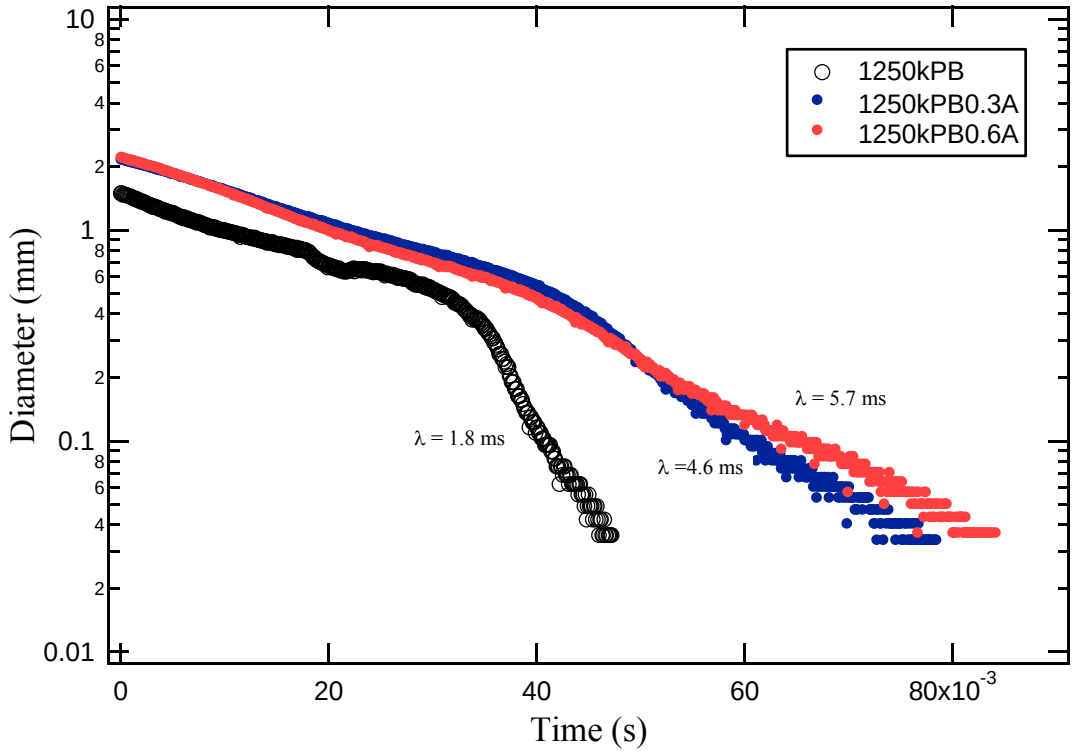

Figure 2.14 Time evolution of filament diameter during capillary breakup experiments for 1250kPB, 1250kPB0.3A, and 1250kPB0.6A polymers at 1.5 wt % total polymer content in Jet-A (corresponding to $c = 6c^*$ for 1250kPB prepolymer). All tests were performed with 8 mm diameter plates, at initial and final aspect ratios of 1.0 and 2.5, respectively. Solution shear viscosities were 48 mPa.s, 83 mPa.s, and 95 mPa.s for the 1250kPB, 1250kPB0.3A, and 1250kPB0.6A solutions, respectively. The characteristic relaxation times of the solutions, determined from the slope of the exponential decay of the filament diameter vs. time, are represented on the figure.

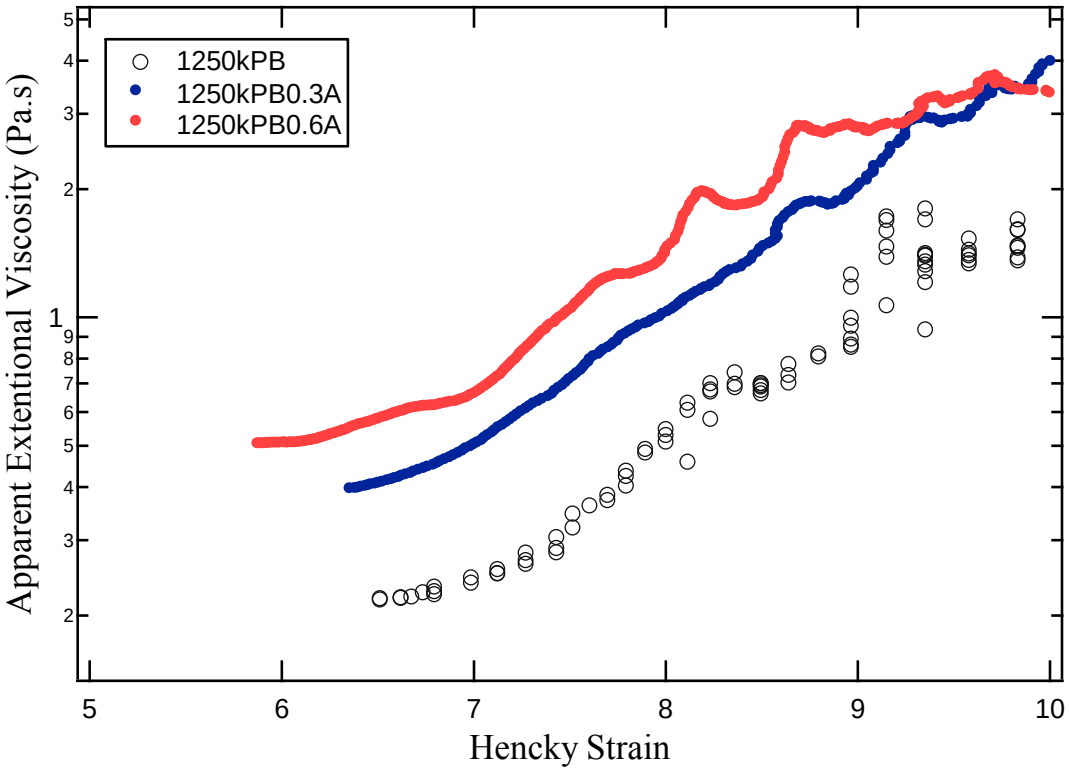

Figure 2.15 Effect of pairwise, self-associations on apparent extentional viscosity during capillary breakup rheology (refer to Figure 2.14 for experimental details).

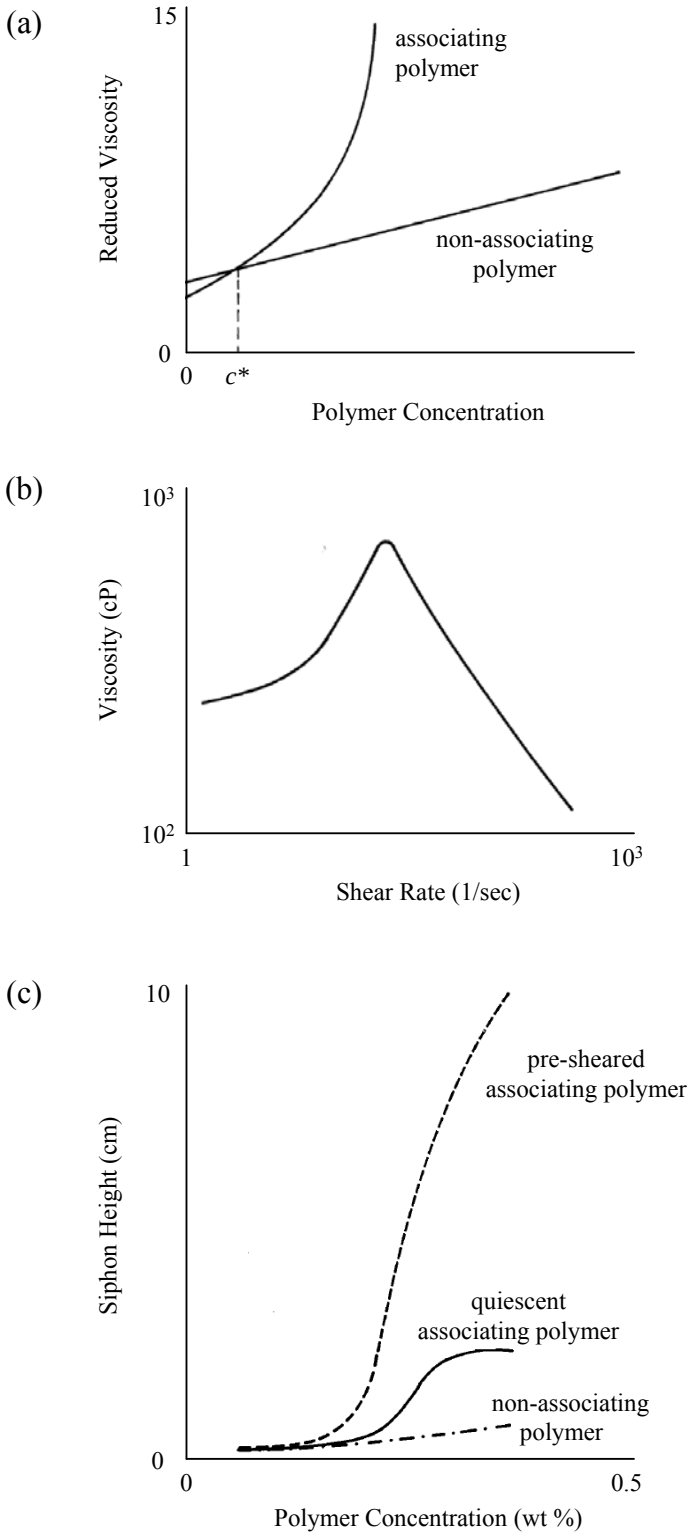

Figure 2.16 Prior understanding of the physical properties of solutions of self-associating polymer of low concentrations, according to Schulz et al.[14] Siphon height is a measure of extensional viscosity.[24] (Reproduced with permission.)

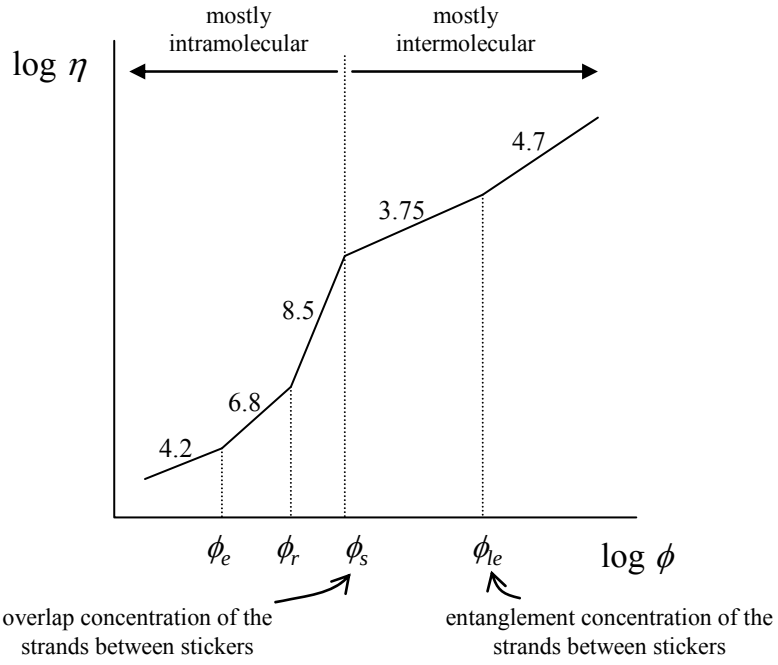

Figure 2.17 Predictions of Rubinstein and Semenov's model[12] for the concentration dependence of the viscosity of entangled reversible networks in good solvent. (Reproduced with permission. Refer to footnotes[20] for identification of the crossover concentrations). The numbers above each line segment indicate the predicted scaling exponent.

Scheme 2.1 Synthesis of Acid-Functionalized Derivatives of Polybutadiene Polymers Containing 98% 1,2 Adducts (a) and 8% 1,2 Adducts (b)

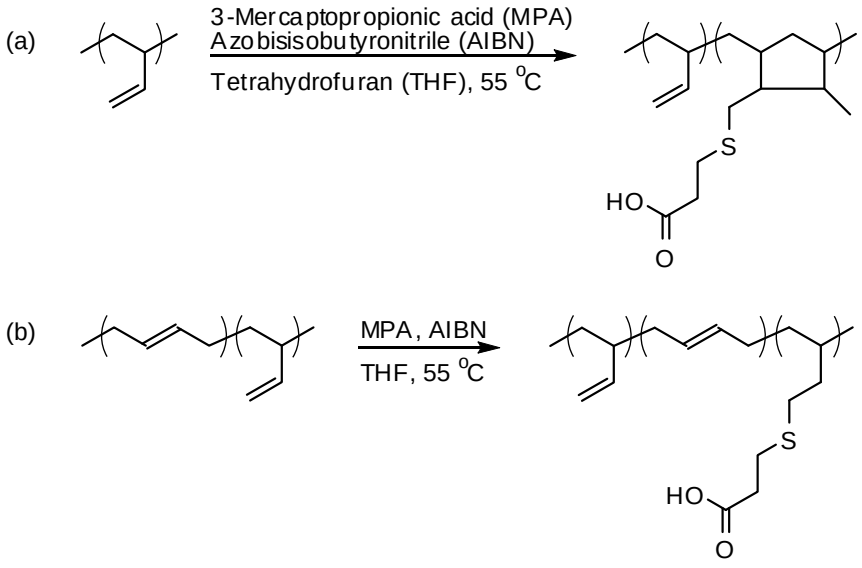

Table 2.1 Reaction Conditions and Results for Polybutadiene Functionalization with 3-Mercaptopropionic Acid

Entry[a]	[PB] (g/mL)	[MPA][b]	[AIBN] (mg/mL)	Rxn time (hrs)	Funct.[c] %	PDI[d]	rxn rate[e] ($mL^{3/2}/mol^{3/2}$ s)
510kPB0.2A	0.016	0.023	0.52	1.2	0.2	1.24	37
510kPB0.3A	0.016	0.021	0.52	2.5	0.3	1.20	30
510kPB1.0A	0.020	0.040	0.65	1.7	1.0	1.23	55
510kPB1.8A[f]	0.018	0.064	0.57	1.8	1.8	1.28	73
510kPB4.7A	0.017	0.13	0.52	1.5	4.7	1.23	130
510kPB7.1A	0.014	0.16	0.49	1.6	7.1	1.28	170
1250kPB0.2A[g]	0.010	12	0.46	0.58	0.2	1.15	41
1250kPB0.3A	0.009	16	0.62	0.55	0.3	1.29	44
1250kPB0.4A	0.009	16	0.52	1.1	0.4	1.17	35
1250kPB0.6A	0.009	16	0.54	1.2	0.6	1.23	43

[a]Functionalized PB polymers were named so that the prefix corresponds to the molecular weight of the precursor chain, and the suffix represents the mol percent of monomers bearing pendent acid groups. [b]In molar equivalent of 1,2-PB units, which are 98% of the units of 510kPB and 8% of the units of 1250kPB. [c]Molar fraction of functionalized monomers based on the total number of PB monomers (both 1,2 and 1,4 units). [d]Reported values correspond to aged samples (12-18 months for 510kPBxxA polymers, and 6-12 months for 1250kPBxxA polymers), and reflect the slow cross-linking of the polymer chains that occurs with time upon storage (see text). The 510kPB and 1250kPB prepolymers had PDI values of 1.15 and 1.09, respectively. [e]Average reaction rate divided by [1,2PB units][MPA][AIBN]$^{1/2}$. [f] ^{1}H NMR spectrum is shown in Figure 2.3. [g]GPC trace is given in Figure 2.4.

Table 2.2 Solubility Constraint on Functionalization with 3-Mercaptopropionic Acid (mol % Monomer Basis) in Various Solvents at Room Temperature

	510k 1,2 PB[a]	1250k 1,4 PB[b]
Dodecane	1.0% < < 1.8%	< 0.2%
Chlorododecane	1.0% < < 1.8%	> 0.6%
Jet-A	1.0% < < 1.8%	> 0.6%
Tetrachloroethane	1.8% < < 4.7%	> 0.6%
Chloroform	4.7% < < 7.1%	> 0.6%

[a]The lower degree of functionalization was found to be soluble at all concentrations tested; the upper degree of functionalization exhibited phase separation at low concentrations (500-2500 ppm). [b]Four degrees of functionalization were examined for 1250kPB (Table 2.1): none were soluble at low concentration (500-2500 ppm) in dodecane; all were soluble in the other solvents.

Table 2.3 Zero-Shear Specific Viscosity[a] of 1250 kg/mol 1,4-Polybutadiene Chains as a Function of 3-Mercaptopropionic Acid Content and Concentration in Jet-A at 25 ºC

c (wt %)	0% A	0.2%A	0.3%A	0.6%A
0.25	1.04	0.99	0.92	0.77
0.5	2.7	3.0	2.8	2.4
1.5	32	42	56	65

[a] $\eta_{sp} \equiv \eta_{solution}/\eta_{solvent} - 1$, where solvent viscosity was 1.45 mPa.s. Measurement reproducibility was typically within 0.03 mPa.s or 3% of the measurement (whichever is greater).

Table 2.4 Normalized Apparent Hydrodynamic Radii of Functionalized 1250 kg/mol 1,4-Polybutadiene Chains in Jet-A and Chlorododecane (CDD)[a]

	0.2%A[b]		0.3%A[b]		0.4%A[b]		0.6%A[b]	
c (by wt, in ppm)	Jet-A	CDD	Jet-A	CDD	Jet-A	CDD	Jet-A	CDD
500	1.02	-	1.07	0.95	1.07	1.02	1.06	0.91
900	1.03	-	1.10	0.99	1.12	1.07	1.10	0.96
1500	1.10	-	1.21	1.05	1.25	1.15	1.23	1.07
2500 ≈ c*	1.14	-	1.27	1.14	1.32	1.30	1.29	1.23

[a]Measurements were carried out at 25 ºC and results are reported as normalized hydrodynamic radii relative to the unfunctionalized chains (for which at 500 ppm R_h = 25.2 nm in Jet-A and 47.9 nm in CDD). The standard deviation of measurements was < 2% of the measured value in all cases. [b]The degree of functionalization with 3-mercaptopropionic acid, as indicated in Table 2.1.

2.7 References and Notes

1. Knight, J. *Antimisting additives for aviation fuels*. United States patent 4,396,398, 1983.

2. Peng, S. T. J.; Landel, R. F., Rheological behavior of progressively shear-thickening solutions. *Journal of Applied Physics* **1981,** 52, (10), 5988–5993.

3. Peng, S. T. J.; Landel, R. F., Rheological behavior of FM-9 solutions and correlation with flammability test results and interpretations. *Journal of Non-Newtonian Fluid Mechanics* **1983,** 12, (1), 95–111.

4. Rodd, L. E.; Scott, T. P.; Cooper-White, J. J.; McKinley, G. H., Capillary break-up rheometry of low-viscosity elastic fluids. *Applied Rheology* **2005,** 15, (1), 12–27.

5. Anna, S. L.; McKinley, G. H., Elasto-capillary thinning and breakup of model elastic liquids. *Journal of Rheology* **2001,** 45, (1), 115–138.

6. Bathel, B. F.; Stephen, N.; Johnson, L.; Ratner, A.; Huisenga, M., Prediction of postcontact parameters of fluid droplet impact on a smooth surface. *AIAA Journal* **2007,** 45, (7), 1725–1733.

7. The extent of MPA incorporation was determined upon analysis of ^{1}H NMR spectra by integration of backbone and side-group peaks, with the following complication. For PB functionalization with MPA, we expect two peaks between 2.85 and 2.55 ppm corresponding to $HO_2CC\mathbf{H_2}CH_2S$- protons and $HO_2CCH_2C\mathbf{H_2}S$-, with one or more additional peaks (depending on whether cyclic structures are formed or not) around 2.55 ppm, corresponding to $HO_2CCH_2CH_2SC\mathbf{H_2}$- protons. Experimental results consistently showed two large, partially overlapping peaks between 2.825 and 2.575 ppm, and a much smaller, broad overlapping shoulder below 2.575 ppm, extending in some cases down to 2.4 ppm (for instance, for 510kPB4.7A polymer that shoulder peak was about 1/3 of the size of the first two). These observations indicate that the signal for $HO_2CCH_2CH_2SC\mathbf{H_2}$- is broad, with significant overlap with the middle peak, and that for simplicity the 2.85-2.4 ppm range should be integrated as a whole, accounting for 6 protons for each functionalized monomer. The complication is that the integration of the small shoulder region between 2.55 and 2.4 ppm was found to be completely unreliable (due both to its small size at the very low extents of functionalization investigated, and apparently to the presence of the very large neighboring PB backbone peak): in many cases, the software-computed integral was a physically nonsensical negative number. As a result, extents of MPA functionalization were calculated instead in all cases by integrating between 2.825 and 2.575 ppm and estimating that that integral accounted for 5 protons for each functionalized monomer.

8. Davis, M. M., In *Acid-Base Behavior in Aprotic Organic Solvents*, 1968; pp. 31–37.

9. Alessi, P.; Cortesi, A.; Sacomani, P.; Valles, E., Solvent Polymer Interactions in Polybutadienes. *Macromolecules* **1993,** 26, (23), 6175–6179.

10. $\eta_{sp} = 2.5\phi$ for non-interacting, rigid, spherical particles dispersed in a liquid medium, meaning that the particles' contribution to solution viscosity depends only their total volume fraction in solution ϕ, and is independent of their size.

11. Rubinstein, M.; Semenov, A. N., Thermoreversible gelation in solutions of associating polymers. 2. Linear dynamics. *Macromolecules* **1998,** 31, (4), 1386–1397.

12. Rubinstein, M.; Semenov, A. N., Dynamics of entangled solutions of associating polymers. *Macromolecules* **2001,** 34, (4), 1058–1068.

13. Semenov, A. N.; Rubinstein, M., Thermoreversible gelation in solutions of associative polymers. 1. Statics. *Macromolecules* **1998,** 31, (4), 1373–1385.

14. Schulz, D. N.; Bock, J., Synthesis and fluid properties of associating polymer systems. *Journal of Macromolecular Science—Chemistry* **1991,** A28, 1235–1243.

15. Schulz, D. N.; Kitano, K.; Duvdevani, I.; Kowalik, R. M.; Eckert, J. A., Hydrocarbon-soluble associating polymers as antimisting and drag-reducing agents. *ACS Symposium Series* **1991,** 462, 176–189.

16. A semi-Markov chain is a stochastic process that takes on a finite number of states, that moves from one state to the next according to transition probabilities P_{ij} (P_{ij} is the probability to transition from state i into state j), and such that the amount of time it spends in any state i, before proceeding to the next state, is a random variable with distribution T_i. When the time spent in every state is always 1, the semi-Markov process is just a Markov chain.

17. Kowalik, R. M.; Duvdevani, I.; Peiffer, D. G.; Lundberg, R. D.; Kitano, K.; Schulz, D. N., Enhanced drag reduction via interpolymer associations. *Journal of Non-Newtonian Fluid Mechanics* **1987,** 24, (1), 1–10.

18. The Zeigler-Natta method of polymerization used in the preparation of the materials characteristically results in very high product polydispersity.

19. Stadler, R.; Freitas, L. D., Complex-formation and dynamics in polymer melts. *Makromolekulare Chemie—Macromolecular Symposia* **1989,** 26, 451–457.

20. Rubinstein and Semenov's model describes the static and dynamic properties of solutions of linear chains randomly functionalized with pairwise, self-associating groups. They assumed monodisperse chains of N Kuhn monomers, containing f stickers capable of forming pairwise associations of energy εkT, located at constant intervals (i.e., separated by $l = N/f$ monomers) along the entire chains. For entangled polymer chains with strongly associating stickers, above the gel point and in good solvent, the model predicts a rich cascade of scaling regimes in the concentration dependence of viscosity shown in Figure 2.17 (Rubinstein, M.; Semenov, A. N. *Macromolecules* **2001,** 34, (4), 1058-1068). Transitions from one regime to another are predicted to occur at the entanglement concentration ϕ_e, the overlap concentration of the strands between stickers ϕ_s, the entanglement concentration of the strands between stickers ϕ_{le}, and a crossover concentration ϕ_r above which the lifetime of bonds must be renormalized to account for reassociation of the same pair of separated stickers due to a shortage of free partners. Below ϕ_s, any sticker's closest partners in space are its neighbors on the same chain, so interactions are mostly intramolecular. The steep increase in viscosity with concentration between ϕ_e and ϕ_s corresponds to a transition from predominantly intramolecular to predominantly intermolecular pairing. For comparison, the concentration dependence of viscosity for linear, non-associating chains is $\eta \sim \phi^{1.3}$ below ϕ_e and $\eta \sim \phi^{3.9}$ above ϕ_e according to de Gennes' reptation model. We note that the $\eta \sim \phi^{5.3}$ relationship which we observed above ϕ_e for unmodified PB is consistent with the well-known observation that the simple reptation model underestimates the value of the exponent for real chains (Rubinstein, M.; Colby, R. H., In *Polymer Physics*, Oxford: 2003; p 374).

21. Obtained using published equilibrium constants of associations (Davis, M. M., In *Acid-Base Behavior in Aprotic Organic Solvents*, 1968; pp 31–37) as explained in Section 4.5.6.

22. Obtained for 510kPB chains in CDD by rearrangement of the scaling relation $\phi^* \approx (b^3/v)^{6\nu-3} N^{1-3\nu}$ (Rubinstein, M.; Colby, R. H., In *Polymer Physics*, Oxford: 2003; Equation 5.19, p 176), using swelling exponent $\nu \approx 0.588$ and overlap concentration $\phi^* \cong 0.003$. In the above equation, v is the excluded volume parameter and b is the Kuhn monomer length. The number of Kuhn monomers N was estimated for chains of $M_w \sim 510$ kg/mol assuming Kuhn monomers of molecular weight ~ 100 g/mol.

23. The overlap concentration of a segment of size N monomers scales with $N^{1-3\nu}$, where the fractal exponent is $\nu \approx 0.588$ in good solvent.

24. Peng, S. T. J.; Landel, R. F., Preliminary Investigation of Elongational Flow of Dilute Polymer-Solutions. *Journal of Applied Physics* **1976,** 47, (10), 4255–4260.

Chapter III Randomly Functionalized Linear Chains with Complementary Groups

3.1 Introduction

Previously we saw that for solutions of self-associating chains (Figure 1.7.1), intrachain pairing is more important than interchain pairing, even up to concentrations $c >> c^*$. In dilute solutions, the addition of self-associating stickers leads to chain collapse and reduces the effect of the polymer on drop breakup. To drive intermolecular associations in dilute solutions,[1] strategies involving the use of complementary functional groups were designed (Figure 1.7.2). In this chapter we study the association behavior of mixtures of tertiary amine and carboxylic acid-functionalized 1,4-polybutadiene chains of size M_w = 1250 kg/mol (Scheme 3.1).

3.1.1 Background

A review of the literature reveals that mixtures of two different linear chain species, one randomly functionalized with hydrogen-bond donating groups and the other with hydrogen-bond accepting groups, exhibit the following behaviors: First, donor and acceptor chains form clusters of increasing size with increasing concentration, even below c^*, and the resulting interpolymer complexes have been reported to exhibit improved shear stability as well as enhanced drag-reduction properties.[2] Second, intermolecular associations nevertheless result in some measure of chain collapse, as well as in non-linear enhancements in shear viscosity with increasing concentration. Here we give a brief literature review of the above and of other relevant behavior of hydrogen donor-acceptor systems, and discuss implications for the design of successful mist-suppression additives.

Donor-acceptor intermolecular associations can cause aggregation of polymer molecules well below the overlap concentration. Malik and Mashelkar[3] investigated the solution properties of blends of poly(dodecyl acrylate-co-methacrylic acid) (DAMA, 3 wt % methacrylic acid) and poly(styrene-co-dodecyl acrylate-co-4-vinyl pyridine) (PSDAVP, 4 wt % vinyl pyridine) (Figure 1.5.b) in kerosene. Using dynamic light scattering, they observed the formation of interpolymer complexes (IPC) whose size increased steeply with increasing polymer concentration near the overlap concentration c^* (see Figure 3.1). Note that

interpolymer complexes at c = 0.3 g/dL were one order of magnitude larger than the component polymers.

Jian and coworkers[4] studied the complexation of poly(styrene-co-vinylphenol) (STVPh) and poly(styrene-co-vinylpyridine) (STVPy) in organic solvents by viscometry and dynamic laser light scattering. They observed the formation of aggregates ~ 1 order of magnitude larger (in hydrodynamic radius R_h) than the individual polymer coils in very dilute blend solutions in both butanone and tetrahydrofuran. (The butanone case is shown in Figure 3.2.)

It should be noted that the observation of interpolymer aggregates in the dilute concentration regime supports the prediction that the strength of the acid-base interaction dwarfs the strength of self-association of the carboxylic acid donor groups via dimerization.

Interpolymer complexation results in a contraction of the polymer chains, causing a decrease in the specific viscosity of the blends compared to that of the component polymer solutions at the same concentration. Jiang and coworkers[4] used viscosity measurements in dilute solutions to evaluate the effect of sticker density (i.e., number density of interacting groups) on complex formation for blends of STVPh and STVP. Large negative deviations in specific viscosity from predicted values for non-associating polymer systems were observed in the dilute regime, indicating coil contraction due to the formation of dense intermolecular complexes (see Figure 3.3). For non-interacting polymer molecules, the specific viscosity $\eta_{sp,m,calc}$ of a ternary polymer$_1$-polymer$_2$-solvent system is simply a weighted average of the specific viscosities of both components:

$$\eta_{sp,m,calc} = \left(\eta_{sp,1}c_1 + \eta_{sp,2}c_2\right)\Big/c_m \tag{3.1}$$

where $\eta_{sp,1}$, $\eta_{sp,2}$ are the specific viscosities of components 1 and 2 at concentration $c_m = c_1 + c_2$. According to Equation 3.1, the reduced viscosity of a non-interacting polymer system would thus exhibit a linear variation from x = 0 to x = 1 in Figure 3.3. For a given value of the x-coordinate (say 0.5), the number density in solution of hydrogen-accepting moieties is fixed while the number density of hydrogen-donating moieties increases as we move down from one curve to the next (i.e., with increasing fraction of vinylphenol in STVPh). As one might expect, this results in an increase in polymer complexation, and specifically in an increase in the number density of paired stickers within the aggregates. The pronounced negative deviation in observed reduced viscosity for the bottom 3 curves in Figure 3.3 is easily understood in terms of a collapse of the coils as polymer molecules aggregate into

more and more compact structures (as the number density of H-bonds between donor and acceptor polymer molecules increases.) In other words, the polymers are making a much smaller contribution to the solution viscosity in the form of collapsed aggregates than in the form of swollen coils.

Wang et al. reported a similar phenomenon for blends of poly(styrene-co-octyl acrylate-co-acrylic acid) and poly(styrene-co-octyl acrylate-co-4-vinylpyridine) in toluene.[5-7] For dilute blends, they observed negative deviations in the measured specific viscosity of the mixture $\eta_{sp,m,exp}$ from the expected value $\eta_{sp,m,calc}$ for non-interacting systems, indicating a reduction in the hydrodynamic volume fraction occupied by the polymer molecules in solution. This was attributed to the aggregation of polymer chains into dense structures as a result of intermolecular associations.

Interpolymer associations result in a non-linear increase of viscosity with concentration even in the dilute concentration regime. Intermolecular interactions make two kinds of contributions to the specific viscosity of solutions of associating polymer systems. In very dilute solutions of strongly associating polymer, negative deviations from the additivity rule (Equation 3.1) are observed due to the aggregation of constituent polymer molecules into relatively compact structures of high physical crosslink density, as observed by Jiang et al.[4, 8, 9] and Wang et al.[5-7] As concentration increases, these compact structures begin to interact, and eventually to form a reversible network, giving rise to a large positive deviation from the value predicted by Equation 3.1. Therefore, due to intermolecular associations, the concentration dependence of reduced viscosity is curved even at very low polymer concentrations (Figure 3.4).

Other solution behavior of donor-acceptor polymer mixtures relevant to mist inhibition applications. As expected, the nature of the solvent exerts a profound influence on interpolymer association. In particular, for polymer interactions based on hydrogen bonding or acid-base interactions, the hydrogen-bonding ability of the solvent has a pronounced effect on the extent of association. For instance, Jiang et al.[4] observed much more pronounced negative deviations in the reduced viscosity of STVPh/STVPy mixtures in $CHCl_3$ than in tetrahydrofuran (THF), even at considerably smaller number density of stickers. This is consistent with a strong competition for H-bonding from the solvent in THF, which reduces

the fraction of the total H-bonds that contribute to complex formation and the physical crosslink density within the aggregates.

In spite of the above understanding, survey of the literature reveals that there is nevertheless little comprehension of the precise structure of interpolymer complexes *at the molecular level*, or of the relationship between molecular or aggregate structure and rheological properties or performance in drop breakup or drag reduction.

Design principles for donor-acceptor associative polymers as mist-control agents. In order to minimize the effects of chain collapse as well as minimize shear viscosity enhancements, future work should focus on polymer molecules with low extents of functionalization with associative groups, and in dilute solutions at concentrations $c < c^*$. The above literature results generate optimism that under these conditions, donor-acceptor specific interactions can be used to achieve formation of large clusters which protect against mechanical degradation and greatly increase extentional viscosity, but only slightly increase shear viscosity.

3.1.2 Scope of Present Work

What part of the variable space should we endeavor to study? Solution behavior will depend on at least the following parameters: solvent, chain lengths, temperature, extents of functionalization of donor and acceptor chains, and concentrations of donor and acceptor chains in solution. In this chapter we restrict our attention to systems which might lead us to a suitable additive for improving the fire safety of jet fuel.

The choice of solvent has such strong effects on the solubility of the functional polymers and their complexes[4,10] that it is necessary to perform experiments using the solvent of interest, here Jet-A. The choice of chain lengths of interest for use in fuel are limited to values that are long enough to confer significant elasticity and short enough to avoid chain scission at high shear rates. We know that the elasticity of solutions of 510 kg/mol and 1250 kg/mol PB chains was too low to be quantitatively measured by CaBER at concentrations below 2 wt % and 1.5 wt % (corresponding to $c \sim 4–6\ c^*$) in low-viscosity hydrocarbon solvents. Therefore, studies of the effect of stickers on elasticity of dilute solutions would benefit from the use of longer chains (recall the strong effect of chain length on elasticity).[11] Unfortunately, MW ~ 1×10^6 g/mol represents the upper limit of chain length for molecules

that resist shear degradation. Therefore, the 1250 kg/mol 1,4-PB chains used in the previous study were used again here. To simplify the task of uncovering the effects of the degrees of functionalization of donor and acceptor chains, of the overall polymer concentration, and of the ratio of donor and acceptor chains, we performed experiments holding temperature fixed (i.e., at room temperature).

3.2 Experimental

3.2.1 Materials

2-(Dimethylamino)ethanethiol hydrochloride (DMAET) was obtained at 95% purity from Aldrich. The 510 kg/mol polybutadiene (510kPB prepolymer), the 1250 kg/mol polybutadiene (1250kPB prepolymer), and all other reagents were obtained and purified as described in the preceding chapter (Section 2.2.1).

3.2.2 Polymer Synthesis and Characterization

The functionalization of 510kPB and 1250kPB with DMAET was performed according to the following representative procedure. To 1250kPB (0.50 g, 0.74 mmol 1,2-PB repeat units) dissolved in 50 mL of THF in a 100 mL Schlenk flask were added DMAET (0.31 g, 2.1 mmol) and azobisisobutyronitrile (AIBN, 51 mg, 0.31 mmol), both dissolved in a mixture of 5 mL THF and 5 mL methanol. The contents of the Schlenk flask were degassed in 3 freeze-pump-thaw cycles, warmed to 55 ºC, and then allowed to react at 55 ºC for 7 hrs. Following the reaction, the polymer solution was transferred to a 100 mL jar containing a small amount of 2,6-di-*tert*-butyl-4-methylphenol (BHT), concentrated by evaporation of all but the last 20 mL solvent under an argon stream, and titrated by addition of potassium hydroxide (0.31 g at 88%, 4.9 mmol, dissolved in a ~1:3:6 water:methanol:THF solution). The solution was cooled in liquid nitrogen and precipitated by addition of 50 mL of cold methanol. Final purification of the polymer was achieved by reprecipitating from a THF solution (containing ca. 1 wt % BHT) once with 50:50 methanol:water, and once again with cold methanol, followed by drying to constant weight under vacuum at room temperature. Reaction conditions and results are summarized in Tables 3.1 and 3.2, and results of product characterization by ^{1}H NMR and GPC are shown in Figures 3.5 and 3.6.

Acid-functionalized 1250 kg/mol 1,4-PB chains used in this study were the same as those used in earlier studies (Section 2.3.1, Table 3.1). The characterization of functionalized

polymer by gel permeation chromatography and ^{1}H NMR was performed as documented previously (Section 2.2.3).

3.2.3 Measurements of Solution Properties

Dilute mixtures of acid-functionalized and amine-functionalized polymer were prepared from stock solutions of the individual polymers by mixing in appropriate ratios to obtain target concentrations. The zero-shear viscosity, apparent hydrodynamic size of polymer clusters, and the fluid break-up and atomization of the solutions were characterized as described in Chapter 2 (Sections 2.2.4 and 2.2.5).

3.3 Results and Discussion

3.3.1 Synthesis of Amine-Functionalized Polybutadiene

Reaction of 1,4-PB (Scheme 3.1) using the procedure outlined in Section 3.2.2 successfully incorporates tertiary amine side-groups (Table 3.1, Figure 3.5). Unfortunately, we were not able to assess the MW distribution of the resultant amine-functionalized 1250kPB by gel permeation chromatography using our instrument: at every injection the RI detector output featured the absence of a polymer peak. Note that this anomalous behavior has been observed in other cases, for example with phenol-functionalized 92 kg/mol 1,2-PB (entry 92kPB12 in Table 5.1). Given that the addition of DMAET to 1,2-PB (using the same procedure) and the addition of 3-mercaptopropionic acid (MPA) to 1,4-PB both proceed without degradation of the polymer backbone (Tables 3.1 and 3.2, Figures 2.4 and 3.6), it is reasonable to expect that the narrow polydispersity of the 1250kPB starting material was also preserved during the addition reaction of DMAET. This is consistent with the result that the viscosities of 1250k1.5N and 1250kPB polymers were identical at the overlap concentration of 2500 ppm in Jet-A (Figure 3.7). For 1250kPB2.6N and 1250kPB5.4N polymers, however, appreciable viscosity enhancements compared to the prepolymer material (Figure 3.7) suggests that a small amount of crosslinking of the polymer occurred, presumably during the workup stage of the preparation of the materials.

3.3.2 Phase Behavior

The degree of functionalization was restricted to be low enough that the individual species dissolve to form homogenous solutions in Jet-A at 25 ºC at all concentrations tested

(up to 1.5 wt % polymer). As a result, the highest degrees of functionalization utilized in this study were 5.4 tertiary amine side-groups per 100 butadiene units, and 0.6 carboxylic acid side-groups per 100 butadiene units (Table 3.1). Nevertheless, intermolecular associations of carboxylic acid and tertiary amine side-groups were found to promote phase separation into polymer-rich (gel) and polymer-poor (sol) phases (Table 3.3). Phase behavior was a strong function of temperature. For example, 1250kPB0.6A polymer separated into gel and sol phases in Jet-A at 0 ºC at all concentrations tested.

We chose to conduct further examination of solution properties only for those pairs of polymers in Table 3.3 that did not yield phase separation. A summary of further experiments is given in Table 3.4.

3.3.3 Aggregate Formation and Effects on Shear Viscosity

Upon inspection of shear viscosity results at the overlap concentration of the 1250kPB chains (corresponding to c^* = 2500 ppm by wt in Jet-A for the unfunctionalized chains, Figure 3.7), we immediately observe an important difference between non-specific, pair-wise self-associations, and specific, donor-acceptor interactions: at that concentration for all the molecules studied, self associations led to negative deviations in η_0 (look at the acid-functionalized molecules by themselves), but interchain donor-acceptor associations led to positive deviations in η_0. This indicates that in the self-associating case, the effects of chain collapse dominate over any positive enhancement in shear viscosity due to formation of polymer clusters; in the donor-acceptor case the opposite holds.

Measuring polymer aggregation in terms of particle size can be readily achieved by dynamic light scattering. Results at 1500 ppm (Figure 3.8) validate our expectations that donor-acceptor interactions can "force" polymer chains to associate even in dilute solutions. At intermediate compositions, objects with hydrodynamic size greater than either individual components are observed. At this dilute condition, self-associating stickers do not cause the acid-functionalized molecules to form large aggregates. Increasing polymer concentration to c^* increases the size of interpolymer complexes (Figures 3.9 and 3.10), in good agreement with literature reports on similar systems (discussed earlier). Large increases in $\langle R_h \rangle$ can be achieved at concentrations as low as c^*: for example, a 3-fold increase in hydrodynamic radius could be obtained at c^* = 2500 ppm for mixtures of 1250kPB0.2A and 1250kPB5.4N (Figure 3.9).

For fixed sticker density on one partner (e.g., 1.5% N), increasing the sticker density on the other partner leads to larger aggregates, at least up to the limit imposed by phase separation. Notice that phase separation precludes simply increasing sticker density on both species as a means to promote larger aggregates. At a certain point, further increases of number density of stickers on one of the chains requires a reduction of the number density of stickers on the partner chains in order to remain in the homogeneous regime. We found that the largest aggregates form when the extent of functionalization of one of the species is pushed up to its single-component solubility limit. Thus, mixtures of 1250kPB0.2A and 1250kPB5.4N polymers, and mixtures of 1250kPB0.8A and 1250kPB1.5N polymers gave the highest enhancement in $\langle R_h \rangle$ at both 1500 and 2500 ppm (Figures 3.8 and 3.9).

For a given pair of acid-functionalized and base-functionalized polymer, we further observe that the largest clusters were obtained in the vicinity of 1:1 weight ratios of the chains, in some cases far from 1:1 molar ratios of the stickers. This very interesting result held for all mixtures tested at both 1500 and 2500 ppm (Figures 3.8 and 3.9).

We close this section by commenting on the relative magnitude of the changes in $\langle R_h \rangle$ and η_0 as a result of interpolymer associations. Except for the mixture involving 1250kPB5.4N, which is measurably crosslinked, deviations in η_0 due to interchain associations were < 20% at the overlap concentration of 2500 ppm (Figure 3.7), compared with up to 300% changes in $\langle R_h \rangle$ (Figure 3.9). It is noteworthy that cluster size is not a good indicator of viscosity enhancements. Indeed, in the following section we find that these large clusters provide no observable enhancements of the elasticity or mist-suppression capacity of the solutions in extensional deformation—contrary to expectations based on the prior literature.

If the concentration is increased in order to confer elasticity to the solutions (and thereby, suppress misting), strong increases of shear viscosity also occur (which hinder application of such solutions in fuel systems). In the following investigation of elasticity and mist suppression, concentrations of 15,000 ppm (1.5 wt %) were required for successful CaBER measurements (see below). At such high concentration, the shear viscosity in donor-acceptor mixtures is increased 2- to 3-fold relative to controls with unfunctionalized polymer or the individual functionalized species. For example, mixtures of 1250kPB2.6N and 1250kPB0.2A in 15:85 and 30:70 wt ratios at total polymer concentrations of 1.5 wt % in

Jet-A were 130 and 180 mPa.s, respectively, compared with 48, 62, and 77 mPa.s for 1250kPB prepolymer, 1250kPB0.2A, and 1250kPB2.6N individual polymers at 1.5 wt % in Jet-A.

3.3.4 Elasticity and Mist Suppression

Drop impact experiments enable us to evaluate the effect of donor-acceptor associations on solution elasticity and drop breakup in very dilute solutions (Figure 3.11). Recall[12] that fluid filaments do not break when 180 ppm of 4200 kg/mol linear PIB are dissolved in Jet-A: the fluid filaments seen in Figure 3.11a simply fall down onto the surface. When chain length is reduced into a range that would survive shear degradation, then substantial fluid is ejected: with 180 ppm of 1250 kg/mol PB, the fluid filaments elongate and some drops escape, which are substantially larger than those ejected from pure Jet-A (Figure 2.1), as a result of polymer elasticity. When stickers are present (Figure 3.11c and 3.11d), there is little evidence of fluid filaments, and numerous, fine droplets are ejected in a manner that resembles Jet-A with no polymer added (Figure 2.1). Thus, donor-acceptor interactions do not overcome the limitations found in self-associating systems (Chapter 2). In fact, the mist-suppression performance of the mixture of acid- and base-functionalized polymers was significantly worse than that of the acid-functionalized polymers by themselves (compare with Figure 2.11). Increasing polymer concentration to 450 ppm (Figure 3.12) does not change this finding: while drop suppression improves for all four systems as a result of increased polymer content, the incorporation of associative groups (c–d) still reduces efficacy relative to the unmodified polymer (b) by a factor of 2-4. Note that the poorest performance in suppression of drop breakup corresponds to the largest extent of interpolymer interactions, at 1:1 wt ratio of the chains (Figures 3.7–3.9).

The above results for dilute solutions of donor-acceptor chains cannot a priori be generalized to more concentrated solutions: physical properties for these systems display a strong concentration dependence in the transition between the dilute and semi-dilute regimes. As noted earlier, the drop impact experiment is not informative near c^*. To compare the effects of interpolymer complexes formed near the overlap concentration to their non-associating parent linear chains, spray experiments were conducted on the mixtures whose viscosity and size measurements are given in Figures 3.7 and 3.9. No large differences in atomization could be discerned as a result of donor-acceptor interpolymer associations at c^*

= 2500 ppm (Figures 3.13–3.18). This was true despite the documented presence of aggregates of hydrodynamic radius up to 3 times that of the unfunctionalized chains (Figure 3.9). In fact, in most cases, the size distribution of droplets generated in the spray experiment shifted to smaller values as a result of interpolymer complexation, as was the case for self-associating polymer systems (Figure 2.13).

To place the above qualitative effects on a more rigorous foundation, quantitative measurements of extensional viscosity and relaxation time were performed using capillary breakup rheology. As mentioned in Chapter 2, solution elasticity was unfortunately too low to be measured for 1250 kg/mol 1,4-PB chains at concentrations below 1.5 wt % (corresponding to $c = 6c^*$) in Jet-A solvent.[13] CaBER results for mixtures of 1250kPB0.2A and 1250kPB2.6N polymers at 1.5 wt % show that intermolecular complexation increased solution relaxation time, apparent extensional viscosity, and breakup time of the filaments (Figures 3.19 and 3.20). However, these increases matched precisely the increases in the shear viscosity of the solutions. Thus, intermolecular complexation did not result in significant improvements of the solutions' extensional viscosity or elasticity, relative to shear viscosity, even well into the semi-dilute concentration regime!

Our above observations of the effects of donor-acceptor polymer-polymer interactions on drop and capillary breakup are surprising in light of literature evidence[1, 3, 14] that interpolymer complexation drives the formation of large aggregates and results in enhanced viscosity, shear-thickening rheology, and enhanced drag-reduction (relative to non-associating and self-associating molecules). Based on the positive correlation between drag-reduction and mist-suppression, and on the positive correlation between polymer size and mist suppression, the adverse effects of interpolymer complexation on drop breakup at $c \leq c^*$—in the presence of large polymer structures—is the opposite of what we expected according to the state of prior understanding. These adverse effects indicate that, in the absence of a macroscopic network at low polymer concentrations, interchain associations, like intrachain associations, hinder the mechanism of mist-suppression. We suggest this occurs as physical bonds inhibit stretching of the chains in extensional flow. This physical phenomenon persists at higher concentrations: in spite of large enhancements in shear viscosity (relative to both unfunctionalized and self-associating chains of the same length) in the semi-dilute regime, to our surprise donor-acceptor molecules showed no improvement in relaxation time or extensional viscosity relative to shear viscosity up to $c = 6c^*$ (Figures 3.19 and 3.20).

3.4 Conclusions

We find that the use of complementary associative groups randomly placed along linear polymer chains (Figure 1.7.2, Scheme 3.1) successfully drives intermolecular interactions even in dilute solutions. However, complementary donor-acceptor stickers, like self-associating stickers, decrease the mist-suppression activity of the polymer chains in dilute solutions at polymer concentrations up to the overlap concentration of linear non-associating chains of the same length. At high concentration, associations increase the shear viscosity relative to the unfunctionalized chains; high viscosity suppresses fluid breakup, but is unacceptable in fuel applications.

Our discoveries thus far lead away from randomly functionalized polymers. In light of the results presented in the foregoing two chapters, we now turn to molecular designs which seek to overcome the effects of chain collapse by clustering associating groups at the end of polymer chains (Figure 1.7.3 and 1.7.4).

3.5 Figures, Schemes, and Tables

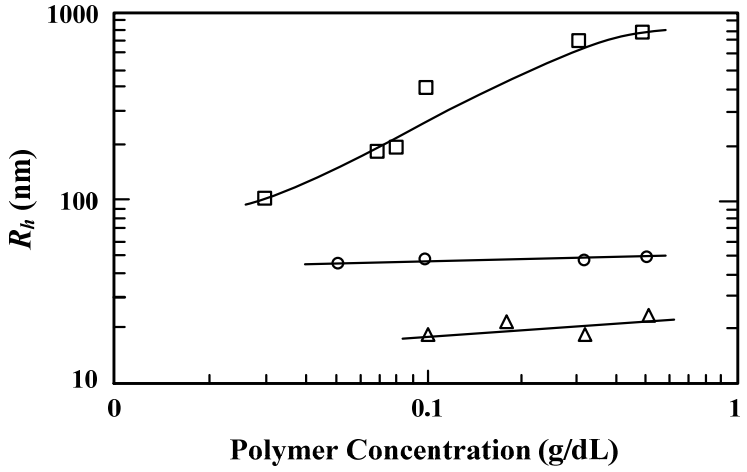

Figure 3.1 Hydrodynamic radii of proton-donating polymer DAMA, proton-accepting polymer PSDAVP, and their mixture (1:1 ratio by weight) in kerosene. The overlap concentration of the chains corresponds to $c^* = 0.3$ g/dL for PSDAVP and $c^* = 0.7$ g/dL for DAMA. (Adapted from Malik and Mashelkar[3] and reproduced with permission.)

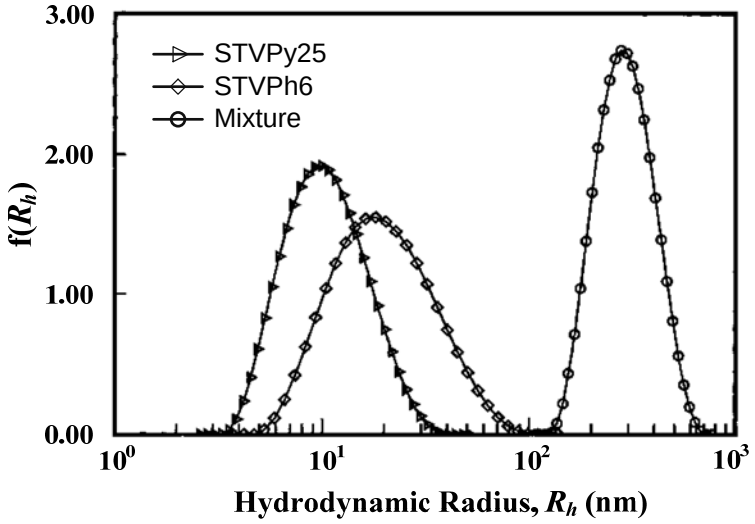

Figure 3.2 Hydrodynamic radius distribution f(R_h) of proton-donating and proton-accepting polymers containing 6 and 25 mol % vinyl phenol and vinyl pyridine monomers, and their mixture (1:1 ratio by weight) in butanone. Measurements were conducted at scattering angle of 15^o for solutions of total polymer concentration 1×10^{-4} g/mL. (Adapted from Xiang et al.[4] and reproduced with permission.)

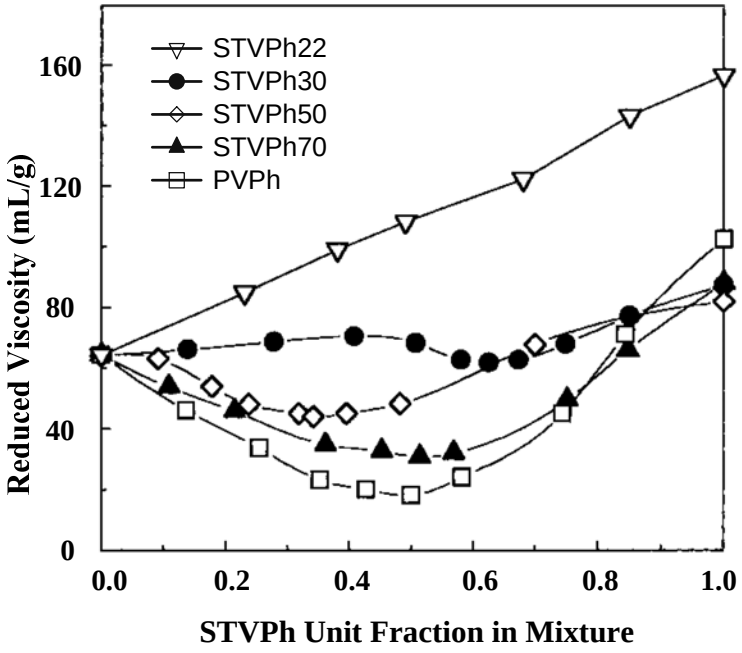

Figure 3.3 Reduced viscosity ($\eta_r = \eta_{sp}/c$, at total polymer concentration c = 1.5 mg/mL) of mixtures of STVPy containing 25% vinyl pyridine monomers and STVPh containing 22-100% vinyl phenol monomers in THF as a function of the unit fraction of STVPh, i.e., the fraction of monomers in solution that belong to STVPh molecules. (Adapted from Xiang et al.[4] and reproduced with permission.)

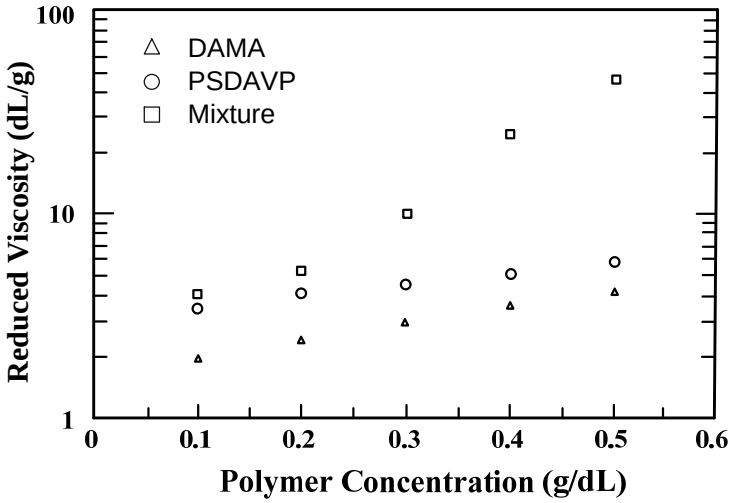

Figure 3.4 Reduced viscosity vs. concentration for proton-donating polymer DAMA, proton-accepting polymer PSDAVP, and their mixture (1:1 ratio by weight) in kerosene, showing that interpolymer associations result in a non-linear increase of viscosity with concentration even at dilute concentrations. The overlap concentration of the chains corresponds to $c^* = 0.3$ g/dL for PSDAVP and $c^* = 0.7$ g/dL for DAMA. (Adapted from Malik and Mashelkar[3] and reproduced with permission.)

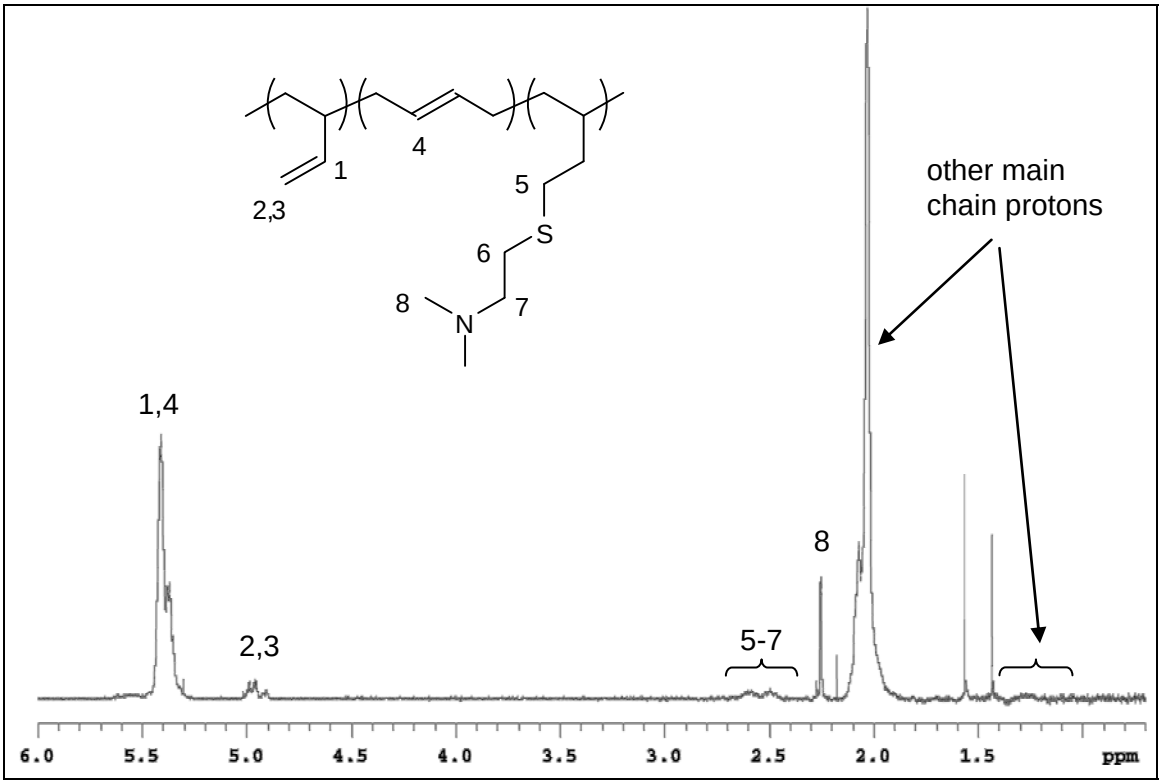

Figure 3.5. Representative ^{1}H NMR spectrum of 1250 kg/mol 1,4-polybutadiene polymer functionalized with 2-(dimethylamino)ethane thiol (1250PB2.6N, refer to Table 3.1). Visible peaks at δ = 2.27 ppm and 1.43 ppm belong to 2,6-ditertbutyl-4-methylphenol (BHT), and the peak near $\delta \sim 1.6$ ppm corresponds to water.

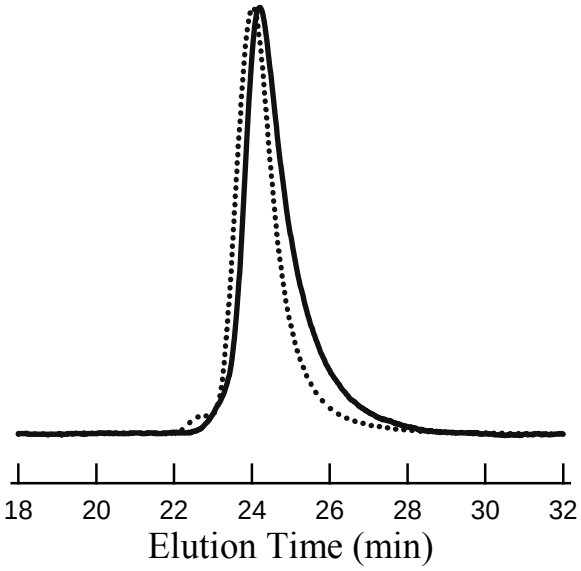

Figure 3.6 Representative gel permeation chromatography (GPC) trace of 1,2-polybutadiene functionalized with DMAET. The dashed line is 510 kg/mol 1,2-PB prepolymer; the solid line corresponds to 510kPB1.6N polymer (refer to Table 3.2) after > 2 years of storage, during which a slight broadening to the right of the size distribution curve was observed to have occurred.

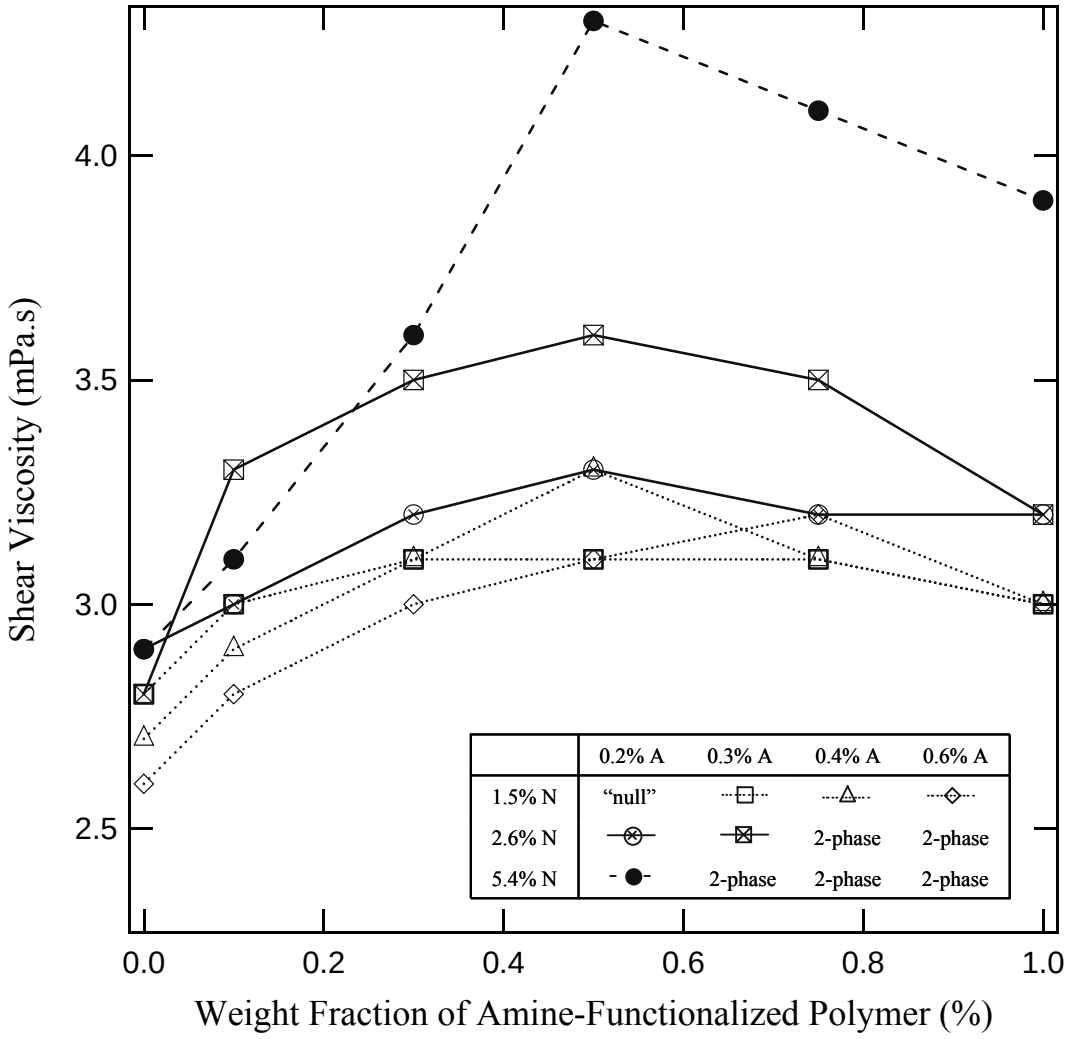

Figure 3.7 Shear viscosity of mixtures of proton-donating (1250kPBxxA) and proton-accepting (1250kPBxxN) chains in Jet-A at total polymer wt fraction of 2500 ppm, as a function of the fraction (wt 1250kPBxxN)/(wt 1250kPBxxN + wt 1250kPBxxA). The viscosities of the solvent and of the 1250k 1,4-PB prepolymer at 2500 ppm in Jet-A were 1.43 and 3.0 mPa.s, respectively.

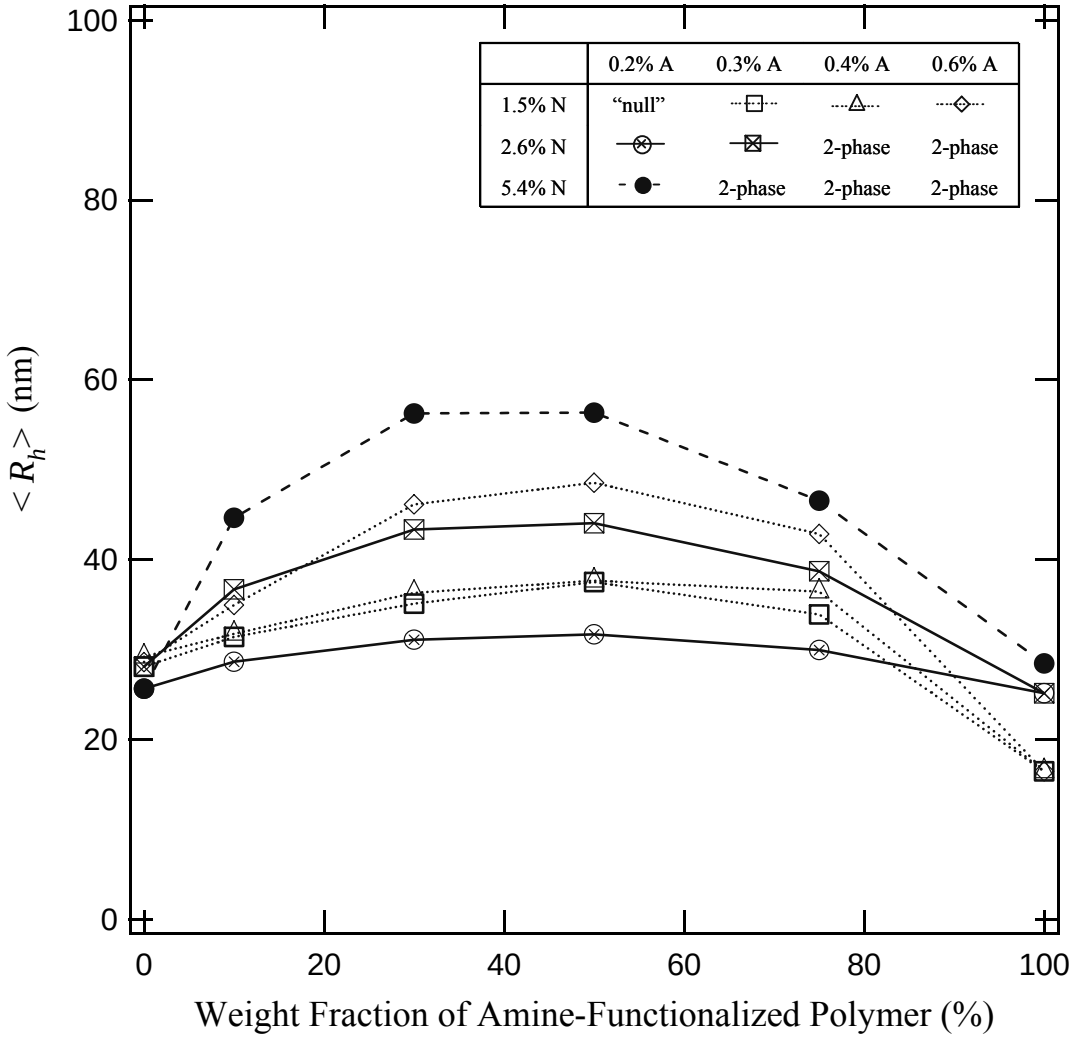

Figure 3.8 Hydrodynamic radii of mixtures of proton-donating (1250kPBxxA) and proton-accepting (1250kPBxxN) chains in Jet-A at total polymer wt fraction of 1500 ppm, as a function of the fraction (wt 1250kPBxxN)/(wt 1250kPBxxN + wt 1250kPBxxA).

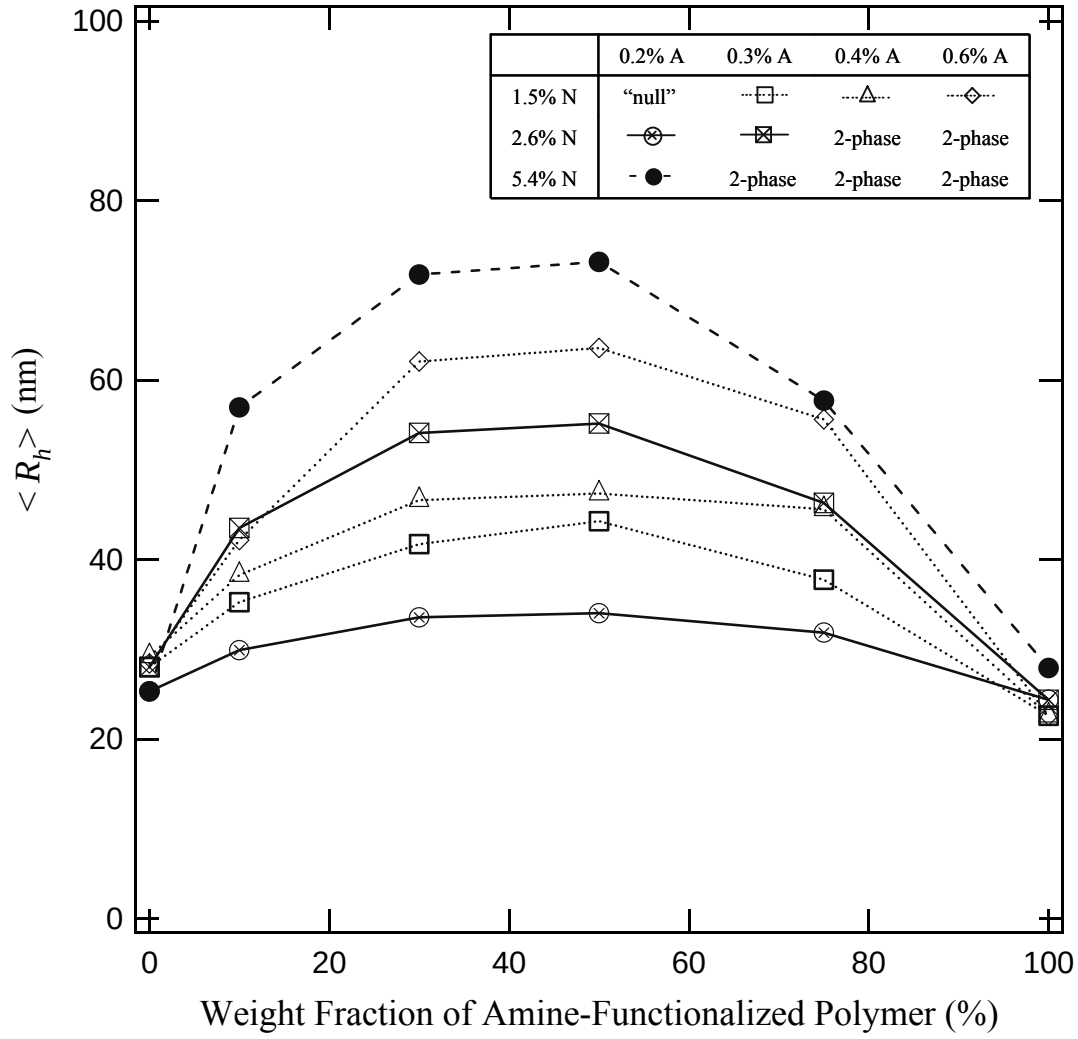

Figure 3.9 Hydrodynamic radii of mixtures of proton-donating (1250kPBxxA) and proton-accepting (1250kPBxxN) chains in Jet-A at total polymer wt fraction of 2500 ppm, as a function of the fraction (wt 1250kPBxxN)/(wt 1250kPBxxN + wt 1250kPBxxA).

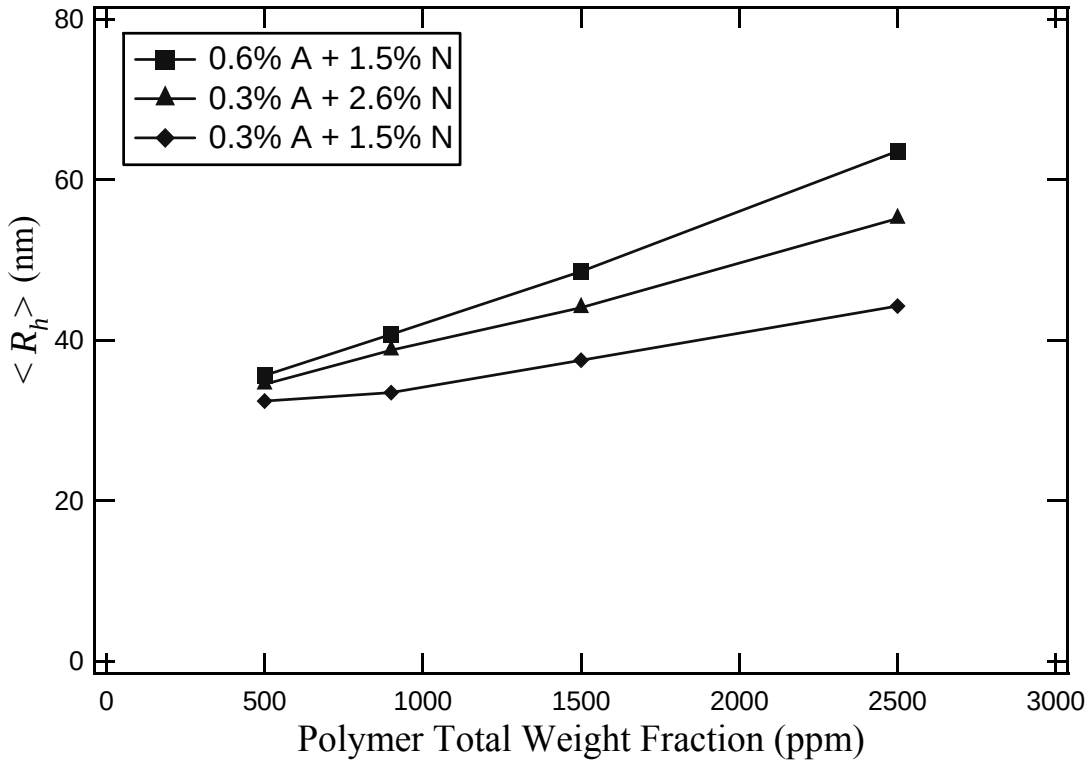

Figure 3.10 Hydrodynamic radii of mixtures of proton-donating (1250kPBxxA) and proton-accepting (1250kPBxxN) chains in 1:1 wt ratio in Jet-A, as a function of increasing total polymer concentration in the dilute regime.

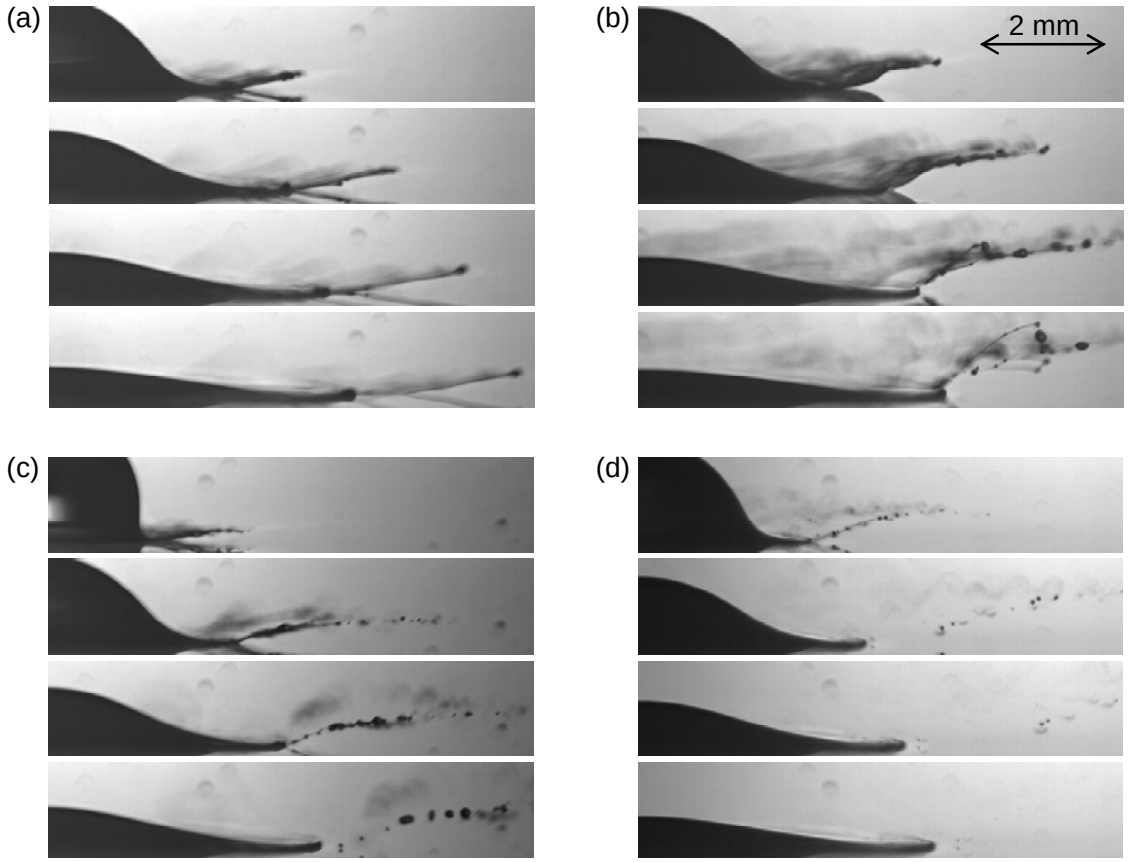

Figure 3.11 High-speed imaging of drop breakup of polymer solutions at 180 ppm by wt in Jet-A: (a) 4200 kg/mol linear, non-associating polyisobutylene chains; (b) 1250 kg/mol linear, unfunctionalized 1,4-polybutadiene (PB) chains; (c) 1250kPB0.3A and 1250kPB2.6N in 3:1 wt ratio; and (d) 1250kPB0.3A and 1250kPB2.6N in 1:1 wt ratio (refer to Table 3.1). For 4200 kg/mol polyisobutylene, satellite droplets were never fully ejected; on the other hand all visible fluid filaments connecting "beads" of fluid together had broken 2 ms, 1 ms, and 0.5 ms after impact for solutions b, c, and d, respectively. The interval between frames is 0.25 ms in all cases.

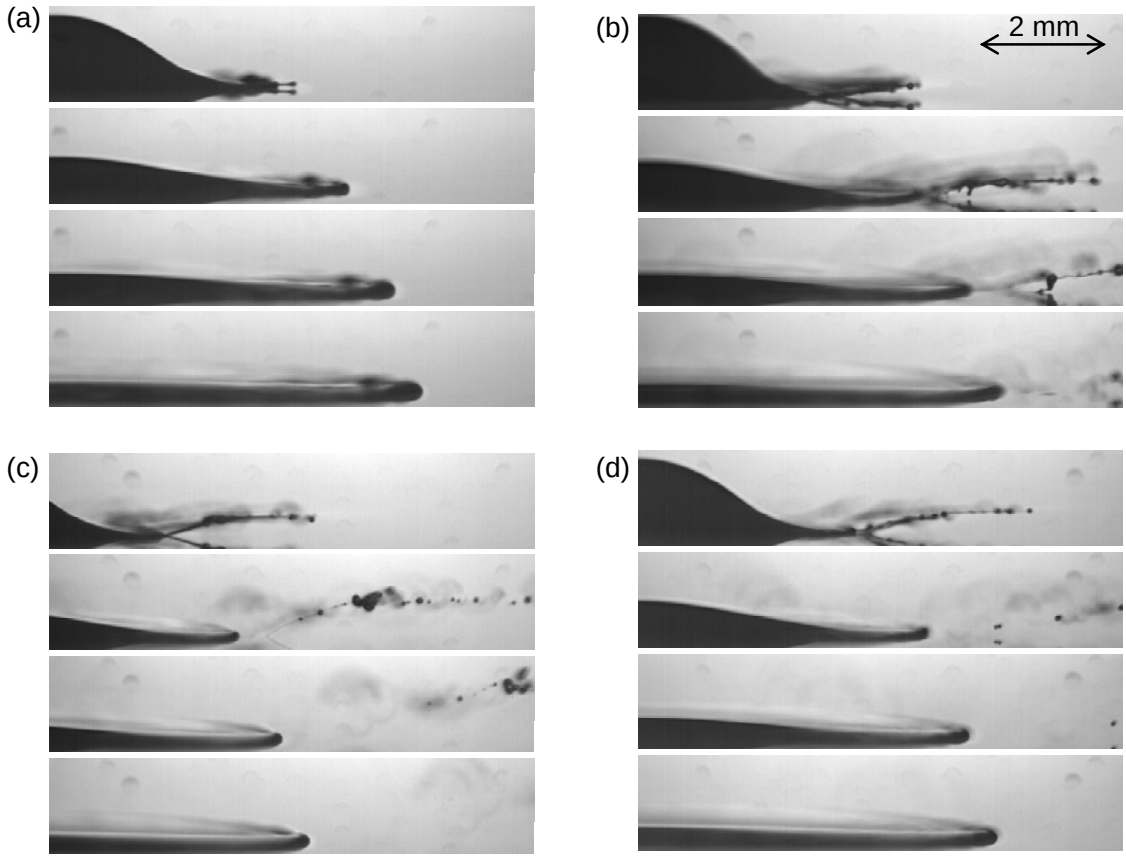

Figure 3.12 High-speed imaging of drop breakup of polymer solutions at 450 ppm by wt in Jet-A: (a) 4200 kg/mol linear, non-associating polyisobutylene chains; (b) 1250 kg/mol linear, unfunctionalized 1,4-polybutadiene (PB) chains; (c) 1250kPB0.3A and 1250kPB2.6N in 3:1 wt ratio; and (d) 1250kPB0.3A and 1250kPB2.6N in 1:1 wt ratio (refer to Table 3.1). For 4200 kg/mol polyisobutylene, there is nearly complete suppression of breakup without formation of satellite droplets; on the other hand all visible fluid filaments connecting "beads" of fluid together had broken 2.5 ms, 1.25 ms, and 0.75 ms after impact for solutions b, c, and d, respectively. The interval between frames is 0.5 ms in all cases.

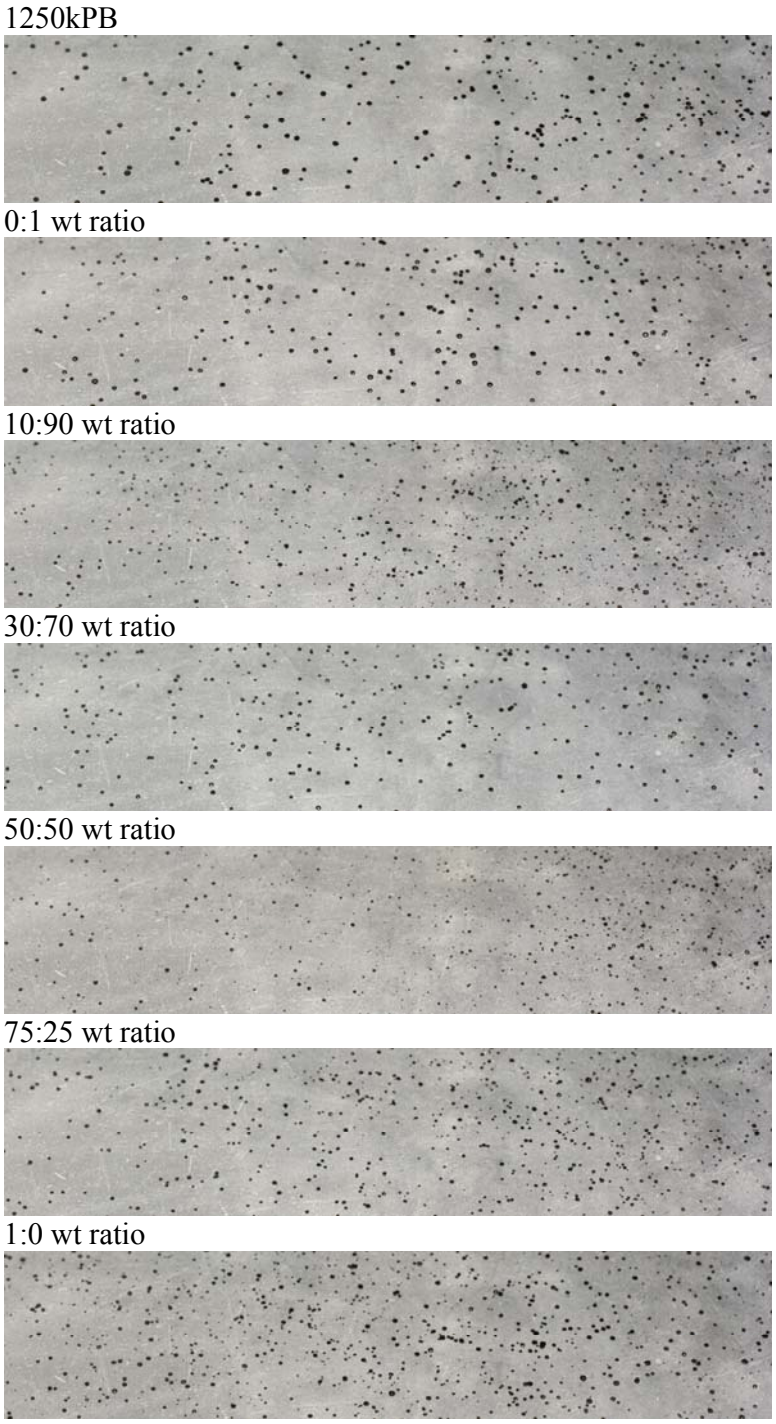

Figure 3.13 Mixture of 1250kPB0.6A and 1250kPB1.5N polymers at total concentration of 2500 ppm by wt in Jet-A, as a function of increasing wt ratio of 1250kPB1.5N to 1250kPB0.6A polymers. The top image corresponds to a reference solution of 1250kPB prepolymer.

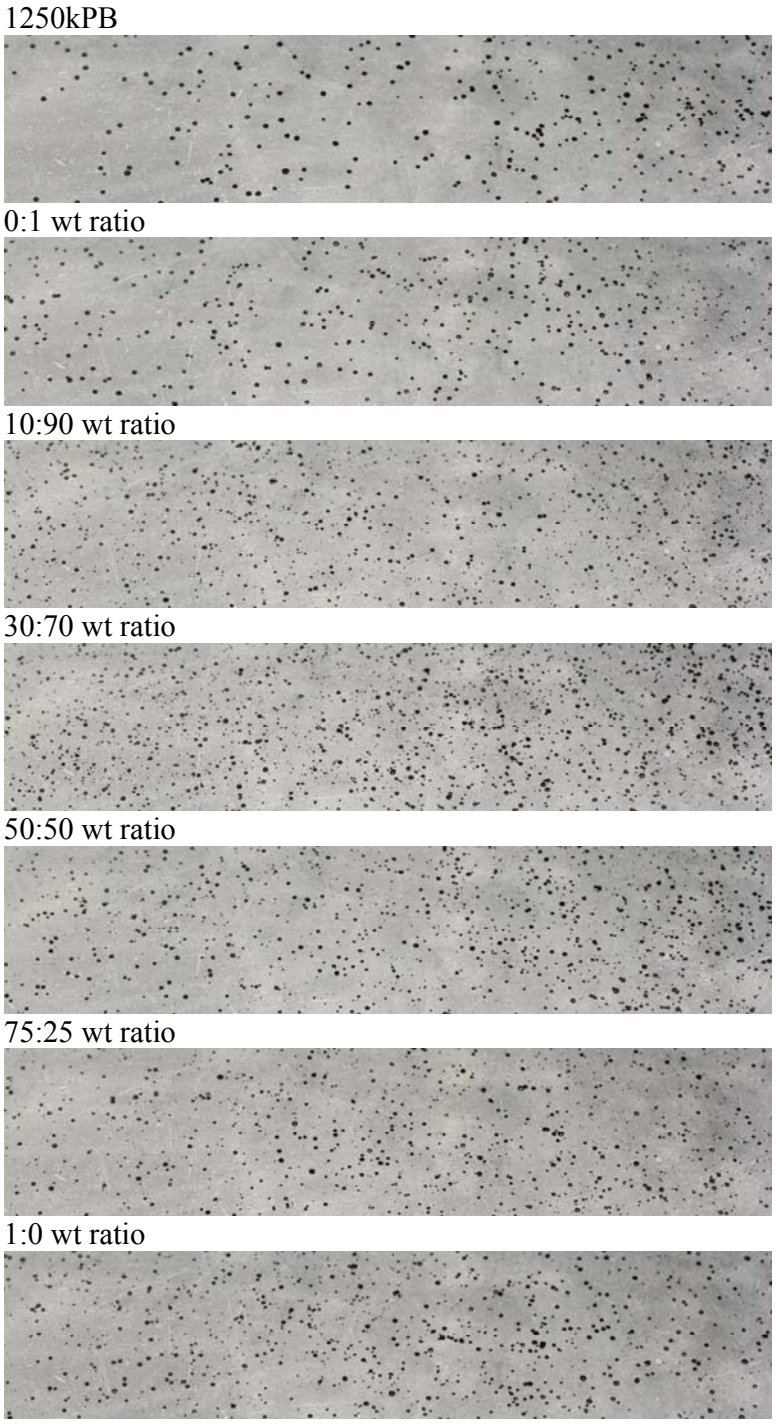

Figure 3.14 Mixture of 1250kPB0.4A and 1250kPB1.5N polymers at total concentration of 2500 ppm by wt in Jet-A, as a function of increasing wt ratio of 1250kPB1.5N to 1250kPB0.6A polymers. The top image corresponds to a reference solution of 1250kPB prepolymer.

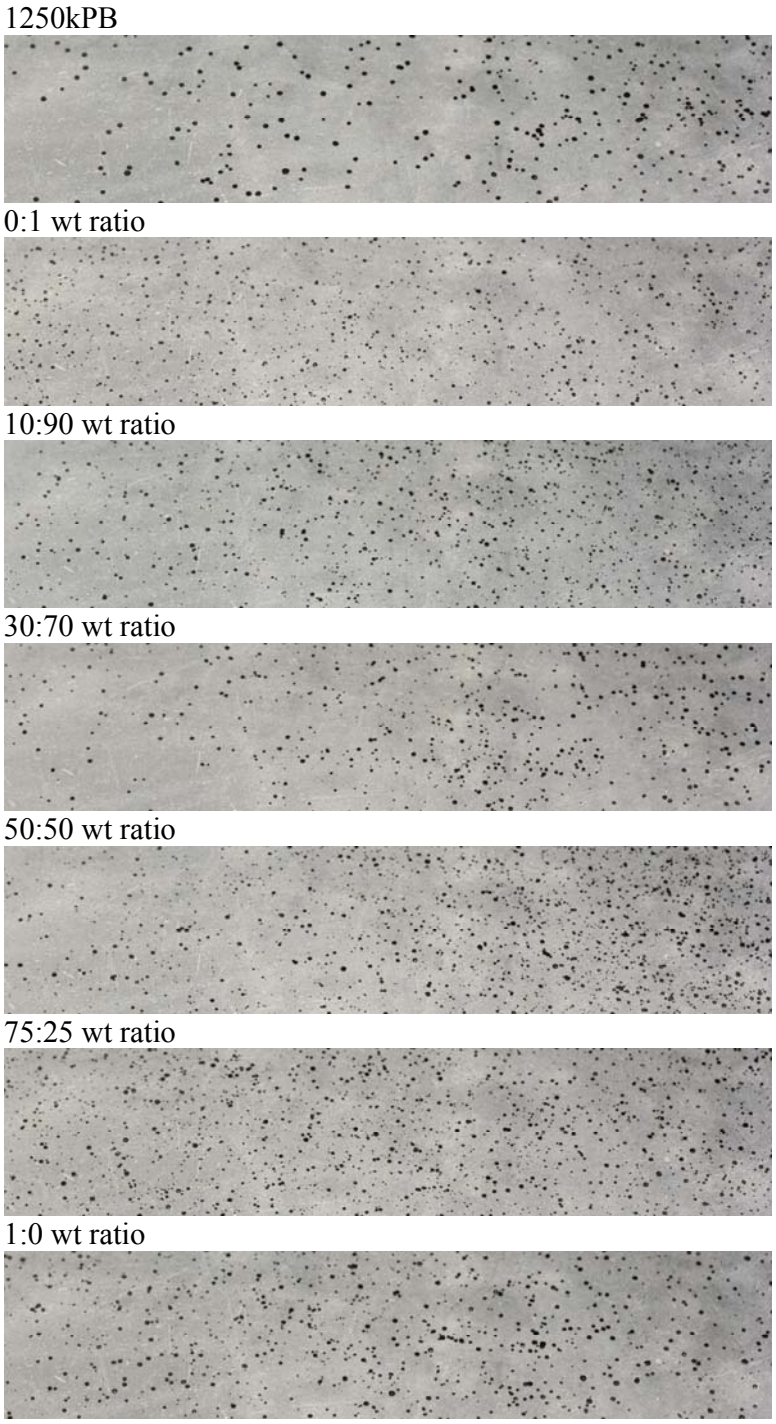

Figure 3.15 Mixture of 1250kPB0.3A and 1250kPB1.5N polymers at total concentration of 2500 ppm by wt in Jet-A, as a function of increasing wt ratio of 1250kPB1.5N to 1250kPB0.6A polymers. The top image corresponds to a reference solution of 1250kPB prepolymer.

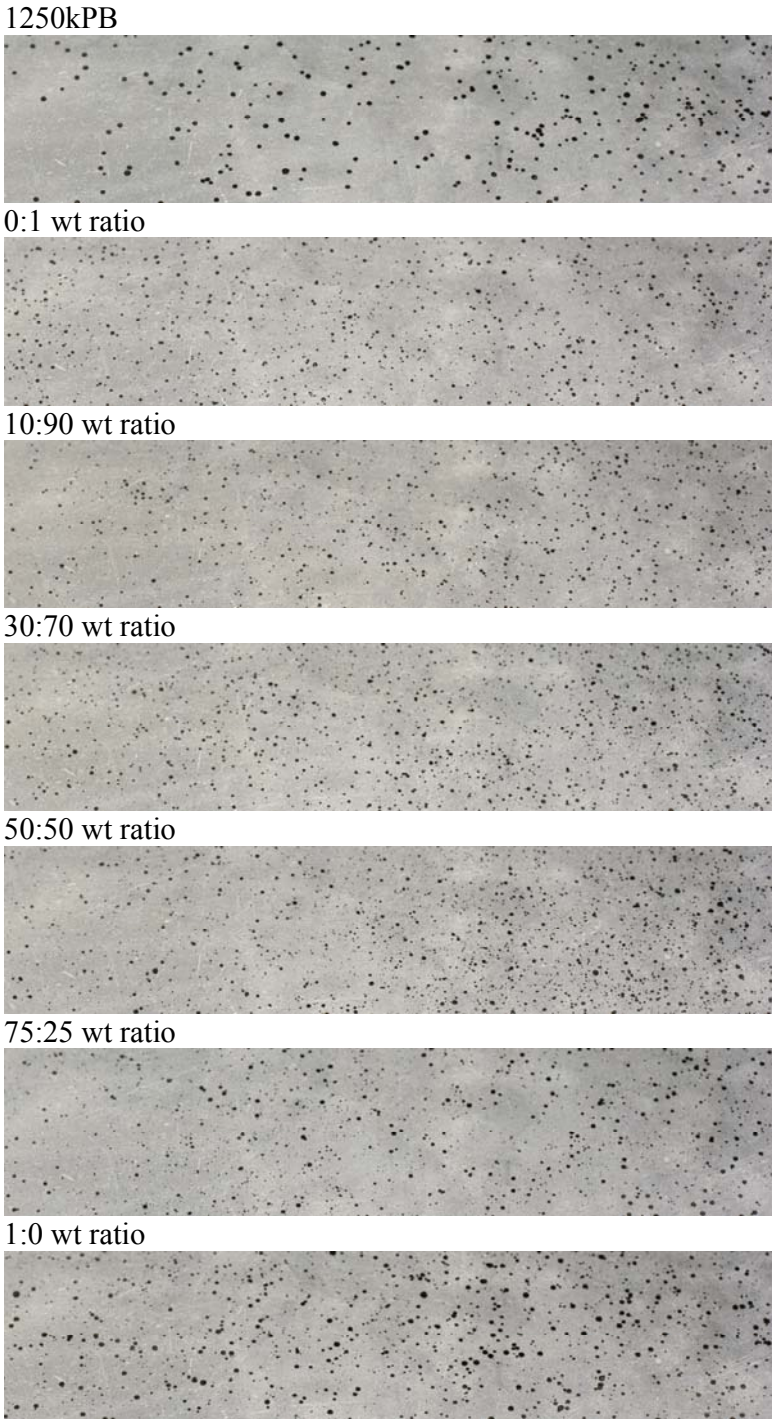

Figure 3.16 Mixture of 1250kPB0.3A and 1250kPB2.6N polymers at total concentration of 2500 ppm by wt in Jet-A, as a function of increasing wt ratio of 1250kPB1.5N to 1250kPB0.6A polymers. The top image corresponds to a reference solution of 1250kPB prepolymer.

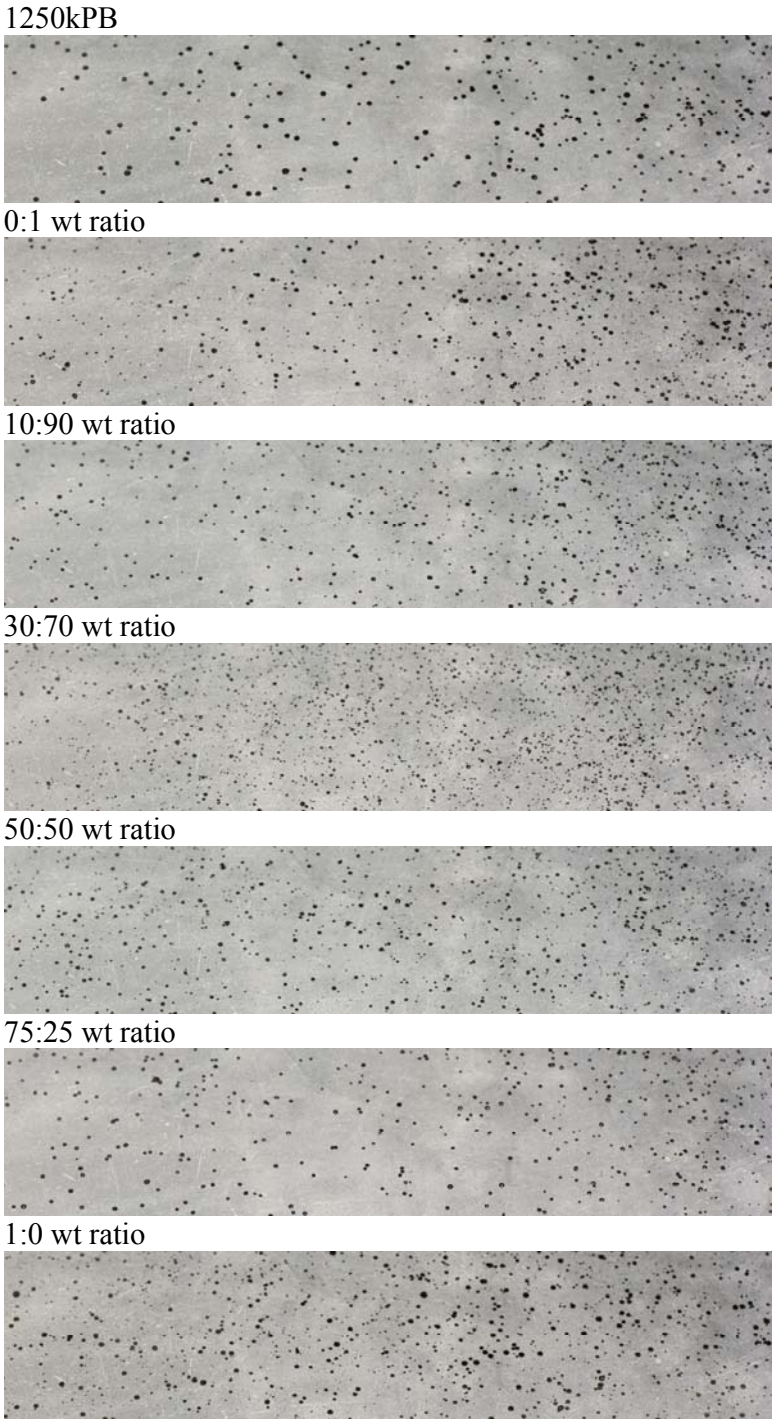

Figure 3.17 Mixture of 1250kPB0.2A and 1250kPB2.6N polymers at total concentration of 2500 ppm by wt in Jet-A, as a function of increasing wt ratio of 1250kPB1.5N to 1250kPB0.6A polymers. The top image corresponds to a reference solution of 1250kPB prepolymer.

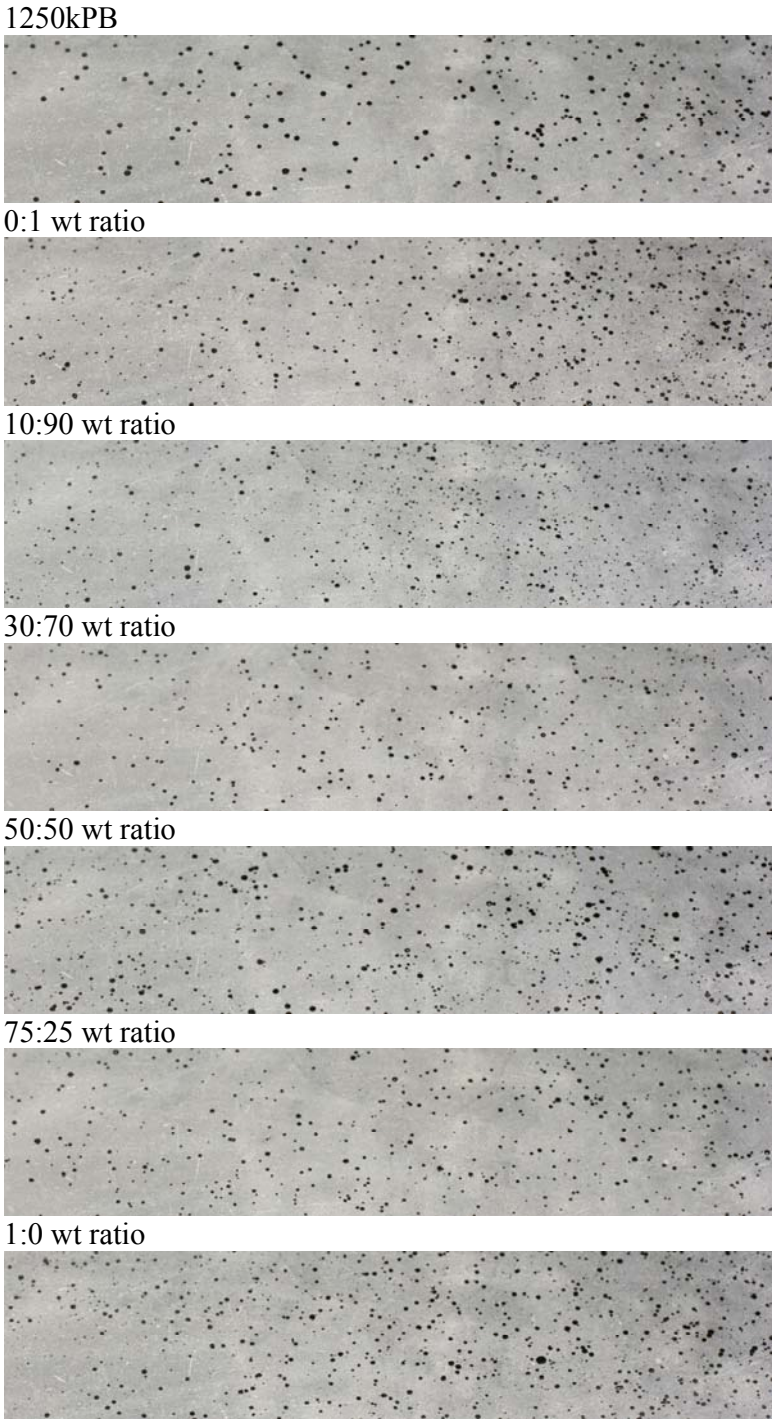

Figure 3.18 Mixture of 1250kPB0.2A and 1250kPB5.4N polymers at total concentration of 2500 ppm by wt in Jet-A, as a function of increasing wt ratio of 1250kPB1.5N to 1250kPB0.6A polymers. The top image corresponds to a reference solution of 1250kPB prepolymer.

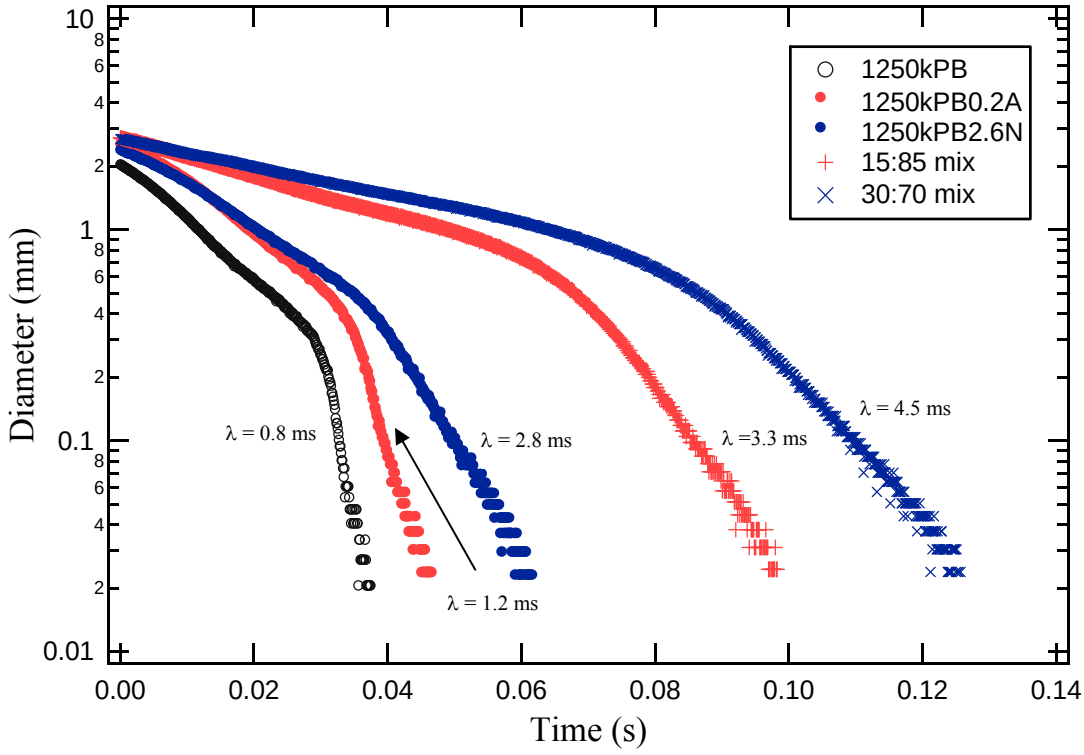

Figure 3.19 Time evolution of filament diameter during capillary breakup experiments for mixtures of 1250k2.6N and 1250k0.2A polymers in 15:85 and 30:70 wt ratios, and for appropriate reference solutions, at 1.5 wt % total polymer content in Jet-A (corresponding to $c = 6c^*$ for 1250kPB prepolymer). All tests were performed with 8 mm diameter plates, at initial and final aspect ratios of 1.0 and 2.2, respectively. Solution shear viscosities were 48 mPa.s, 62 mPa.s, and 77 mPa.s for the 1250kPB, 1250kPB0.2A, and 1250kPB2.6N reference solutions, and 130 mPa.s and 180 mPa.s for the 85:15 and 70:30 mixtures, respectively. The characteristic relaxation times of the solutions, determined from the slope of the exponential decay of the filament diameter vs. time, are represented on the figure.

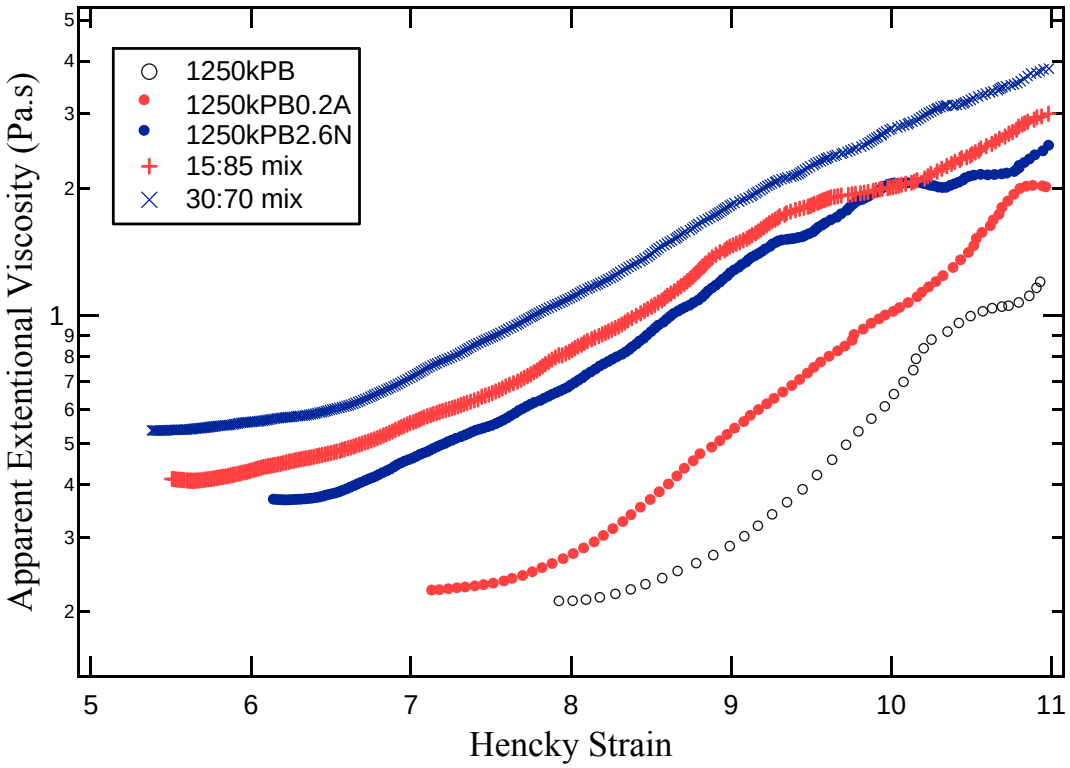

Figure 3.20 Effect of acid-base complementary associations on apparent extentional viscosity during capillary breakup rheology (refer to Figure 3.19 for experimental details).

Scheme 3.1 Preparation of Functionalized 1250 kg/mol 1,4-Polybutadiene Molecules Used in the Present Study: Thiol-Ene Addition of (a) 3-Mercaptopropionic Acid, and (b) Dimethylaminoethanethiol Hydrochloride

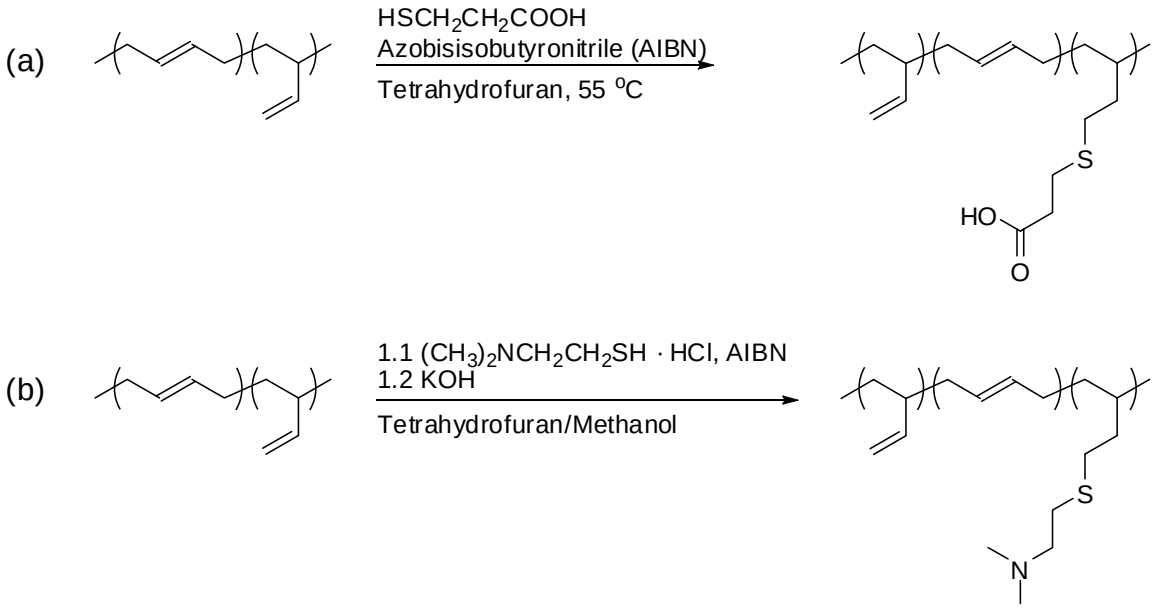

Table 3.1 Reaction Conditions[a] and Results for Functionalization of 1250 kg/mol 1,4-Polybutadiene

Entry[b]	[PB] (g/mL)	[RSH][c]	[AIBN] (mg/mL)	Rxn time (hrs)	Funct.[d] %	PDI[e]
1250kPB1.5N	0.008	2.8	0.86	7.0	1.5	-
1250kPB2.6N[f]	0.011	13	1.1	11[h]	2.6	-
1250kPB5.4N	0.009	20	1.1	12[i]	5.4	-
1250kPB0.2A[g]	0.010	12	0.46	0.58	0.2	1.15
1250kPB0.3A	0.009	16	0.62	0.55	0.3	1.29
1250kPB0.4A	0.009	16	0.52	1.1	0.4	1.17
1250kPB0.6A	0.009	16	0.54	1.2	0.6	1.23

[a]In all cases, reactions were run in THF for functionalization with MPA, and ~ 9:1 THF: methanol for functionalization with DMAET. [b]Functionalized PB polymers were named so that the prefix corresponds to the molecular weight of the precursor chain, and the suffix represents the mol % of monomers bearing functional groups (abbreviated as N for DMAET and A for MPA). [c]In molar equivalent of 1,2-PB units, which are 98% of the units of 510kPB and 8% of the units of 1250kPB. [d]Molar fraction of functionalized monomers based on the total number of PB monomers (both 1,2 and 1,4 units). [e]The 1250kPB prepolymer had a PDI value of 1.09. [f] ^{1}H NMR spectrum shown in Figure 3.5. [g]GPC trace given in Figure 2.4. [h]Reaction temperature was 50 ºC instead of 55 ºC. [i]First 9 hrs at 55 ºC and last 3 hrs at 65 ºC.

Table 3.2 Reaction Conditions[a] and Results for Functionalization of 510 kg/mol 1,2-Polybutadiene

Entry[b]	PB (g)	RSH[c]	AIBN (mg)	Rxn time (hrs)	Funct.[d] %	PDI[e]
510kPB1.6N[f]	0.55	3.9%	11	1.1	1.6	~ 1.2
510kPB4.0N	0.54	9.5%	10	1.1	4.0	~ 1.2
510kPB6.6N	~ 0.3	~ 20%	~ 10	~ 1	6.6	~ 1.2

[a]In all cases, reactions were run in 30 mL of a mixture of THF and methanol in 9:1 volume ratio. [b]Functionalized PB polymers were named as described in the footnote of Table 3.1. [c]In molar equivalent of 1,2-PB units. [d]Molar fraction of functionalized monomers. [e]The 510kPB prepolymer had a PDI value of 1.15. [f]GPC trace given in Figure 3.6.

Table 3.3 Phase Behavior[a] of Mixtures of 1250kPB Proton-Donating and Proton-Accepting Chains in Jet-A Solvent

	0.2% A[b]	0.3% A	0.4% A	0.6% A
1.5% N[c]				
2.6% N				
5.4% N				

[a]Shaded boxes correspond to phase separated mixtures, at 25 ºC and total polymer concentrations of 0.25 wt %. [b]The degree of functionalization with 3-mercaptopropionic acid. [c]The degree of functionalization with 2-(dimethylamino)ethanethiol.

Table 3.4 Summary of Experiments[a] Conducted on Mixtures of 1250kPB Proton-Donating and Proton-Accepting Chains in Jet-A Solvent

	0.2% A[b]	0.3% A	0.4% A	0.6% A
1.5% N[c]				
2.6% N	**CaBER**	**Drop Breakup**		
5.4% N				

[a]Shaded boxes correspond to mixtures for which spray experiments, as well as shear viscosity and size measurements were made for solutions at 25 ºC and total polymer concentrations of 0.25 wt %. [b]The degree of functionalization with 3-mercaptopropionic acid. [c]The degree of functionalization with 2-(dimethylamino)ethanethiol.

3.6 References and Notes

1. Kowalik, R. M.; Duvdevani, I.; Peiffer, D. G.; Lundberg, R. D.; Kitano, K.; Schulz, D. N., Enhanced drag reduction via interpolymer associations. *Journal of Non-Newtonian Fluid Mechanics* **1987,** 24, (1), 1–10.

2. Refer to Chapter 1, Section 1.2.2. Malik and Mashelkar (see reference 3 below) reported that interpolymer complexation resulted in large aggregates with drag-reduction activity up to 6 times greater than that of non-associating counterparts, and further that interpolymer complexation increased shear-stability of the polymer components compared to the stability of the individual components by themselves.

3. Malik, S.; Mashelkar, R. A., Hydrogen-bonding mediated shear stable clusters as drag reducers. *Chemical Engineering Science* **1995,** 50, (1), 105–116.

4. Xiang, M. L.; Jiang, M.; Zhang, Y. B.; Wu, C.; Feng, L. X., Intermacromolecular complexation due to specific interactions .4. The hydrogen-bonding complex of vinylphenol-containing copolymer and vinylpyridine-containing copolymer. *Macromolecules* **1997,** 30, (8), 2313–2319.

5. Qi, G. R.; Wang, Y. H.; Li, X. X.; Peng, H. Y.; Yang, S. L., Viscometric study on the specific interaction between proton-donating polymers and proton-accepting polymers. *Journal of Applied Polymer Science* **2002,** 85, (2), 415–421.

6. Wang, Y. H.; Qi, G. R.; Li, H. L.; Yang, S. L., Effect of chain compositions on interpolymer specific interaction in solutions. *European Polymer Journal* **2002,** 38, (7), 1391–1397.

7. Wang, Y. H.; Qi, G. R.; Peng, H. Y.; Yang, S. L., Interpolymer specific interaction in blends of poly(styrene-co-alkyl acrylate-co-4-vinylpyridine) and poly(styrene-co-alkyl acrylate-co-acrylic acid). *Polymer* **2002,** 43, (9), 2811–2818.

8. Qiu, X. P.; Jiang, M., Intermacromolecular complexation due to specific interactions .1. The hydrogen-bonding complex between poly(methyl methacrylate) and modified polystyrene. *Polymer* **1994,** 35, (23), 5084–5090.

9. Qiu, X. P.; Jiang, M., Intermacromolecular complexation due to specific interactions .3. Miscibility and complexation of Pbma and Ps(Oh). *Polymer* **1995,** 36, (18), 3601–3604.

10. Refer to Section 2.3.2

11. Yu, J. H.; Fridrikh, S. V.; Rutledge, G. C., The role of elasticity in the formation of electrospun fibers. *Polymer* **2006,** 47, (13), 4789–4797.

12. Refer to Section 2.3.6.1

13. Attempts were made, without success, to make capillary breakup measurements of dilute 1250 kg/mol PB chains in a solvent of enhanced shear viscosity, such as Jet-A containing 3–15 wt % 50–500 kg/mol polyisobutylene or polyisoprene chains. In all such attempts solution shear viscosity was still too low to enable elasticity measurements of the 1250 kg/mol PB solutions, or the 1250 kg/mol PB chains phase separated.

14. Schulz, D. N.; Kitano, K.; Duvdevani, I.; Kowalik, R. M.; Eckert, J. A., Hydrocarbon-soluble associating polymers as antimisting and drag-reducing agents. *ACS Symposium Series* **1991,** 462, 176–189.

Chapter IV Modeling of the Association Behavior of Linear Chains with Strongly Associating Endgroups

4.1 Introduction

Our work so far has investigated whether linear chains possessing associating functional groups grafted at random positions along the entire chains can be useful as mist-control additives to aviation fuel. Molecular designs involving both self-associating interactions and donor-acceptor interactions were studied, and the effects of extent of functionalization as well as concentration of polymer components on shear and extensional rheology of dilute solutions in non-polar hydrocarbon solvents were examined. We have found that for both self-associating and donor-acceptor systems, intra- and intermolecular associations cause collapse of the chains and interfere with the mechanism of mist control by inhibiting stretching of the chain in extentional flow. In this chapter, we consider molecular designs that overcome chain collapse by clustering associating groups at the ends of polymer chains. In particular, we construct a model that predicts, for long linear chains endcapped with strongly associating A and B groups, the equilibrium partitioning of the polymer into supramolecular linear chains and supramolecular loops of all sizes (Scheme 4.1). We assume that the A and B endgroups associate with each other pair-wise with interaction energy εkT, but that neither the A nor the B endgroups self-associate.

4.2 Theoretical

To model the equilibrium aggregation of telechelic polymers A----A and B----B into supramolecular cyclic and linear chains of any length (Scheme 4.1), we consider the simpler case of association of telechelic polymers A_1----A_2 and B_1----B_2, and argue that results are the same (Section 4.2.6). In doing so, we assume that the end-groups A_1 and A_2, and likewise B_1 and B_2, are distinguishable but of identical reactivity (as might be the case, for example, if one atom of A_1 were a different isotope than the corresponding atom of A_2). What is the equilibrium distribution of all the aggregates for a given energy of association εkT? We can estimate this equilibrium assuming ideal solutions by making use of the following lattice model.[1]

4.2.1 Model Description

Consider a solution composed of N_s solvent molecules and N_{Atotal} and N_{Btotal} telechelic A_1----A_2 and B_1----B_2 chains, of respective length M_A and M_B elementary units (monomers). The solution volume V is partitioned into lattice sites of volume a^3, where a^3 is the volume of a solvent molecule and also the volume of a monomer. We will assume that there is no volume change upon mixing, so that $V = a^3(N_s + N_{Atotal}M_A + N_{Btotal}M_B) = \Lambda a^3$, where Λ is the total number of "sites." We will use the subscript s to refer to the solvent and the subscripts i or j to refer to single-chain and supramolecular components. Unless otherwise specified, sums $\sum_j$ are over all polymer components in solution, i.e., the telechelic starting materials and all polymer aggregates. The volume fractions of solvent and polymer component j are $\phi_s = N_s/\Lambda$ and $\phi_j = N_jM_j/\Lambda$, where M_j is the number of monomers of polymer component j. Let $\phi = \sum_j M_jN_j/\Lambda = 1-\phi_s$ denote the total polymer volume fraction in solution. The center-of-mass and configurational entropy of the polymer components and solvent is:

$$S = k\sum_j \ln \Omega(0, N_j) + \Delta S_{mix} \tag{4.1}$$

where $\Omega(0,N_j)$ is the number of possible configurations of N_j molecules of polymer component j, each of length M_j, onto M_jN_j sites (referring to pure polymer before mixing), so that the sum accounts for the entropy of all the polymer components before mixing. Here we have retained the notation of Hill[2] for the entropy of a pure solution of N_i linear polymer chains of length M_i:

$$\ln \Omega(0, N_i) = -N_i \ln N_i + N_i + M_iN_i \ln(M_iN_i) - M_iN_i + N_i(M_i - 1)\ln\left(\frac{c-1}{M_iN_i}\right) \tag{4.2}$$

where c is the coordination number, i.e., the number of sites neighboring any given monomer where the next monomer on the chain may be found. The entropy of mixing of the solvent and all polymer components, $\Delta S_{mix,}$ is approximated using the Flory-Huggins expression:

$$\Delta S_{mix} = -k\left(N_s \ln \phi_s + \sum_j N_j \ln \phi_j\right). \tag{4.3}$$

Equation 4.1 does not account for the entropic cost of loop closure for supramolecular cycles; that contribution will instead be absorbed into the standard chemical potential of the cyclic components, as discussed later. The entropic contribution to the mixture's free energy is therefore:

$$\begin{aligned} F_S &= -T\Delta S_{mix} - kT\sum_j \ln\Omega(0,N_j) \\ &= kT\left[N_s \ln\left(\frac{N_s}{\Omega}\right) + \sum_j N_j \ln\left(\frac{N_j}{\Omega}\right)\right] + kT\sum_j N_j \ln\left(M_j\right) - kT\sum_j \ln\Omega(0,N_j). \end{aligned} \tag{4.4}$$

Next, the contribution to the solution free energy due to solvent-solvent, polymer-solvent, and polymer-polymer interactions is estimated by the random mixing approximation:

$$F_{int} = \Omega\delta\left[(1-\phi)^2 h_{ss} + \phi^2 h_{pp} + 2\phi(1-\phi)h_{ps}\right] \tag{4.5}$$

where δ is one-half the local coordination number, and h_{ij} are the microscopic interaction energies of the polymer and solvent species. The total free energy F of the solution is the sum of F_S, F_{int}, and of contributions from the internal free energy of solvent and polymer components:

$$F = F_{int} + F_S + N_s\mu_s^0 + \sum_j N_j\mu_j^0 \tag{4.6}$$

where μ_i^0 is the standard chemical potential of the single-chain or supramolecular chain component i. Using $\phi = (M_iN_i + \sum_{j\neq i} M_jN_j)/\Lambda$ with $\Lambda = N_s + M_iN_i + \sum_{j\neq i} M_jN_j$, the contribution to the chemical potential of polymer component i due to interactions is:

$$\mu_{int,i} = \left.\frac{\partial F_{int}}{\partial N_i}\right|_{N_{j\neq i}} = -\omega M_i\phi_s^2 + \omega_{pp}M_i \tag{4.7}$$

where for convenience we have introduced $\omega_{mn} = \delta h_{mn}$ and $\omega = \omega_{pp} + \omega_{ss} - 2\,\omega_{ps}$. The entropic contribution to the chemical potential of polymer component i is:

$$\begin{aligned} \frac{\mu_{S,i}}{kT} = \frac{1}{kT}\left.\frac{\partial F_S}{\partial N_i}\right|_{N_{j\neq i}} &= \ln\left(\frac{\phi_i}{M_i}\right) + 1 - \phi_i - M_i\left[\phi_s + \sum_{j\neq i}\frac{\phi_j}{M_j}\right] + \ln M_i \\ &\quad -1 - M_i\left[\ln(c-1) - 1\right] - \ln M_i + \ln(c-1) \end{aligned} \tag{4.8}$$

or, after rearranging:

$$\frac{1}{kT}\left.\frac{\partial F_S}{\partial N_i}\right|_{N_{j\neq i}} = \ln\left(\frac{\phi_i}{M_i}\right) - M_i\left[\phi_s + \sum_j \frac{\phi_j}{M_j}\right] + f_i \tag{4.9}$$

where f_i = ln(c-1) + M_i[1-ln(c-1)]. Differentiation of Equation 4.6 and substitution of Equations 4.7 and 4.9 give the following expression for the chemical potential of component i, valid for the single-chain building blocks and all aggregates:

$$\mu_i = \left.\frac{\partial F}{\partial N_i}\right|_{N_{j\neq i}} = \mu_i^0 + kT\left\{\ln\left(\frac{\phi_i}{M_i}\right) - M_i\left[\phi_s + \sum_j \frac{\phi_j}{M_j}\right] + f_i\right\} - \omega M_i \phi_s^2 + \omega_{pp} M_i . \quad (4.10)$$

Consider a supramolecular component i made up of n_i A_1----A_2 building blocks and m_i B_1----B_2 building blocks: its size is $M_i = n_i M_A + m_i M_B$. At the equilibrium partitioning of the telechelic building blocks into aggregates of all size, its chemical potential satisfies the equilibrium condition:

$$\mu_i = n_i \mu_A + m_i \mu_B \quad (4.11)$$

where μ_A and μ_B are the chemical potentials of building blocks A_1----A_2 and B_1----B_2, respectively. Substituting the expressions for μ_i, μ_A, and μ_B from Equation 4.10 into Equation 4.11 above, we obtain, after rearrangement, the following mass-action relation for polymer component i:

$$\mu_i^0 + kT\left[\ln\left(\frac{\phi_i}{M_i}\right) + f_i\right] = n_i\mu_A^0 + m_i\mu_B^0 + kT\left[n_i \ln\left(\frac{\phi_A}{M_A}\right) + m_i \ln\left(\frac{\phi_B}{M_B}\right) + n_i f_A + m_i f_B\right] \quad (4.12)$$

where ϕ_A, ϕ_B are the volume fractions of the telechelic building blocks A_1----A_2 and B_1----B_2, respectively. Equation 4.12 above can be rewritten as follows:

$$\left(\frac{\phi_i}{n_i M_A + m_i M_B}\right) = \left(\frac{\phi_A}{M_A}\right)^{n_i}\left(\frac{\phi_B}{M_B}\right)^{m_i} \exp(\Gamma_i) \quad (4.13)$$

where
$$\Gamma_i = \frac{1}{kT}(n_i\mu_A^0 + m_i\mu_B^0 - \mu_i^0) + (n_i + m_i - 1)\ln(c-1). \quad (4.14)$$

The conservation equations are then:

$$\begin{aligned}
\phi_{Atotal} &= \sum_j \phi_j \left(\frac{n_j M_A}{n_j M_A + m_j M_B}\right) = \sum_j n_j M_A \left(\frac{\phi_A}{M_A}\right)^{n_j}\left(\frac{\phi_B}{M_B}\right)^{m_j} \exp(\Gamma_j) \\
\phi_{Btotal} &= \sum_j \phi_j \left(\frac{m_j M_B}{n_j M_A + m_j M_B}\right) = \sum_j m_j M_B \left(\frac{\phi_A}{M_A}\right)^{n_j}\left(\frac{\phi_B}{M_B}\right)^{m_j} \exp(\Gamma_j).
\end{aligned} \quad (4.15)$$

In our construction of the model, terms arising from microscopic interactions, as well as terms arising from the center-of-mass and configurational entropy (except loop closure) of polymer components and solvent in solution have been carried out explicitly. On the other hand, terms arising from (i) the energy of association of the endgroups within a polymer aggregate, and (ii) the entropic cost of loop closure for cyclic supramolecular aggregates, are instead absorbed into the standard chemical potentials μ_j^0 of the aggregates. We now proceed to derive expressions accounting for these effects.

4.2.2 Entropic Cost of Loop Closure

The entropic cost of loop closure is determined by calculating the probability of loop closure, as follows: For Gaussian linear chains of N Kuhn monomers of length b, the probability density function for the end-to-end vector $\mathbf{r}$ is:[3]

$$G_{Gaussian}(\mathbf{r},N)=\left(\frac{3}{2\pi Nb^2}\right)^{\frac{3}{2}}\exp\left\{-\frac{3\mathbf{r}^2}{2Nb^2}\right\}. \tag{4.16}$$

The argument within the exponential is $-3\mathbf{r}^2/(2Nb^2) \cong 0$ for $\|\mathbf{r}\| << \langle\mathbf{r}^2\rangle^{1/2}$, so the probability that the chain ends be within a small distance x of each other, where $x/b \sim O(1)$, is:

$$\begin{aligned} G_{cyc,Gaussian} &= \left(\frac{3}{2\pi Nb^2}\right)^{\frac{3}{2}}\int_0^{2\pi}d\phi\int_0^{\pi}d\theta\sin\theta\int_0^{a}dr\cdot r^2\exp(0) \\ &= 4\pi\left(\frac{3}{2\pi Nb^2}\right)^{\frac{3}{2}}\int_0^{a}dr\cdot r^2\exp(0)=\left(\frac{6}{\pi N^3}\right)^{\frac{1}{2}}\left(\frac{x}{b}\right)^3. \end{aligned} \tag{4.17}$$

For real chains, excluded volume interactions of the monomers at chain ends reduce the probability density function $G(\mathbf{r},N)$ by the factor

$$\frac{G_{real}(\mathbf{r},N)}{G_{Gaussian}(\mathbf{r},N)}\sim\left(\frac{\|\mathbf{r}\|}{\sqrt{\langle\mathbf{r}^2\rangle}}\right)^g \qquad \text{for } \frac{\|\mathbf{r}\|}{\sqrt{\langle\mathbf{r}^2\rangle}}<<1 \tag{4.18}$$

where the exponent $g \cong 0.28$,[4] so that the probability of cyclization becomes

$$G_{cyc,real}\approx 4\pi\left(\frac{3}{2\pi Nb^2}\right)^{\frac{3}{2}}\left(\frac{1}{bN^{\nu}}\right)^g\int_0^{a}dr\cdot r^{2+g}\exp(0)\sim N^{-3/2-g\nu} \tag{4.19}$$

where the fractal exponent ν is 0.588 in good solvent. The loop closure probability thus scales as $N^{-3/2}$ for Gaussian chains and $N^{-1.66}$ for swollen chains. The entropic cost of loop closure is simply $\Delta S_{loop} = -k\ln G_{cyc}$.

In dilute or semi-dilute solutions, all chain segments smaller than the thermal blob $g_T \approx b^6/v^2$ (where v is the excluded volume parameter) have nearly Gaussian statistics because excluded volume interactions are weaker than the thermal energy. If, for our solution composed of any number of different (single and supramolecular) chains j of size M_j, at total polymer volume fraction $\phi = \sum_j \phi_j$, we assume that the polymer chains are dilute enough to ignore polymer-polymer interactions, we can use the following expression in the calculation of the entropic cost of loop closure $\Delta S_{loop} = -k\ln G_{cyc}$ for any cyclic aggregate q:

$$G_{cyc,q} \approx \left(\frac{6}{\pi g_T^3}\right)^{\frac{1}{2}} \left(\frac{x}{b}\right)^3 \left(\frac{M_q}{g_T}\right)^{-1.66} . \tag{4.20}$$

By doing so we are simply assuming that all chain segments larger than g_T are fully swollen.

4.2.3 Inventory of Polymer Components

As a starting point in classifying the polymer aggregates, we group them together as shown in Figure 4.1. Let index g refer to groups, and ϕ_g refer to the cumulative volume fraction of all the polymer components that belong to group g. All the polymer components j that belong to any particular group g have the same values of $M_j = M_g$, $n_j = n_g$, $m_j = m_g$, and $\Gamma_j = \Gamma_g$, so the equilibrium condition and the conservation equations can be rewritten as:

$$\left(\frac{\phi_g}{n_g M_g + m_g M_g}\right) = \Omega_g \left(\frac{\phi_A}{M_A}\right)^{n_g} \left(\frac{\phi_B}{M_B}\right)^{m_g} \exp(\Gamma_g) \tag{4.21}$$

$$\begin{aligned} \phi_{Atotal} &= \sum_g n_g M_A \Omega_g \left(\frac{\phi_A}{M_A}\right)^{n_g} \left(\frac{\phi_B}{M_B}\right)^{m_g} \exp(\Gamma_g) \\ \phi_{Btotal} &= \sum_g m_g M_B \Omega_g \left(\frac{\phi_A}{M_A}\right)^{n_g} \left(\frac{\phi_B}{M_B}\right)^{m_g} \exp(\Gamma_g) \end{aligned} \tag{4.22}$$

where Ω_g refers to the number of distinct species in group g.

How many components belong to each group? For linear aggregates there are two possibilities: (i) if $n_g + m_g$ is even (i.e., $n_g = m_g$), then no sequence read from left to right will

be the same as a sequence read from right to left, so the number of ways to arrange the molecules is $\Omega_g = 2^{n_g+m_g}$; (ii) if $n_g + m_g$ is odd, then every sequence read from left to right will have a matching sequence read from right to left, so the number of ways to arrange the molecules is $\Omega_g = 2^{n_g+m_g-1}$. Supramolecular cycles can only be formed if $n_g = m_g$. The number of ways to form such a loop is derived below; to a very good approximation it is $\Omega_{cyc,g} = 2 + (2^{2n_g-1} - 2)/n_g$.

4.2.4 Number of Ways to Form Loops

We seek to determine the number of different loops that can be formed by linking n A_1----A_2 and n B_1----B_2 telechelic chains end-to-end via association of A and B endgroups, as shown in Figure 4.2 (left). We are assuming that A_1 groups are distinguishable from A_2 groups, and likewise B_1 groups are distinguishable from B_2 groups, but that the n A_1----A_2 molecules are indistinguishable, and likewise are the n B_1----B_2 molecules. The question is equivalent to the combinatorial problem of counting necklaces formed using beads of different colors, in which two necklaces are considered equivalent if one can be rotated to give the other. The way to recognize the equivalence is to break up the loops into adjacent pairs of telechelics (with one A_1----A_2 and one B_1----B_2 molecule per pair), and map the loops into necklaces made up of n beads of 4 different colors as shown in Figure 4.2. The formula for the number of different necklaces is:[5]

$$m(n) = \frac{1}{n}\sum_{d|n}\left[\varphi(d)\cdot 4^{n/d}\right] \tag{4.23}$$

where the sum is over all numbers d that divide n, and $\varphi(d)$ is the Euler phi function.

In reality, the above formula overcounts the number of ways to form polymer loops by a factor of 2. To see this, observe that any loop can be "read" in two ways (clockwise and counter-clockwise) to give two *distinct* necklaces. This is true because we cannot create an arbitrary loop which can be "read" the same clockwise and counterclockwise, no matter where we begin to read (Figure 4.3). Consider now the $m(n)$ distinct necklaces obtained from n beads, and the $s(n)$ distinct loops obtained from n A_1----A_2 and n B_1----B_2 telechelic chains, forming sets $\{\text{necklaces}_n\}$ and $\{\text{loops}_n\}$. Each necklace in $\{\text{necklaces}_n\}$ uniquely maps into a polymer loop in the set $\{\text{loops}_n\}$, but every loop in $\{\text{loops}_n\}$ maps back to two different necklaces, which must belong to $\{\text{necklaces}_n\}$. The elements of $\{\text{necklaces}_n\}$ can therefore

be arranged pairwise as shown in Figure 4.4, revealing that there are twice as many elements in {necklaces$_n$} than in {loops$_n$}. The number of distinct loops $s(n)$ that can be formed by linking n A_1----A_2 and n B_1----B_2 telechelic chains end-to-end via association of A and B endgroups is therefore:

$$s(n) = \frac{1}{2n}\sum_{d|n}\left[\varphi(d)\cdot 4^{n/d}\right]. \tag{4.24}$$

4.2.5 Standard Chemical Potential of Polymer Aggregates

In Equations 4.13–4.15 and 4.21–4.22, we chose to absorb into the expressions for the standard chemical potential of the aggregates μ_j^0 the contributions due to the energy of association of the endgroups and to the entropic cost of loop closure. The equation for the standard chemical potential of any polymer component j within group g is therefore:

$$\mu_g^0 = \begin{cases} n_g\mu_A^0 + m_g\mu_B^0 - \varepsilon kT(n_g+m_g) - kT\ln G_{cycl,g} & \text{if cyclic} \\ n_g\mu_A^0 + m_g\mu_B^0 - \varepsilon kT(n_g+m_g-1) & \text{if linear,} \end{cases} \tag{4.25}$$

so that Γ_g in the equilibrium and conservation relationships (Equation 4.21 and 4.22) is:

$$\Gamma_g = \begin{cases} \varepsilon(n_g+m_i) + (n_i+m_i-1)\ln(c-1) + \ln G_{cycl,g} & \text{if cyclic} \\ \varepsilon(n_g+m_g-1) + (n_g+m_g-1)\ln(c-1) & \text{if linear.} \end{cases} \tag{4.26}$$

4.2.6 Distinguishable versus Indistinguishable Endgroups

Consider the reversible association reactions shown in Scheme 4.2 (endgroups are indistinguishable in case b, but distinguishable in c). In each of cases a, b, and c, let ϕ_A and ϕ_B be the volume fractions of the starting materials, and ϕ_{dimer} be the total volume fraction of product dimers. For the product in case a and each of the products in case c, the equilibrium condition (Equation 4.13) is the same:

$$\left(\frac{\phi_{dimer}}{M_A+M_B}\right) = \left(\frac{\phi_A}{M_A}\right)\left(\frac{\phi_B}{M_B}\right)\exp(\Gamma) \qquad \text{in case a} \tag{4.27}$$

and

$$\left(\frac{\tfrac{1}{4}\phi_{dimer}}{M_A+M_B}\right) = \left(\frac{\phi_A}{M_A}\right)\left(\frac{\phi_B}{M_B}\right)\exp(\Gamma) \qquad \text{in case c} \tag{4.28}$$

where M_A and M_B are the number of monomers in the starting materials, and $\Gamma = \varepsilon + \ln(c\text{-}1)$ according to Equation 4.26. In Equation 4.28, ¼ ϕ_{dimer} is the volume fraction of each of the product dimers, so the difference in Equations 4.27 and 4.28 simply reflects the difference in the number of ways to form dimers, i.e., $\Omega_c = 4$ while $\Omega_a = 1$. The correspondingly larger equilibrium fraction of dimers in case c can be intuitively understood to be a mere consequence of the increased contact probability of the endgroups to form the product: the rate of dissociation of dimers is equal in both cases, but the rate of association of reactants is expected to be 4 times greater in case b.

What is the equilibrium condition for the total volume fraction of product dimers in case b? If the endgroups A, A_1, and A_2 have precisely the same reactivity, and likewise the endgroups B, B_1, and B_2, there cannot be any difference in the equilibrium partitioning of the molecules in cases b and case c, so that the equilibrium condition for case b is Equation 4.28, not Equation 4.27. We generalize this argument to conclude that the solution to the equilibrium problem presented in Scheme 4.1, where endgroups are indistinguishable, is expected to be that solution which we developed for telechelics A_1----A_2 and B_1----B_2, where endgroups are distinguishable. A less careful modeling of the association of telechelic polymers A----A and B----B might miscalculate the cumulative equilibrium volume fraction of polymer aggregates that fall within any group g by omitting the factor Ω_g in Equation 4.21.

4.2.7 Addition of End-Capping Chains

Addition of "end-capping chains" can be used to alter the relative partitioning into linear vs. cyclic aggregates, and the model can be extended to capture that behavior. Consider the addition of $N_{captotal}$ end-capping A---- chains, of length M_{cap} and total volume fraction $\phi_{captotal}$. Let $p_j = p_g$ refer to the number of end-capping A---- chains in any polymer component j belonging to group g and let ϕ_{cap} be the equilibrium volume fraction of free A---- chains. The equilibrium condition for any group g becomes:

$$\left(\frac{\phi_g}{n_g M_A + m_g M_B + p_g M_{cap}}\right) = \Omega_g \left(\frac{\phi_A}{M_A}\right)^{n_g} \left(\frac{\phi_B}{M_B}\right)^{m_g} \left(\frac{\phi_{cap}}{M_{cap}}\right)^{p_g} \exp(\Gamma_g) \qquad (4.29)$$

with
$$\Gamma_g = \begin{cases} \varepsilon(n_g + m_g) + (n_g + m_g - 1)\ln(c-1) + \ln G_{cycl,g} & \text{if cyclic} \\ (n_g + m_g + p_g - 1)\left[\varepsilon + \ln(c-1)\right] & \text{if linear} \end{cases} \qquad (4.30)$$

where for endcapped aggregates $\Omega_{cap,g} = 2^{n_g+m_g} / p_g$, and the expressions for Ω_g for cyclic and non-endcapped linear aggregates are given in Section 4.2.3. The conservation equations become:

$$\begin{aligned}
\phi_{Atotal} &= \sum_g n_g M_A \Omega_g \left(\frac{\phi_A}{M_A}\right)^{n_g} \left(\frac{\phi_B}{M_B}\right)^{m_g} \left(\frac{\phi_{cap}}{M_{cap}}\right)^{p_g} \exp(\Gamma_g) \\
\phi_{Btotal} &= \sum_g m_g M_B \Omega_g \left(\frac{\phi_A}{M_A}\right)^{n_g} \left(\frac{\phi_B}{M_B}\right)^{m_g} \left(\frac{\phi_{cap}}{M_{cap}}\right)^{p_g} \exp(\Gamma_g) \\
\phi_{captotal} &= \sum_g p_g M_{cap} \Omega_g \left(\frac{\phi_A}{M_A}\right)^{n_g} \left(\frac{\phi_B}{M_B}\right)^{m_g} \left(\frac{\phi_{cap}}{M_{cap}}\right)^{p_g} \exp(\Gamma_g).
\end{aligned} \tag{4.31}$$

4.3 Computational

We want to test whether linear chains possessing strongly associating endgroups can be useful as mist-control additives to aviation fuel. In the present chapter, computational results are given for a case of practical significance that can be tested experimentally using anionically polymerized telechelics: monodisperse polyisoprene (PI) chains with strongly associating endgroups, in dilute solutions in Jet-A solvent. We will address the nature of the endgroups in Section 4.5.6.

4.3.1 Choice of Parameters

The model has assumed that solvent molecules and polymer elementary units have the same size a^3. In general, we cannot expect that to be the case. If the volume of a solvent molecule (v_s) differs from that of a monomer, how should we choose the lattice size a, and how many lattice sites M should be assigned to a polymer chain of molecular weight MW_p?

We want to model a mixture of N_s solvent molecules and N_p monodisperse polymer chains of molecular weight MW_p. If we wish to preserve the volume fraction and number densities of polymer and solvent molecules, then we require that $N_s a^3 = N_s v_s$ and $N_p M a^3 = N_p(MW_p/MW_o)v_{mon}$, where v_{mon} and MW_o are the volume and molecular weight of a chemical monomer. These conditions require that $a^3 = v_s$ and $M = (MW_p/MW_o)\ (v_{mon}/a^3)$, meaning that the number and size of the elementary units into which we break up the chains is determined by the solvent size v_s. In this way, we have sacrificed the freedom to map the polymer chain as we might otherwise wish to: for instance, use of Equations 4.16–4.20 assumes that the

polymer chain has been mapped into an equivalent freely jointed chain with $M = MW_p/MW_K$ Kuhn monomers, where MW_K is the molecular weight of a Kuhn momomer.

An alternative is to model a solution of N_p monodisperse polymer molecules of given number density N_p/V and volume fraction ϕ_p. This method lets the monomer size determine the lattice size and renormalizes the number of solvent molecules, as follows. Preserving the polymer volume fraction and number density requires that $N_{s,model}a^3 = N_{s,real}v_s$ and $N_pMa^3 = N_p(MW_p/MW_o)v_{mon}$, where $N_{s,real}$ and $N_{s,model}$ are the number of real and model solvent molecules dissolving the polymer chains, and other parameters are the same as above. In this manner we are free to map the polymer chains in whatever way we choose to. The cost of that improvement is that the number density of the solvent molecules is not preserved, but since that number does not appear in the equilibrium equations (Equation 4.13–4.14), it seems inconsequential.

In what follows, we have adopted the latter approach and chosen to break up the chain into $M = MW_p/MW_K$ Kuhn monomers using $a^3 = v_{mon}MW_K/MW_o = v_K$, where v_K is the volume of a Kuhn monomer, and $N_{s,model} = N_{s,real}v_s/v_K$.

4.3.2 Parameter Values

We are choosing to break-up the polymer into Kuhn monomers of molecular weight MW_K, and to set the lattice size as $a^3 = v_K = MW_K/(\mathcal{N}_A\rho)$, where $\mathcal{N}_A$ is Avogadro's constant and ρ is the polymer density. For 1,4-PI polymer,[6] $\rho = 0.83$ g/cm^3 and $MW_K = 113$ g/mol, giving $a \approx 6.1$ Å. To quantitate the entropic cost of loop closure, numerical values are needed for the end-to-end distance x we require to close the loop and for the number of monomers in a thermal blob $g_T \approx b^6/v^2$. For simplicity we arbitrarily choose $x/b = 1$. The excluded volume parameter v was estimated[7] to be such that $v/b^3 \approx 0.10$ for PI in Jet-A, giving $g_T \approx 100$. Finally, we assume that the random walks of the chains on the lattice correspond to a coordination number of $c = 6$.

4.3.3 Computations

The following procedure was used to calculate the volume fraction of all polymer components (i.e., single-chain starting materials and aggregates of all sizes) at equilibrium, for polymer solutions of A_1----A_2 and B_1----B_2 telechelics and A---- "end-cap" chains of

specified molecular weights at specified initial concentrations ϕ_{Atotal}, ϕ_{Btotal}, and $\phi_{captotal}$ (polymer components were grouped as shown in Figure 4.5):

- First, choose a number of groups T_{groups} to include in the analysis (even though there is an infinite number of possible polymer components, we expect that above a certain size, polymer aggregates will have negligible equilibrium volume fraction and can therefore be ignored)
- Calculate n_g, m_g, M_g, Ω_g, $G_{cyc,g}$ (if appropriate), and Γ_g for polymer group g, for g = 1… T_{groups}
- Solve the three conservation equations, Equations 4.31, for (ϕ_A, ϕ_B, ϕ_{cap})
- Calculate ϕ_g for g = 1… T_{groups} using Equation 4.29
- Repeat with a new value of T_{groups} twice that of the previous one until changes in the calculated values of ϕ_g from one value of T_{groups} to the next are negligible.

4.4 Results

To translate model results into terms relevant to experiment, the equilibrium distribution of aggregates is described in terms of the concentration of the various size supramolecular species. In the context of polymer-induced mist-suppression, all linear aggregates of a given length are equivalent, and all cyclic aggregates of a given length are likewise equivalent. Therefore, the cumulative volume fractions ϕ_{linear}(MW) and ϕ_{loop}(MW) of all the linear species and of all the cyclic species of a given molecular weight MW will be used to evaluate the impacts of the following parameters on rheological solution properties: binding energy, concentration and degree of polymerization of the single-chain building blocks, and presence or absence of "end-capping" chains (Figures 4.6–4.11).

4.4.1 Mixtures of A----A and B----B Chains Only

At the lowest level of complexity, we consider solutions of telechelics of equal molecular weights ($MW_A = MW_B = MW_p$) and equal initial volume fractions ($\phi_{Atotal} = \phi_{Btotal} = \phi_{total}/2$). In this case, the problem is reduced to understanding the association behavior as a function of MW_p, ϕ_{total}, and the energy of interaction ε. The rationale for the part of the parameter space which we investigate here is given in the Section 4.5.2.

Comparison of model results for MW_p = 10^6 g/mol (labeled 1000k in figures) at total polymer volume fraction ϕ_{total} of 1400 ppm and 800 ppm (Figures 4.6–4.7) demonstrates two important effects of total polymer concentration. First, at fixed MW_p and ε, increasing concentration results in a higher fraction of the polymer becoming involved in larger linear aggregates (compare first and second rows in Figures 4.6–4.7): the decrease in ϕ_{linear} with increasing aggregate MW is not as sharp at 1400 ppm, and the position of the peak in ϕ_{linear} vs. MW is shifted to the right at 1400 ppm for each ε (most visibly for ε =18, left column of Figure 4.7). Second, the relative partitioning of the polymer into linear rather than cyclic aggregates is insensitive to total polymer concentration ϕ_{total}.

Consider now the effect of the length of the individual chains (MW_p), by comparing results for 5 × 10^5 chains at 1400 ppm (third row, Figures 4.6–4.7) and 1 × 10^6 g/mol chains at 800 ppm (second row). These concentrations were chosen to correspond to one-fourth of the overlap concentration of the single-chains, i.e., ϕ_{total} = ¼ ϕ^* based on the respective values of MW_p. We observe that the shape of the ϕ_{linear} vs. MW curves for both these systems is nearly identical, for each value of ε investigated. On the other hand, the relative proportion of loops vs. linear chains is substantially higher for the shorter chains, due to the smaller entropic cost of cyclization for shorter loops.

Finally, the effect of the energy of association on the equilibrium distributions is very pronounced (the columns of Figures 4.6–4.7 are in ascending order by association energy). First, higher values of ε strongly increase the population of loops of all sizes, i.e., increasing ε increases the relative fraction of loops compared to linear aggregates. Second, increasing ε greatly broadens the distribution of ϕ_{linear} vs. MW, decreasing the magnitude of the peak in the distribution. At values of $\varepsilon \leq 14$, aggregates are few and the dominant components are the telechelic building block themselves. At values of $\varepsilon \geq 20$, the dominant components are cycles of low MW, but the distribution of linear supramolecules is nearly flat, meaning that very large aggregates have a significant cumulative volume fraction at equilibrium. Intermediate values of the energy of association, corresponding to $16 \leq \varepsilon \leq 18$, provide a balance of interactions strong enough to drive formation of large superchains and weak enough to accommodate a significant population with unpaired ends (i.e., linear superchains).

4.4.2 Mixtures of A----A, B----B, and A---- Chains

Important changes in the partitioning of the polymer occur as end-capping A---- chains are added to solutions of A----A and B----B telechelics. At the lowest level of complexity again, we consider solutions of polymer additives of equal molecular weight ($MW_A = MW_B = MW_{cap} = MW_p$). We consider solution compositions that maintain equal number densities of A and B endgroups, i.e., such that $\phi_{captotal} = 2(\phi_{Btotal} - \phi_{Atotal})$. Therefore, the total polymer fraction of A---- end-capping chains, $\phi_{captotal}$, must be in the range from 0 to 2/3. Define $X = \phi_{Atotal}/\phi_{Btotal}$ as the ratio of telechelics A----A to telechelics B----B; that ratio decreases from 1 to 0 as the fraction of A---- increases from 0 to 2/3.

Results obtained for solutions of $MW_p = 10^6$ g/mol at total volume fraction $\phi_{Atotal} + \phi_{Btotal} + \phi_{captotal}$ = 800 ppm (Figures 4.8–4.11) confirm that introducing end-caps favors the formation of linear species. At fixed ε, MW_p, and ϕ_{total}, the fraction of polymer involved in cycles decreases with increasing volume fraction of A---- end-caps, as expected (see top row of Figures 4.8–4.11). This is true at all values of ε and occurs simply because the presence of A---- components decreases the fraction of linear chains that *can* form loops. Note that the increase in the concentration of linear species upon addition of A---- (offsetting the decrease in ϕ_{loop}) heavily favors short, rather than long aggregates: in fact, the population of very long linear superchains is reduced by adding end-caps (decreasing X), and this was also true at all values of ε (most visible in bottom row of Figures 4.8 and 4.9). In other words, increasing the volume fraction $\phi_{captotal}$ of end-capping chains causes a narrowing of the distribution of linear aggregates, meaning that a higher fraction of polymer is involved in smaller linear supramolecules.

A striking qualitative difference between the binary (A----A + B----B) and the ternary systems is in the behavior as $\varepsilon \rightarrow \infty$. In the absence of end-capping A----, the ratio of linear to cyclic supramolecules vanishes as $\varepsilon \rightarrow \infty$ (Figure 4.7). As the free energy penalty for leaving unpaired stickers diverges, no linear chains can survive in the absence of end-caps. When end-caps are present, one is free to increase ε without extinction of linear species; instead as $\varepsilon \rightarrow \infty$ a limiting distribution is achieved (Figure 4.11) in which doubly end-capped linear species and cyclic species equilibrate in a manner that can be quantitatively controlled by the choice of the relative number of A---- single chains.

4.5 Discussion

4.5.1 Using the Model to Design Anti Misting Additives

While the model may find wide utility for diverse applications involving rheology modifiers, here we wish to identify a set of parameter values for which the equilibrium distribution of the polymer components is suitable for mist-suppression applications. The figures of merit for this application are deduced from the prior literature on ultra-long polymers, which themselves are not acceptable because turbulent flow during transport of fuel cleaves the chains and eliminates their effectiveness. As a guide to experiments to determine whether or not the efficacy of ultra-long chains and the resistance to shear degradation of associative polymers can be combined, we use the present model to guide the selection of chain lengths, association strengths, and mixture compositions that hold the greatest promise.

Chao and coworkers[8] reported that polyisobutylene chains of molecular weight ~ 5×10^6 g/mol were satisfactory mist-suppressing agents at concentrations as low as 50 ppm in kerosene. Considering that cyclic polymer chains are expected only to be as effective as linear chains of half their size, the cumulative amount of linear species of MW $\geq 5 \times 10^6$ g/mol and cycles of MW $\geq 10 \times 10^6$ g/mol should be 50 ppm or more. Given that aviation fuel is continuously circulated on the aircraft as a heat transfer fluid, the kinetics of equilibration may play a role, i.e., in practice long linear aggregates may not achieve their equilibrium distribution (refer to Section 4.5.4). If so, polymer designs and mixture compositions that maximize the *equilibrium fraction* of polymer involved in linear supramolecular aggregates in the 5–10 $\times$ 10^6 g/mol range may lead to maximal mist suppression in practice.

4.5.2 Parameter Space

By restricting the level of complexity (choosing the A----A, B----B, and A---- building blocks to be of the same molecular weight MW_p, and by requiring that A and B endgroups have equal number densities in solution), the parameter space is reduced to 4 dimensions. Within the parameter space $\{MW_p, \varepsilon, \phi_{total}, X\}$, we seek to optimize the equilibrium partitioning of the polymer for mist-control applications given the constraints of the problem.

Here we consider the bounds that are imposed on MW_p and ϕ_{total} in the context of fuel additives.

First, we should use the highest possible values of MW_p, since at fixed ε and ϕ_{total} the total fraction of polymer trapped in loops decreases monotonically with increasing MW_p. In reality the upper-bound of MW_p is limited by mechanical degradation of the polymer. Unintentional chain scission of our telechelics would result in an excess of end-capping species that would greatly reduce the size of supramolecular chains that form. Literature on shear degradation shows that flexible linear chains of less than a few million g/mol resist degradation associated with flow through pumps and turbulent pipeline flow. Therefore, we imposed $MW_p = 10^6$ g/mol as our upper bound and compared results with $MW_p = 0.5 \times 10^6$ g/mol in order to quantitate sensitivity to changes in MW_p.

Next, implementation of a polymer-based mist-control technology cannot be possible unless changes in shear viscosity of the fuel due to polymer addition are very small. Here we chose an upper bound in total volume fraction of polymer to be one-fourth of the overlap concentration of the A----A and B----B, and A---- building blocks, recognizing that supramolecular chains formed by physical associations may reach or exceed their overlap concentration. So long as the very long supramolecules remain below their particular c^*, the shear viscosity of the solution is expected to remain within permissible bounds. For the two chain lengths selected above, this constraint imposes a maximum polymer volume fraction of 800 ppm for $MW_p = 10^6$ g/mol and 1400 ppm for $MW_p = 5 \times 10^5$ g/mol. To quantify the improvements in mist control arising from increases in concentration, results for 10^6 g/mol chains at both 800 and 1400 ppm were compared.

With the above choices for MW_p and ϕ_{total}, the problem is reduced to two dimensions, ε and X, which were examined over their physically relevant ranges.

4.5.3 Implication for Mist-Control Applications

Our criterion for optimal results with regard to mist-suppressing applications corresponds to maximizing the equilibrium fraction of polymer involved in linear supramolecular aggregates in the 5–10 $\times 10^6$ g/mol range. Two key features of the distributions that satisfy this objectives are (i) favorable partitioning of the polymer into linear rather than cyclic

aggregates, and (ii) a concentration vs. molecular weight curve for linear aggregates that is narrowly distributed and centered around ~ 5×10^6 g/mol.

According to the above criteria, model results show that partitioning of the polymer into linear superchains is favored at higher values of MW_p and ϕ_{total}, as expected, but that ~ 2-fold changes in MW_p or ϕ_{total} about the ~ {10^6 g/mol, 800 ppm} upper-boundary determined by the problem constraints yield only small changes in the overall *shapes* of the ϕ_{linear}, ϕ_{loop} distributions (compare first and second rows, and first and third rows at fixed ε in Figures 4.6 and 4.7). Effects of the energy of interaction were much more pronounced. For example, a $\leq$ 15% change in ε from 14 to 16 yielded a dramatic change in the shape of the size distribution of aggregates for all values of {MW_p, ϕ_{total}} (Figure 4.6).

The strong dependence of the size distribution of linear and cyclic aggregates on energy of interactions has important implications for mist-control applications. For mixtures of A----A and B----B molecules, model predictions indicate that "good" results are only achieved in a narrow range of association energy, $16 \leq \varepsilon \leq 18$. The following two complications immediately arise. First, the preparation of telechelic chains of such length (~ 10^6 g/mol) terminated with endgroups that all bind with a precise target strength of interaction of such magnitude (> 16 kT) poses a tremendous synthetic challenge (see Section 4.5.6). Second, the strength of physical associations is strongly temperature dependent and the operating temperature range of interest for aviation fuel is very broad (-50 to +50 ^oC), so it is doubtful that any system could be designed to maintain the binding energy of the polymer endblocks within such a narrow range.

Addition of A---- end-capping chains to A----A + B----B mixtures solves the above problem, at least under equilibrium conditions. For instance, model results for 10^6 g/mol chains at ϕ_{total} = 800 ppm and X = 0.5 (Figure 4.11) show that for any value of $\varepsilon \geq 20$, the equilibrium volume fraction of linear superchains of 5×10^6 g/mol is greater than 100 ppm and that of 7×10^6 g/mol superchains is greater than 50 ppm. This means that the mist-suppression effectiveness of such a polymer solution under equilibrium conditions will be robust with respect to fluctuation in ε due to temperature variations or to variations in molecular structure of the endgroups. The model, therefore, indicates that it should be feasible to create polymers whose equilibrium distribution of aggregates provides the requisite concentration of very long supramolecular chains over a wide range of temperature.

At this point, we need to inquire whether it is reasonable to expect that equilibrium partitioning of the polymer will be found under conditions of practical import.

4.5.4 Time to Reach the Equilibrium Distribution

Earlier we explored whatever values of $\{\varepsilon, X\}$ allowed us to optimize the equilibrium distribution of polymer components. In doing so we assumed that under conditions of practical importance, equilibrium is restored as fast it is disturbed. How long does it take to reach the equilibrium partitioning of the polymer into aggregates of all sizes? Let us start by considering the lifetime of a bond. The relaxation time $\tau_0 \sim \eta b^3/kT$ of a monomer in solution of shear viscosity ~ 1 mPa.s is on the order of 10^{-10} sec, so the lifetime of a donor-acceptor physical bond $\tau_b \sim \tau_0 \exp(\varepsilon)$ is on the order of 0.001–10 sec for ε = 17–25. Therefore, even if we assumed that equilibrium could be reached with a mere 10^3 bond breaking and bond forming events, for endgroups associating with energy 20–25kT, that time is on the order of $1–10^4$ s. Consider now that processes such as recirculation of the fuel within an aircraft are expected to breakup polymer aggregates down to individual components at intervals of a few minutes during, for example, passage through pumps. Given the level of uncertainty in our calculations, experimentation is required to reach a definite conclusion about whether or not solutions of A----A plus B----B plus A---- polymer chains reassociate into large superchains sufficiently rapidly to be used as mist-suppressing agents for aviation fuel.

4.5.5 From Telechelics to Heterotelechelics

What experiments do the model results motivate us to conduct? We found that ternary mixtures of A----A, B----B, and A---- chains in dilute solutions deserve the effort required to synthesize the polymer. Unfortunately, they suffer to some extent from the same problems as mixtures of A----A and B----B chains only (whose binary mixtures do not appear to be viable candidates for mist-suppressing applications): (i) to provide 50 ppm of superchains > 5×10^6 g/mol, the overall polymer concentration must be several hundred ppm because a lot of polymer is "lost" in useless small cycles and small linear aggregates, and (ii) the reassembly of superchains takes time, and the longer the superchain the longer it takes for its population to build up to its equilibrium value.

The above insight suggests that a better alternative would involve the design of a polymer system for which loops are prohibited and associations would result in the systematic

formation of well-defined linear chains. An example of such a design is shown in Scheme 4.3. It involves two sets of specific interactions, such that A endgroups interact only with B endgroups, and C endgroups likewise only with D endgroups. The molecules in Scheme 4.3 are designed such that for a stoichiometric blend of the building blocks and at high enough binding affinity of the A+B and C+D associations, nearly all the polymer chains should assemble into pentamers (in 4 bond-forming events only) even at arbitrarily low polymer volume fraction ϕ_{total}. As a result, satisfactory mist suppression could be achieved with < 100 ppm of A----A, B----C, and D---- chains of size $MW = 10^6$ g/mol.

4.5.6 Nature of the Endgroups

We now address an important synthetic challenge. What chemical moieties might we use at the chain ends to generate association energies in the 17–25kT range? Let A and B refer to the small molecules corresponding to these endgroups. We first inquire what equilibrium constant of association K_{ass} the above association energies correspond to. For the association reaction of the free-endgroups A + B → AB, our model predictions are:

$$\frac{\phi_{AB}}{M_{AB}} = \left(\frac{\phi_A}{M_A}\right)\left(\frac{\phi_B}{M_B}\right)\exp\left[-\frac{1}{kT}\left(\mu_{AB}^0 - \mu_A^0 - \mu_B^0\right)\right] = \exp(\varepsilon)\,. \tag{4.32}$$

For small molecules in dilute solution, this expression is consistent with the equilibrium condition for ideal solutions (Raoult's law), $x_{AB}/x_A x_B = \exp[-(\mu_{AB}^0 - \mu_A^0 - \mu_B^0)]$, where x is mole fraction. It follows from Equation 4.32 that $K_{ass} \equiv C_{AB}/C_A C_B = \upsilon_s \exp(\varepsilon)$, where C is molar concentration and υ_s is the molar volume of the solvent. Thus, achieving binding energies of the endgroups in the range of ε = 17–25 corresponds to association constants K_{ass} on the order of 10^7 to 10^{10} M^{-1}!

Although interacting chemical structures of binding constants up to 10^6 M^{-1} are known (Figure 4.12), the synthetic challenge of preparing telechelic polymer chains of size 10^6 g/mol with well-defined endgroups of binding constants ~ 10^7 to 10^{10} M^{-1} is daunting. In addition to the challenge of finding a suitable donor-acceptor pair, synthesis of telechelics becomes increasingly more difficult with increasing size. Furthermore, the possible poisoning of the endgroups (which would be present at < ppb levels in dilute polymer solutions) by minute amounts of acids, bases, metals etc… present in the solvent, thereby rendering the polymer ineffective, is an important concern.

A worthwhile alternative involves the use of short polymer endblocks featuring an arbitrary number of donor-acceptor type functional groups. For example, synthesis of 10^6 g/mol polymer chains endcapped with 1,2-PB endblocks of a few thousands g/mol would enable the preparation of associating polymer of tunable binding affinities by post-polymerization functionalization of the 1,2-PB. This strategy would provide more flexibility in the choice of binding energy and also facilitate fast and effective optimization of material properties via rapid adjustments in the number and the identity of the functional side-groups.

4.6 Conclusions

In this chapter we developed a model to understand the self-assembling behavior of polymer chains designed to overcome the effect of chain collapse (refer to Chapters 2 and 3) by clustering stickers at the ends of polymer chains. We showed that symmetric linear chains displaying strongly associating endgroups (A----A and B----B binary mixtures) suffer instead from loop formation, which traps large amounts of the polymer into small cyclic aggregates with low mist-control properties. We found that more favorable equilibrium distributions for the purpose of mist-control applications can be achieved by addition of end-capping A---- chains. Future work might involve experimentation to determine whether ternary mixtures of A----A, B----B, and A---- polymer chains that associate end-to-end with binding energies > 10^7 M^{-1} can build up large superchains sufficiently rapidly to be used as mist-suppressing agents for aviation fuel. This presents a synthetic challenge which we addressed above. We reasoned that functional endgroups would best be achieved by synthesis of short polymer endblocks bearing a suitable number of selected functional groups (hydrogen bond donor and acceptor pairs, for instance).

Insight generated from the present model also suggests the design of end-to-end associating molecules which cannot form loops. Breaking symmetry to enable the exclusive formation of large linear supramolecules from self-assembly of end-functionalized polymer chains (Scheme 4.3) requires synthesis of polymer molecules featuring several orthogonal (i.e., non-interacting) pairs of complementary (i.e., donor-acceptor) endgroups. Preparation of such materials required the development of new synthetic tools: in the next chapter we present straightforward and rapid protocols for the preparation of functional polymer materials of controlled architecture and functionality.

4.7 Figures and Schemes

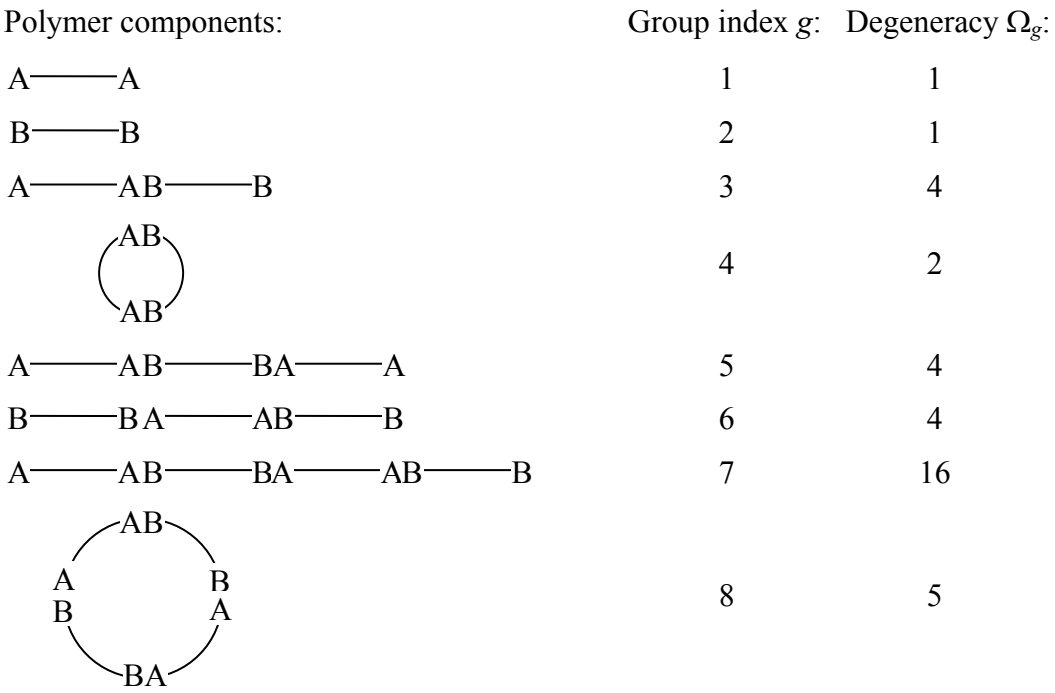

Figure 4.1 Grouping of polymer components, where A and B generically refer to A_1 or A_2 and B_1 or B_2 endgroups. Each group is composed of all the different possible aggregates obtained by the assembly of the A_1----A_2 and B_1----B_2 building blocks. For example, group 3 is composed of the following 4 distinct aggregates: A_1----A_2B_1----B_2, A_1----A_2B_2----B_1, A_2----A_1B_1----B_2, and A_2----A_1B_2----B_1.

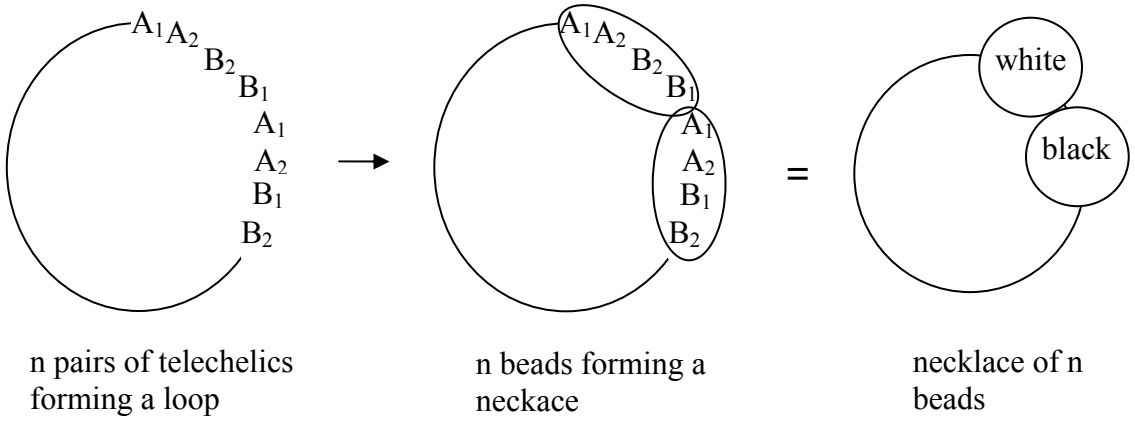

Figure 4.2 Mapping of polymer loops into necklaces of 4 colors. The 4 colors correspond to: $A_1A_2B_1B_2$, $A_1A_2B_2B_1$, $A_2A_1B_1B_2$, $A_2A_1B_2B_1$. For example, we can choose $A_1A_2B_1B_2$ = black, $A_1A_2B_2B_1$ = white, $A_2A_1B_1B_2$ = blue, and $A_2A_1B_2B_1$ = green.

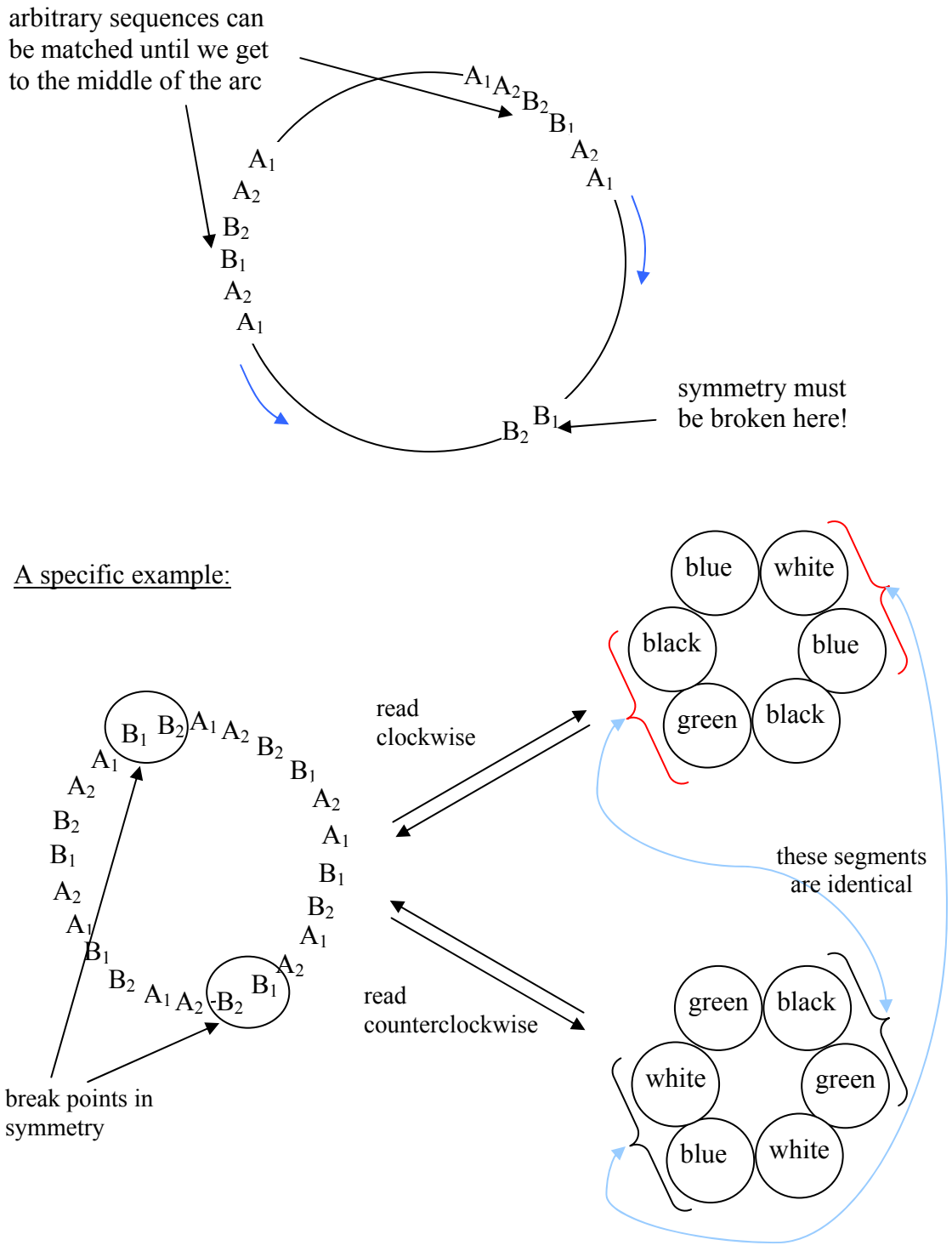

Figure 4.3 We cannot arbitrarily create a loop that "reads" the same clockwise and counterclockwise. Therefore, every loop maps into exactly two distinct necklaces. (Color assignments are given in Figure 4.2.)

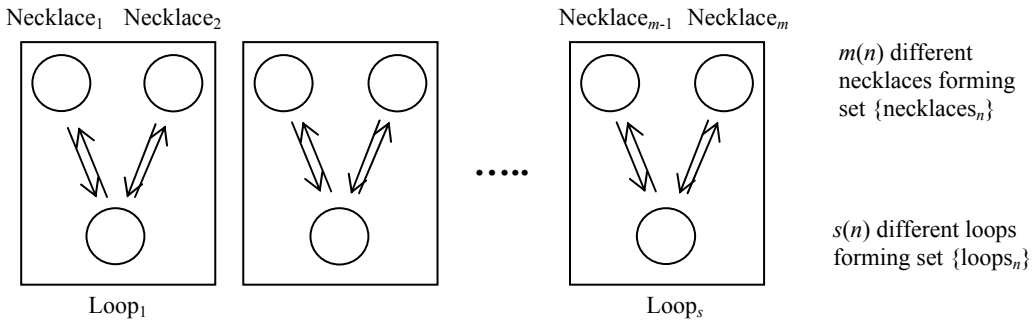

Figure 4.4 There are twice as many distinct necklaces as there are distinct loops.

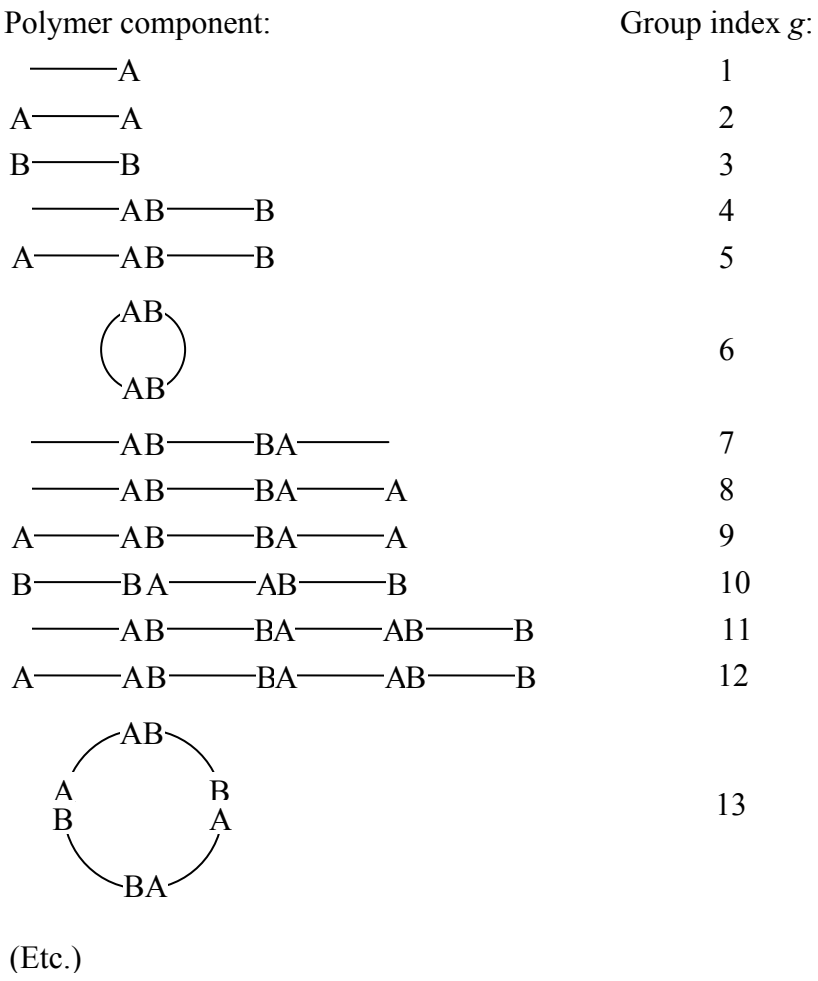

Figure 4.5 Grouping of polymer components in the presence of A---- end-capping chains. Each group is composed of all the different possible aggregates obtained by the assembly of the A_1----A_2, B_1----B_2, and A---- building blocks, as before (Figure 4.1).

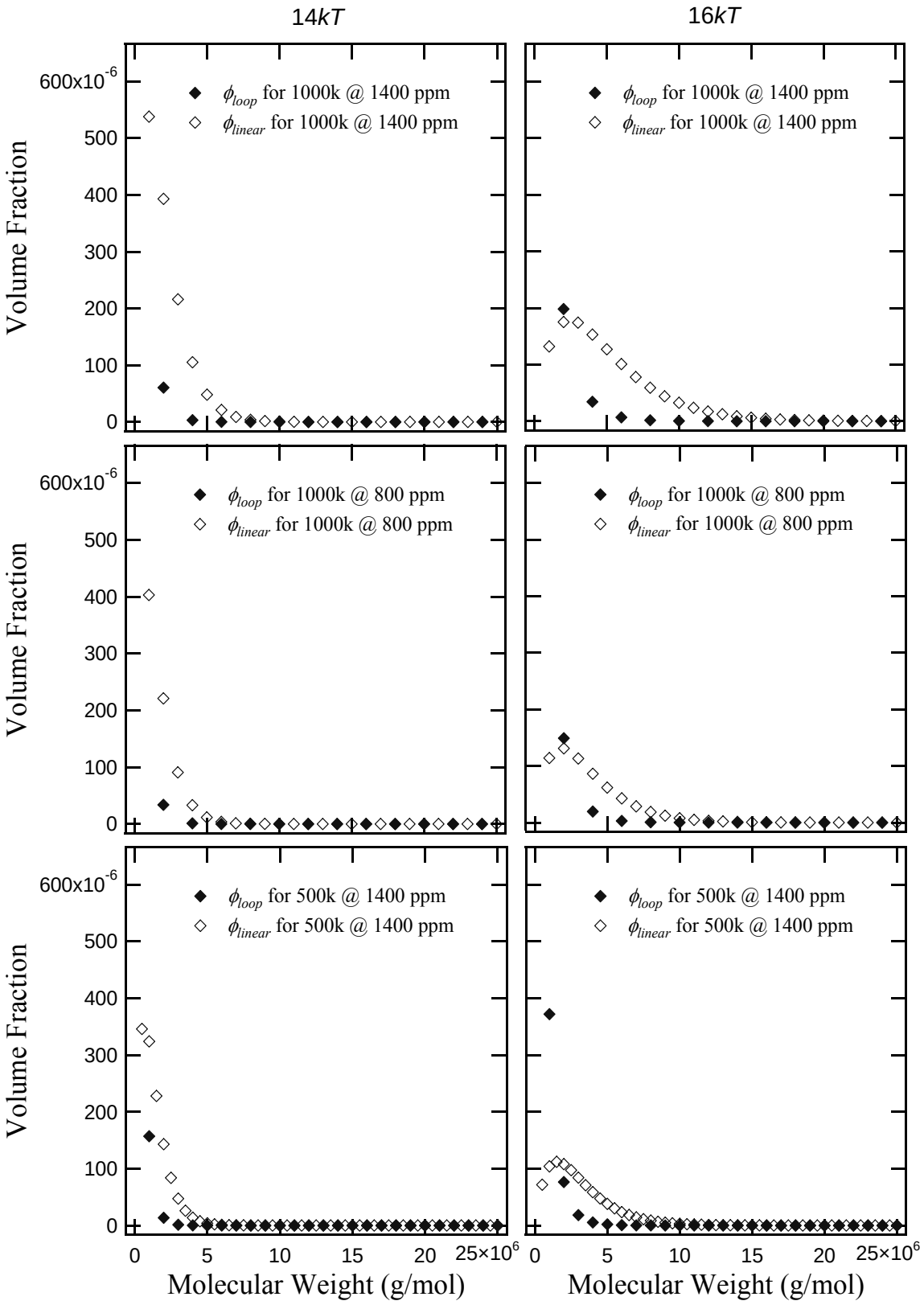

Figure 4.6 Model predictions for strength of interaction $\varepsilon kT = 14kT$ (left) and $\varepsilon kT = 16kT$ (right).

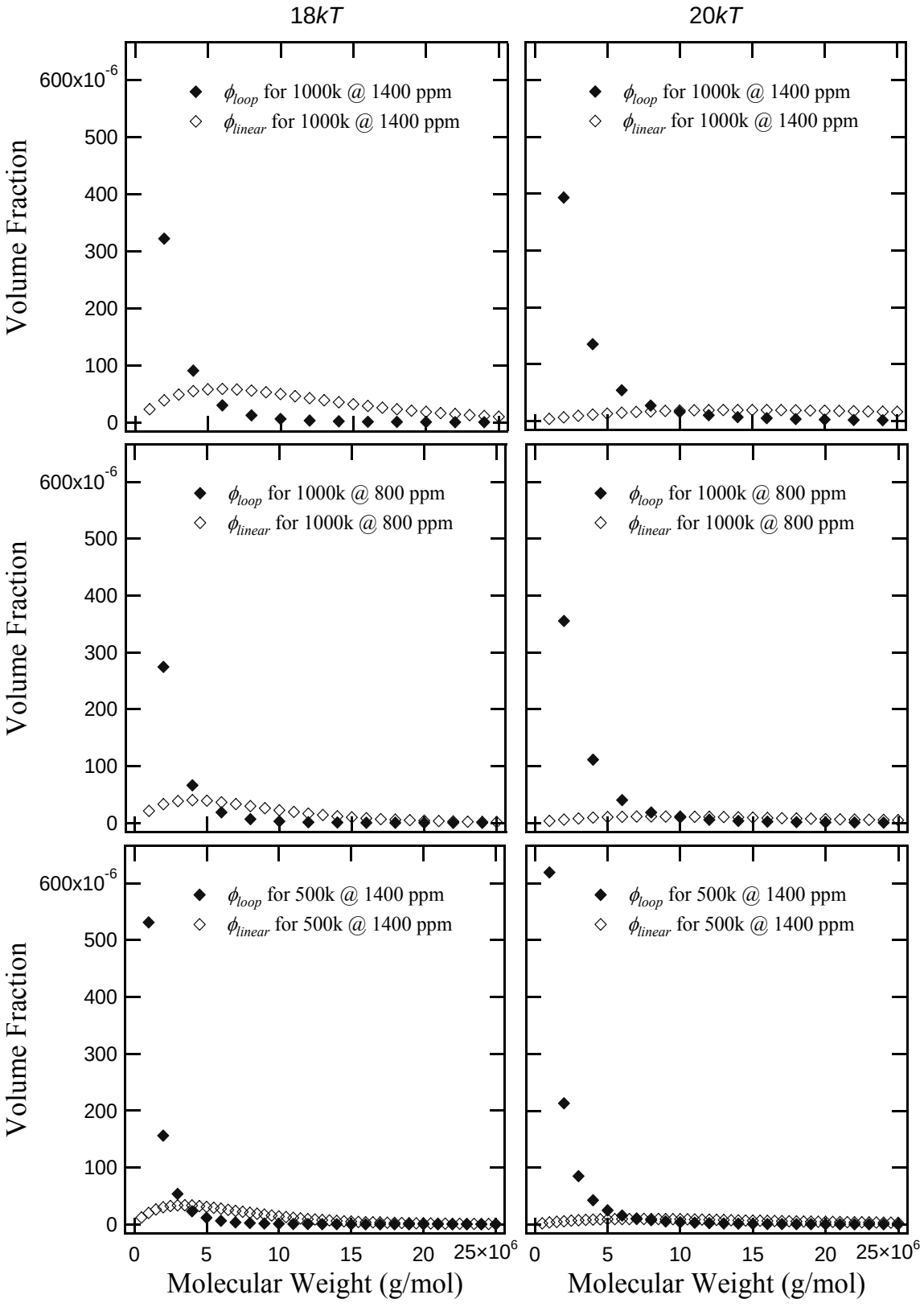

Figure 4.7 Model predictions for strength of interaction $\varepsilon kT = 18kT$ (left) and $\varepsilon kT = 20kT$ (right).

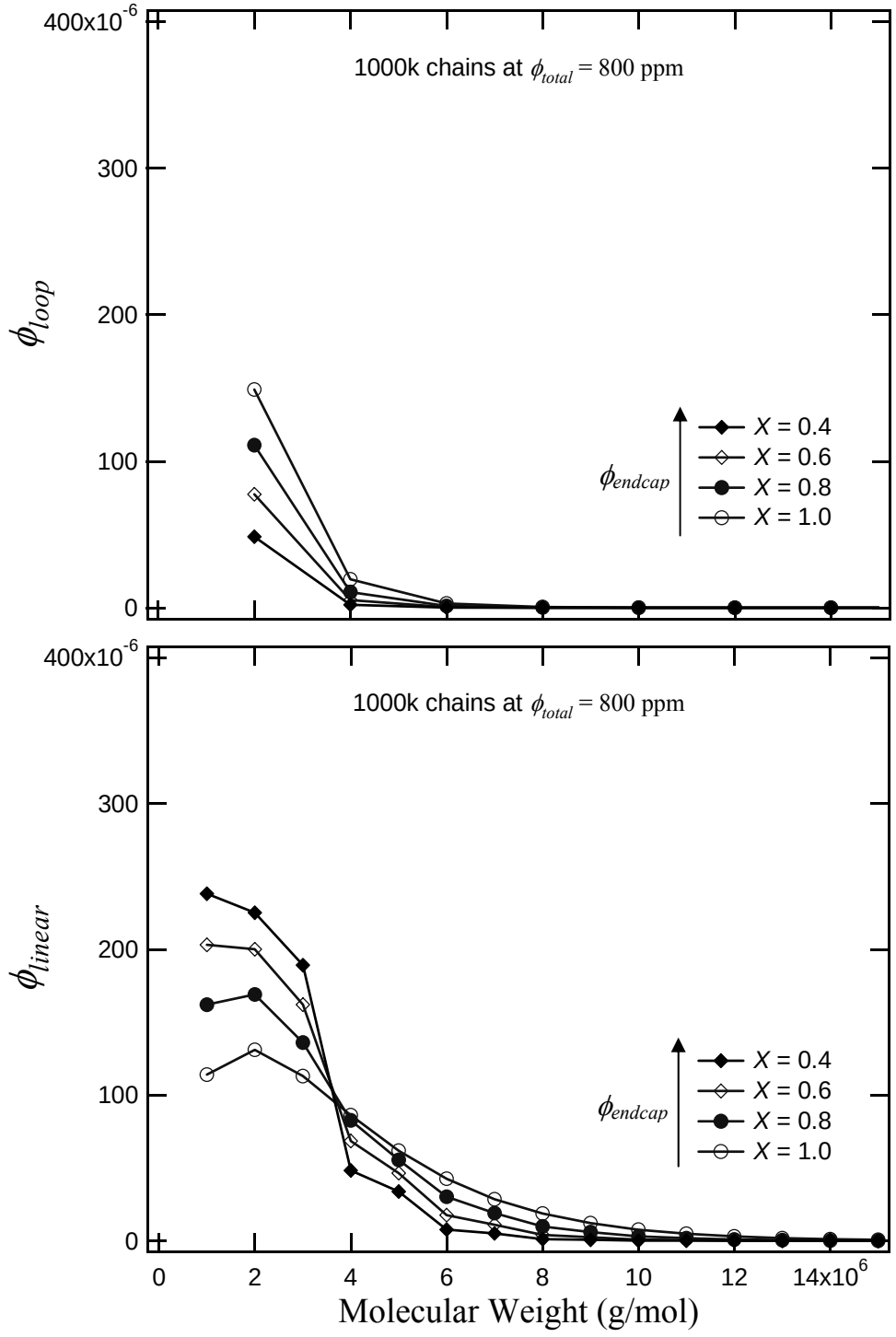

Figure 4.8 Model predictions in the presence of end-capped chains, when $\varepsilon kT = 16kT$.

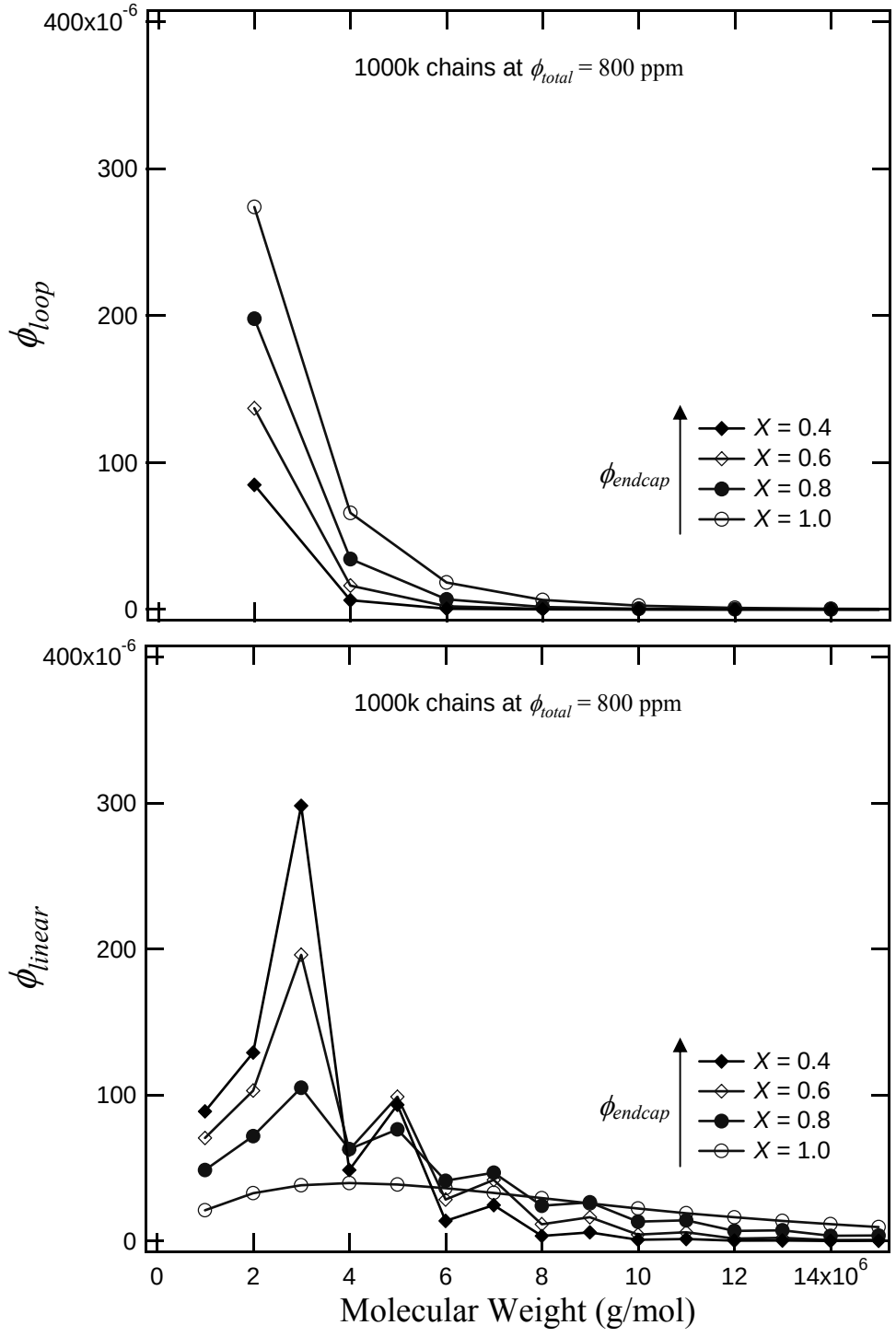

Figure 4.9 Model predictions in the presence of end-capped chains, when $\varepsilon kT = 18kT$.

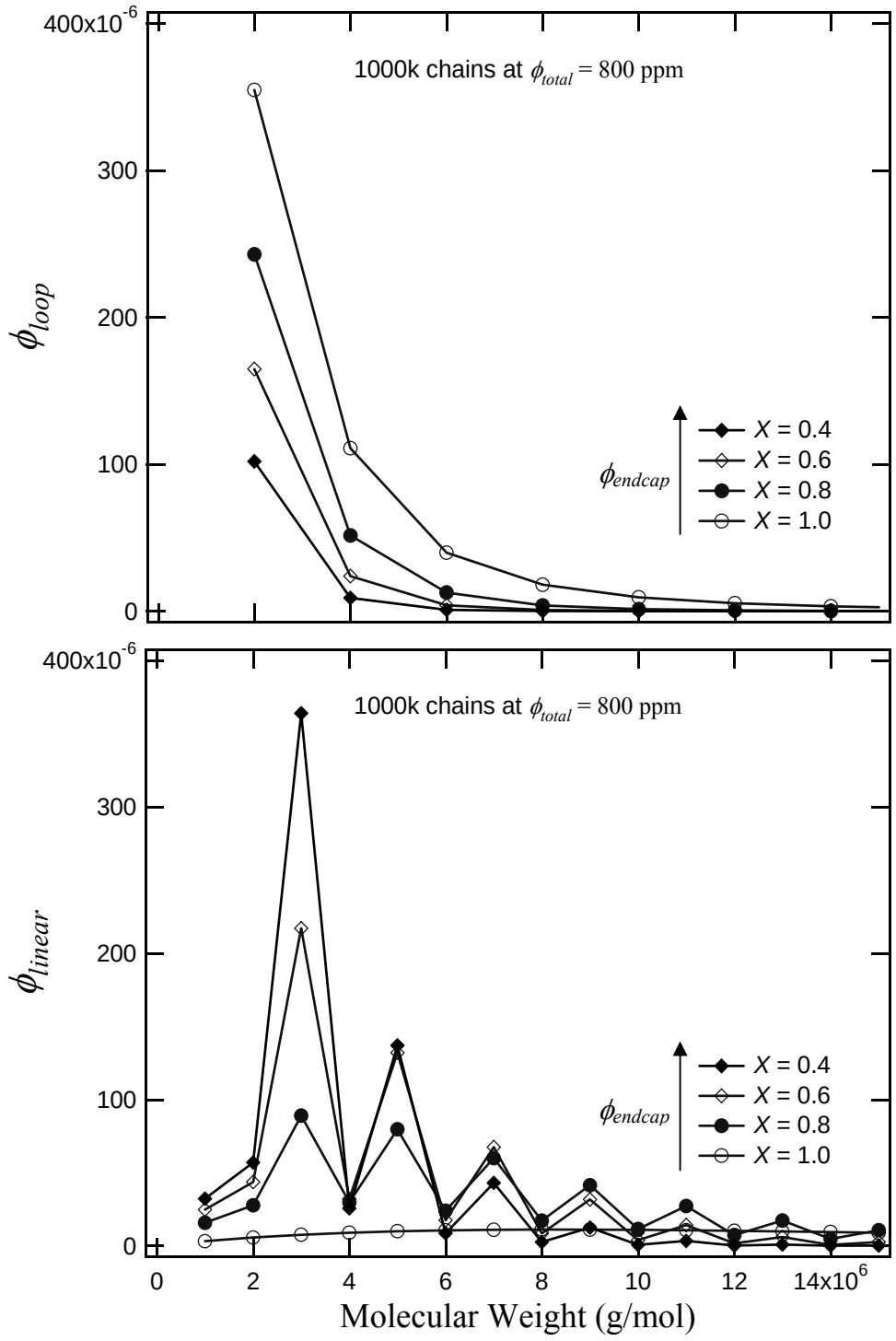

Figure 4.10 Model predictions in the presence of end-capped chains, when $\varepsilon kT = 20kT$.

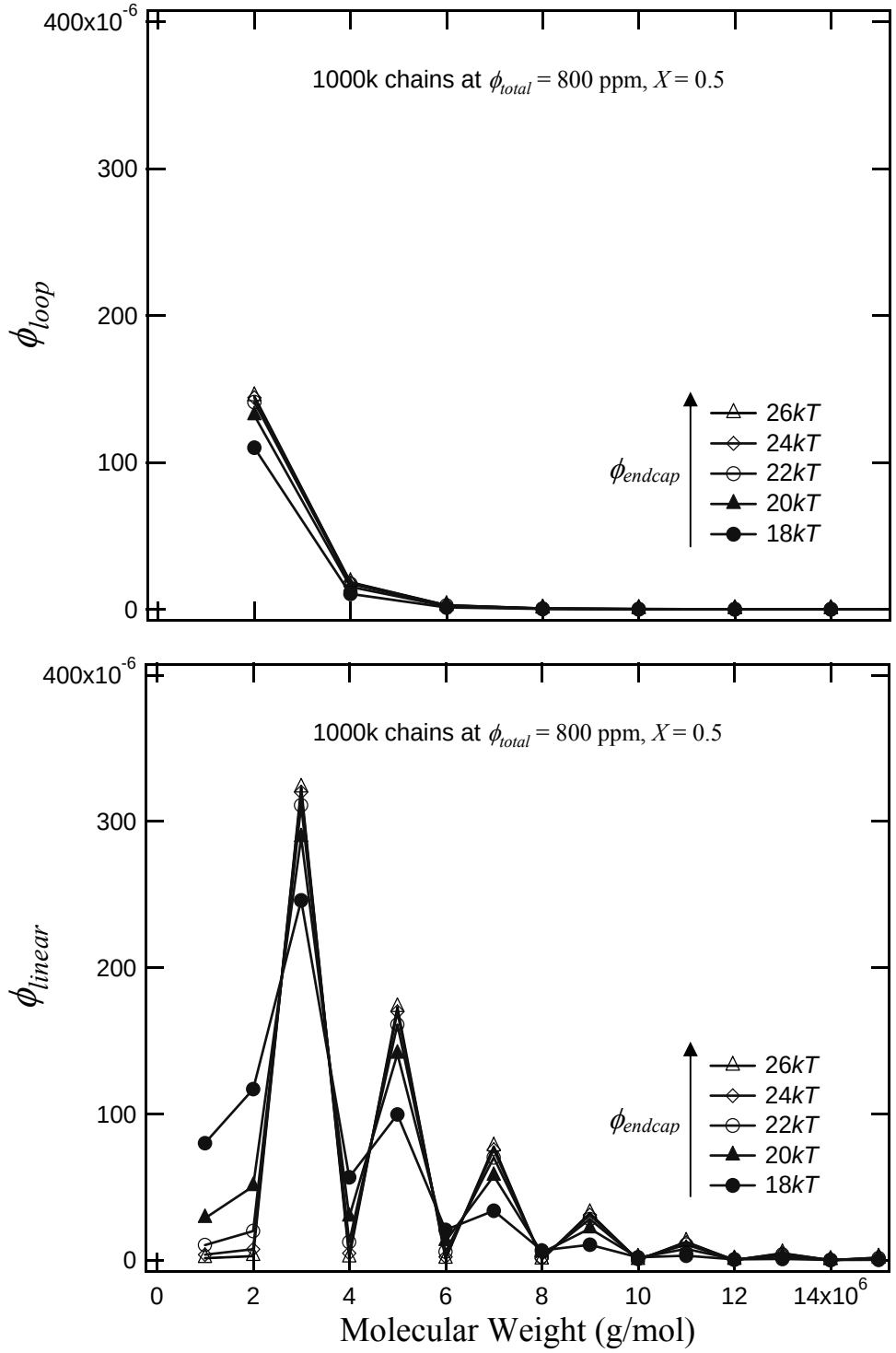

Figure 4.11 Limiting equilibrium distribution (as $\varepsilon \rightarrow \infty$) obtained in the presence of end-capping A---- polymer chains.

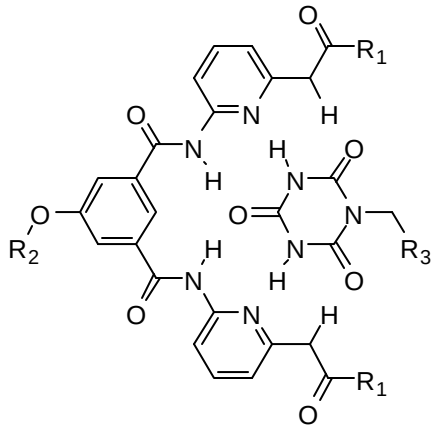

Figure 4.12 Sextuple hydrogen-bonding motifs derived from nucleobase structures, of binding constants ~ 10^6 M^{-1} in organic solvents of low polarity.[9, 10]

Scheme 4.1 Molecular Design for Self-Assembly of Difunctional Polymeric Building Blocks into Larger Linear Chains via Physical Interactions

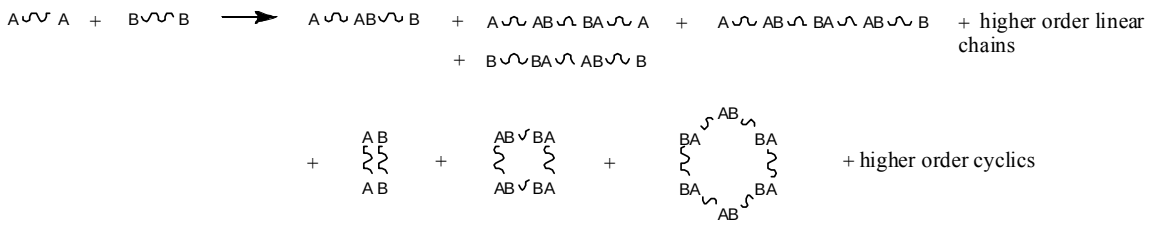

Scheme 4.2 Contact Probabilities and Equilibria

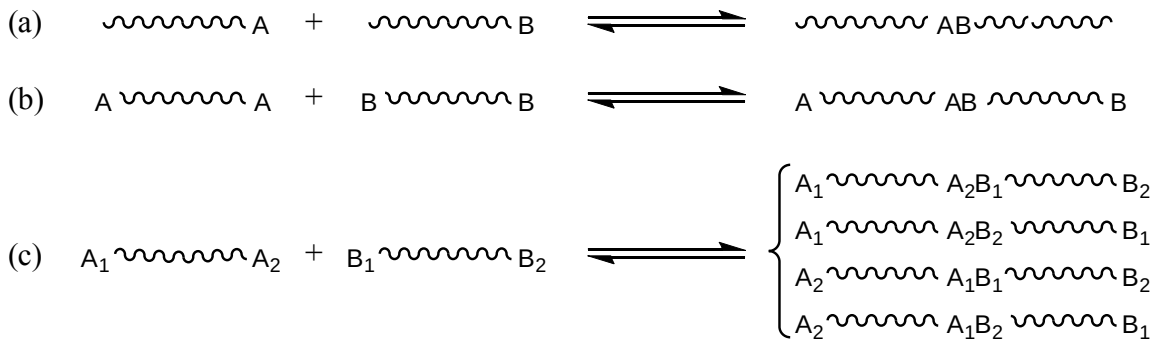

Scheme 4.3 Molecular Design Aimed at the Exclusive Formation of Well-Defined Supramolecular Linear Chains

4.8 References and Notes

1. Compare with lattice model of Goldstein (Goldstein, R. E., Model for Phase-Equilibria in Micellar Solutions of Nonionic Surfactants. *Journal of Chemical Physics* **1986,** 84, (6), 3367–3378).

2. Hill, T. L., In *An Introduction to Statistical Thermodynamics*, Dover Publications: 1986; pp. 402–404.

3. Rubinstein, M.; Colby, R. H., In *Polymer Physics*, Oxford: 2003; p. 70.

4. Rubinstein, M.; Colby, R. H., In *Polymer Physics*, Oxford: 2003; pp. 121–122.

5. van Lint, J. H.; Wilson, R. M., In *A Course in Combinatorics*, Cambridge University Press: 2001; pp. 522–525.

6. Rubinstein, M.; Colby, R. H., In *Polymer Physics*, Oxford: 2003; p. 53, Table 2.1.

7. Obtained from viscosity measurements of 580 kg/mol polyisoprene chains, of polydispersity index 1.22, in Jet-A solvent, by rearrangement of the scaling relation $\phi^* \approx (b^3/v)^{6\nu-3}N^{1-3\nu}$ (Rubinstein, M.; Colby, R. H., *Polymer Physics*. Oxford: 2003, Equation 5.19, p. 176) using swelling exponent $\nu \approx 0.588$ and overlap concentration $\phi^* \cong 0.0049$. The number of Kuhn monomers N was estimated using $MW_K = 113$, and the overlap concentration was determined according to the criterion $[\eta]\phi^* \cong 1$.

8. Chao, K. K.; Child, C. A.; Grens, E. A.; Williams, M. C., Antimisting action of polymeric additives in jet fuels. *AICHE Journal* **1984,** 30, (1), 111–120.

9. Binder, W. H.; Kunz, M. J.; Kluger, C.; Hayn, G.; Saf, R., Synthesis and analysis of telechelic polyisobutylenes for hydrogen-bonded supramolecular pseudo-block copolymers. *Macromolecules* **2004,** 37, (5), 1749–1759.

10. Kolomiets, E.; Buhler, E.; Candau, S. J.; Lehn, J. M., Structure and properties of supramolecular polymers generated from heterocomplementary monomers linked through sextuple hydrogen-bonding arrays. *Macromolecules* **2006,** 39, (3), 1173–1181.

Chapter V Facile, Efficient Routes to Diverse Protected Thiols and to Their Deprotection and Addition to Create Functional Polymers by Thiol-Ene Coupling

5.1 Introduction

Well-defined homopolymers and block copolymers containing covalently or noncovalently attached functionalities are of much interest as materials with tailored properties (refer, for instance, to work by Antonietti[1-4] and Weck,[5-9] among others). To synthesize these functional macromolecules, the chemical modification of well-defined prepolymer chains (i.e., polymer analogous synthesis) is a valuable alternative to the traditional route of direct polymerization or copolymerization of functional monomers by living ionic, group-transfer, radical, or ring-opening methods. Living polymerization methods commonly require intense purification of reagents and solvents, protection of functional groups in monomers, and inert reaction conditions. Further, polymerization by any one of the living mechanisms cited above places restriction on the nature of monomers and comonomers that can be used. Polymer analogous synthesis extends the accessible range of functional polymers and copolymers, with important advantages. Control of the polymer architecture and length is afforded by the choice of prepolymer material, while functionality control is achieved by the modification reaction conditions; therefore, control of polymer structure and of polymer functionality are decoupled. In addition, rapid adjustments in the nature of the side-group and/or the extent of functionalization allow fast and effective optimization of molecular properties for a given application.

Chemical functionalization of unsaturated polymers has received particular attention[10] because of the availability of the parent materials and of the reactivity of the featured double bonds. In particular, polybutadiene (PB) has been successfully functionalized with a diversity of side-groups by hydroboration/oxidation,[11-13] epoxidation followed by oxirane ring-opening using nucleophiles or acid chlorides,[1] hydrosilylation,[13, 14] and radical additions of thiols[15-21] and alkyl iodides.[22]

Polymer analogous synthesis becomes attractive when the coupling reaction is efficient and robust, and free of degradation or cross-linking side reactions. We have come to appreciate several advantages of thiol-ene coupling from our experience functionalizing 1,2-PB. First, the method can be used for grafting various functionalities in a one-step polymer reaction (as opposed to hydroboration or epoxidation). Thiol-ene coupling proceeds under mild reaction conditions and is tolerant of a large number of functional groups. In particular, the chemistry is water insensitive, which renders it considerably simpler than hydrosilylation, for instance. Of paramount importance to our work, thiol addition also proceeds with minimal cross-linking or chain scission in comparison to other modification reactions such as hydroboration/oxidation[13] and hydrosilylation.[23, 24] Finally, desired side-groups are incorporated via unobtrusive thioether linkages, without the introduction of additional functionalities (in contrast to functionalization by epoxidation or radical addition of alkyl iodides, which add one molar equivalent of hydroxyl, chloro, or iodo functionalities per grafted side-group).

Thiol-ene addition to PB offers tremendous versatility for molecular design. The excellent tolerance of thiol-ene coupling to numerous functional groups combines with the good availability of PB-containing prepolymers of well-defined microstructures (e.g., content of 1,2-adducts), macromolecular structure (such as chain topology and incorporation of other polymer blocks), and size (from $< 10^4$ to $> 10^6$ g/mol). The method is well suited to produce homologous series of model materials (i.e., having precisely matched degree of polymerization, but varying in functionality and/or in extents of functionalization) that elucidate macromolecular physical phenomena. Examples from our own activities include studies of (i) association behavior of donor-acceptor chains in dilute solutions, (ii) sticky reptation, and (iii) solution properties of liquid-crystalline polymers bearing mesogenic side-groups.[23, 24]

The functional groups required for our research extend beyond the range of commercially available mercaptans (essentially limited to carboxylic acid, alcohol, 1,2-diol, amine, alkyl, and fluoroalkyl functionalities). Therefore, rapid, high-yield synthetic methods to prepare desired functional thiols are needed to make thiol-ene functionalization widely useful. Furthermore, technological application requires that these synthetic methods be amenable to scale up. We found that indirect preparation of thiols through thioester intermediates presents significant advantages with regard to safety, yield, and product stability. We

developed facile procedures to deprotect the thiols and—without isolation—proceed to functionalize 1,2-PB (Scheme 5.1). Thus, this contribution demonstrates how to conveniently extend the number of candidate side-groups for functionalization of polymers by thiol-ene coupling.

The present work documents highly efficient synthetic routes to an array of protected thiols which were chosen both (i) because the featured side-groups are important functionalities in their own right, and (ii) because each is representative of a general pathway for incorporation of the thiol moiety (Scheme 5.2). Specifically, phenol and pyridine functionalities are described because of their relevance as hydrogen-bond donor and acceptor; carbazole and dinitrobenzoate are of interest as electron donor and acceptor, and relevant to materials with novel electronic properties; and 4-cyano-4'-hydroxybiphenyl is of interest for its liquid-crystalline properties. Of paramount practical significance, the featured chemistry involves: (i) inexpensive, readily available reagents of moderate toxicity and reactivity, (ii) no elaborate equipment or procedures, (iii) rapid, quantitative conversions of limiting reagents in all steps without measurable formation of side-products, and (iv) simple purification (enabled by the clean synthetic routes) using scalable separation processes (principally liquid-liquid extraction and washes and occasionally recrystallization but no column separations).

5.2 Experimental

5.2.1 Materials and Instrumentation

Except for thiobenzoic acid (Alfa Aesar, 94%), carbazole (Aldrich, 95%), 4'-hydroxy-4-carbonitrile (TCI, 95%), thioacetic acid (Aldrich, 96%), allyl bromide (Aldrich, 97%), hydrazine monohydrochloride (Acros Organics, 98%), *p*-toluenesulfonyl chloride (Alfa Aesar, 98%), and *p*-toluenesulfonic acid monohydrate (Aldrich, 98.5%), all reagents were obtained at 99% purity from Aldrich, Alfa Aesar, or Mallinckrodt Chemicals. 2,2′-Azobis(2-methylpropionitrile) (AIBN) was recrystallized biweekly in methanol (10 mL solvent per g AIBN) and stored at 4 ºC; all other reagents were used as received without further purification. Polybutadiene polymer chains (98% 1,2-content) of size 92×10^3 and 820×10^3 g/mol and narrow molecular weight distribution (of polydispersity index 1.07 and 1.26, respectively) were kindly donated by Dr. Steven Smith of Procter and Gamble Company. ^{1}H and ^{13}C NMR spectra were obtained using a Varian Mercury 300 spectrometer (300 MHz for

^{1}H and 74.5 MHz for ^{13}C); all spectra were recorded in $CDCl_3$ and referenced to tetramethylsilane. Polymer molecular weight measurements were obtained by gel permeation chromatography using one of two systems. Measurements were either carried out (i) in tetrahydrofuran (THF) at 25 ºC eluting at 0.9 mL/min through four PLgel 10-μm analytical columns (Polymer Labs, 10^6 to 10^3 A in pore size) connected to a Waters 410 differential refractometer detector (λ = 930 nm) or (ii) in THF on two PLgel 5-μm mixed-C columns (Polymer Labs) connected in series to a DAWN EOS multi-angle laser light scattering (MALLS) detector (Wyatt Technology, Ar laser, λ = 690 nm) and an Optilab DSP differential refractometer (Wyatt Technology, λ = 690 nm). In the former case, molecular weight measurements were analyzed based on calibration using polystyrene standards; in the latter case no calibration standards were used, and d*n*/d*c* values were obtained for each injection by assuming 100% mass elution from the columns.

5.2.2 Synthesis of Benzoyl- or Acetyl-Protected Thiols (Scheme 5.2)

All reactions were monitored by ^{1}H NMR spectroscopy. Analysis of reaction mixtures was generally performed by washing a ~ 1-mL aliquot with water and extracting organic reactants and products into an appropriate solvent, followed by solvent evaporation, and redissolving in $CDCl_3$ for NMR analysis. ^{13}C NMR resonances of compounds **1, 3, 6, 8, 10, 12,** and **13** are documented in Appendix B.

2-Chloroethyl-*p*-toluenesulfonate (1). *p*-Toluenesulfonyl chloride (172 g, 0.884 mol) and pyridine (59 g, 0.75 mol) were added to 180 mL of dichloromethane (DCM) in a 1-L round-bottom flask (RBF) which was placed in an ice bath for ~ 5 min. 1-Chloroethanol (40.3 g, 0.496 mol) was added slowly, and the RBF was taken out of the ice bath and left to stir at room temperature for 15 h. The reaction mixture was poured into a 1-L separatory funnel, washed twice with 300 mL water + 50 mL pyridine, and again with 300 mL water + 75 mL 36 wt % aqueous HCl (discarding the aqueous phase after each wash). Removal of the solvent at reduced pressure yielded analytically pure **1** as a faint yellow, thick syrup (116 g, 0.494 mol, 100% yield). ^{1}H NMR: δ = 7.81 (d, 2 aromatic H meta to CH_3, J = 8.3 Hz), 7.37 (d, 2 aromatic H ortho to CH_3, J = 8.3 Hz), 4.23 (t, OCH_2, J = 5.9 Hz), 3.66 (t, CH_2Cl, J = 5.9 Hz), 2.46 (s, CH_3).

4'-(2-(Benzoylthio)ethoxy)[1,1'-biphenyl]-4-carbonitrile (3). 4'-Hydroxy[1,1'-biphenyl]-4-carbonitrile (5.1 g, 0.025 mol), 2-chloroethyl-*p*-toluenesulfonate (**1**, 9.2 g, 0.039

mol), and potassium carbonate (5.3 g, 0.038 mol) were stirred at 57 ºC in 100 mL of dimethyl sulfoxide (DMSO) for 22 h, resulting in quantitative conversion to **2** (verified by NMR analysis). Potassium chloride (2.1 g, 0.028 mol) was added to the reaction mixture, which was stirred 3 h at 85 ºC to convert the excess **1** into dichloroethane. The reaction mixture was poured into a 1-L separatory funnel containing 300 mL water and extracted with 200 mL of 2-butanone (MEK). The aqueous phase was extracted with another 300 mL MEK, and the organic extracts were combined and washed 3 times with 300 mL water. Finally, solvent and dichloroethane were evaporated under reduced pressure at 80 ºC to give **2** (6.4 g, 0.025 mol, 100% yield) as a brown-orange syrup which solidifies upon cooling. To the previous product in 100 mL of *N*,*N*-dimethylformamide (DMF) in a 250 mL RBF were added thiobenzoic acid (7.3 g, 0.050 mol) and potassium bicarbonate (6.8 g, 0.068 mol), and the mixture was stirred at room temperature until CO_2 effervescence ceased and then at 45 ºC for 4 h. The reaction mixture was transferred to a 1-L separatory funnel containing 250 mL of water, extracted with 400 mL of ethyl acetate, and the organic phase was washed twice with 250 mL of water before solvent removal under reduced pressure. The crude product was purified by dissolving in 300 mL of ethanol at 90 ºC (under slight pressure), and allowing to recrystallize by slowly cooling to room temperature, then by letting stand overnight at 4^{o} C. Filtration of the crystals and removal of solvent under reduced pressure gave analytically pure **3** as ultra-fine, pale brown needles (7.9 g, 0.022 mol, 88% overall yield in 2 steps). ^{1}H NMR: δ = 8.02-7.96 (m, 2 aromatic H ortho to COS), 7.72-7.43 (m, 3 aromatic H meta and para to COS, 4 aromatic H ortho and meta to CN, and 2 aromatic H meta to OCH_2), 7.05 (d, 2 aromatic H ortho to OCH_2, J = 8.7 Hz), 4.25 (t, OCH_2, J = 6.6 Hz), 3.50 (t, SCH_2, J = 6.6 Hz).

4'-(2-(2-(Benzoylthio)ethoxy)ethoxy) [1,1'-biphenyl]-4-carbonitrile (6). 4'-Hydroxy[1,1'-biphenyl]-4-carbonitrile (4.9 g, 0.024 mol), 2-(2-chloroethoxy)ethanol (12.7 g, 0.101 mol) and potassium phosphate tribasic ($K_3PO_4.xH_2O$, 22 g at ~ 25 wt % water, 0.078 mol) were stirred at 110 ºC in 150 mL of DMSO for 12 h, resulting in quantitative conversion to **4** (verified by NMR analysis). The reaction mixture was poured into a 1-L separatory funnel containing 200 mL of chloroform and washed 5 times with 400 mL of water to remove all of the chloroalcohol. The resultant organic phase was dried with $MgSO_4$ and filtered, and the solvent was removed under reduced pressure at 60 ºC to afford analytically pure **4** (6.5 g, 0.023 mol, 96% yield) as a pale yellow-orange syrup which solidifies upon

cooling. To this product in 100 mL of DCM at 0 ºC were added *p*-toluenesulfonyl chloride (22.2 g, 0.115 mol) and pyridine (7.2 g, 0.091 mol), after which the reaction vessel was allowed to warm up to room temperature and left to stir at room temperature for 24 h. The reaction mixture was transferred to a 500-mL separatory funnel, washed twice with 150 mL of water + 25 mL of pyridine, and again with 150 mL of water and 40 mL of 36 wt % aqueous HCl (discarding the aqueous phase after each wash). The organic phase was again dried with $MgSO_4$, filtered, and the solvent was removed under reduced pressure at 40 ºC to yield analytically pure **5** (9.5 g, 0.022 mol, 95% yield), which was finally reacted to generate **6** as follows. To 1.96 g (4.5 mmol) of the said product in 40 mL of DMF were added thiobenzoic acid (0.69 g, 4.7 mmol, 1.05 equiv) and potassium bicarbonate (1.0 g, 10 mmol), and the mixture was stirred at room temperature until CO_2 effervescence ceased, then at 40 ºC for 12 h. The reaction mixture was transferred to a 500-mL separatory funnel containing 200 mL of water, extracted with 100 mL of ethyl acetate, and the organic phase was washed three additional times with 200 mL of water, dried with $MgSO_4$, and gravity filtered before solvent removal at 80 ºC under reduced pressure to give analytically pure **6** as an orange syrup which crystallizes upon cooling (1.80 g, 4.5 mmol, 91% overall yield in 3 steps). ^{1}H NMR: δ = 8.00-7.93 (m, 2 aromatic H ortho to COS), 7.72-7.39 (m, 3 aromatic H meta and para to COS, 4 aromatic H ortho and meta to CN, and 2 aromatic H meta to OCH_2), 7.02 (d, 2 aromatic H ortho to OCH_2, J = 8.7 Hz), 4.19 (t, $ArOCH_2$, J = 4.8 Hz), 3.90 (t, $ArOCH_2CH_2$, J = 4.8 Hz), 3.79 (t, SCH_2CH_2, J = 6.5 Hz), 3.33 (t, SCH_2CH_2 , J = 6.5 Hz).

Thiobenzoic Acid *S*-[2-(9-carbazolyl)ethyl] Ester (8). Carbazole (15.2 g, 0.086 mol), 2-chloroethyl-*p*-toluenesulfonate (**1**, 60.2 g, 0.256 mol), and potassium hydroxide (88 wt % pellets, 13.7 g, 0.215 mol) were stirred at room temperature in 300 mL of DMSO for 18 h, resulting in quantitative conversion to **7** (verified by NMR analysis). Trichloroacetic acid (TCA, 22 g, 0.135 mol) and potassium chloride (20 g, 0.268 mol) were added to the reaction mixture, which was stirred 4 h at 100 ºC to convert the excess **1** to dichloroethane. After titration of the excess TCA by potassium bicarbonate (15.5 g, 0.155 mol), the reaction mixture was poured into a 1-L separatory funnel containing 180 mL of water and extracted with 300 mL of chloroform. The organic phase was washed twice with 400 mL of water; the solvent was evaporated under reduced pressure; and the crude product was purified by dissolving in 475 mL of boiling ethanol and allowing it to recrystallize at room temperature overnight, yielding analytically pure **7** (16.5 g, 0.072 mol, 83% yield) after filtration and

solvent removal. To 6.8 g (0.030 mol) of this product in 110 mL of DMF were added thiobenzoic acid (8.9 g, 0.061 mol) and potassium bicarbonate (8.0 g, 0.080 mol); the mixture was swirled with gentle heating until CO_2 effervescence ceased and then was allowed to react for 4 h at 50 ºC. The reaction mixture was poured into a 500-mL separatory funnel containing 100 mL of water, extracted with 100 mL of chloroform, and the organic phase was washed twice with 150 mL of water before solvent removal under reduced pressure. The crude product was purified by first dissolving in 35 mL of hot chloroform, adding 200 mL of boiling ethanol, and allowing it to recrystallize overnight at room temperature. Filtration of the crystals and removal of solvent under reduced pressure gave analytically pure **8** as very fine, orange-pink needles (8.3 g, 0.025 mol, 70% overall yield in 2 steps). ^{1}H NMR: δ = 8.10 (d, 2 carbazole H, J = 7.5 Hz), 8.03-7.96 (m, 2 aromatic H ortho to COS), 7.64-7.57 (m, 3 aromatic H meta and para to COS), 7.54-7.43 (m, 4 carbazole H), 7.30-7.21 (m, 2 carbazole H), 4.55 (t, NCH_2, J = 7.8 Hz), 3.44 (t, SCH_2, J = 7.8 Hz).

3,5-Dinitrobenzoic Acid 3-(acetylthio)propyl Ester (10). Potassium bicarbonate (7.2 g, 0.072 mol) was added to 3,5-dinitrobenzoic acid (10.0 g, 0.047 mol) in 150 mL of DMSO in a 500-mL RBF, and the slurry was swirled with gentle heating until CO_2 effervescence ceased. Allyl bromide (11.8 g, 0.095 mol) was added next, and the RBF was placed in an oil bath to stir at 70 ºC for 2.5 h. The reaction mixture was poured into a 1-L separatory funnel containing 250 mL of chloroform and washed twice with 400 mL of water (discarding the aqueous phase after each wash), yielding **9** (10.7 g, 0.042 mol, 91% yield) in > 99% purity after removal of allyl bromide and solvent at 80 ºC under reduced pressure. To this product in 100 mL of toluene was added thioacetic acid (9.8 g, 0.124 mol), and the reaction was carried out at 85 ºC with argon purge via radical mechanism using AIBN as the initiator (0.70 g, 4.3 mmol, in 0.175-g increments at 1-hr intervals). After 6 h the reaction mixture was poured into a 1-L separatory funnel containing 16 g sodium bicarbonate ($NaHCO_3$, 0.19 mol) in 300 mL of water, extracted with 100 mL of chloroform, and the organic phase was washed twice with 300 mL of water before solvent removal under reduced pressure. The crude product was purified by washing four times in 50 mL of hexane at 60 ºC, yielding **10** in > 99% purity as a viscous, dark brown syrup (9.1 g, 0.028 mol, 59% overall yield in 2 steps). ^{1}H NMR: δ = 9.24 (t, 1 aromatic H para to CO_2, J = 2.1 Hz), 9.19 (d, 2 aromatic H ortho to CO_2, J = 2.1 Hz), 4.52 (t, OCH_2, J = 6.3 Hz), 3.07 (t, SCH_2, J = 6.9 Hz), 2.37 (s, CH_3), 2.15 (tt, $OCH_2CH_2CH_2S$, J = 6.9, 6.3 Hz).

4-Hydroxybenzoic acid 2-(benzoylthio)ethyl Ester (12). 4-Hydroxybenzoic acid (10 g, 0.072 mol) and 1-chloroethanol (60 g, 0.73 mol) were reacted in the bulk at 110 ºC for 16 h with *p*-toluenesulfonic acid monohydrate (2.7 g, 0.014 mol) as catalyst. The reaction mixture was transferred to a 500-mL separatory funnel containing 5 g of sodium bicarbonate in 125 mL of water, extracted with 150 mL of ethyl acetate, and the organic phase was washed 4 times with 125 mL of water before solvent removal under reduced pressure, yielding **11** in ~ 97% purity (13 g, 0.063 mol, 88% yield). To this product in 100 mL of DMF were added thiobenzoic acid (18 g, 0.12 mol) and potassium bicarbonate (16 g, 0.16 mol), and the mixture was stirred at room temperature until CO_2 effervescence ceased and then at 50 ºC for 4 h. The reaction mixture was poured into a 500-mL separatory funnel containing 100 mL of water and extracted with 100 mL of chloroform, and the organic phase was washed 3 times with 150 mL of water before solvent removal at reduced pressure. The crude product was finally purified by first dissolving it in 50 mL of hot chloroform, then adding 25 mL of boiling hexane and allowing it to recrystallize overnight in the freezer. Filtration of the crystals and removal of the solvent under reduced pressure gave analytically pure **12** as a pink powder (14.5 g, 0.048 mol, 67% overall yield in 2 steps). ^{1}H NMR: δ = 8.02-7.93 (m, 2 aromatic H ortho to CO_2 and 2 aromatic H ortho to COS), 7.59 (tt, 1 aromatic H para to COS, J = 7.5, 1.2 Hz), 7.51-7.42 (m, 2 aromatic H meta to COS), 6.87 (d, 2 aromatic H meta to CO_2, J = 8.7 Hz), 5.8 (br, ArO*H*), 4.50 (t, OCH_2, J = 6.5 Hz), 3.47 (t, SCH_2, J = 6.5 Hz).

Thiobenzoic Acid *S*-[3-pyridinylmethyl] Ester (13). Potassium bicarbonate (12.3 g, 0.123 mol) was added to thiobenzoic acid (14.2 g, 0.097) in 200 mL of ethanol in a 500-mL RBF, and the slurry was swirled with gentle heating until CO_2 effervescence ceased. 3-(Chloromethyl)pyridine hydrochloride (10.2 g, 0.060 mol) was added next, and the RBF was placed in an oil bath to stir at 50 ºC for 2.5 h. The reaction mixture was poured into a 1-L separatory funnel containing 10 g of potassium carbonate (K_2CO_3, 0.072 mol) in 250 mL of water and extracted with 150 mL of DCM, and the organic phase was washed twice with 250 mL of water, gravity filtered, and evaporated to dryness under reduced pressure. The crude product was purified further by washing in 50 mL of hot hexane to give, after removal of leftover solvent under reduced pressure, **13** as a brown solid in ~ 96% purity (11.4 g, 0.050 mol, 80% yield). ^{1}H NMR: δ = 8.64 (d, 1 aromatic H ortho to CH_2 at the second C of the pyridine ring, J = 1.8 Hz), 8.50 (dd, 1 aromatic H para to CH_2 at the sixth C of the pyridine ring, J = 4.8, 1.5 Hz), 7.99-7.90 (m, 2 aromatic H ortho to COS), 7.71 (ddd, 1 aromatic H

ortho to CH_2 at the fourth C of the pyridine ring, J = 7.8, 1.8, 1.5 Hz), 7.58 (tt, 1 aromatic H para to COS, J = 7.5, 1.2 Hz), 7.49-7.39 (m, 2 aromatic H meta to COS), 7.24 (dd, 1 aromatic H meta to CH_2 at the fifth C of the pyridine ring, J = 7.8, 4.8 Hz), 4.29 (s, CH_2).

5.2.3 Polymer Functionalization

General Procedure for 1,2-PB Functionalization Using a Protected Thiol PhCOSR (Scheme 5.1). To the thioester PhCOSR (1–4 mmol) dissolved in 25–75 mL of DMF in a 250-mL RBF were added hydrazine monohydrochloride (~ 4 equiv, 4–16 mmol) and sodium acetate (~ 8 equiv, 8–32 mmol). The RBF was purged with argon for ~ 10 min and left to stir at room temperature for 2–4 h, resulting in 95–100% cleavage of the thioester (verified by NMR analysis). The thiol product was extracted into 30–40 mL of chloroform after addition of 100 mL of water; the organic phase was washed 4 times with 150 mL of water, and transferred into a 100-mL Schlenk tube containing 1,2-PB (0.1–0.2 g, 2–4 mmol, dissolved in 10 mL of chloroform) and AIBN (50–250 mg, 0.3–1.5 mmol). The contents of the Schlenk tube were degassed in three freeze-pump-thaw cycles, and then allowed to react at 55 ºC for 2–6 h. Following reaction, the polymer solution was transferred to a 100-mL jar containing a small amount of 2,6-di-*tert*-butyl-4-methylphenol (BHT), concentrated by evaporation of all but the last 10 mL solvent under an argon stream, and precipitated with cold methanol. Final purification of the polymer was achieved by reprecipitation from a DCM or THF solution (containing ca. 1 wt % BHT) with cold methanol (repeated 2–4 times), followed by drying to constant weight under vacuum at room temperature.

General Procedure for 1,2-PB Functionalization Using an Acyl Chloride RCOCl (Scheme 5.3). To 1,2-PB (0.1–0.5 g, 2–9 mmol) dissolved in 15–30 mL THF in a 100-mL Schlenk tube was added a 10 mL THF solution of 2-mercaptoethanol (BME, 0.5–2 equiv, 1–20 mmol) and AIBN (15–50 mg, 0.1–0.3 mmol). The contents of the Schlenk tube were degassed in three freeze-pump-thaw cycles, and then allowed to react at 55 ºC for 2–3 h. Following reaction, the polymer solution was transferred to a 100-mL jar containing a small amount of BHT and precipitated in cold methanol. The polymer was purified by reprecipitation from a THF solution (containing ~ 1 wt % BHT) with cold methanol (repeated 1–2 times), followed by drying to constant weight under vacuum at room temperature. To the 2-hydroxyethylthio-functionalized 1,2-PB polymer (0.1–0.5 g) dissolved in 10–25 mL of DCM in a 100-mL RBF were added triethylamine (Et_3N, 3–5 mol equiv of functionalized

monomer units) and the acyl chloride RCOCl (2.5–3 mol equiv of functionalized monomer units), and the reaction mixture was stirred 3–4 h at room temperature. Following reaction, the polymer solution was transferred to a 100- or 250-mL jar containing a small amount of BHT, washed with 50–100 mL of water and again with 50–100 mL of aqueous sodium bicarbonate (discarding the wash each time), concentrated by evaporation of all but the last 10 mL of DCM under an argon stream, and finally precipitated with cold methanol. Final purification of the polymer was achieved by reprecipitation from a DCM solution (containing ~ 1 wt % BHT) with cold methanol (repeated 2–3 times), followed by drying to constant weight under vacuum at room temperature.

5.3 Results

5.3.1 Synthesis of Protected Thiols

The set of protected thiols was chosen to illustrate clean, high-yield synthetic routes to introduce the thiol moiety onto functional molecules. Molecules were selected for the importance of their functionalities and for their reactive groups available for derivatization (Scheme 5.2). Thus, we exemplify the synthesis of protected mercaptans using an accessible phenol or alcohol group (compounds **3** and **6**), a heterocyclic nitrogen atom (compound **8**), an accessible carboxylic acid group (compounds **10** and **12**), a terminal olefin group (compound **10**), or an available halide atom (compounds **3**, **8**, **12**, and **13**). Compounds **3** and **6** illustrate convenient methods to control the distance between the grafted side-group and the polymer backbone after thiol-ene coupling. Note that an 8-atom spacer can be incorporated by replacing $H(OCH_2CH_2)_2Cl$ with commercially available $H(OCH_2CH_2)_3Cl$ in the described procedure for the synthesis of **4**. We will return to address synthetic crossroads for introduction of the thioester functionality in Section 5.4.3.

Reaction conditions for the synthesis of compounds **2–13** demonstrate highly efficient and *scalable* methods of significant synthetic utility. ^1H NMR analysis of crude reaction mixtures showed that all reaction steps resulted in quantitative conversion to desired product (except synthesis of **9** and **11**, for which conversion was ~ 90%). The clean synthetic steps made it possible to isolate products in 95–100% purity and 90–100% yield by mere use of liquid-liquid extraction/washes, and evaporation of low-boiling compounds. In some cases, further purification was achieved by recrystallization to yield analytically pure product (compounds **3**, **7**, **8**, and **12**).

5.3.2 Alkylation of Nucleophiles to Introduce Primary Halide or Alcohol Moieties

To generate ω-chloroalkyl or ω-bromoalkyl derivatives, alkylation of nucleophiles is usually done using α,ω dibromo- or dichloroalkanes, e.g., reaction of 4'-hydroxy-biphenyl-4-carbonitrile with 1,6-dibromohexane[25] or carbazole with 1,2-dichloroethane.[26] Unfortunately, when using these reagents bisubstitution is always an issue. In addition, in the case of very basic nucleophiles (e.g., deprotonated carbazole), elimination competes effectively; hence, yields tend to be low and product purification usually requires column chromatography. We were not, for instance, able to achieve yields > 50% for the synthesis of **7** according to published methods[26] using KOH/K_2CO_3 as base in 1,2 dichloroethane with tetrabutylammonium bromide as phase-transfer catalyst. We found, however, that chloroethylation of nucleophiles with 2-chloroethyl-*p*-toluenesulfonate (**1**) in DMSO at low to moderate temperatures overcame both problems stated above. First, the use of *p*-toluenesulfonate (tosylate) as the leaving group and of a polar aprotic solvent both favor substitution over elimination;[27] second, because tosylate is a significantly better leaving group than chlorine, quantitative conversion of both carbazole and 4'-hydroxy-biphenyl-4-carbonitrile to the chloroethyl derivatives (compounds **7**, **2**) was achieved without measurable formation of side-products. Excess **1** could be reacted quantitatively to 1,2-dichloroethane with KCl in a few hours, so that product in quantitative yields and > 95% purity could be obtained by mere liquid-liquid extraction and removal of solvent and dichloroethane at reduced pressure.

Alkylation of nucleophiles to generate ω-hydroxyalkyl derivatives is usually done using ω-bromo-1-alkanols or ω-chloro-1-alkanols with K_2CO_3 or NaH as base in DMF, acetone, or ethanol as solvent (for instance, alkylation of 4'-hydroxy-biphenyl-4-carbonitrile with bromodecanol[28] or chlorohexanol[29]). Published yields for such reactions are usually < 85 %, and column chromatography is typically necessary for isolation of the product. We found, however, that alkylation of 4'-hydroxy-biphenyl-4-carbonitrile with commercially available $H(OCH_2CH_2)_nCl$ (n = 1–3, inexpensively available from Wako Chemicals) in DMSO with K_3PO_4 as base gave quantitative conversion, and that product (compound **4** or analog) in > 99% purity could be obtained by mere washes due to the good water solubility of the chloride reagent.

5.3.3 Functionalization of 1,2-PB

Reaction conditions for 1,2-PB functionalization given in Table 5.1 incorporate functional side-groups while preserving the narrow molar mass distribution of the precursor polymer material (Table 5.1, Figures 5.1–5.4). Depending on the application, degrees of functionalization from ≤ 1% to ≥ 50% are of interest; here, we demonstrate systematic control of functionalization (X_{funct}) from a few % to 40% (Table 5.1). PB chains with very high 1,2-content tend to form cyclic adducts, which limit functionalization to ≤ 50% unless very high thiol concentrations are used.[18, 19] Accounting for the formation of ring structures by random cyclization of adjacent repeat units during the addition reaction, the general structure of the functionalized polymer is as shown in Figure 5.1. That structure is solved by considering that either five- or six-member rings can be formed, and that polycyclic structures are possible. Note that any cyclic or polycyclic structure involves at most one five-member ring (on either side of which can be fused any number of six-member rings), and that there are exactly as many methyl groups in the functionalized polymer as there are five-member rings. Let X_{funct} be the fraction of reacted 1,2-PB repeat units bearing functional groups, $X_{unreact}$ be the fraction of unreacted 1,2-PB repeat units, and X_{cycl} be the fraction of reacted 1,2-PB repeat units that are unfunctionalized. Thankfully, analysis of the general structure (Figure 5.1) provides an unambiguous relationship between X_{funct}, $X_{unreact}$, X_{cycl} and three quantities that are readily determined from the ^{1}H NMR spectra: the relative values of the integrals of RC**H$_2$**S- methylene protons (S_1), **H$_2$**C=CH- alkenic protons (S_2), and aliphatic protons of chemical shifts below 2.2 ppm (S_3). In terms of the indices defined in Figure 5.1, $S_1 \sim 2(n + m + m')$ and $S_2 \sim 2u$. Furthermore, since none of the side-groups R in the present study display protons with $\delta < 2.2$ ppm, $S_3 \sim [5\,n + 4\,(m + m') + 6\,(p + p' + t) + 7\,(q + v) + 3\,u]$. Because there are as many beginnings as ends in both *y* and *z* structures (Figure 5.1, top), $m = q$, and $m' = v$; therefore, $(p + p' + t + q + v) = (2S_3 - 3S_2 - 5S_1)/12$. Thus, X_{funct}, $X_{unreact}$, and X_{cycl} can be calculated by the expressions below without any knowledge of the relative amounts of the repeat units *m*, *m*', *p*, *p*', *q*, *t*, or *v* in the functionalized polymer:

$$X_{funct} = \frac{n+m+m'}{n+m+m'+p+p'+t+q+v+u} = \frac{6S_1}{S_1+3S_2+2S_3}$$

$$X_{unreact} = \frac{u}{n+m+m'+p+p'+t+q+v+u} = \frac{6S_2}{S_1+3S_2+2S_3}$$

$$X_{cycl} = 1 - X_{funct} - X_{unreact} \quad .$$

Functional polymer could also be obtained in a two-step polymer modification procedure, by thiol-ene addition of β-mercaptoethanol (BME), followed by esterification of the incorporated hydroxyl groups with a suitable acyl halide (Scheme 5.3, Table 5.2). We found that the narrow polydispersity of well-defined precursor polymer material could also be preserved throughout this process (Table 5.2), so that the procedure offers a useful alternative to direct coupling of a thiol derivative when an acyl chloride compound featuring the desired functionality is readily accessible.

5.3.4 Molecular Structure of Functionalized 1,2-PB Polymer

Let us first see why there are indisputably cyclic structures. To begin, the potential to form cyclic structures follows from the reaction mechanism. The addition reaction is initiated by abstraction of a thiol hydrogen by a cyanopropyl free radical. The resultant thiyl radical (RS·) adds to a double bond of 1,2-PB in anti-Markovnikov fashion,[16-18] generating a polymeric alkyl radical (e.g., structure **I** in Figure 5.5). As shown in the figure, transfer of hydrogen from another thiol molecule completes the addition reaction (structure **II**) and regenerates a new RS$^{\bullet}$ participant; alternatively, intramolecular reactions of **I** compete with hydrogen transfer to form structures **III** and **IV**. As evidence for the formation of ring structures by intramolecular cyclization, Schlaad[18, 19] pointed to incomplete functionalization at full conversion of double bonds using 1,2-PB-*block*-poly(ethylene oxide) as starting material, i.e., typically only 60–80 functional side-groups were found for every 100 reacted 1,2-PB repeat units. Direct evidence of cyclization is seen in the ^{1}H NMR spectra in the present study (bottom trace in Figure 5.2 and spectra in Appendix B): the broad peaks below 2.2 ppm are not consistent with the structures of repeat units *w* and *x* in Figure 5.1, but consistent with cyclohexyl or cyclopentyl proton signals. Further, the observed multiple peaks assignable to the $RCH_2SC\mathbf{H_2}$- protons of the functionalized polymer (protons 4, 5, 6; Figure 5.2) cannot be explained in the absence of cyclization, but are consistent with a combination of the repeat units *n*, *m*, and *m*' in Figure 5.1.

The question now arises whether radical **I** in Figure 5.5 predominantly forms **III** or **IV** during cyclization. On the basis of the relative thermodynamic stability of secondary vs. primary radical intermediates, Schlaad and coworkers[18] have suggested that six-member rings (**III**) should be preferred over their five-member counterparts (**IV**); however, experimental results discussed in the next few paragraphs give instead evidence to the contrary. First, our

data reveals a high content of five-member rings in reacted polymer. NMR analysis of our product for highly functionalized chains shows (i) a strong peak around 17 ppm in the solid state ^{13}C spectra (Figure 5.3), and (ii) a strong signal at 1–0.9 ppm in the ^{1}H NMR spectra (Figure 5.2, bottom). Both these signals are consistent with the methyl group of structure *v* in Figure 5.1. Since there are exactly as many five-member rings as methyl groups in the functionalized polymer, we deduce that a large number of unfunctionalized, reacted monomers cyclized into five-member rings.

Next, literature results[22, 30] on the radical addition of primary alkyl iodides to 1,2-PB and α,ω-alkadienes provides further evidence. Although the initiation, addition, and transfer steps for RI vs. RSH radical addition involve molecules of substantially different reactivity, the intermediate radicals involved in *intra*molecular cyclization have essentially the same structure (i.e., replace RS by R in structures **I**, **III**, and **IV** of Figure 5.5). Thus, the relative rates of formation of five- vs. six-member ring structures should be comparable. According to reports on the radical addition of perfluoroalkyl iodides to 1,2-PB[22] and 1,6 heptadiene,[30] intramolecular reaction of polymer radical **I** is expected to form primarily five-, instead of six-, member cyclic intermediates (structure **IV** rather than **III**).

In order to make further progress, let us now consider the competition between H-abstraction by **I** (forming **II**) vs. cyclization of **I** (to form **III** or **IV**). This competition depends on both thiol concentration and steric hindrance as chain modification proceeds. Let r_1, r_2, r_3 and p_1, p_2, p_3 denote the reaction rates and transition probabilities for the pathways **I→ II**, **III,** or **IV**, respectively (Figure 5.5). Consider a thiol-ene coupling event that yields a radical with a neighboring vinyl group, such as **I**. The fraction of events that proceed to form simple pendant groups **II** vs. cycles (**III** or **IV**) is $p_1/(p_2+p_3)$. Furthermore, $p_1/(p_2+p_3) = r_1/(r_2+r_3)$, which is proportional to [RSH], since r_1 is first-order and r_2 and r_3 are zero-order in thiol concentration. Let the coefficient of proportionality be k, i.e., $p_1/(p_2+p_3) = k$[RSH], where k may vary with the extent of conversion due to steric hindrance. Given that $p_1/(p_2+p_3) = p_1/(1-p_1)$, we see that $p_1 = k$[RSH]/(1+k[RSH]); hence, p_1 increases linearly with [RSH] at low thiol concentration ([RSH]<<1/k) and saturates to 1 at [RSH]>>1/k (Figure 5.6). Schlaad[18] reported saturation of the extent of functionalization for [RSH] >10M. With decreasing [RSH], he further observed that cyclization began to compete significantly at [RSH] ≤ 5M. Using k[RSH] ~ O(10) at the onset of competition (Figure 5.6), we deduce k ~ O(1 M^{-1}).

The above result has important implications for the relative formation of five- vs. six-member rings. First, the finding that $k \sim O(1\ M^{-1})$ leads immediately to the realization that under the functionalization conditions used in the present study ([RSH] ~ $O(10^{-1}$ M or less), radical **I** (Figure 5.5) primarily undergoes intramolecular reaction, i.e., $p_1 \approx p_1/(p_2+p_3) \sim O(10^{-1}$ or less). Second, the fact that very little of radical **I** proceeds to abstract H from RSH under these conditions suggests that likewise very little of radical **III** would abstract H under the same conditions (judging reactivity based on structure similarity). Therefore, if, as Schlaad suggests, intramolecular cyclization of **I** led primarily to the six-member rings **III**, the similarity of **I** and **III** would cause **III** to propagate a ladder of many six-member cycles prior to concluding with H-abstraction from RSH. In that case, our functionalized polymer would then display (i) very high ratios of cyclization to functionalization, $X_{cycl}/X_{funct} >> 1$, and (ii) very few five-member rings. Both these results are contrary to our observations.

We conclude by suggesting that the data is consistent with the following predominant pathway: **I** → **IV** → **V** (Figure 5.5) for thiol concentrations on the order of 10^{-2}–10^{-1} M. That is, **I** cyclizes predominantly (and preferably to form five-member rings), but **IV** abstracts hydrogen predominantly. Note that such different relative reactivity for radicals **I** and **IV** are reasonable based on their structures. Further, this reaction pathway successfully explains the observed ratios of X_{funct}/X_{cycl} in the relatively narrow range of 0.65–1 (Tables 5.1 and 5.2) over the > 1 order of magnitude range of thiol concentration spanned by our experiments. If the reaction proceeded exclusively from **I** to **IV** to **V** ($p_1 = p_2 = p_5 = 0$), then $X_{funct}/X_{cycl} = 1$ and the polymer structure would consist exclusively of unreacted 1,2 units and functionalized five-member rings. In reality, deviations from $p_2 = 0$ or $p_5 = 0$ account for values of X_{funct}/X_{cycl} smaller than 1, and deviation from $p_1 = 0$ account for values of X_{funct}/X_{cycl} larger than 1. Increasing [RSH] increases p_1, leading to a greater number of acyclic functionalized units. The general predominant polymer structure is therefore the one given in Scheme 5.1.

5.4 Discussion

5.4.1 Direct or Indirect Functionalization?

The utility of indirect functionalization by esterification of 2-hydroxyethylthio-modified PB (Scheme 5.3) is somewhat limited by the high reactivity of acyl halides, which renders them incompatible with a number of important functional groups and working conditions. Furthermore, our experience with polymers that are susceptible to cross-linking (such as high

MW 1,2-PB) indicates that best results are typically achieved by minimizing the number of synthetic steps involving macromolecules. Finally, we found that the time invested in the synthesis of protected thiols is easily regained in subsequent tailoring of polymer properties by quicker adjustments in the number density of grafted side-groups. Thus, we find that direct polymer functionalization according to Scheme 5.1 is preferable in most cases. However, indirect functionalization according to Scheme 5.3 becomes useful when (i) a suitable acyl halide is commercially available, and (ii) Scheme 5.1 fails for one reason or another; e.g., due to unsatisfactory deprotection of a suitable thiol. For instance, deprotection of compound **10** to give the corresponding mercaptan did not give acceptable results due to apparent partial reduction of the nitro groups.

5.4.2 Choice of Protecting Group

The motivation for using protected thiols arises from issues of safety, yield, efficiency, and product stability. Direct preparation of thiols can be achieved by addition of hydrogen sulfide (H_2S) to alkenes or by substitution of alkyl halides with hydrogen sulfide or hydrosulfide (HS^-). These methods have the following disadvantages: first, both hydrogen sulfide and hydrosulfide present considerable health hazards, and second, sulfide byproducts are usually formed in significant amounts.[27, 31] Alternatively, the thiol functionality can be incorporated indirectly using other sulfur-containing compounds such as thiolcarboxylic acids, thiourea, or the thiolsulphate ion, followed by bond cleavage via, e.g., hydrolysis of the intermediates to generate the desired mercaptan.[31] The extra step required by any indirect method is balanced by the advantages of cleaner, less-wasteful reactions, and the use of less-toxic reagents. Because thiols are prone to oxidation (e.g., in air on standing), storage of protected thiols is also often considered a wiser choice.

On the basis of adverse side reactions that occur with the triphenylmethyl (trityl) group, we found it necessary to turn to other protecting groups. The widespread use of the trityl group[32] reflects the ease by which it is first incorporated by substitution of halides using triphenylmethyl mercaptan, and the ease with which it is quantitatively removed (< 2 hours in DCM at room temperature in the presence of TFA and triethyl- or triisopropylsilane[33-36]). Our interest in the trityl sulfide group was generated by the hope that both deprotection of the sulfide and addition of the resultant thiol to PB could be successfully carried out in one pot by using chloroform as the solvent (procedure described in Appendix B). Unfortunately,

experiments with 9-[2-(triphenylmethyl)thio]ethyl]carbazole (**14**, Scheme 5.4, Appendix B) showed that although both deprotection and addition reactions proceeded as desired, unacceptable degradation of the polymer also occurred under such conditions (Figure 5.7, right; Appendix B). It is also worth noting that triphenylmethyl mercaptan is a comparatively expensive reagent for the introduction of the thiol functionality.

Thioesters have been used extensively in the past as protecting groups of the thiol functionality, with more or less success towards selective deprotection based on the reagents and method used[37]. Recent literature reports[38-40] described selective, quantitative hydrolysis of thioesters to thiols under mild conditions, i.e., in < 2 hours at room temperature with hydrazine acetate in DMF. Oxygen esters were found to be resistant to hydrolysis under these conditions. These reports motivated us to use thioacetic acid or thiobenzoic acid as reagents for the indirect synthesis of mercaptans, with good success toward preparation of functionalized polybutadienes as documented in the present report. We found that thioacetic acid and thiobenzoic acid were essentially equivalent in reactivity, but that thiobenzoic acid offers the advantage of simpler purification of the thioester product due to differences in both solubility and melting point between products and impurities. For instance, the higher molecular weight products obtained with PhCOSH were usually solid compounds amenable to recrystallization.

5.4.3 Synthetic Crossroads for the Introduction of the Thioester Functionality

Thioesters can be generated using thioacetic acid or thiobenzoic acid either from nucleophilic displacement of a leaving group or from radical addition to a terminal alkene (Scheme 5.2). Reaction of a halide or tosylate is considerably more convenient than reaction of an alkene, since the nucleophilic displacement (i) does not require oxygen-free conditions and (ii) essentially does not generate any impurities. Indeed, quantitative radical reaction of alkenes (e.g., synthesis of **10**) is accompanied by the formation of radical termination products (0.05 to 0.3 molar equiv) which can greatly complicate the purification process.

In some cases a leaving group (e.g., synthesis of **13**) or alkene may be directly available, otherwise they can be introduced in one of the following ways: (i) alcohols can be converted into good leaving groups by tosylation (e.g., synthesis of **5**), (ii) carboxylic acids can be reacted by Fisher esterification with, e.g., 2-chloroethanol (e.g., synthesis of **11**), and (iii) nucleophiles can be alkylated with, for instance, allyl bromide (e.g., synthesis of **9**) or 2-

chloroethyl-*p*-toluenesulfonate (compound **1**, e.g., synthesis of **2** or **7**). The following considerations affect decision making regarding alkylation of nucleophiles. On the one hand, allyl bromide is considerably more reactive and available than **1**, and its reaction with nucleophiles proceeds cleanly (in contrast, care must be taken in choosing reaction conditions with compound **1** to prevent bisubstitution and minimize elimination). On the other hand, the use of allyl bromide suffers in the conversion of the resulting alkene to the desired protected thiol (e.g., **9** to **10**). As noted earlier, that reaction is air sensitive, and the side-products are often difficult to separate from the desired one. As a result, the ease of conversion and purification of thioesters from halides (e.g., **3** from **2**) often justifies the additional care required in the coupling of **1** to the molecule of interest (e.g., **1** to **2**).

Functional precursors bearing nucleophilic atoms also afford a convenient method to control the spacer length between the functional group of interest and the polymer backbone. For instance, 3-, 5- and 8-atom spacers can be accessed by alkylation of a nucleophile with inexpensively available $H(OCH_2CH_2)_nCl$ (n = 1,2,3; Wako Chemicals), followed by conversion to a protected thiol as in the synthesis of **6**.

5.4.4 Deprotection of Acetyl- or Benzoyl-Thioesters

In all cases (with the exception of compound **10**), cleavage of thioesters was achieved in > 95% yields (verified by ^{1}H NMR analysis) in 2–4 h with hydrazine acetate in DMF at room temperature (Scheme 5.1, step 1.1). Significantly, we found that hydrazine acetate could be generated in situ by ion exchange in DMF from considerably less expensive hydrazine hydrochloride and sodium acetate, with equally successful results.

A most compelling advantage of Scheme 5.1 for functionalization of PB using acetyl or benzoyl thioesters consists in the direct addition of the deprotected mercaptan to PB without its isolation as a purified intermediate. Extraction of the DMF reaction mixture with chloroform or DCM and subsequent washing of the organic phase (Scheme 5.1, step 1.2) yields in ~ 30 min a remarkably pure solution of the thiol in which the only impurities are *small amounts* of disulfide (due to exposure to air), unreacted thioester (< 5% of initial amount), DMF, and moisture. Radical addition of the thiol to PB is highly tolerant of these impurities and proceeds unaffected by their presence (Table 5.1).

5.4.5 Effect of Impurities

The radical addition of mercaptans to alkenes is known to be highly tolerant of a vast array of functional groups.[27] Indeed, we found that most impurities (such as disulfides, thioesters, solvents, water, etc.) were inconsequential during thiol-ene functionalization of PB, with the following notable exceptions. First, in one-pot reaction procedures after detritylation of triphenylmethyl sulfides, some unidentified compound(s) caused chain scission of 1,2-PB (as mentioned earlier, Figure 5.7, right). Second, we found that the presence of benzoyl disulfide (PhCOSSOCPh) resulted in significant cross-linking. For example, use of a sample of thiobenzoic acid *S*-[3-(9-carbazolyl)propyl] ester (**16**, Appendix B) containing ~ 0.2 molar equiv of benzoyl disulfide caused polydispersity to increase from PDI = 1.07 to 1.34 at 19% functionalization (Figure 5.7, left; Appendix B).

5.4.6 Implications of Extents of Cyclization for 1,2-PB

Depending on the reason for modifying the polymer, degrees of functionalization from a few % up to ~100% are of interest. Our experiments show cyclization to functionalization ratios X_{cycl}/X_{funct} of 1–1.5, meaning that during the course of the addition reaction, approximately as many reacted monomers were functionalized as were consumed without functionalization by intramolecular cyclization. We found this to be the case for reaction conditions spanning more than 1 order of magnitude in thiol concentration in the range $10^{-2} < [\text{RSH}] < 3 \times 10^{-1}$ M. That is, 1,2-PB functionalization at moderately low to very low thiol concentrations proceeds without excessive amounts of cyclization (which would be expected if radical **I** in Figure 5.5 led primarily to six-member rings, as explained earlier). The implications of this result are 2-fold. First, low target levels of functionalization can be readily achieved at low or very low [RSH], with minimal changes in the physical properties of the polymer product resulting from cyclic/polycyclic structures. This enables good control of the extent of reaction and minimizes waste of potentially highly valuable thiol reagent. Second, the result suggests an alternative synthetic strategy to using extremely high thiol concentration (on the order of 10 M!) in order to achieve high degrees of functionalization (e.g., > 70%). Taking advantage of the fact that cyclization to functionalization ratios remain in the narrow range of 1–1.5 at thiol concentrations of 0.01–0.1 M, the strategy involves synthesis of thioester compounds featuring two functional side-groups per molecule. Deprotection and addition to 1,2-PB according to Scheme 5.1 using thiol concentrations on

the order of 0.1 M will result in incorporation of, e.g., 80% side-groups at 40% functionalization. For instance, our lab is now attempting to synthesize compound **17** as shown in Scheme 5.5.

5.5 Conclusion

Functionalization of polymers bearing pendant vinyl groups by thiol-ene coupling is quickly gaining popularity as a powerful and versatile method to prepare well-defined polymeric materials with tailored properties. However, commercially available mercaptans are limited to a select few functional groups. Our research interests have prompted us to develop rapid, high-yield synthetic methods to prepare new functional thiols. In this contribution, we show that the synthesis of acetyl or benzoyl thioesters to introduce the thiol moiety enables clean, nonwasteful, scalable preparation of stable compounds suitable for long-term storage; these can then be painlessly deprotected and added to the polymer in one continuous, straightforward procedure (Scheme 5.1). The deprotection and addition can be completed in a matter of hours, and the addition is devoid of degradation or cross-linking side reactions. Hence, the method enables synthesis of new polymeric materials whose molecular properties can be rapidly tailored by quick adjustments in the nature or quantity of the side-group(s). The facile routes for both synthesis of the protected thiols and their deprotection-addition make thiol-ene functionalization attractive for diverse applications including drug delivery, organic electronics, and polymer compatibilization. Future work might explore surface modification, which could be performed in a spatially resolved manner using photogeneration of radicals in the absence of photoinitiators[41] to perform thiol-ene coupling in the irradiated region.

5.6 Figures, Schemes, and Tables

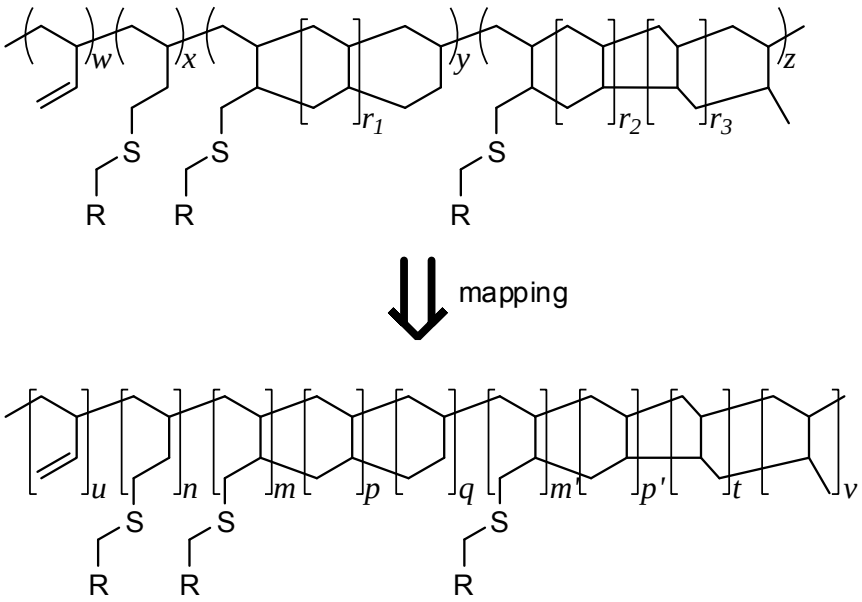

Figure 5.1 General structure of functionalized 1,2-polybutadiene (1,2-PB) and calculation of the fraction of 1,2-PB repeat units that are functionalized, cyclized, and unreacted. For any cyclic or polycyclic structure of type *y* or *z*, the number of repeat units r_1, r_2, and r_3 can be any non-negative integers. The mapping is interpreted as follows: *u* is the total number of unreacted monomers in the polymer chain; *p* is the total number of reacted, unfunctionalized monomers involved in six-member rings "in the middle" of a polycyclic ring structure of type *y*; *p*' and *v* are the total number of reacted, unfunctionalized monomers involved in six member rings "to the left" and "to the right," respectively, of the five-member ring in a polycyclic structure of type *z*; etc. Pairs of indices (*m* and *m*', *p* and *p*') refer to groups that contribute identically to NMR spectra.

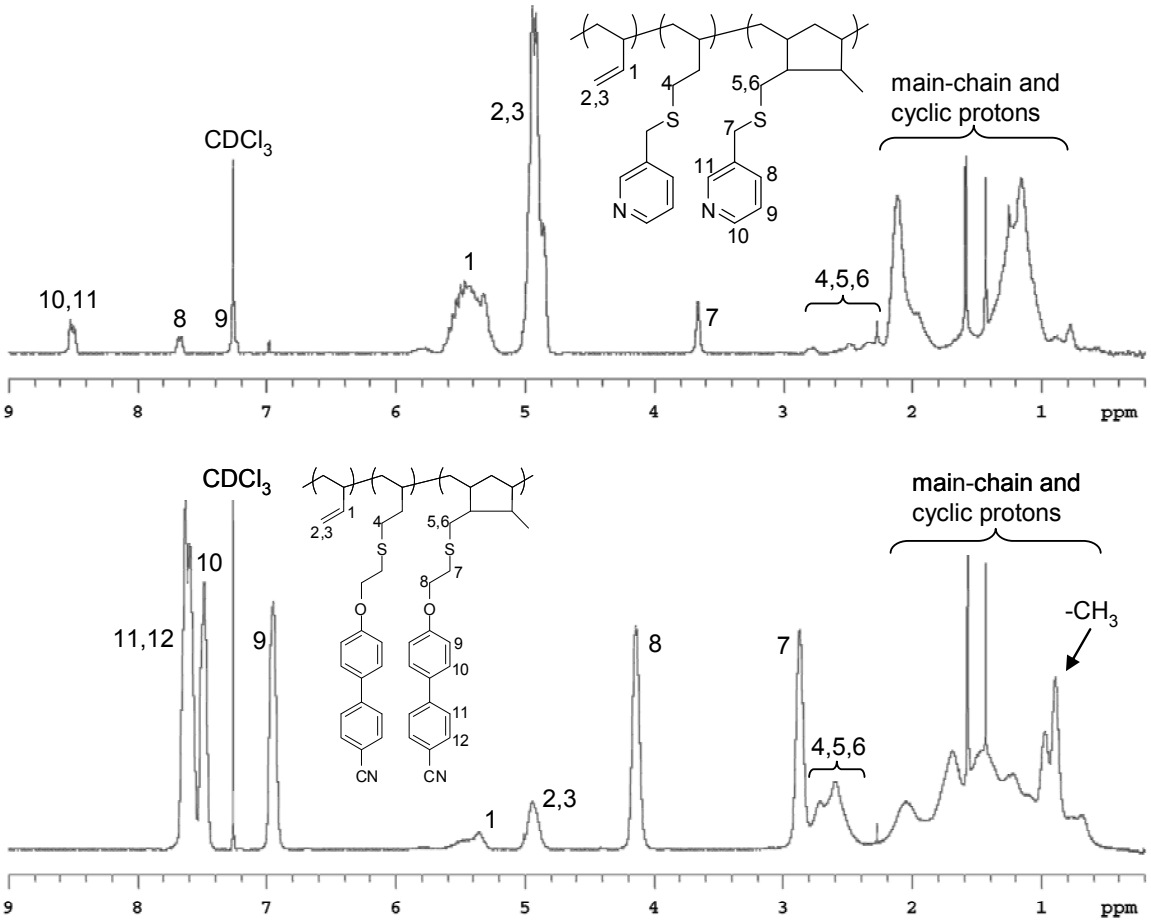

Figure 5.2 Representative ^{1}H NMR spectra of functionalized 1,2-polybutadiene polymers (92kPB13, top trace, and 92kPB3, bottom trace; refer to Table 5.1). Note that the two protons of the $RCH_2SC\mathbf{H_2}$- methylene groups directly attached to ring structures are not equivalent and hence give separate signals. In both spectra, visible peaks at δ = 6.97, 2.27, and 1.43 ppm belong to 2,6-di-*tert*-butyl-4-methylphenol (BHT), and peaks near δ = 1.6 ppm correspond to water.

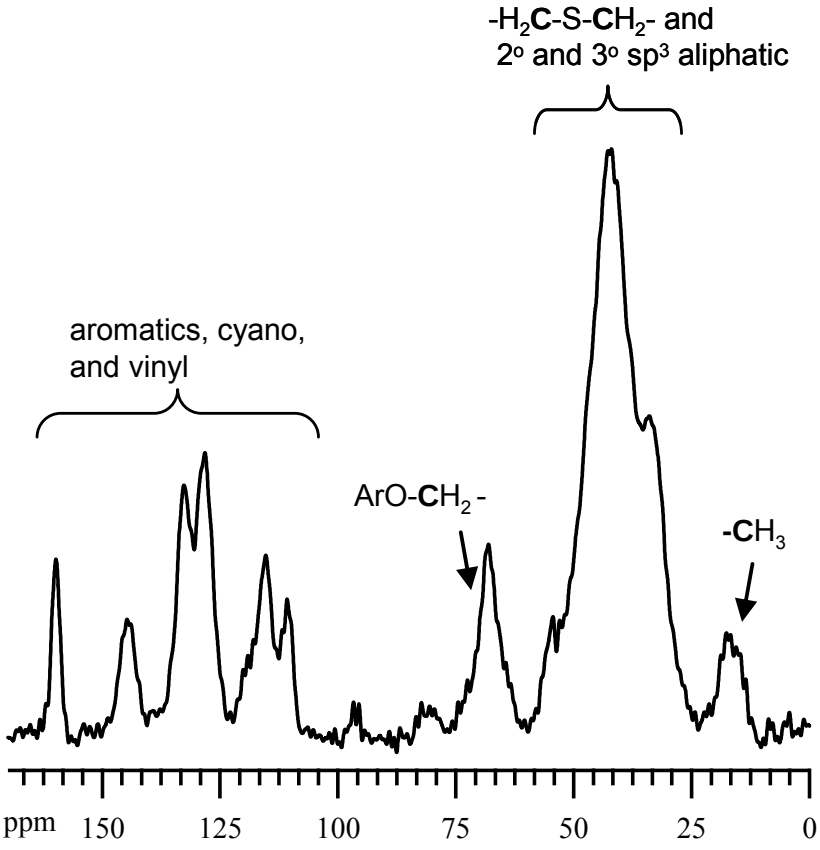

Figure 5.3 Representative solid-state ^{13}C NMR spectrum of functionalized 1,2-polybutadiene polymer (92kPB3; refer to Table 5.1 and to the structure at the bottom of Figure 5.2).

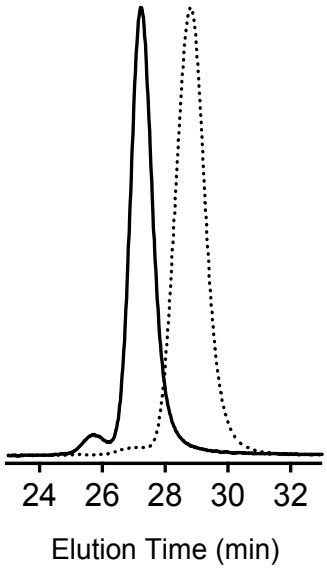

Figure 5.4 Representative gel permeation chromatography trace of functionalized 1,2-polybutadiene (1,2-PB) polymer. The solid line corresponds to 92kPB3 (refer to Table 5.1); the dashed line is 92 kg/mol 1,2-PB prepolymer.

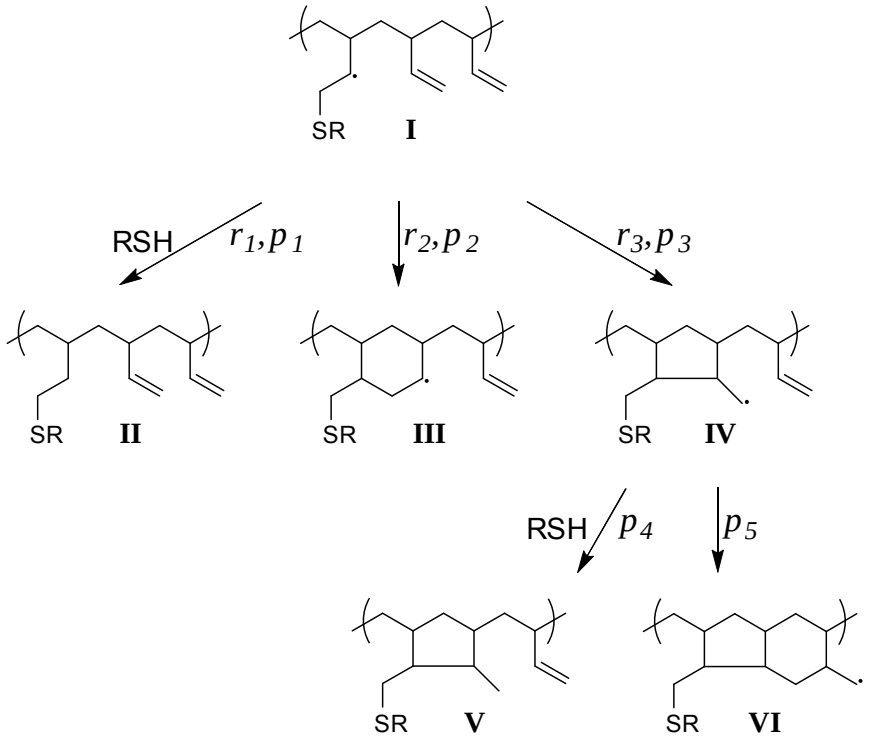

Figure 5.5 Possible reaction pathways for radical thiol addition to 1,2-polybutadiene and competing cyclization reactions.

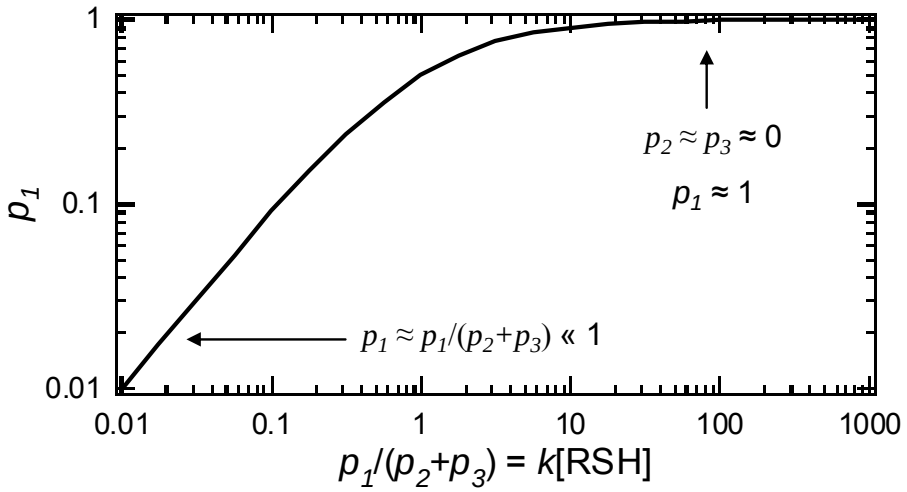

Figure 5.6 Fraction p_1 of species **I** (Figure 5.5) to proceed to abstract hydrogen from RSH as a function of [RSH]. It exhibits a linear increase at low concentration and saturates above a characteristic concentration that corresponds to $p_1/(p_2 + p_3) \approx 10$ (refer to text).

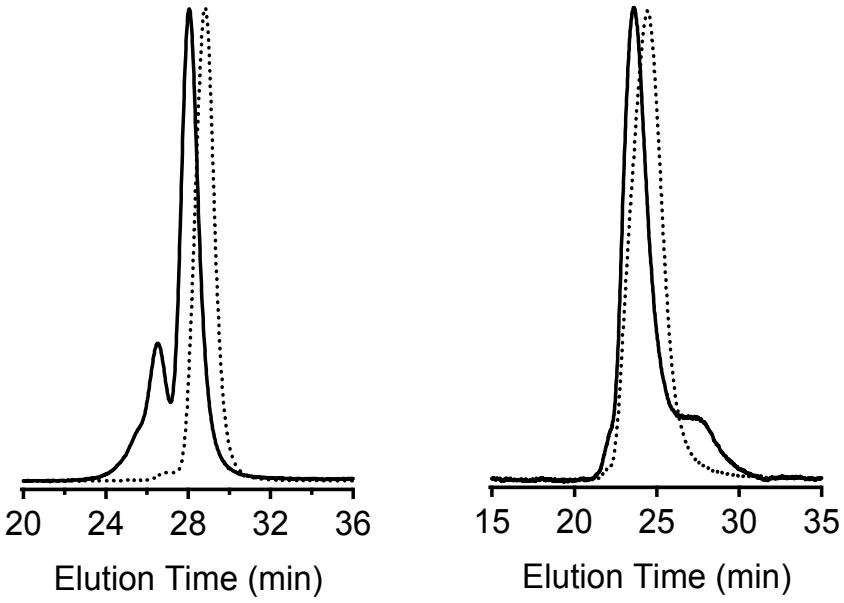

Figure 5.7 Particular reaction conditions (refer to Appendix B, Sections 3 & 4 and Table B.1) to be avoided because of cross-linking (left) or chain scission (right): gel permeation chromatography traces of 1,2-polybutadiene functionalized by reaction in the presence of dibenzoyl disulfide (solid line, left, 92kPB16), and in a one pot synthesis after deprotection of triphenylmethyl sulfide derivatives (solid line, right, 820kPB14). The dashed lines correspond to prepolymer starting materials.

Scheme 5.1 Use of a Thioester RSCOPh in the Functionalization of 1,2-Polybutadiene (1,2-PB) by Thiol-Ene Coupling of Unavailable Mercaptans

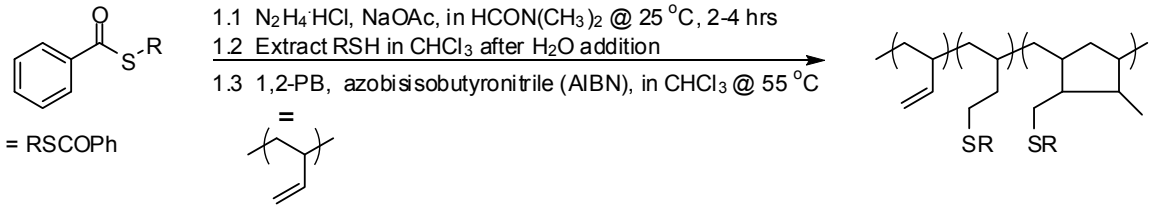

Scheme 5.2 Synthesis of Benzoyl- or Acetyl-Protected Thiols[a]

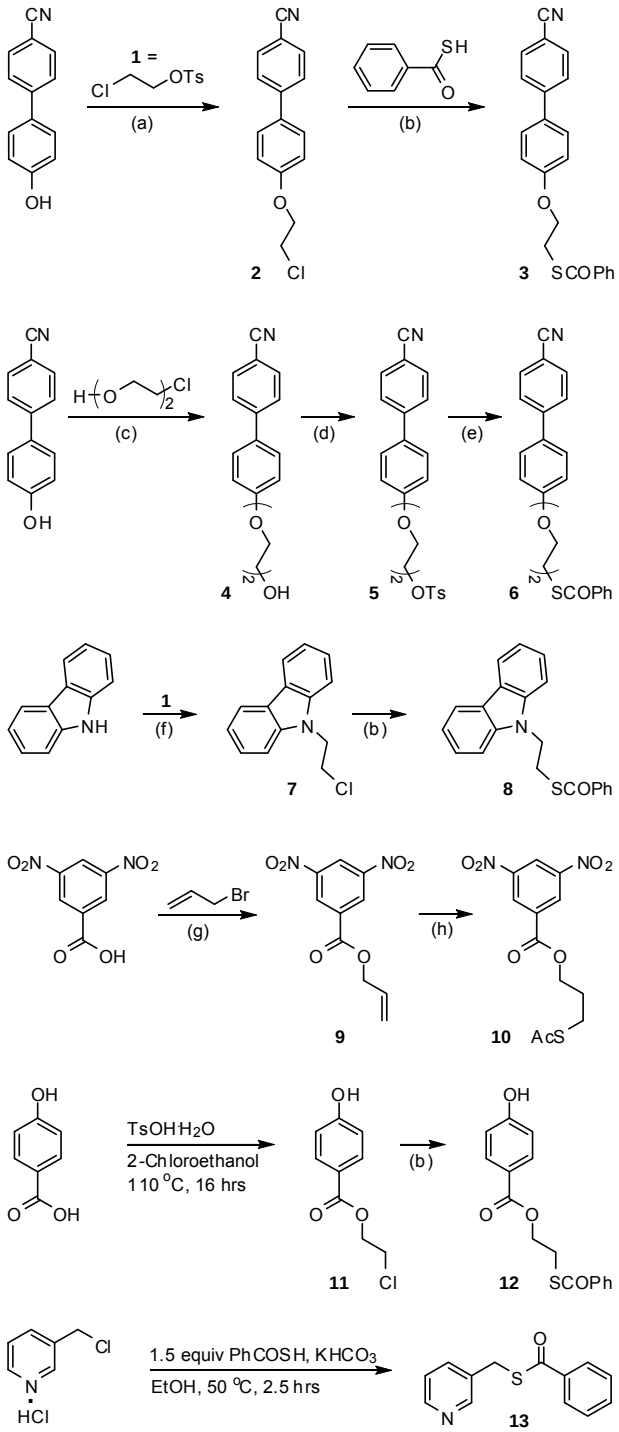

[a] Key: (a) 1.5 equiv of **1**, K_2CO_3, dimethyl sulfoxide (DMSO), 57 ºC, 22 h; (b) 2 equiv of PhCOSH, $KHCO_3$, *N*,*N*-dimethylformamide (DMF), 45–50 ºC, 4 h; (c) 4 equiv of 2-(2-chloroethoxy)ethanol, K_3PO_4, DMSO, 110 °C, 12 h; (d) 5 equiv of tosyl chloride, 4 equiv of pyridine, CH_2Cl_2, 25 ºC, 24 h; (e) 1.05 equiv of PhCOSH, $KHCO_3$, DMF, 40 ºC, 12 h; (f) 3 equiv of **1**, 2.5 equiv of KOH, DMSO, 25 ºC, 18 h; (g) 2 equiv of allyl bromide, $KHCO_3$, DMSO, 70 ºC, 2.5 h; (h) 3 equiv of AcSH, 2,2′-azobis(2-methylpropionitrile), toluene, 85 ºC, 6 h.

Scheme 5.3 Alternative Route to New Functional Derivatives of 1,2-Polybutadiene by Thiol-Ene Coupling Using an Acyl Chloride RCOCl

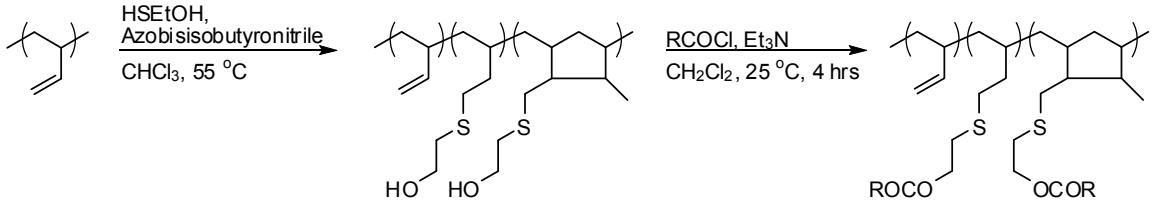

Scheme 5.4 Synthesis of Trityl-Protected 9-(2-Mercaptoethyl)carbazole

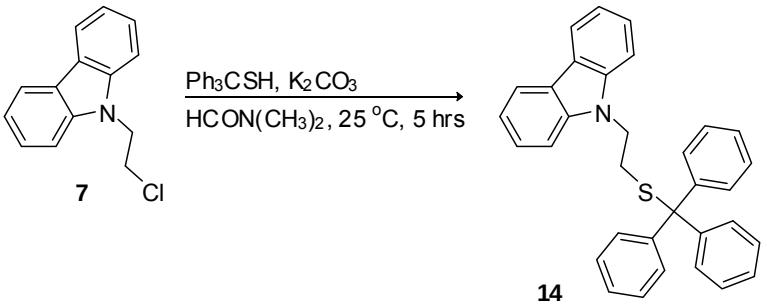

Scheme 5.5 Synthesis of a Protected Thiol Bearing Two Mesogenic Side-Groups

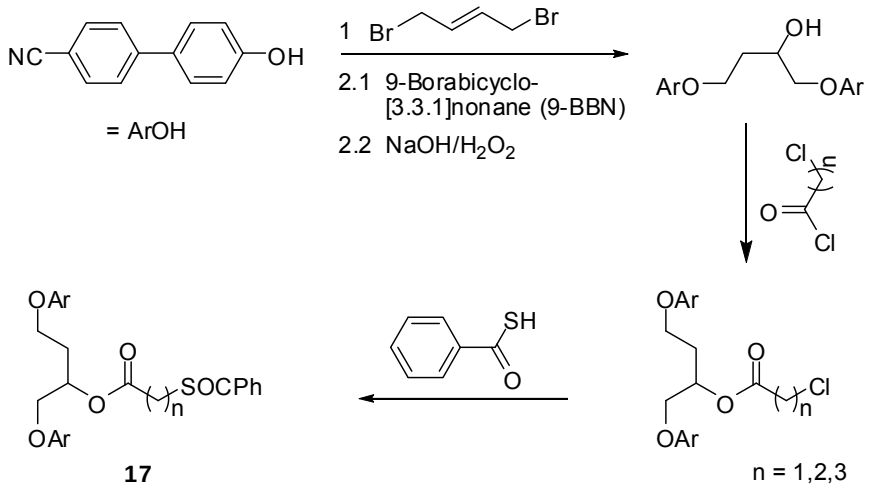

Table 5.1 Reaction Conditions and Results for 1,2-Polybutadiene Functionalization Using a Protected Thiol PhCOSR

entry[a]	[PB] (g/mL	[Thiol][b]	[AIBN] (g/mL)	rxn time (h)	X_{funct}[c] %	X_{cycl}[c] %	M_W[d] (kg/mol)	PDI[d]	new ^{1}H NMR peaks above 2.2 ppm for modified PB (all peaks are broad)
92kPB3[e,g]	0.004	1.6	0.005	6.2	40 ± 2	48 ± 3	199	1.07	7.71-7.43 (6H), 7.01-6.88 (2H), 4.22-4.08 (2H), 2.95-2.43 (4H)
92kPB6[f]	0.003	0.5	0.002	3.7	22 ± 2	34 ± 3	194	1.07	7.71-7.58 (4H), 7.54-7.46 (2H), 7.05-6.95 (2H), 4.19-4.12 (2H), 3.90-3.82 (2H), 3.77-3.67 (2H), 2.77-2.39 (4H)
92kPB8	0.004	1.2	0.001	4.4	36 ± 2	41 ± 3	146	1.06	8.12-7.95 (2H), 7.53-7.12 (6H), 4.53-4.26 (2H), 2.95-2.72 (2H), 2.65-2.2 (2H)
92kPB12	0.009	1.5	0.001	3.6	16 ± 1	18 ± 2	98	1.02	7.93-7.83 (2H), 7.88-7.80 (2H), 4.43-4.34 (2H), 2.87-2.44 (4H)
92kPB13[e]	0.003	1.9	0.001	2.0	4 ± 1	6 ± 2	122	1.07	8.55-8.46 (2H), 7.70-7.63 (1H), 7.28-7.22 (1H), 3.70-3.62 (2H), 2.82-2.43 (2H)
820kPB3	0.003	0.3	0.001	1.5	4 ± 1	4 ± 2	1420	1.45[h]	7.69-7.56 (4H), 7.56-7.45 (2H), 7.00-6.91 (2H), 4.19-4.10 (2H), 2.92-2.80 (2H), 2.74-2.49 (2H)
820kPB8[f]	0.004	1.3	0.002	3.0	27 ± 2	36 ± 3	1200	1.25	8.11-7.95 (2H), 7.49-7.12 (6H), 4.52-4.28 (2H), 2.94-2.71 (2H), 2.61-2.2 (2H)
820kPB12[f]	0.007	0.2	0.002	3.0	7 ± 1	11 ± 2	579	1.48[h]	7.94-7.87 (2H), 6.87-6.79 (2H), 4.45-4.33 (2H), 2.88-2.41 (4H)
820kPB13	0.007	0.2	0.002	2.5	2 ± 1	3 ± 2	1310	1.26	8.55-8.46 (2H), 7.70-7.64 (1H), 7.28-7.22 (1H), 3.68-3.62 (2H), 2.82-2.43 (2H)

[a]Modified PB polymers were named so that the prefix corresponds to the molecular weight of the starting 1,2-PB chain (98% 1,2 content), and the suffix represents the thioester reagent (Scheme 5.2) used. [b]In molar equivalents of 1,2-PB monomer units, estimated from the mass ratio of the protected thiol PhCOSR and 1,2-PB. [c]The fraction of reacted 1,2-PB units that bear functional groups (X_{funct}) and that are not functionalized (X_{cycl}); refer to text. The reported uncertainties were calculated based on the following uncertainties for the integrals S_1, S_2, and S_3: the measurement of S_3 is ~ 3% accurate, and the uncertainties in S_1 and S_2 are both < 1% of (S_1+S_2). [d]Measured as described in Section 5.2.1 using the Waters setup, except for polymer 92kPB12 (measurements obtained by MALLS). The 1,2-PB prepolymers had PDI of 1.07 and 1.26 for the 92 kg/mol and 820 kg/mol 1,2-PB chains, respectively. [e] ^{1}H NMR spectra are given in Figure 5.2. [f] ^{1}H NMR spectra are given in Appendix B. [g] ^{13}C NMR spectrum and GPC trace are given in Figures 5.3 and 5.4, respectively. [h]A small amount of cross-linking is believed to have occurred during workup and handling of the polymer product.

Table 5.2 Reaction Conditions and Results for 1,2-Polybutadiene Functionalization Using 3,5-Dinitrobenzoyl Chloride (DNBC)

entry[a]	[PB] (g/mL)	[BME][b]	[AIBN] (g/mL)	rxn time (h)	X_{funct}[d] %	X_{cycl}[d] %	M_W[e] (kg/mol	PDI[e]	new ^{1}H NMR peaks above 2.2 ppm for modified PB (all peaks are broad)
92kPB-OH[f]	0.03	0.6	0.002	1.9	20 ± 1	28 ± 2	151	1.07	3.77-3.65 (2H), 2.76-2.2 (4H)
820kPB-OH	0.02	0.4	0.001	3.0	15 ± 1	24 ± 2	1170	1.24	3.77-3.66 (2H), 2.76-2.3 (4H)

entry[a]	[PB-OH] (g/mL)	[DNBC][c]	[Et_3N][c]	rxn time (h)	X_{funct}[d] %	X_{cycl}[d] %	M_W[e] (kg/mol)	PDI[e]	new H NMR peaks above 2.2 ppm for modified PB (all peaks are broad)
92kPB-DNB[f]	0.02	3.3	5.0	4.0	20 ± 1	28 ± 2	158	1.08	9.24-9.20 (1H), 9.20-9.12 (2H), 4.64-4.51 (2H), 2.97-2.81 (2H), 2.81-2.41 (2H)
820kPB-DNB	0.02	2.5	3.5	3.3	15 ± 1	24 ± 2	1410	1.28	9.24-9.20 (1H), 9.20-9.12 (2H), 4.65-4.51 (2H), 2.97-2.83 (2H), 2.80-2.42 (2H)

[a]Modified PB polymers were named so that the prefix corresponds to the molecular weight of the starting 1,2-PB chain (98% 1,2 content), and the suffix represents the functional group added. [b]In molar equivalents of 1,2-PB monomer units. [c]In molar equivalents of 2-hydroxyethylthio- functionalized monomer units. [d]The fraction of reacted 1,2-PB units that bear functional groups (X_{funct}) and that are not functionalized (X_{cycl}); refer to text. The reported uncertainties were calculated based on the following uncertainties for the integrals S_1, S_2, and S_3: the measurement of S_3 is ~ 3% accurate, and the uncertainties in S_1 and S_2 are both < 1% of (S_1+S_2). [e]Measured as described in Section 5.2.1 using the Waters setup. The 1,2-PB prepolymers had PDI of 1.07 and 1.26 for the 92 kg/mol and 820 kg/mol 1,2-PB chains, respectively. [f] ^{1}H NMR spectra are given in Appendix B.

5.7 References and Notes

1. Antonietti, M.; Forster, S.; Hartmann, J.; Oestreich, S., Novel amphiphilic block copolymers by polymer reactions and their use for solubilization of metal salts and metal colloids. *Macromolecules* **1996,** 29, (11), 3800–3806.

2. Kramer, E.; Forster, S.; Goltner, C.; Antonietti, M., Synthesis of nanoporous silica with new pore morphologies by templating the assemblies of ionic block copolymers. *Langmuir* **1998,** 14, (8), 2027–2031.

3. Kukula, H.; Schlaad, H.; Antonietti, M.; Forster, S., The formation of polymer vesicles or "peptosomes" by polybutadiene-block-poly(L-glutamate)s in dilute aqueous solution. *Journal of the American Chemical Society* **2002,** 124, (8), 1658–1663.

4. Forster, S.; Antonietti, M., Amphiphilic block copolymers in structure-controlled nanomaterial hybrids. *Advanced Materials* **1998,** 10, (3), 195–217.

5. Pollino, J. M.; Stubbs, L. P.; Weck, M., One-step multifunctionalization of random copolymers via self-assembly. *Journal of the American Chemical Society* **2004,** 126, (2), 563–567.

6. Carlise, J. R.; Weck, M., Side-chain functionalized polymers containing bipyridine coordination sites: Polymerization and metal-coordination studies. *Journal of Polymer Science Part A—Polymer Chemistry* **2004,** 42, (12), 2973–2984.

7. Meyers, A.; Weck, M., Design and synthesis of Alq(3)-functionalized polymers. *Macromolecules* **2003,** 36, (6), 1766–1768.

8. Kimyonok, A.; Weck, M., Poly(cyclooctene)s with pendant fluorescent and phosphorescent metal complexes. *Macromolecular Rapid Communications* **2007,** 28, (2), 152–157.

9. South, C. R.; Burd, C.; Weck, M., Modular and dynamic functionalization of polymeric scaffolds. *Accounts of Chemical Research* **2007,** 40, (1), 63–74.

10. Schulz, D. N.; Turner, S. R.; Golub, M. A., Recent advances in the chemical modification of unsaturated polymers. *Rubber Chemistry and Technology* **1982,** 55, (3), 809–859.

11. Chung, T. C.; Raate, M.; Berluche, E.; Schulz, D. N., Synthesis of functional hydrocarbon polymers with well-defined molecular structures. *Macromolecules* **1988,** 21, (7), 1903–1907.

12. Ramakrishnan, S., Well-defined ethylene vinyl alcohol copolymers via hydroboration—control of composition and distribution of the hydroxyl-groups on the polymer backbone. *Macromolecules* **1991,** 24, (13), 3753–3759.

13. Kempe, M. D. *Rheology and Dynamics of Side-Group Liquid Crystalline Polymers in Nematic Solvents*. Ph.D. Thesis, California Institute of Technology, Pasadena, CA, 2003.

14. Guo, X. Y.; Farwaha, R.; Rempel, G. L., Catalytic hydrosilylation of diene-based polymers. 1. Hydrosilylation of polybutadiene. *Macromolecules* **1990,** 23, (24), 5047–5054.

15. Ameduri, B.; Boutevin, B.; Nouiri, M., Synthesis and properties of fluorinated telechelic macromolecular diols prepared by radical grafting of fluorinated thiols onto

hydroxyl-terminated polybutadienes. *Journal of Polymer Science Part A—Polymer Chemistry* **1993,** 31, (8), 2069–2080.

16. Boutevin, G.; Ameduri, B.; Boutevin, B.; Joubert, J. P., Synthesis and use of hydroxyl telechelic polybutadienes grafted by 2-mercaptoethanol for polyurethane resins. *Journal of Applied Polymer Science* **2000,** 75, (13), 1655–1666.

17. Schapman, F.; Couvercelle, J. P.; Bunel, C., Low molar mass polybutadiene made crosslinkable by silane moieties introduced via addition of thiol to double bond: 3. Synthesis and kinetic study. *Polymer* **1998,** 39, (20), 4955–4962.

18. Justynska, J.; Hordyjewicz, Z.; Schlaad, H., Toward a toolbox of functional block copolymers via free-radical addition of mercaptans. *Polymer* **2005,** 46, (26), 12057–12064.

19. Justynska, J.; Hordyjewicz, Z.; Schlaad, H., New functional diblock copolymers through radical addition of mercaptans. *Macromolecular Symposia* **2006,** 240, 41–46.

20. Geng, Y.; Discher, D. E.; Justynska, J.; Schlaad, H., Grafting short peptides onto polybutadiene-block-poly(ethylene oxide): A platform for self-assembling hybrid amphiphiles. *Angewandte Chemie-International Edition* **2006,** 45, (45), 7578–7581.

21. Hordyjewicz-Baran, Z.; You, L. C.; Smarsly, B.; Sigel, R.; Schlaad, H., Bioinspired polymer vesicles based on hydrophilically modified polybutadienes. *Macromolecules* **2007,** 40, (11), 3901–3903.

22. Ren, Y.; Lodge, T. P.; Hillmyer, M. A., A simple and mild route to highly fluorinated model polymers. *Macromolecules* **2001,** 34, (14), 4780–4787.

23. Scruggs, N. R. *Coupling Polymer Thermodynamics and Viscoelasticity to Liquid Crystalline Order: Self-Assembly and Relaxation Dynamics of Block Copolymers in a nematic Solvent*. Ph.D. Thesis, California Institute of Technology, Pasadena, CA, 2007.

24. Verduzco, R. *Self-Assembled Liquid Crystal Polymer Gels*. Ph.D. Thesis, California Institute of Technology, Pasadena, CA, 2007.

25. Yamaguchi, A.; Maeda, Y.; Yokoyama, H.; Yoshizawa, A., Self-assembly of amphiphilic liquid-crystalline oligomers possessing a semiperfluorinated alkyl chain. *Chemistry of Materials* **2006,** 18, (24), 5704–5710.

26. Bogdal, D.; Yashchuk, V.; Pielichowski, J.; Ogul'Chansky, T.; Warzala, M.; Kudrya, V., Synthesis and spectral investigation of alkyl methacrylates with halogenated carbazolyl pendant groups for photonics applications. *Journal of Applied Polymer Science* **2002,** 84, (9), 1650–1656.

27. Smith, M. B.; March, J., *March's Advanced Organic Chemistry. Reactions, Mechanisms, and Structure*. 5th ed.; John Wiley & Sons, Inc: 2001.

28. Nakatsuji, S.; Ikemoto, H.; Akutsu, H.; Yamada, J. I.; Mori, A., Novel radical compounds bearing mesogenic cores with long alkyl substituents. *Journal of Organic Chemistry* **2003,** 68, (5), 1708–1714.

29. Bhatt, J. J., Preparation and thermal properties of 4-alkoxy-4'-cyanobiphenyl esters of ferrocenedicarboxylic acid. *Journal of Organometallic Chemistry* **1991,** 413, 263.

30. Brace, N. O., Cyclization reactions of perfluoroalkyl-substituted radicals. *Journal of Organic Chemistry* **1966,** 31, (9), 2879–2885.

31. Patai, S., *The Chemistry of the Thiol Group, Part 1*. Wiley: 1974; ch 4.

32. Kocienski, P. J., *Protecting Groups*. 3rd ed.; Thieme: 2004; ch 5.

33. Fabris, L.; Antonello, S.; Armelao, L.; Donkers, R. L.; Polo, F.; Toniolo, C.; Maran, F., Gold nanoclusters protected by conformationally constrained peptides. *Journal of the American Chemical Society* **2006,** 128, (1), 326–336.

34. Moreau, X.; Campagne, J. M., Approaches toward the total synthesis of the nine-membered thio-lactone core of griseoviridin. *Journal of Organic Chemistry* **2003,** 68, (25), 9874–9874.

35. Narayan, R. S.; VanNieuwenhze, M. S., Versatile and stereloselective syntheses of orthogonally protected beta-methylcysteine and beta-methyllanthionine. *Organic Letters* **2005,** 7, (13), 2655–2658.

36. Oila, M. J.; Tois, J. E.; Koskinen, A. M. P., Synthesis of a novel carboxy functionalized PyOX-ligand. *Tetrahedron Letters* **2005,** 46, (6), 967–969.

37. Wuts, P. G. M., *Greene's Protective Groups in Organic Synthesis: Peter G.M. Wuts and Theodora W. Greene*. 4th ed.; Wiley-Interscience: 2007; ch 6.

38. Hinou, H.; Sun, X. L.; Ito, Y., Systematic syntheses and inhibitory activities of bisubstrate-type inhibitors of sialyltransferases. *Journal of Organic Chemistry* **2003,** 68, (14), 5602–5613.

39. Morii, Y.; Matsuda, H.; Ohara, K.; Hashimoto, M.; Miyairi, K.; Okuno, T., Synthetic studies on oligosaccharides composed of 5-thioglucopyranose units. *Bioorganic & Medicinal Chemistry* **2005,** 13, (17), 5113–5144.

40. Rich, J. R.; Wakarchuk, W. W.; Bundle, D. R., Chemical and chemoenzymatic synthesis of S-Linked ganglioside analogues and their protein conjugates for use as immunogens. *Chemistry—A European Journal* **2006,** 12, (3), 845–858.

41. Cramer, N. B.; Scott, J. P.; Bowman, C. N., Photopolymerizations of thiol-ene polymers without photoinitiators. *Macromolecules* **2002,** 35, (14), 5361–5365.

Appendix A Numerical Approach for Chain Statistics of Self-Associating Chains at Infinite Dilution in θ-Solvent

A.1 Model Description

Our objective is to determine the size of a linear chain of N monomers, f of which are modified to act as stickers capable of forming pair-wise only, physical associations. The stickers are assumed to be equidistantly spaced l monomers apart along the chain, and the energy of association is εkT. We will assume Gaussian chain statistics for any segment of the chain whose configuration is unrestrained by reversible crosslinks.

To calculate the size of the chain in the very dilute regime (all associations are intramolecular), we define a semi-Markov process X(t), $t > 0$ such that each state i is fully specified by identifying which pairs of stickers form bonds. (Note here that a given state has an infinite number of chain configurations.) The chain goes from one state to the next by either breaking or forming a bond, as illustrated in Figure A.1.

This semi-Markov process is completely specified if we know both (a) the distribution of times T_i the chain spends in any given state i and (b) the probabilities P_{ij} that once it leaves state i it next enters state j. Thus, if we can determine the distributions of T_i, compute the transition probabilities P_{ij}, and calculate relevant properties of the chain in any state i, then we can estimate the long-run average of chain properties such as size by simply running the Markov process for a sufficiently long time. Fortunately, although the total number of states is extremely large for f as small as 20, the number of states that are *accessible in one step* from any given state is much more manageable, that is, $P_{ij} = 0$ for most values of j for a given state i.

Assume the polymer chain enters state i at time t. Clearly, the state it enters next is determined by which bond is broken or formed first; and the time spent in the present state is the time it took for that bond-breaking or bond-forming event to take place. Because the times for bond breaking and bond forming are random variables, in order to solve the problem we need to determine the distribution of the breaking time and the forming time of all the possible bonds, for any state i.

Consider the breaking of a single bond. A bond that has been "alive" for any given time s is just as strong as a bond which has just formed; in other words the expected time to break a bond given that is has been "alive" for time s is independent of s. Accordingly, bond breaking is a memoryless (hence exponential) process, and the time to break a bond is given by the exponential density function:

$$f_{T_b}(t) = \frac{1}{\tau_b}\exp\left(-\frac{t}{\tau_b}\right) \qquad t \geq 0$$

where τ_b is the expected time to break a bond, and has the same value for all bonds. Bond forming can also be argued to be an exponential process, as discussed below, with expected time τ_f dependent on the number of monomers $L_{qq'}$ in the shortest connected path between the two free stickers q and q'. Observe that the shortest path $L_{qq'}$ between stickers depends on the pair of stickers q and q' and on the current state of the chain; for example, the shortest distance between stickers 1 and 6 in state (b) of Figure A.1 is $L_{1,6} = 2l$.

Let's now see if we can determine expressions for τ_b and τ_f. Rubinstein and Semenov[1] give $\tau_b = \tau_0 \exp(\varepsilon + \varepsilon_a)$, where τ_0 is the monomer relaxation time and $\varepsilon_a kT$ is a potential barrier for bond breaking and also the activation energy for bond forming. I get $\tau_f \cong \tau_0/p_c p_s$ to a first approximation (as discussed below), where $p_c = (6/\pi L^3)^{1/2}$ is the contact probability that the two stickers separated by L monomers be within distance b of each other (b is the Kuhn length, assumed to be the maximum distance over which the stickers can associate), and p_s is the sticking probability that a bond is formed at any given "visit." If $p_s \approx (V_b/b^3)\exp(-\varepsilon_a)$ where V_b is the bond volume, then we get $\tau_f \approx \alpha\,\tau_0 \exp(\varepsilon_a)\, L^{3/2}$ where $\alpha = (b^3/V_b)(\pi/6)^{1/2}$.

Let $\{pp'\}_i$ be the set of all pairs of stickers that are bonded in state i, and $\{T_{b,pp'}\}_i$ be the set of random variables corresponding to their breaking time. Among the unpaired stickers in state i, let $\{qq'\}_i$ be the set of all possible pairings for formation of a new bond, and $\{T_{f,qq'}\}_i$ be the set of random variables corresponding to their expected bond-forming time. For a given state i, then, we have independent, exponential random variables $\{T_{b,pp'}\}_i$ and $\{T_{f,qq'}\}_i$, with expected values $E[T_{b,pp'}] = \tau_b$ and $E[T_{f,qq'}] = \alpha\,\tau_0 \exp(\varepsilon_a)\,(L_{qq'[i]})^{3/2}$, where $L_{qq'[i]}$ is the number of monomer in the shortest connected path between the two free stickers p and p' in state i. The probability that the next state is achieved by breaking a specific bond pp', or by

forming a specific bond *qq'* is the probability that $T_{b,pp'}$ or $T_{f,qq'}$ is the shortest of all the breaking and forming times. For independent exponential random variables this probability is (the rate of the given exponential variable)/(the sum of all the rates). Thus, the probability that the next state is obtained from forming a bond between any two free stickers *q* and *q'* is:

$$P = \frac{\alpha^{-1} e^{\varepsilon} L_{qq'[i]}^{-3/2}}{Q + \alpha^{-1} e^{\varepsilon} \cdot \sum_{qq'} L_{qq'[i]}^{-3/2}}$$

where *Q* is the number of bonds in the present state *i* and the sum is over all the possible pairs of unpaired stickers in the present state. The probability that the next state is obtained from breaking a given bond is:

$$P = \frac{1}{Q + \alpha^{-1} e^{\varepsilon} \cdot \sum_{qq'} L_{qq'[i]}^{-3/2}} .$$

Note that these probabilities are independent of the activation energy. Given that all the breaking times and forming times are independent exponential random variables, the time T_i to transition from any state *i* to the next is also exponentially distributed, with rate equal to 1/(sum of all the rates), so with mean:

$$\tau_i = \frac{\tau_b}{Q + \alpha^{-1} e^{\varepsilon} \cdot \sum_{qq'} L_{qq'[i]}^{-3/2}} .$$

In this case (exponentially distributed transition times), the semi-Markov process is a continuous-time Markov chain. Continuous-time Markov chains are characterized by the Markovian property that, given the present state, the future is independent of the past. This result is intuitive for the bond-breaking and bond-forming processes which determine the time-evolution of our chains: given the present state, the next state and the time to transition into the next state are both independent of what states were visited previously or how long the chain has been in the present state already. As a result of the memoryless property of a continuous-time Markov chain, the amount of time T_i spent in state *i*, and the next state visited are *independent* random variables. The reader is referred to a text by Ross[2] for an excellent description of Markov chains, semi-Markov chains, and continuous-time Markov chains.

A.2 Distribution Function for the Time to Form a Bond

Consider a strand of L monomers with 2 stickers at its ends. What is the probability density function of the random variable T_f, the time for the stickers to form a bond (given that they are not bonded at the present time)?

Clearly there is an infinite number of configurations for the strand, where a configuration is specified by specifying the position vectors $\mathbf{r_1}$, $\mathbf{r_2}$,..., $\mathbf{r_L}$ of all the monomers. However, if we break up space into a 3D lattice with arbitrarily small but finite volume elements, then there is now a finite number of strand configurations. If we further define a macroscopic time τ_0 over which the polymer configuration does not change (and renormalize time in units of τ_0), then the configurations the strand takes over time constitute an irreducible (all the states communicate), positive recurrent (the expected time to return to the present state is finite for all the states) Markov chain. Therefore, there exist stationary probabilities $\pi_v = \lim_{n\to\infty} P_{uv}^n$ independent of initial state u for all states v.

Given a probability density function for the initial polymer configuration, there exists a distribution function for T_f, the time it will take for the stickers to bond *given* that they are not bonded at the present time $t = 0$. If the probability density of the initial chain configuration is the stationary probability density, and *given* that the sticker ends have not bonded after time s, the probability density to find the chain in any given configuration at time s is still equal to the stationary probability density. Therefore, nothing has changed after time s, so that the remaining time it will take to form a bond is independent of s. Accordingly, bond forming is a memoryless (hence exponential) process, and the time to break a bond is given by:

$$f_{T_b}(t) = \frac{1}{\tau_b}\exp\left(-\frac{t}{\tau_b}\right)$$

where τ_f is the expected value of T_f. To determine τ_f for a strand of L monomers with stickers at its ends, we need to know the time it takes for the stickers to come within close enough distance of each other to associate. Assume stickers form a bond with sticking probability p_s if they come within distance b (= Kuhn length) of each other. Consider another semi-Markov process with the following two states only: the strand is in state 1 if the stickers are within distance b of each other, and in state 2 otherwise. Let μ_1 and μ_2 be the mean times spent in states 1 and 2, respectively (we do not need to know the distribution of transition times). For

$\varepsilon = 0$ (corresponding to a non-associating strand of L monomers), the long-run fraction of time spent in state 1 is:

$$\frac{\frac{1}{2}\mu_1}{\frac{1}{2}\mu_1 + \frac{1}{2}\mu_2} = p_c = \left(\frac{6}{\pi \cdot L^3}\right)^{1/2}$$

where p_c is the contact probability for the chain ends to be within distance b of each other, and the only assumption is that of Gaussian statistics. But the mean time spent in state 1 is $\mu_1 \approx \tau_0$, from which we get $\mu_2 \approx \tau_0 (1-p_c)/p_c$. Note here that the above expression for μ_1 is also valid when $\varepsilon \neq 0$ if stickers fail to stick while the strand is in state 1, and that the above expression for μ_2 is likewise also valid when $\varepsilon \neq 0$. By conditioning on the present state of the chain, the expected time to form a bond is:

$$\begin{aligned} \mathrm{E}\left[\mathrm{T}_f\right] &= \mathrm{E}\left[\mathrm{T}_f \middle| 1\right]\mathrm{P}_1 + \mathrm{E}\left[\mathrm{T}_f \middle| 2\right]\mathrm{P}_2 \\ &= \mathrm{E}\left[\mathrm{T}_f \middle| 1\right] p_c + \left(\mu_2 + \mathrm{E}\left[\mathrm{T}_f \middle| 1\right]\right)(1 - p_c) \\ &= \mu_2 (1 - p_c) + \mathrm{E}\left[\mathrm{T}_f \middle| 1\right]. \end{aligned}$$

We find the expected time to bond given that the strand is in state 1, $\mathrm{E}[\mathrm{T_f}|1]$, by conditioning on whether the stickers stick the first time around:

$$\mathrm{E}\left[\mathrm{T}_f \middle| 1\right] \approx p_s \tau_0 + \left(\mu_1 + \mu_2 + \mathrm{E}\left[\mathrm{T}_f \middle| 1\right]\right)(1 - p_s)$$

where $\mathrm{p_s} \approx (\mathrm{V_b}/\mathrm{b}^3) \exp(-\varepsilon_a)$ is the probability that the stickers form a bond while the chain segment is in state 1. So after rearranging:

$$\mathrm{E}\left[\mathrm{T}_f \middle| 1\right] \approx \frac{\mu_1 + \mu_2}{p_s} - \mu_2 .$$

Substituting, we get: $$\mathrm{E}\left[\mathrm{T}_f\right] \approx \frac{\tau_0 (1 - p_c)(1 - p_c p_s)}{p_c p_s} \approx \frac{\tau_0}{p_c p_s}.$$

A.3 Simplifying Assumptions of the Model

We made two simplifying assumptions in our construction of the model. First, we have assumed Gaussian statistics for any strand whose configuration is unrestrained by reversible crosslinks. This assumption is reasonable in θ-solvents only to the extent that congestion is not an issue. In reality there is a limit to the number of monomers that can be collapsed into

a given volume, and for a high-enough number density of paired stickers and long-enough chains, congestion is expected to become important.

Second, in our derivation of the time for bond formation we assumed that the initial configuration of the strand between the stickers was chosen according to the stationary probabilities π_u, where a state u corresponds to a specific configuration of the strand. Justification for this assumption is derived from the fact that the probability density of the strand configuration *will* reach the stationary probability density, for any arbitrary initial probability density, after a sufficiently long time during which the stickers do not pair up. The assumption however presents limitations for a pair of stickers right after their bond is broken: due to spatial proximity, these may reassociate before the strand between them reaches its stationary probability density. In other words, the memoryless Markovian property may be violated to that extent in that the future is not completely independent of the past.

A.4 References and Notes

1. Rubinstein, M.; Semenov, A. N., Dynamics of entangled solutions of associating polymers. *Macromolecules* **2001,** 34, (4), 1058–1068.

2. Ross, S. M., *Introduction to Probability Models*. 8th ed.; Academic Press: 2003.

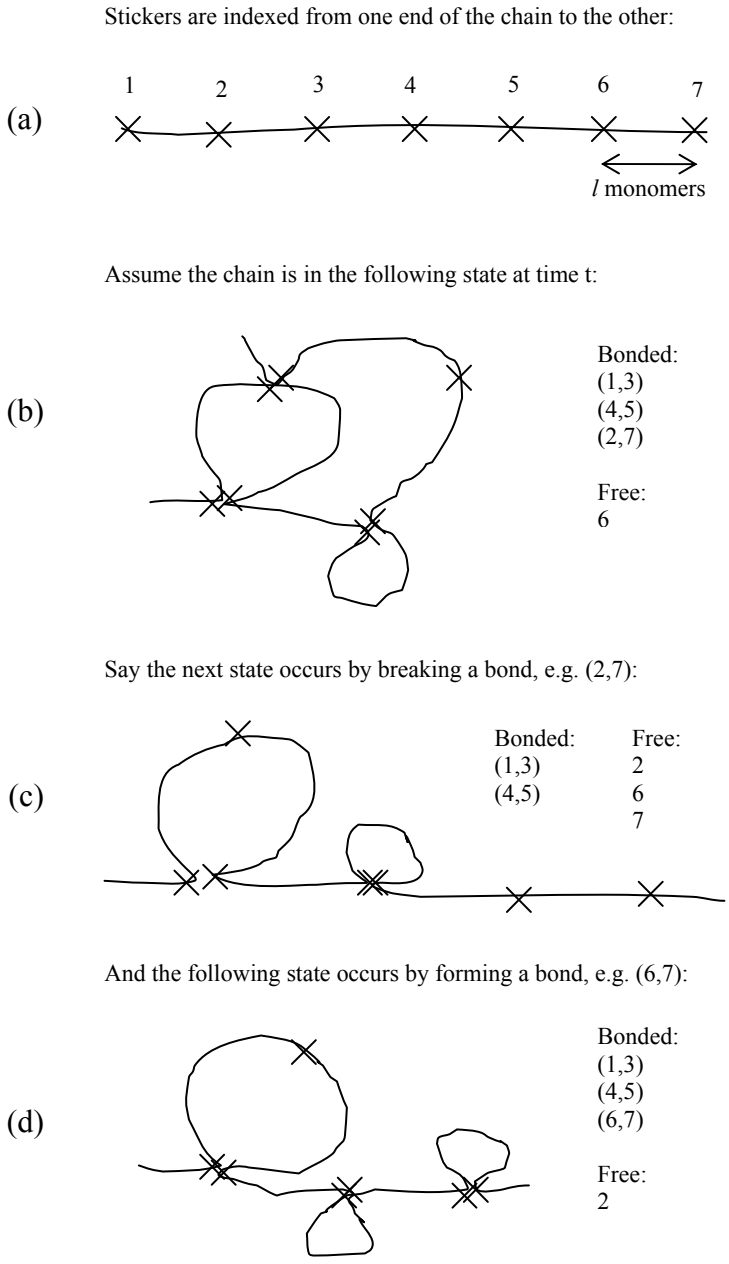

Figure A.1 Schematic illustration of the transition from one state of the chain to another by bond breaking and bond forming, for a chain with $f = 7$ stickers.

Appendix B Supplementary Information to Chapter V

B.1 ^{13}C NMR Resonances of Select Compounds

All ^{13}C NMR spectra were obtained using a Varian Mercury 300 spectrometer (corresponding to 74.5 MHz for ^{13}C), recorded in $CDCl_3$, and referenced to tetramethylsilane. The authors referred to information compiled in the Spectral Database for Organic Compounds (available online at http://riodb01.ibase.aist.go.jp/sdbs/cgi-bin/direct_frame_top.cgi) in the process of assigning ^{13}C NMR resonances.

2-Chloroethyl-*p*-toluenesulfonate (1). ^{13}C NMR: δ = 145.30 (e), 132.44 (b), 130.00 and 127.97 (c and d), 69.02 (f), 40.83 (g), 21.67 (a).

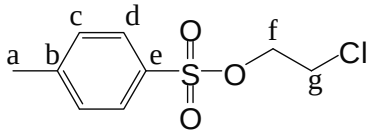

4'-(2-(Benzoylthio)ethoxy)[1,1'-biphenyl]-4-carbonitrile (3). ^{13}C NMR: δ = 191.40 (e), 159.00 (j), 145.11 (n), 136.64 (d), 133.69 (a), 132.57 (p), 131.89 (m), 128.70 and 127.30 (b and c), 128.43 (l), 127.13 (o), 119.09 (r), 115.21 (k), 110.14 (q), 66.70 (g), 28.13 (f).

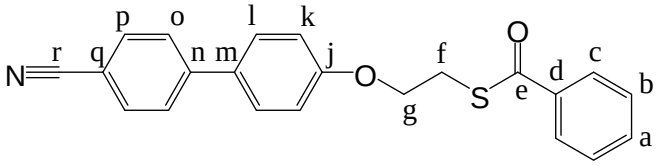

4'-(2-(2-(Benzoylthio)ethoxy)ethoxy) [1,1'-biphenyl]-4-carbonitrile (6). ^{13}C NMR: δ = 191.54 (e), 159.35 (j), 145.12 (n), 136.82 (d), 133.48 (a), 132.54 (p), 131.63 (m), 128.61 and 127.23 (b and c), 128.30 (l), 127.07 (o), 119.10 (r), 115.22 (k), 110.06 (q), 70.05 and 69.38 (h and i), 67.50 (g), 28.65 (f).

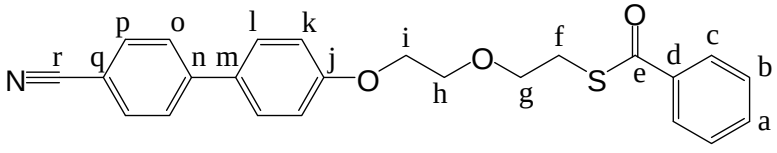

Thiobenzoic acid S-[2-(9-carbazolyl)ethyl] ester (8). ^{13}C NMR: δ = 191.73 (e), 140.07 (h), 136.71 (d), 133.73 (a), 128.74 and 127.35 (b and c), 125.91 (j), 122.98 (m), 120.40 (l), 119.26 (k), 108.74 (i), 42.42 (g), 27.28 (f).

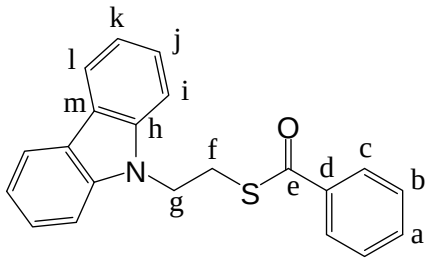

3,5-Dinitrobenzoic acid 3-(acetylthio)propyl ester (10). ^{13}C NMR: δ = 195.36 (b), 162.49 (f), 148.67 (i), 133.81 (g), 129.52 (h), 122.47 (j), 65.21 (e), 30.64 (a), 28.68 and 25.50 (c and d).

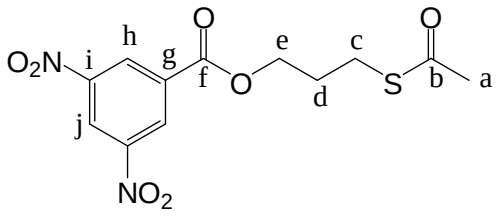

4-Hydroxybenzoic acid 2-(benzoylthio)ethyl ester (12). ^{13}C NMR: δ = 191.42 (e), 166.27 (h), 160.24 (l), 136.65 (d), 133.68 (a), 132.09 (j), 128.70 and 127.32 (b and c), 122.13 (i), 115.28 (k), 63.11 (g), 27.86 (f).

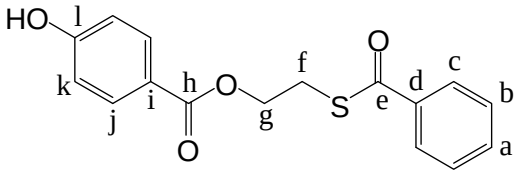

Thiobenzoic acid S-[3-pyridinylmethyl] ester (13). ^{13}C NMR: δ = 190.74 (e), 150.14 (h), 148.62 (i), 136.48 and 136.42 (d and k), 133.70 and 133.65 (a and g), 128.71 and 127.31 (b and c), 123.46 (j), 30.38 (f).

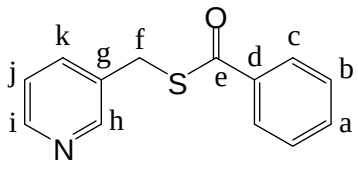

B.2 ^{1}H NMR Spectra of Select Functionalized Polymers

All spectra were taken in $CDCl_3$, resulting in a solvent peak in each case at δ = 7.24 ppm. Peaks near 1.6 ppm correspond to water, and visible peaks at δ = 6.97, 2.27, and 1.43 ppm belong to BHT.

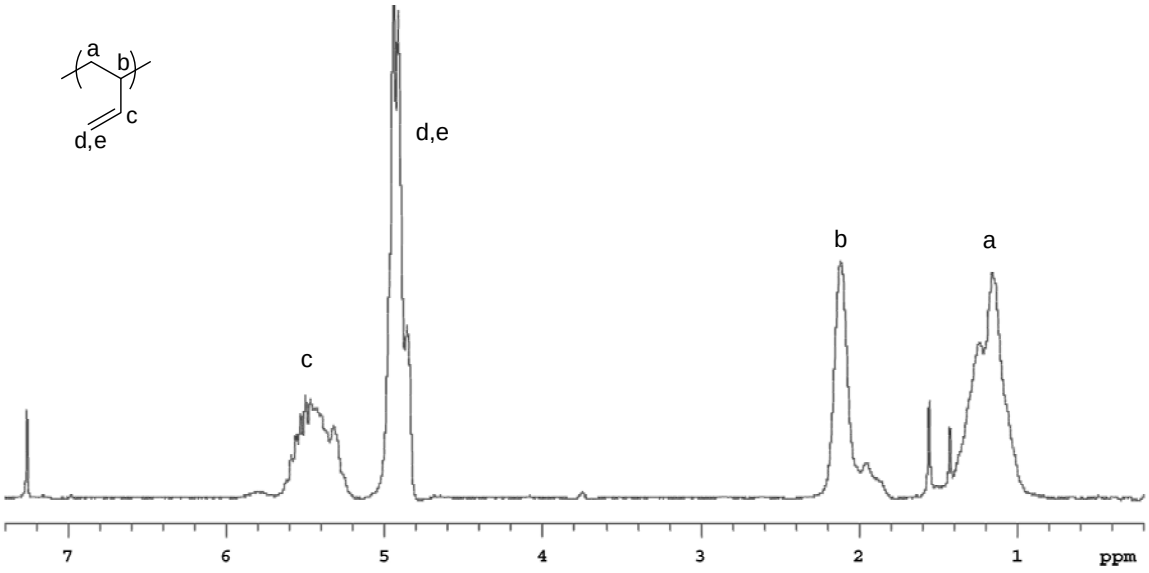

Figure B.1 ^{1}H NMR trace of unfunctionalized 92 kg/mol 1,2-polybutadiene polymer.

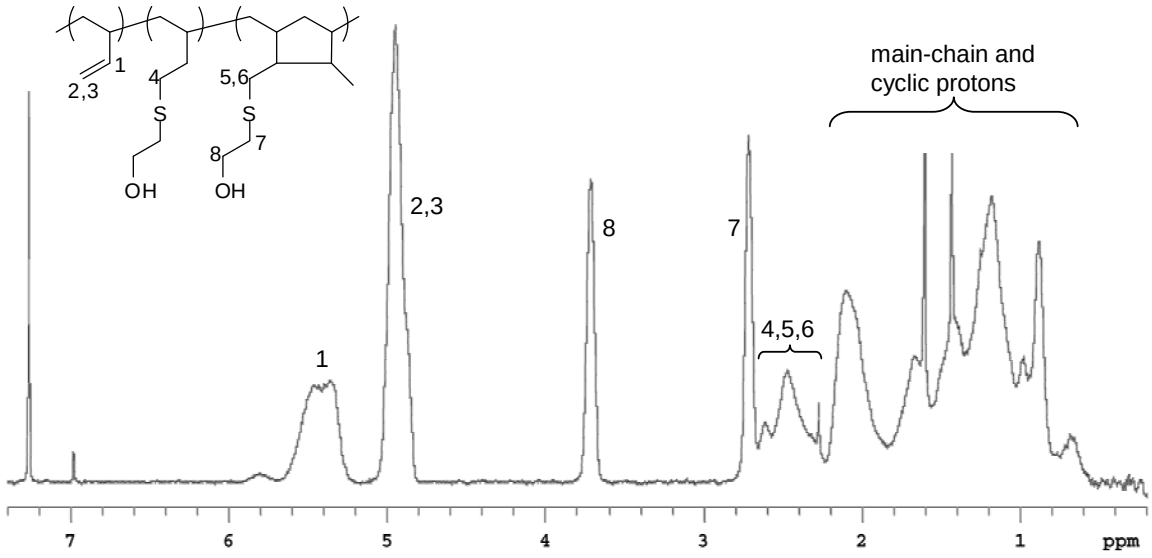

Figure B.2 ^{1}H NMR trace of functionalized 1,2-PB polymer 92kPB-OH (experimental conditions are given in Table 5.2).

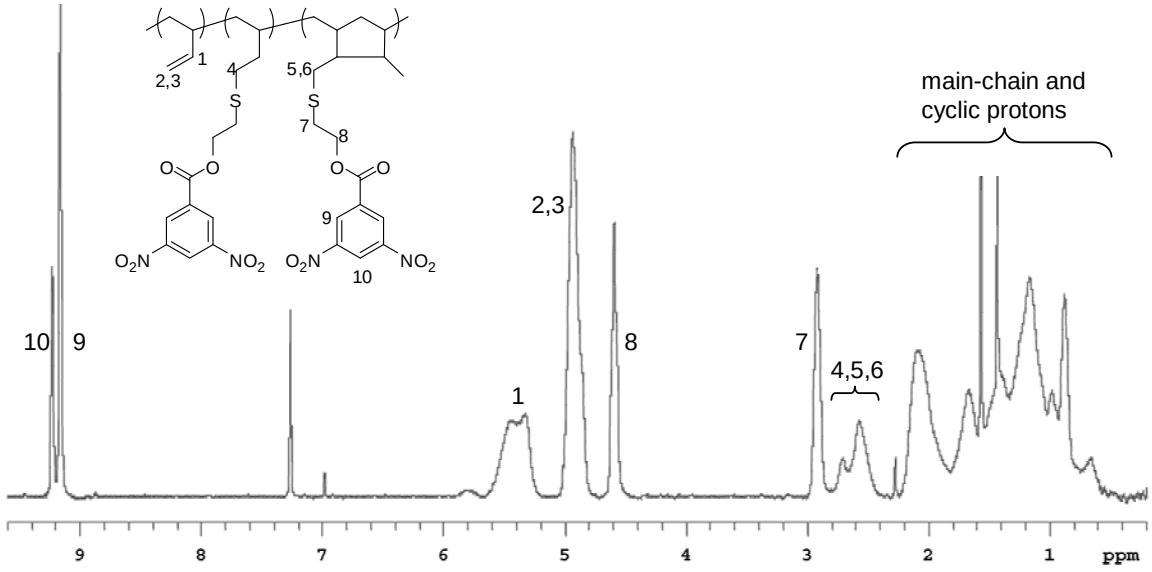

Figure B.3 ^{1}H NMR trace of functionalized 1,2-PB polymer 92kPB-DNB (experimental conditions are given in Table 5.2).

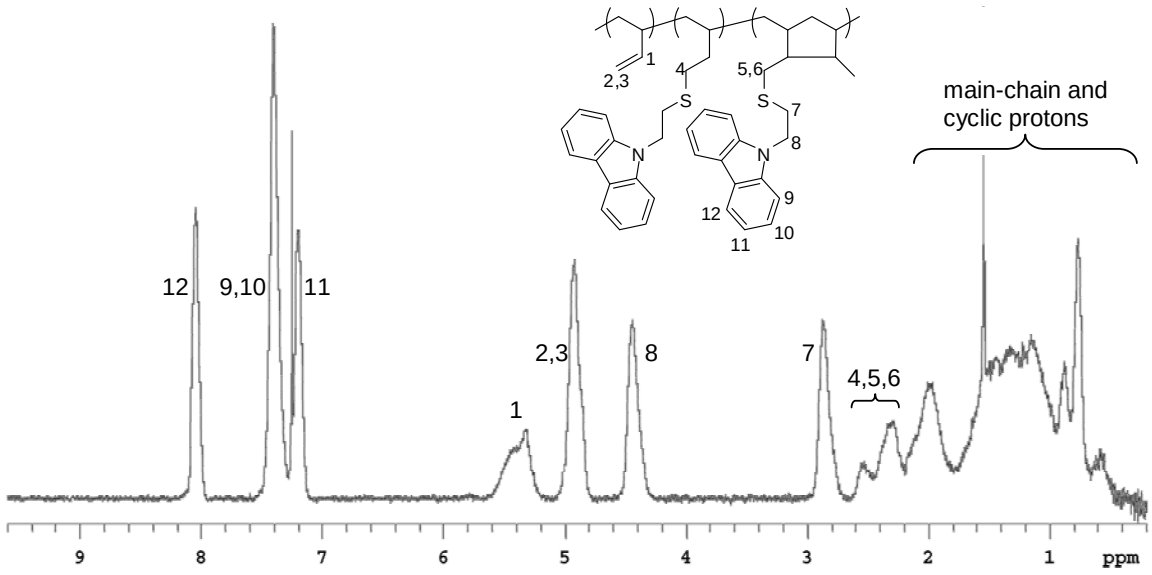

Figure B.4 ^{1}H NMR trace of functionalized 1,2-PB polymer 820kPB8 (experimental conditions are given in Table 5.1).

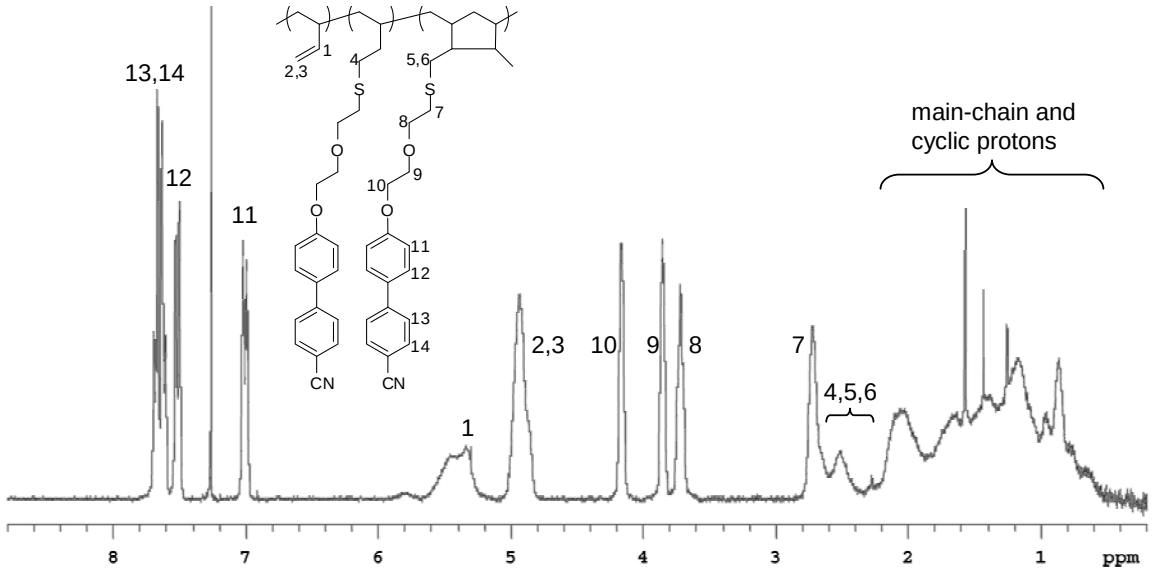

Figure B.5 ^{1}H NMR trace of functionalized 1,2-PB polymer 92kPB6 (experimental conditions are given in Table 5.1).

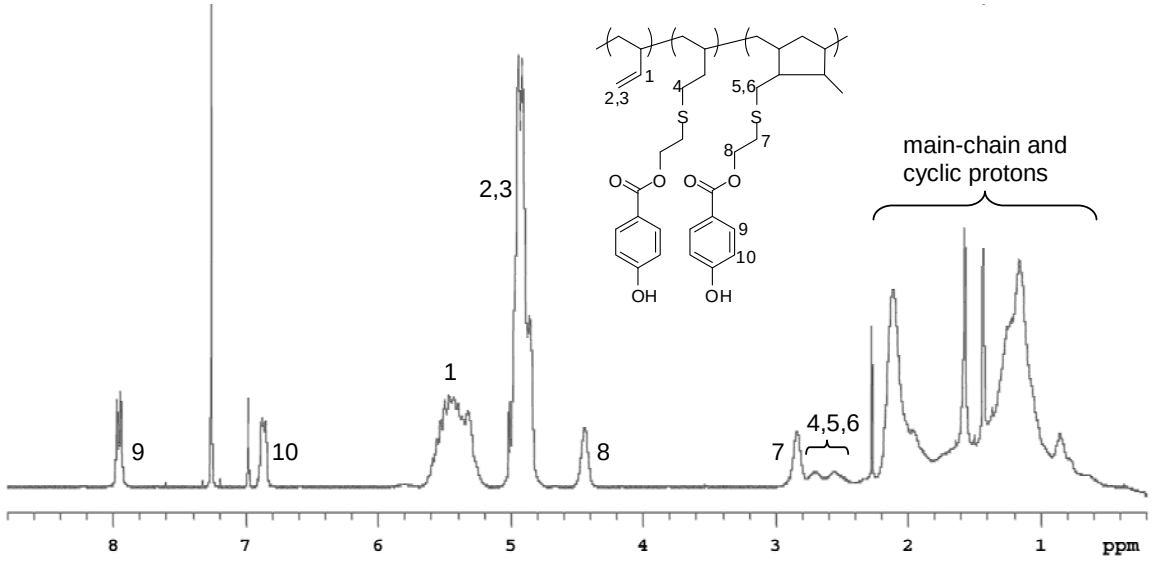

Figure B.6 ^{1}H NMR trace of functionalized 1,2-PB polymer 820kPB12 (experimental conditions are given in Table 5.1).

B.3 1,2-Polybutadiene Functionalization Using 9-[2-[(Triphenylmethyl)thio] ethyl]carbazole (14)

Synthesis of 9-(2-Chloroethyl)carbazole (7). The procedure was outlined in the description of the preparation of **8**. ^{1}H NMR (300 MHz, $CDCl_3$): δ = 8.09 (d, 2 carbazole H, J = 7.8 Hz), 7.50-7.37 (m, 4 carbazole H), 7.29-7.20 (m, 2 carbazole H), 4.60 (t, NCH_2, J = 7.2 Hz), 3.83 (t, CH_2Cl, J =7.2 Hz). ^{13}C NMR (300 MHz, $CDCl_3$): δ = 140.07, 125.91, 123.07, 120.50, 119.50, 108.43, 44.64, 40.99.

Synthesis of 9-[2-[(Triphenylmethyl)thio]ethyl]carbazole (14). Potassium carbonate (4.4 g, 32 mmol), triphenylmethyl mercaptan (Alfa Aesar, 98%, 3.1 g, 11 mmol), and 9-(2-chloroethyl)carbazole (2.1 g, 9.1 mmol) were stirred at room temperature in 50 mL of DMF for 5 h, after which the reaction mixture was transferred to a 500-mL separatory funnel containing 100 mL of water and extracted with 50 mL of chloroform. The organic layer was washed twice with 100 mL of water, the solvent was evaporated under reduced pressure, and the crude product was purified by washing 3 times in 75 mL of hot ethanol. Filtration of the solids and removal of remaining solvent under reduced pressure gave analytically pure **14** as ultra-fine, white needles (3.1 g, 6.6 mmol, 72% yield). ^{1}H NMR (300 MHz, $CDCl_3$): δ =

8.03 (d, 2 carbazole H, J = 7.8 Hz), 7.43-7.14 (m, 4 carbazole H and 15 phenyl H), 7.00 (d, 2 carbazole H, J = 8.1 Hz), 4.06 (t, NCH_2, J = 8.1 Hz), 2.75 (t, SCH_2, J = 8.1 Hz). ^{13}C NMR (300 MHz, $CDCl_3$): δ = 144.61, 139.76, 129.69, 128.01, 126.86, 125.56, 122.79, 120.27, 119.00, 108.54, 67.39, 42.37, 30.22.

Functionalization Procedure and Results. To compound **14** (0.25 g, 0.5 mmol) dissolved in 10 mL of chloroform in a 100-mL Schlenk tube were added triethylsilane (Alfa Aesar, 98%, 0.08 g, 0.7 mmol) and trifluoroacetic acid (TFA, 0.5 mL, 5 %vol), and the mixture was stirred 1–2 h at room temperature. After addition of 1,2-PB (0.2 g, 4 mmol vinyl groups, dissolved in 10 mL chloroform) and AIBN (0.03 g, 0.2 mmol), the contents of the Schlenk tube were degassed in three freeze-pump-thaw cycles, then allowed to react at 55 ºC for 3 h. Following reaction, the polymer solution was transferred to a 100-mL jar containing a small amount of BHT, concentrated by evaporation of all but the last 10 mL of solvent under an argon stream, and precipitated in cold methanol. Final purification of the polymer was achieved by reprecipitation from a DCM solution with cold methanol (2–3 times), followed by drying to constant weight under vacuum at room temperature Reaction conditions and results for a specific example are given in Table B.1 (first entry).

B.4 1,2-Polybutadiene Functionalization Using Thiobenzoic acid S-[3-(9-carbazolyl)propyl] ester (16)

Synthesis of 9-Allylcarbazole (15). Carbazole (10.1 g, 0.057 mol) and potassium hydroxide (88 wt % pellets, crushed, 7.1 g, 0.11 mol) were stirred in 100 mL of DMSO at 50 ºC for 30 min before dropwise addition of allyl bromide (14.7 g, 0.118 mol). After 15 min the reaction mixture was poured into a 500-mL separatory funnel containing 100 mL of chloroform and washed 5 times with 200 mL of water to give, after solvent evaporation at 60 ºC under reduced pressure, compound **15** in > 99% purity as a dark brown, viscous syrup which solidified upon cooling (11.9 g, 0.057 mol, 100% yield). ^{1}H NMR (300 MHz, $CDCl_3$): δ = 8.14-8.06 (m, 2 carbazole H), 7.49-7.32 (m, 4 carbazole H), 7.28-7.19 (m, 2 carbazole H), 6.04-5.90 (m, CH=CH_2), 5.19-5.10 (m, Z-HCH=CH), 5.07-4.97 (m, E-HCH=CH), 4.92-4.85 (m, NCH_2). ^{13}C NMR (300 MHz, $CDCl_3$): δ = 140.34, 132.27, 125.67, 122.90, 120.33, 119.00, 116.74, 108.74, 45.21.

Synthesis of Thiobenzoic acid S-[3-(9-carbazolyl)propyl] ester (16). Thiobenzoic acid (30 g, 0.20 mol) was added to 9-allylcarbazole (11.9 g, 0.057 mol) in 100 mL of toluene, and the reaction was carried out at 90 ºC with argon purge via radical mechanism using AIBN as the initiator (1.8 g, 11 mmol, in 300-mg increments at 1-hr intervals). After 6 h the reaction mixture was poured into a 1-L separatory funnel containing 20 g of sodium bicarbonate ($NaHCO_3$, 0.24 mol) in 250 mL of water, extracted with 100 mL of chloroform, and the organic phase was washed twice with 200 mL of water before solvent removal under reduced pressure. The crude product was subsequently washed in 100 mL of hot hexane, 150 mL of ethanol, and finally 150 mL of 15:1 of ethanol:chloroform. Evaporation of leftover solvent at 80 ºC under reduced pressure yielded compound **16** in ca. 90% purity as a dark brown, viscous syrup which solidified upon cooling (9.35 g, 0.024 mol, 42% yield, ~ 10 wt % dibenzoyl disulfide). ^{1}H NMR (300 MHz, $CDCl_3$): δ = 8.10 (d, 2 carbazole H, J = 8.1 Hz), 8.00-7.95 (m, 2 aromatic H ortho to COS), 7.62-7.41 (m, 3 aromatic H meta and para to COS plus 4 carbazole H), 7.27-7.19 (m, 2 carbazole H), 4.43 (t, NCH_2, J = 6.9 Hz), 3.06 (t, SCH_2, J = 6.9 Hz), 2.26 (tt, $NCH_2CH_2CH_2S$, J = 6.9, 6.9 Hz). ^{13}C NMR (300 MHz, $CDCl_3$): δ = 191.56, 140.25, 136.88, 133.50, 128.65, 127.23, 125.75, 122.91, 120.41, 119.00, 108.55, 41.65, 28.95, 26.41.

Functionalization Procedure and Results. The functionalization procedure followed the general method outlined in Section 5.2.3. Reaction conditions and results for a specific example are given in Table B.1 (second entry).

Table B.1 Reaction Conditions and Results for 1,2-PB Functionalization Using Compounds **14** and **16**

Entry[a]	[PB] (g/mL)	[Thiol][b]	[AIBN] (g/mL)	Rxn time (h)	X_{funct}[c] %	M_W[d] (kg/mol)	PDI[d]	New ^{1}H NMR peaks above 2.2 ppm for modified PB (all peaks are broad)
820kPB14	0.011	0.1	0.002	2.9	6	945	2.08	8.12-8.04 (2H), 7.52-7.39 (4H), 7.27-7.19 (2H), 4.56-4.43 (2H), 2.97-2.83 (2H)
92kPB16	0.003	1.1	0.003	3.0	19	187	1.34	8.15-8.03 (2H), 7.56.-7.37 (4H), 7.28-7.15 (2H), 4.50-4.27(2H), 2.62-2.30 (4H)

[a]Modified PB polymers were named so that the prefix corresponds to the molecular weight of the starting 1,2-PB chain, and the suffix represents the reagent used. [b]In molar equivalents of 1,2-PB monomer units. [c]The fraction of reacted 1,2-PB units that bear functional groups (refer to text). [d]Measurements as described in Section 5.2.1 using the Waters setup (the 1,2-PB prepolymers had PDI values of 1.07 and 1.26 for the 92 kg/mol and 820 kg/mol chains, respectively).